

Phenomenological Aspects of Majorana Neutrino Mass Matrices

Dissertation

zur Erlangung des Grades eines
Doktors der Naturwissenschaften
der Abteilung Physik
der Universität Dortmund

vorgelegt von

Werner Rodejohann

November 2001

Für meine Mutter

Contents

1	Introduction	3
1.1	Historical introduction	5
1.2	Neutrino masses and the see–saw mechanism	7
1.2.1	Neutrino masses	7
1.2.2	See–saw mechanism	8
1.2.3	Diagonalization of Majorana neutrino mass matrices	9
1.3	Neutrino mixing and experimental evidence	13
1.3.1	Oscillation	13
1.3.2	Experiments and their results	13
2	Neutrinoless Double Beta Decay and Neutrino Oscillations	19
2.1	Basics, experiments and uncertainty	20
2.1.1	Calculation of the nuclear matrix elements	23
2.2	Formalism	25
2.2.1	General considerations	25
2.2.2	Special cases	25
2.2.3	Maximal values for different schemes	28
2.3	Dependence on the parameters	30
2.3.1	Hierarchical scheme	30
2.3.2	Inverse hierarchical scheme	30
2.3.3	Degenerate scheme	32
2.3.4	Summary	39
2.4	An analysis of $\langle m \rangle$ as a function of the smallest mass state	41
2.4.1	Best–fit values	41
2.4.2	Results for the complete data set	42
2.4.3	Implications from the dark side	52
2.5	Summary and final remarks	54
3	Analogue of $0\nu\beta\beta$ I: Production of heavy Majorana Neutrinos at Colliders	57
3.1	Calculation of inverse neutrinoless double beta decay	59
3.1.1	Unitarity	61
3.1.2	Limits on heavy neutrinos and properties of the cross section	62

3.1.3	Evading the limits	64
3.2	Neutrino–nucleon scattering	66
3.2.1	Calculation	66
3.2.2	Results of the Monte Carlo	67
3.2.3	Experimental considerations	71
3.3	High energy neutrino factory	72
3.3.1	Properties of neutrino factories	76
3.3.2	Experimental considerations	77
3.3.3	Is it observable?	78
3.4	Positron–proton scattering at HERA	80
3.4.1	Analysis and results	80
3.4.2	Experimental considerations	84
3.5	HERA’s isolated leptons and heavy Majorana neutrinos	85
3.5.1	Two become one	86
3.5.2	Signals and observables	89
3.6	Summary and final remarks	95
4	Analogues of $0\nu\beta\beta$ II: Effects of $m_{\alpha\beta}$ and $\frac{1}{m_{\alpha\beta}}$	97
4.1	The entries of the mixing matrix	98
4.1.1	CP violating case, $\delta \neq 0$	98
4.1.2	CP conserving case, $\delta = 0$	100
4.2	The other entries of the mass matrix	102
4.2.1	Properties of the plots	102
4.2.2	Summary of the allowed range of $m_{\alpha\beta}$	105
4.3	Direct and indirect limits on and from $m_{\alpha\beta}$	107
4.3.1	Analogues of neutrinoless double beta decay	107
4.3.2	Limits on lepton number violating processes from indirect limits on $m_{\alpha\beta}$	109
4.3.3	More on the influence of $\langle m \rangle$ on $m_{\alpha\beta}$	114
4.4	Effective heavy Majorana masses: $\frac{1}{m_{\alpha\beta}}$	115
4.4.1	Direct limits on $\frac{1}{m_{\alpha\beta}}$	115
4.4.2	Indirect limits on $\frac{1}{m_{\alpha\beta}}$	116
4.4.3	Limits on lepton number violating processes from indirect limits of $\frac{1}{m_{\alpha\beta}}$	118
4.4.4	An example for future limits: high energy Neutrino factory	118
4.5	Model dependent considerations for heavy neutrinos	121
4.5.1	Right–handed Majorana neutrinos and see–saw models	121
4.5.2	Unitarity revisited	122
4.6	Summary and final remarks	124
5	Summary	127

A	Mass matrix elements	131
B	The matrix element	133
B.1	Left-handed Majorana neutrino	133
B.2	Right-handed Majorana neutrino	134
C	Derivation of the neutrino spectrum from muon decay	135
	References	139

Preface

This thesis consists of studies of different aspects of Majorana neutrinos.

Chapter 2 “Neutrinoless Double Beta Decay and Neutrino Oscillations” is a continuation of work presented in [1] and the result of a study performed together with Dr. C. Peña–Garay, which is new and not yet published. Part of the chapter bases on [1]

- W. Rodejohann, *Cancellations in Neutrinoless Double Beta Decay and the Neutrino Mass Matrix*, Nucl. Phys. **B 597**, 110 (2001) [Section 2.3.3].

The second Chapter “Analogues of $0\nu\beta\beta$ I: Production of heavy Majorana Neutrinos at Colliders” has emerged from collaborations with Dr. M. Flanz and Priv. Doz. K. Zuber [2–5]:

- M. Flanz, W. Rodejohann, and K. Zuber, *Trimuon production in νN scattering as a probe of massive neutrinos*, Eur. Phys. J. **C 16**, 453 (2000) [Section 3.2].
- W. Rodejohann, K. Zuber, *“Neutrinoless Double Beta Decay” at a Neutrino Factory*, Phys. Rev. **D 63**, 054031 (2001) [Section 3.3].
- M. Flanz, W. Rodejohann, and K. Zuber, *Bounds on effective Majorana neutrino masses at HERA*, Phys. Lett. **B 473**, 324 (2000), erratum *ibid.* **480**, 418 (2000) [Section 3.4].
- W. Rodejohann, K. Zuber, *Signatures of heavy Majorana neutrinos and HERA’s isolated lepton events*, Phys. Rev. **D 62**, 094017 (2000) [Section 3.5].

Chapter 4, “Analogues of $0\nu\beta\beta$ II: Effects of $m_{\alpha\beta}$ and $\frac{1}{m_{\alpha\beta}}$ ” is also based on the publications given above as well as on a more detailed analysis as the one presented in [6]. The work in Section 4.4 is new and has not been published yet. The remaining part of the Chapter bases on [6]

- W. Rodejohann, *Neutrino oscillation experiments and limits on lepton number and lepton flavor violating processes*, Phys. Rev. **D 62**, 013011 (2000) [Sections 4.1, 4.2 and 4.3].

Chapter 1

Introduction

This thesis is devoted to observable effects of light and heavy Majorana neutrinos. Since the strong evidence in favor of neutrino oscillations found by the SuperKamiokande collaboration, neutrino physics has become one of the most exciting and active fields of particle physics. The experimental observation of a significant reduction of neutrino flux from the atmosphere and the Sun finds its simplest explanation by means of neutrino oscillations. This in turn requires the neutrinos to be massive. Thus, for the first time, we are provided with evidence for physics beyond the Standard Model, which in the past has been confirmed to a high degree of precision over and over again. Neutrino mass and mixing can now be considered as established physical objects. Though it is possible to modify the Standard Model in a trivial manner by adding right-handed neutrinos to its particle content and thus producing a conventional Dirac mass term, the implied smallness of the neutrino masses remains puzzling. The next heaviest fermion, the electron, is at least five orders of magnitude heavier, the heaviest known particle, the top quark, at least eleven orders of magnitude. Certainly, a way to produce neutrino masses, different from the Standard Model Higgs mechanism, would be more than welcome. In fact, the see-saw mechanism can explain tiny neutrino masses due to their inverse proportionality to a heavy scale, the mass of additional heavy neutrinos.

The other important prediction of the see-saw mechanism is the Majorana nature of the light and heavy neutrinos. This introduces lepton number violation to the theory, a property after which is intensively searched. Since neutrino oscillation implies that lepton flavor is not conserved, it is natural to ask if lepton number itself is also not conserved. This is expected in Grand Unified Theories, when leptons and quarks are members of the same multiplet. In the search for lepton number violation, neutrinoless double beta decay ($0\nu\beta\beta$) stands out as the most important low energy process. In the present thesis this process and several other aspects of lepton number violation mediated by Majorana neutrinos are studied. The range of the Majorana mass matrix and observable effects of its entries are analyzed.

- In Chapter 2 an analysis of the connection between neutrino oscillation and $0\nu\beta\beta$ will be performed. After studying the dependence of the effective electron

neutrino Majorana mass on the oscillation parameters, a detailed analysis of the dependence on the smallest mass eigenstate is performed. In a degenerate scheme, limits on the neutrino mass in various situations are obtained. The CP conserving and violating cases are studied and ways to distinguish these two cases experimentally are proposed. It is commented on the consequences of the “dark side” of the parameter space.

- In Chapter 3 production of heavy Majorana neutrinos at colliders is studied. The diagram of $0\nu\beta\beta$ is applied to neutrino–nucleon and positron–proton scattering. For the former case, past fixed target as well as future neutrino factory experiments are considered. Then, for positron–proton scattering a possible explanation of an anomaly in the HERA experiment H1 is given.
- In Chapter 4 we turn to analogues of $0\nu\beta\beta$ and their observable effects. For this study, the allowed range of the neutrino mixing matrix as well as the Majorana mass matrix is analyzed. This is applied to a variety of lepton number violating processes. The predicted rates and signals are compared with current experimental bounds on these quantities. A similar analysis is performed for effects of heavy Majorana neutrinos.
- Finally, in Chapter 5 the main results of this thesis are summarized. Some useful formulas e.g. for the mass matrix elements or the matrix elements for production of Majorana neutrinos at colliders are relegated to the Appendix.

1.1 Historical introduction

Neutrinos were “invented“ in 1930 by Wolfgang Pauli in a desperate attempt to explain the continuous β -spectrum. In a legendary letter [7] to a conference in Tübingen, he proposed new light neutral spin 1/2 particles called “neutrons”, which exist in nuclei. Later, they were christened by Fermi to their now familiar name neutrinos, meaning “little neutrons” in Italian. It was not before 1956 that Cowans and Reines [8] observed the electron antineutrino in reactor experiments. Pontecorvo proposed neutrino oscillations in 1957 [9] and Goldhaber found that neutrinos are emitted only left-handed in 1958 [10]. In 1962 Lederman, Schwartz and Steinberger discovered that there is a different kind of neutrino, namely the one that is predominately produced in π decays [11]. In the same year the theory of neutrino mixing was studied by Maki, Nakagawa and Sakata [12], actually predating the proposal of quark mixing by one year. Seven years later Gribov and Pontecorvo [13] proposed the first phenomenological theory of neutrino mixing and oscillations. In 1978 Wolfenstein as well as Mikheev and Smirnov [14] studied neutrino mixing in the presence of a medium.

The theoretical explanation in favor of neutrino masses and mixing is based on models beyond the Standard Model (SM). In such models (see, for example, [15]) the fields of quarks, charged leptons and neutrinos are grouped within the same multiplets and the generation of the masses of quarks and charged leptons through the Higgs mechanism provides also masses for the neutrinos.

The see-saw mechanism for the generation of neutrino masses was proposed in 1979 [16]. This mechanism connects the smallness of neutrino masses with the possible violation of lepton number at a very large scale. The mechanism also predicts Majorana neutrinos, whose properties have been studied by Majorana already in 1937 [17].

The total number of light active neutrinos was inferred from the invisible part of the Z_0 -width to be approximately three in 1992 by the LEP experiments [18]. Finally, the year 2000 saw the discovery of the tau neutrino, found by the DONUT experiment [19].

At present the effects of neutrino masses and mixings are investigated in many different experiments. There are three types of experiments in which the effects of small neutrino masses (of the order of 1 eV or smaller) and mixing can be revealed:

1. Neutrino oscillation experiments
2. Experiments on the search for neutrinoless double beta decay
3. Experiments on the measurement of the electron neutrino mass

Three indications in favor of neutrino masses and mixing have been found so far, obtained in the following experiments:

1. Solar neutrino experiments (Homestake [20], Kamiokande [21], GALLEX [22], SAGE [23], GNO [24], SuperKamiokande [25] and SNO [26])
2. Atmospheric neutrino experiments (IMB [27], Soudan [28], MACRO [29], Kamiokande [30] and SuperKamiokande [31])
3. The accelerator LSND experiment [32]

Many other neutrino oscillation experiments from reactor and accelerators did not find any evidence for neutrino oscillations. In the experiments on the search for neutrinoless double beta decay no indications for non-zero neutrino mass were found (see Chapter 2). The present upper bound for the electron neutrino mass obtained in the Mainz experiment [33] is 2.2 eV. The upper limits on the masses of the ν_μ and ν_τ are 170 keV [34] and 18.2 MeV [35], respectively.

Only a small part of the recent developments in neutrino physics can be given in this introduction, for more extensive reviews see [36]. In Section 1.2, we will now introduce the see-saw mechanism and discuss some properties of Majorana neutrinos. The diagonalization of a mass matrix is identified as the reason for neutrino mixing. The phenomenology of neutrino mixing and the resulting oscillation as well as the results of neutrino experiments are summarized in Section 1.3. It is also discussed to which mass and mixing schemes the experiments lead.

1.2 Neutrino masses and the see-saw mechanism

1.2.1 Neutrino masses

In the SM masses for quarks and leptons were introduced through Yukawa couplings to the Higgs doublet. The neutrino was massless because it was assumed that the right-handed neutrino did not exist. This may be a conservative assumption because for all other particles right-handed components were introduced. Once one accepts the presence of right-handed neutrinos N_R , one observes that they are singlets under $SU(2)$. The representation content for the electron sector is

$$\Psi_L = \begin{pmatrix} \nu \\ e \end{pmatrix}_L, N_R \text{ and } e_R. \quad (1.1)$$

A mass term of the form

$$\mathcal{L}_D = m_D \bar{\nu}_L N_R + \text{h.c.} \quad (1.2)$$

is possible. It is generated from the Yukawa coupling

$$\mathcal{L}_Y^\nu = \sum f_{\alpha\beta} \bar{\Psi}_L^\alpha \hat{\Phi} N_R^\beta + \text{h.c.} \quad (1.3)$$

where Φ is the standard Higgs doublet with

$$\hat{\Phi} = i\tau_2 \Phi^* = \begin{pmatrix} \bar{\Phi}_0 \\ -\Phi^- \end{pmatrix} \xrightarrow{\text{breaking}} \begin{pmatrix} \bar{\Phi}_0 + v \\ 0 \end{pmatrix}, \quad (1.4)$$

and $f_{\alpha\beta}$ is the Yukawa coupling matrix. This is the conventional Dirac mass term. The formalism is similar to that of quarks and charged leptons. However, the observed extreme smallness of neutrino masses seems to require a special treatment. In addition, this smallness can in a very elegant way be related to a high scale, the mass of heavy neutrinos. Lepton number can be conserved by applying a global symmetry via $\psi \rightarrow \psi e^{iL}$. A Dirac mass term is invariant under this symmetry and L can be identified as the lepton number.

In a Dirac mass term ν_L annihilates a left-handed neutrino and creates a right-handed antineutrino. Correspondingly, the field $\bar{\nu}_L$ creates a left-handed neutrino and annihilates a right-handed antineutrino. Left-handed neutrinos ν_L and right-handed antineutrinos $\bar{\nu}_R = \bar{\nu}_L$ are indeed the only observed states in nature. Thus, in principle one can assume that right-handed neutrinos ν_R and left-handed antineutrinos $\bar{\nu}_L = \bar{\nu}_R$ do not exist at all.

If L is violated, there is no quantum number that makes the neutral ν and $\bar{\nu}$ different and a new kind of mass term is possible. For a massive neutrino, the positive helicity state that Lorentz invariance demands to be associated with the state ν_L of given momentum can be $\bar{\nu}_R$. If neutrinos and antineutrinos are no distinct particles, both Lorentz and CPT invariance are satisfied by just allowing ν_L and $\bar{\nu}_R$. If L is violated a so-called Majorana mass term

$$\mathcal{L}_L = \overline{(\nu_L)^c} m_L \nu_L = \nu_L^T C m_L \nu_L \quad (1.5)$$

is allowed, where $C = i\gamma_2$ is the charge conjugation matrix in Dirac space. It has the properties

$$\begin{aligned} -C &= C^T = C^{-1} = C^* = C^\dagger \\ C^{-1}\gamma_\mu C &= -\gamma_\mu^T, \quad C^{-1}\gamma_5 C = \gamma_5^T. \\ \psi^c &= C\bar{\psi}^T, \quad \bar{\psi}^c = -\psi^T C^{-1} \end{aligned} \quad (1.6)$$

Clearly, in the mass term (1.5) lepton number is violated by two units, $\Delta L = 2$. In the SM ν_L transforms as a weak isospin doublet, thus the mass term transforms as a component of an isospin triplet.

If L is violated and in addition ν_R exists, then a second type of Majorana mass is allowed,

$$\mathcal{L}_R = \overline{(\nu_R)^c} M_R \nu_R = \nu_R^T C M_R \nu_R. \quad (1.7)$$

Also this mass term has $\Delta L = 2$ but since ν_R is a gauge singlet, (1.7) is invariant under the SM gauge group.

In conclusion, if ν_R does not exist, we can only have a Majorana mass term \mathcal{L}_L if L is violated. If ν_R exists and L is violated, both Dirac \mathcal{L}_D and Majorana masses $\mathcal{L}_{L,R}$ are allowed. As already mentioned, since oscillation experiments show that lepton flavor L_α is not a conserved quantum number, it is natural to expect that also the lepton number L is violated.

1.2.2 See–saw mechanism

The most general mass term is a combination of Dirac and Majorana terms [16]. It is a symmetric matrix and reads

$$-\mathcal{L} = \left(\overline{\nu_L}, \overline{(\nu_R)^c} \right) \begin{pmatrix} m_L & m_D \\ m_D & M_R \end{pmatrix} \begin{pmatrix} (\nu_L)^c \\ \nu_R \end{pmatrix} + \text{h.c.} \quad (1.8)$$

This is obviously a Majorana mass term. The mass term has the form $\overline{\chi^c} m \chi$ with $\chi^c = \chi$, which is the definition of a Majorana particle. Diagonalizing this symmetric matrix leads to eigenvalues $m_{1,2}$,

$$m_{1,2} = \frac{1}{2} \left[m_L + M_R \pm \sqrt{(m_L - M_R)^2 + 4m_D^2} \right]. \quad (1.9)$$

The mixing angle is

$$\tan 2\theta = \frac{2m_D}{M_R - m_L}. \quad (1.10)$$

The eigenfields are

$$\chi = \begin{pmatrix} \nu_1 \\ \nu_2 \end{pmatrix} = \hat{U}^\dagger \begin{pmatrix} \nu_L \\ (\nu_R)^c \end{pmatrix} + \hat{U}^T \begin{pmatrix} (\nu_L)^c \\ \nu_R \end{pmatrix}, \quad (1.11)$$

which are again Majorana particles. Now assume that $M_R \gg m_L, m_D$. Then,

$$\begin{aligned} m_1 &\simeq m_L - \frac{m_D^2}{M_R} \\ m_2 &\simeq M_R \end{aligned} \quad (1.12)$$

$$\tan 2\theta \simeq \frac{2m_D}{M_R} \Rightarrow \cos \theta \simeq 1 \text{ and } \sin \theta \simeq \frac{m_D}{M_R}.$$

It is interesting to note that

$$\cos^2 \theta m_1 + \sin^2 \theta m_2 = m_L. \quad (1.13)$$

If in addition $m_D \gg m_L$, then the mixing between the light and heavy states is a function of m_1/m_2 ,

$$m_1 = \frac{m_D^2}{M_R} \text{ and } \sin^2 \theta \simeq \frac{m_1}{m_2}. \quad (1.14)$$

The sum in Eq. (1.13) vanishes now. It is therefore always the left-handed triplet entry of the mass term Eq. (1.8). The eigenfields in Eq. (1.11) simplify to

$$\begin{aligned} \nu_1 &\equiv \nu \simeq \nu_L + (\nu_L)^c \\ \nu_2 &\equiv N \simeq \nu_R + (\nu_R)^c \end{aligned} \quad (1.15)$$

The result is thus a light Majorana neutrino ν with mass m_D^2/M_R and a heavy Majorana neutrino N . Identifying ν with the standard model neutrinos explains their lightness by the heavy scale M_R . This is the see-saw mechanism. It follows a hierarchical mass scheme for the neutrinos and $m_\nu \simeq 10^{-2}$ eV leads to $M_R \simeq 10^{16}$ GeV for a Dirac scale of 1 GeV. Since this is a typical Grand Unified Theory (GUT) scale, the model is very popular and appealing. However, the masses M_R, m_L, m_D and thus their mixing can assume arbitrary values and are a priori constrained only by experiment. Chapter 3 and part of Chapter 4 will be devoted to look for observable effects of these intermediate Majorana neutrinos.

1.2.3 Diagonalization of Majorana neutrino mass matrices

A Majorana neutrino mass matrix is always symmetric: since $\overline{\nu_\alpha^c} \nu_\beta = -\nu_\alpha^T C^{-1} \nu_\beta = \nu_\beta^T (C^{-1})^T \nu_\alpha = -\nu_\beta^T C^{-1} \nu_\alpha = \overline{\nu_\beta^c} \nu_\alpha$, it follows that $\overline{\nu_\alpha^c} m_{\alpha\beta} \nu_\beta = \overline{\nu_\beta^c} m_{\alpha\beta} \nu_\alpha = \overline{\nu_\alpha^c} m_{\beta\alpha} \nu_\beta$. In general, m_L is a 3×3 , whereas m_D can be a $3 \times s$ and M_R a $s \times s$ matrix, where s is an arbitrary natural number. Neglecting m_L , the 3×3 neutrino mass matrix reads

$$m = -m_D M_R^{-1} m_D^T. \quad (1.16)$$

Now m has to be further diagonalized in order to get from the non-diagonal flavor basis to the diagonal mass basis. In case of CP invariance m is real and can be diagonalized by an orthogonal matrix O ,

$$O^T m O = \text{diag}(\eta_1 m_1, \eta_2 m_2, \eta_3 m_3), \quad (1.17)$$

with $\eta_i = \pm 1$ and $m_i \geq 0$, where $i = 1, 2, 3$. At the cost of a complex O the CP parities can also be absorbed in the mixing matrix via the identity

$$\eta_i = e^{i\pi/2(\eta_i-1)}. \quad (1.18)$$

For complex m and thus CP violation the diagonalization of the mass term is done by an unitary matrix,

$$U^T m U = \text{diag}(m_1, m_2, m_3). \quad (1.19)$$

Appropriate choice of U can always make $m_i \geq 0$. Conventionally one chooses

$$m_3 > m_2 > m_1. \quad (1.20)$$

With the help of Eq. (1.18) the matrices U and O are connected via

$$U_{\alpha i} = O_{\alpha i} e^{i\pi/4(\eta_i-1)}. \quad (1.21)$$

Note that since $\eta_i = \pm 1$ for the mixing matrix elements holds

$$U_{\alpha i}^* = U_{\alpha i} \eta_i. \quad (1.22)$$

The mixing matrix is thus always complex and the neutrinos get transformed via

$$\nu_\alpha = U_{\alpha i} \nu_i. \quad (1.23)$$

This is exactly the equation needed to produce neutrino oscillations, the neutrino mixing is thus produced by the diagonalization of the neutrino mass matrix. U is denoted Maki–Nakagawa–Sakata (MNS) matrix.

The Majorana mass term has the form $\nu^T \nu$. For this reason, there are two additional phases in the parametrisation of the MNS matrix U . A very convenient form of U is

$$\begin{aligned} U &= U_{\text{CKM}} P = U_{\text{CKM}} \text{diag}(1, e^{i\alpha}, e^{i(\beta+\delta)}) \\ &= \begin{pmatrix} c_1 c_3 & s_1 c_3 & s_3 e^{-i\delta} \\ -s_1 c_2 - c_1 s_2 s_3 e^{i\delta} & c_1 c_2 - s_1 s_2 s_3 e^{i\delta} & s_2 c_3 \\ s_1 s_2 - c_1 c_2 s_3 e^{i\delta} & -c_1 s_2 - s_1 c_2 s_3 e^{i\delta} & c_2 c_3 \end{pmatrix} \text{diag}(1, e^{i\alpha}, e^{i(\beta+\delta)}), \end{aligned} \quad (1.24)$$

where $c_i = \cos \theta_i$ and $s_i = \sin \theta_i$. The two additional phases α and β , which do not appear in the quark mixing parametrisation are included in the diagonal matrix P . It is seen that the ee element of m in Eq. (1.19) is only depending on the three masses m_i , two angles θ_1, θ_3 and these two extra phases.

A parametrisation of U for two flavors reads

$$U = \begin{pmatrix} \cos \theta & \sin \theta e^{i\phi} \\ -\sin \theta e^{-i\phi} & \cos \theta \end{pmatrix}, \quad (1.25)$$

where ϕ is the Majorana phase, which would not appear for Dirac neutrinos.

For CP invariance it can be shown that η_i is connected to the intrinsic CP parity of the Majorana neutrino. First we show that the CP parity of Majorana neutrinos is complex. In general, the CP property of a neutrino is given by

$$U_{CP}\nu U_{CP}^{-1} = \eta_{CP}\gamma_0\nu(x'), \quad (1.26)$$

where U_{CP} is the CP conjugation operator, η_{CP} the CP parity and $x' = (t, -\vec{x})$. Since $\gamma_0 C = -C\gamma_0$ one finds

$$U_{CP}\nu^c U_{CP}^{-1} = -\eta_{CP}^*\gamma_0\nu^c(x'). \quad (1.27)$$

Due to the Majorana condition $\nu^c = \nu$ it follows

$$U_{CP}\nu U_{CP}^{-1} = -\eta_{CP}^*\gamma_0\nu(x'), \quad (1.28)$$

which means that

$$\eta_{CP} = \pm i \quad (1.29)$$

for Majorana neutrinos. Therefore, for a Majorana neutrino holds

$$U_{CP}\nu_\alpha U_{CP}^{-1} = i\gamma_0\nu_\alpha(x'). \quad (1.30)$$

From this equation we will show that $\eta_{CP}(\nu_i) = i\eta_i$. Starting with

$$\nu_i = U_{\alpha i}^*\nu_\alpha \quad (1.31)$$

one gets

$$\gamma_0\nu_\alpha^c(x') = U_{\alpha j}^*\gamma_0\nu_j^c(x'). \quad (1.32)$$

On the other hand, from Eq. (1.30) it is found that

$$U_{CP}\nu_i U_{CP}^{-1} = i\gamma_0 U_{\alpha i}^*\nu_\alpha^c(x'). \quad (1.33)$$

Inserting now (1.32) into (1.33) and taking (1.22) into account, one finds

$$U_{CP}\nu_i(x)U_{CP}^{-1} = iU_{\alpha i}^*U_{\beta j}^*\gamma_0\nu_j^c(x') = i\eta_i\nu_i^c(x'), \quad (1.34)$$

which gives the desired result that

$$\eta_{CP}(\nu_i) = i\eta_i. \quad (1.35)$$

Within the parametrisation of U given in Eq. (1.24) and with the help of identity (1.18) it is easy to show that the CP conserving cases correspond to special cases of the phases, to be precise

$$\begin{aligned} \eta_1 = \eta_2 = \eta_3 = +1 & \leftrightarrow \alpha = \beta = \pi & (+ + +) \\ \eta_1 = -\eta_2 = -\eta_3 = +1 & \leftrightarrow \alpha = \beta = \pi/2 & (+ - -) \\ \eta_1 = -\eta_2 = \eta_3 = -1 & \leftrightarrow \alpha = \beta/2 = \pi/2 & (- + -) \\ \eta_1 = \eta_2 = -\eta_3 = -1 & \leftrightarrow \alpha = 2\beta = \pi & (- - +) \end{aligned} \quad (1.36)$$

The $(\pm \pm \pm)$ denote the sign of the three mass eigenvalues. In conventional CP violation the phase π is not distinguishable from the CP conserving case. For processes involving Majorana neutrinos also $\pi/2$ is such a special value.

In conclusion, the neutrino mixing matrix U is derived by diagonalizing the Majorana mass term in the Lagrangian:

$$-\mathcal{L}_{\text{mass}} = \overline{\nu}_\alpha^c m_{\alpha\beta} \nu_\beta + \text{h.c.} \quad (1.37)$$

The Majorana mass matrix can be written as

$$m_{\alpha\beta} = \left(U^T \text{diag}(m_1, m_2, m_3) U \right)_{\alpha\beta} = \sum_i m_i U_{\alpha i} U_{\beta i}. \quad (1.38)$$

Chapter 2 will be devoted to the ee element of this matrix and part of Chapter 4 will deal with the other entries of m .

1.3 Neutrino mixing and experimental evidence

1.3.1 Oscillation

The probability for a flavor state ν_α to oscillate into ν_β is denoted $P_{\alpha\beta}$ and reads

$$P_{\alpha\beta} = \delta_{\alpha\beta} - 2 \operatorname{Re} \sum_{j>i} U_{\alpha i} U_{\alpha j}^* U_{\beta i}^* U_{\beta j} (1 - \exp i\Delta_{ji}) , \quad (1.39)$$

where in practical units

$$\Delta_{ij} = \frac{\Delta m_{ij}^2 L}{2E} = 2.48 \frac{L}{\text{km}} \frac{\Delta m_{ij}^2 \text{ GeV}}{\text{eV}^2 E} \quad (1.40)$$

and $\Delta m_{ij}^2 = m_i^2 - m_j^2$. This formula defines the sensitivity for any given experiment, since $\frac{\Delta m_{ij}^2 L}{E}$ should not be much smaller than one. As a function of baseline, the maximum of oscillation occurs at $L \simeq 2E/\Delta m_{ij}^2$. It is easy to show that the two extra phases α and β do not influence the oscillation probability. Only the third phases δ is responsible for CP violating effects [37] in oscillations.

For two neutrino families, the probability simplifies to

$$\begin{aligned} P_{\alpha\alpha} &= 1 - \sin^2 2\theta \sin^2 \Delta_{12}/2 \\ P_{\alpha\beta} &= 1 - P(\nu_\alpha \rightarrow \nu_\alpha) \end{aligned} \quad (1.41)$$

A mono-energetic neutrino beam thus oscillates with amplitude $\sin^2 2\theta$ and wave number $\Delta m^2/4E$. Oscillation only measures the difference of two squared masses, leaving the smallest mass eigenstate as a free parameter, whose range goes from zero to 2.2 eV. In Chapter 2 a way to bound this smallest mass value is presented.

1.3.2 Experiments and their results

The three experiments with evidence for neutrino oscillation can each be successfully analyzed in simple two-flavor frameworks, though at least one more flavor exists. The reason is that the equations for the probability decouple, as will be shown below. In the following, we will ignore the result of the LSND experiment, since it is not independently confirmed by other experiments. In addition, its result together with the ones from the solar and atmospheric experiments requires the introduction of a light fourth, sterile neutrino. Atmospheric experiments are explained by large mixing, $\tan^2 \theta \simeq 1$, and a mass scale of $\Delta m_A^2 \simeq 3 \cdot 10^{-3} \text{ eV}^2$. For solar experiments, three distinct areas in the parameter space are identified:

- The large mixing Mikheyev–Smirnov–Wolfenstein (MSW) solution (LMA) with large mixing and a mass scale of $\Delta m_\odot^2 \simeq (10^{-5} \dots 10^{-4}) \text{ eV}^2$. A typical best-fit point is $\tan^2 \theta_1 = 1$ and $\Delta m_\odot^2 = 5 \cdot 10^{-5} \text{ eV}^2$.

- The small mixing MSW solution (SMA) with small mixing $\tan^2 \theta \simeq 10^{-3}$ and a mass scale of $\Delta m_{\odot}^2 \simeq (10^{-6} \dots 10^{-5}) \text{ eV}^2$. A typical best-fit point is $\tan^2 \theta_1 = 5 \cdot 10^{-4}$ and $\Delta m_{\odot}^2 = 5 \cdot 10^{-6} \text{ eV}^2$.
- The quasi-vacuum solution (QVO) with large mixing and a mass scale of $\Delta m_{\odot}^2 \simeq (10^{-10} \dots 10^{-7}) \text{ eV}^2$. A typical best-fit point is $\tan^2 \theta_1 = 1$ and $\Delta m_{\odot}^2 = 10^{-8} \text{ eV}^2$.

Reactor and accelerator neutrino experiment find no evidence for oscillation. With the relation

$$\Delta m_{\odot}^2 \ll \Delta m_{\text{A}}^2 \quad (1.42)$$

and identifying $\Delta m_{21}^2 = \Delta m_{\odot}^2 \ll \Delta m_{\text{A}}^2 = \Delta m_{31}^2 \simeq \Delta m_{32}^2$ we have for a short baseline reactor experiment such as CHOOZ [38]

$$P_{ee}^{\text{CHOOZ}} = 1 - 4|U_{e3}|^2(1 - |U_{e3}|^2) \sin^2 \Delta_{31}/2. \quad (1.43)$$

The negative results mean that $|U_{e3}|$ is either small or close to one. The survival probability for solar neutrinos is

$$P_{ee}^{\odot} = (1 - |U_{e3}|^2)^2 \left(1 - 4 \frac{|U_{e1}|^2 |U_{e2}|^2}{(1 - |U_{e3}|^2)^2} \sin^2 \Delta_{21}/2 \right) + |U_{e3}|^4. \quad (1.44)$$

Experimentally, P_{ee}^{\odot} is significantly lower than one and also energy dependent, therefore $|U_{e3}|^2 \ll 1$ and

$$P_{ee}^{\odot} = 1 - 4|U_{e1}|^2 |U_{e2}|^2 \sin^2 \Delta_{21}/2. \quad (1.45)$$

Finally, atmospheric neutrinos oscillate with

$$P_{\mu\tau}^{\text{A}} = 4|U_{\mu 3}|^2 |U_{\tau 3}|^2 \sin^2 \Delta_{31}/2. \quad (1.46)$$

The relation between the two Δm^2 (1.42) and the smallness of $|U_{e3}|$ allows the simple two-flavor description of the experiments. Roughly, one can assume $|U_{e3}| \simeq 0$, maximal atmospheric mixing and maximal (QVO or LMA) or vanishing (SMA) solar mixing. Ignoring the phases one finds for the MNS matrix

$$U \simeq \begin{cases} \begin{pmatrix} 1 & 0 & 0 \\ 0 & 1/\sqrt{2} & 1/\sqrt{2} \\ 0 & -1/\sqrt{2} & 1/\sqrt{2} \end{pmatrix} & \text{SMA} \\ \begin{pmatrix} 1/\sqrt{2} & 1/\sqrt{2} & 0 \\ -1/2 & 1/2 & 1/\sqrt{2} \\ 1/2 & -1/2 & 1/\sqrt{2} \end{pmatrix} & \text{QVO or LMA} \end{cases}. \quad (1.47)$$

These two special matrices go under the name single maximal and bimaximal mixing, respectively. There exists a third special matrix, denoted trimaximal mixing, which is

basically ruled out and given for historical reasons,

$$U \simeq \begin{pmatrix} 1/\sqrt{3} & 1/\sqrt{3} & 1/\sqrt{3} \\ -1/2(1 + 1/\sqrt{3}) & 1/2(1 - 1/\sqrt{3}) & 1/\sqrt{3} \\ 1/2(1 - 1/\sqrt{3}) & -1/2(1 + 1/\sqrt{3}) & 1/\sqrt{3} \end{pmatrix}. \quad (1.48)$$

These simple forms of U have been discussed extensively in the literature and may be summarized as follows:

- Single maximal [39]
Maximal atmospheric mixing and a vanishing angle in solar and the CHOOZ experiment, resulting in $|U_{e1}| = 1$.
- Bimaximal [40]
Both solar and atmospheric mixing is maximal, $|U_{e3}|$ is zero. Then $|U_{e1}| = |U_{e2}| = |U_{\mu 3}| = |U_{\tau 3}| = 1/\sqrt{2}$.
- Trimaximal [41]
All U_{ei} and $U_{\alpha 3}$ have the same magnitude and $|U_{e1}| = |U_{e2}| = |U_{e3}| = 1/\sqrt{3}$. The model gives a very poor fit to the oscillation data and is given only for the sake of completeness.

All three of these special cases will be of later use when estimates of the entries of the mass matrix are made. More precise values of the entries in U will be given in Section 4.1. Since at the moment large mixing seems to be favored [42], a simple picture emerges: the atmospheric muon neutrinos oscillate into tau neutrinos and the solar electron neutrinos into $1/\sqrt{2}(\nu_\mu + \nu_\tau)$. Within the parameterization (1.24) one can identify θ_1 as the solar angle, θ_2 as the atmospheric angle and θ_3 as CHOOZ's angle. The phase δ is at the moment not bounded, since CP violating effects are suppressed when one uses the currently available neutrino sources. Different upcoming experiments can probe CP violation [37]. In Chapter 2 another way to detect leptonic CP violation is presented.

Global three-flavor fits are necessary to calculate the allowed ranges of the oscillation parameters. For most of the analyses in this thesis the results by one group [42] are used, the approximate values of the 99% C.L. areas are given in Tables 1.1 and 1.2. The analysis does not include the recent SNO data, which will however not affect any of the results significantly. For LMA and QVO the angle can lie in the "dark side" [43] $\tan^2 \theta_1 > 1$. For the atmospheric parameters, matter effects play no significant role, that is why the parameter space is symmetric with respect to the maximal mixing line $\tan^2 \theta_2 = 1$. The CHOOZ angle $\sin^2 \theta_3$ is indeed very small and, depending on the solar solution, is bounded by 0.06 to 0.08. The three different solar solutions can be measured in upcoming experiments such as KAMLAND [44], BOREXINO [45] or detailed SNO measurements [46]. In Chapter 2 another way to distinguish the different solar solutions will be presented.

s_3^2	t_2^2	Δm_A^2 [10^{-3} eV 2]
0...0.02	0.4...3	1...6
0.03...0.04	0.5...3	1...4
0.05	0.5...3	1...3
0.05...0.07	0.6...3	2...3

Table 1.1: Approximate 99 % C.L. values of the atmospheric oscillation parameters. We defined $t_2^2 = \tan^2 \theta_2$.

s_3^2	LMA		QVO	
	t_1^2	Δm_\odot^2 [eV 2]	t_1^2	Δm_\odot^2 [eV 2]
0...0.02	0.1...3	$(0.2...6) \cdot 10^{-4}$	0.1...5	$(0.005...3) \cdot 10^{-7}$
0.03	0.2...1	$(0.2...4) \cdot 10^{-4}$	0.1...5	$(0.005...3) \cdot 10^{-7}$
0.04	0.2...0.7	$(0.2...4) \cdot 10^{-4}$	0.5...5	$(0.005...2) \cdot 10^{-7}$
0.05	0.2...0.5	$(0.2...1) \cdot 10^{-4}$	0.5...2	$(0.4...1) \cdot 10^{-7}$
0.06	0.2...0.5	$(0.2...1) \cdot 10^{-4}$	—	—
0.07	0.3...0.5	$(3...5) \cdot 10^{-5}$	—	—

SMA		
s_3^2	t_1^2	Δm_\odot^2 [eV 2]
0...0.02	$(0.2...3) \cdot 10^{-3}$	$(0.4...1) \cdot 10^{-5}$
0.03	$(0.2...3) \cdot 10^{-3}$	$(0.4...1) \cdot 10^{-5}$
0.04	$(0.3...2) \cdot 10^{-3}$	$(0.6...1) \cdot 10^{-5}$
0.05	$(0.3...1) \cdot 10^{-3}$	$(0.6...1) \cdot 10^{-5}$
0.06	$(5...8) \cdot 10^{-4}$	$(5...9) \cdot 10^{-6}$

Table 1.2: Approximate 99 % C.L. values of the solar oscillation parameters. We defined $t_1^2 = \tan^2 \theta_1$.

In calculating the mixing matrix it was assumed that $\Delta m_{21}^2 = \Delta m_\odot^2 \ll \Delta m_A^2 = \Delta m_{31}^2 \simeq \Delta m_{32}^2$. This is denoted “normal scheme”. The second possibility would be $\Delta m_{32}^2 = \Delta m_\odot^2 \ll \Delta m_A^2 = \Delta m_{21}^2 \simeq \Delta m_{31}^2$, for which the name “inverse scheme” has been chosen. Due to this fact, the small element in U is now U_{e1} and not anymore U_{e3} . In this second scheme one should therefore introduce a parameterization different than (1.24) in order to identify one angle with one experiment. One can avoid that by changing the order of the mass eigenstates in the condition (1.20), i.e. in the inverse scheme holds

$$m_1 > m_2 > m_3. \quad (1.49)$$

Then the oscillation probabilities are the same as in Eqs. (1.43,1.45,1.46) but the identification of the mass squared differences changes. To be precise, $\Delta m_{32}^2 = \Delta m_\odot^2 \ll \Delta m_A^2 = \Delta m_{21}^2 \simeq \Delta m_{31}^2$ changes to $\Delta m_{12}^2 = \Delta m_\odot^2 \ll \Delta m_A^2 = \Delta m_{23}^2 \simeq \Delta m_{13}^2$. One can summarize

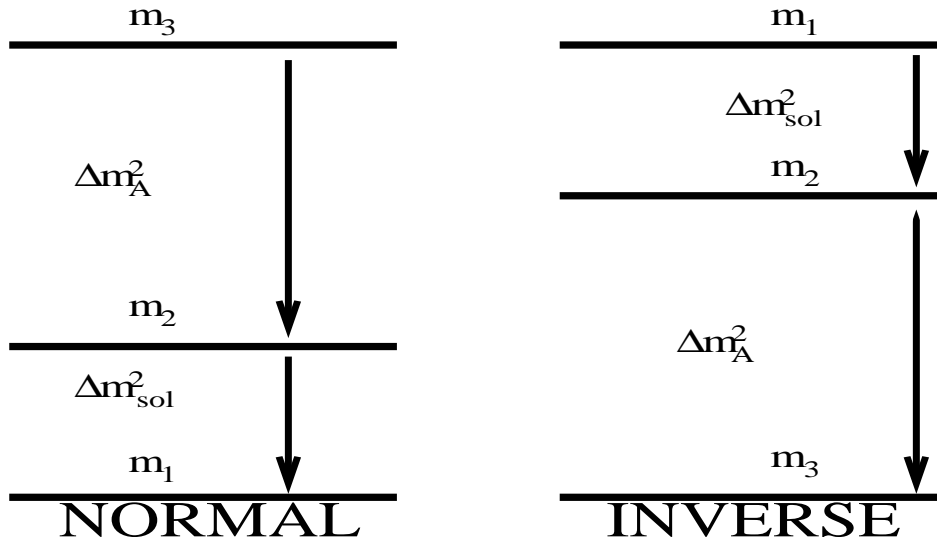


Figure 1.1: The normal and inverse mass scheme.

the two schemes as follows:

$$\begin{array}{cc}
 \text{NORMAL} & \text{INVERSE} \\
 m_3 = \sqrt{\Delta m_A^2 + m_1^2} & m_1 = \sqrt{\Delta m_A^2 + m_3^2} \\
 m_2 = \sqrt{\Delta m_{\odot}^2 + m_1^2} & m_2 = \sqrt{-\Delta m_{\odot}^2 + m_1^2} . \\
 m_1 = 0 \dots 2.2 \text{ eV} & m_3 = 0 \dots 2.2 \text{ eV}
 \end{array} \tag{1.50}$$

The value of the lightest mass state governs the precise shape of the scheme. A thorough study of the possibilities will be presented in Section 2.2.3. A sketch of the two schemes can be seen in Fig. 1.1. They can be distinguished in future oscillation experiments due to matter effects [47]. In Chapter 2 another way to distinguish both possibilities will be presented.

To sum up, neutrino oscillations provide evidence for neutrino masses, with the following remaining still as open problems: the selection of the solar solution, the value of the absolute mass scale, the mass scheme and the presence of leptonic CP violation. Moreover, the implied smallness of the neutrino masses finds a simple explanation through the see-saw mechanism, whose important prediction is the Majorana nature of light and heavy neutrinos. In the next Chapter it will be shown that $0\nu\beta\beta$ can provide answers to all of the open problems mentioned above. Chapters 3 and 4 are then devoted to the search for processes analogue to $0\nu\beta\beta$, which may be able to provide information about all entries of the light and heavy Majorana mass matrices.

Chapter 2

Neutrinoless Double Beta Decay and Neutrino Oscillations

In this chapter the connection of neutrinoless double beta decay and neutrino oscillation is studied. After presenting the general formalism, some introductory examples of the dependence of $\langle m \rangle$ on the oscillation parameters are given. Then an analysis of the allowed range of $\langle m \rangle$ will be presented, using a global three-flavor fit from C. Peña-Garay *et al.* [42]. We concentrate on the dependence on the smallest neutrino mass.

Oscillation experiments measure the differences of the squares of neutrino masses, therefore one has to make assumptions concerning the mass values and the spectrum in order to determine $\langle m \rangle$. Consequently, any limit or value of $\langle m \rangle$ may rule out or constrain schemes and mass values. The situation is complicated by the fact that oscillation experiments are not sensitive to the two extra phases that appear in the MNS matrix for Majorana particles. These phases might cause cancellations among the contributions to $\langle m \rangle$. Even for the case of CP conservation the mass eigenvalues may have different signs and thus also cause cancellations. We illustrate this fact with several examples.

Many recent works dealt with these facts [48]. The point that justifies this analysis is the fact that for the first time the oscillation parameters from a full three-flavor fit are used, which includes very recent data. This complete five-dimensional parameter space takes automatically the high correlation of the data into account, which was ignored in most previous works. It is commented on the so-called “dark side” [43] of the parameter space, $\tan^2 \theta_1 > 1$, and the consequences of its inclusion on $\langle m \rangle$ are discussed.

The chapter is organized as follows. In Section 2.1 the experimental and theoretical basic aspects of $\langle m \rangle$ and $0\nu\beta\beta$ are described, followed in Section 2.2 by a summary of the form of $\langle m \rangle$ in different mass schemes. Introductory examples are given in Section 2.3. Then the results on the range of $\langle m \rangle$ as a function of the smallest mass are given in Section 2.4. Finally, Section 2.5 summarizes our conclusions.

2.1 Basics, experiments and uncertainty

Neutrinoless double beta decay has been first discussed by Furry [49] in 1939. The diagram is shown in Fig. 2.1. It is a process of second order in Fermi interaction and given by [50]

$$(Z, A) \rightarrow (Z + 2, A) + 2 e^- . \quad (2.1)$$

The emission of two W bosons by the nuclei is described by nuclear physics. The subsequent production of the electron pair via exchange of a neutrino mass eigenstate ν_i is given by particle physics. Obviously, lepton number is violated by two units, $\Delta L = 2$. We will calculate a similar process in Chapter 3, here only some hand-waving arguments are given to show the dependence on the neutrino properties. The Majorana condition $\nu^c = \nu$ can be used to write (see also Eq. (1.15))

$$\nu = \nu_L + (\nu_L)^c , \quad (2.2)$$

since $(\nu_L)^c = (\nu^c)_R$. Therefore, the left- and right-handed components of Majorana neutrinos are connected. This is not the case for Dirac neutrinos. The neutrino, which is emitted at the first vertex $W \rightarrow e^- \nu$ is right-handed, whereas the one at the second vertex $\nu W \rightarrow e^-$ is left-handed. Thus, the process is only possible for Majorana neutrinos. The amplitude for the emission of a left-handed neutrino and the absorption of a right-handed one is of order m_i/E , where E is its energy. If neutrinos are massless and/or Dirac particles, the amplitude vanishes.

In addition, for every vertex of the neutrino state ν_i and the electron a factor U_{ei} appears. Also the neutrino propagator has to be taken into account. The complete amplitude of neutrinoless double beta decay is therefore proportional to

$$\mathcal{M}(0\nu\beta\beta) \propto \sum_i U_{ei}^2 \frac{m_i}{q^2 - m_i^2} , \quad (2.3)$$

where q is the momentum of the Majorana neutrino. This can be estimated by $1/r \simeq (10 \dots 100)$ MeV, where $r \simeq (10^{-12} \dots 10^{-13})$ cm is the average distance between the two decaying nuclei. Thus, for neutrinos with mass of order eV there remains no mass dependence in the denominator and the matrix element is proportional to

$$\mathcal{M}(0\nu\beta\beta) \propto \sum_i U_{ei}^2 m_i \equiv \langle m \rangle . \quad (2.4)$$

Comparing this with Eq. (1.38) shows that this is just the ee element of the Majorana neutrino mass matrix. The inverse half-life can be written as

$$(T_{1/2}^{0\nu})^{-1} = A |\langle m \rangle|^2 , \quad (2.5)$$

where A includes the highly nontrivial nuclear matrix element, whose calculation is treated in the next section.

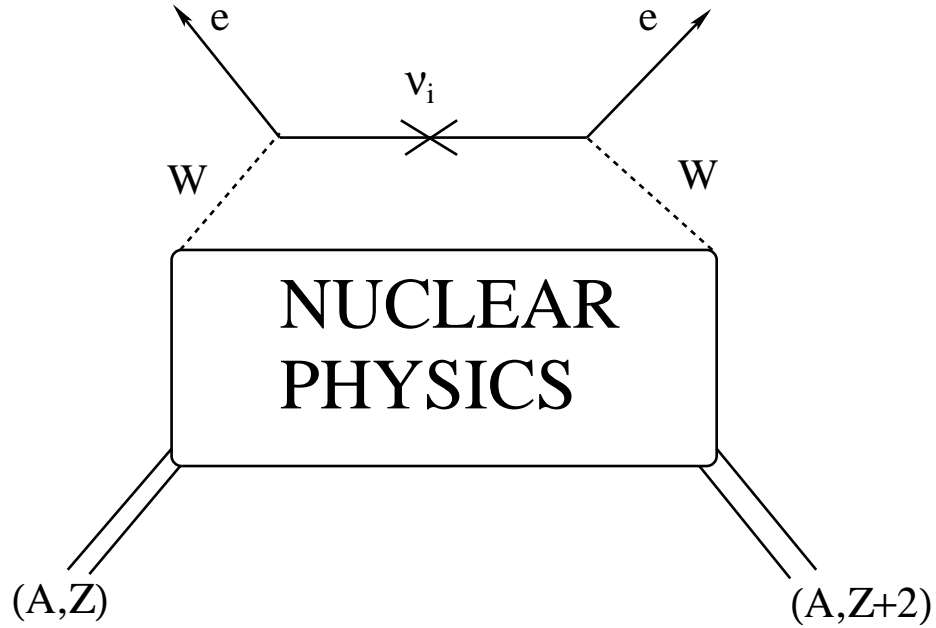


Figure 2.1: Diagram of neutrinoless double beta decay.

Different calculations using different techniques yield values for A that vary within a factor of ten. Consequently, the limits on $\langle m \rangle$ obtained from limits on half-lives vary within a factor of 2 – 3. The best limit on $0\nu\beta\beta$ comes from the Heidelberg–Moscow experiment, whose half-life limit on the neutrinoless double beta decay of ^{76}Ge is [51]

$$T_{1/2}^{0\nu} > 1.9 \cdot 10^{25} \text{ y}. \quad (2.6)$$

From this, using the nuclear matrix element calculation from [52] the collaboration quotes a limit on $\langle m \rangle$ of

$$\langle m \rangle < 0.35 \text{ eV} \quad (2.7)$$

at 90 % C.L. and 0.26 eV at 68 % C.L. Several experiments running or being planned will try to improve this limit. Among them are CUORE [53], MOON [54], NEMO [55] and GENIUS [56], which typically aim at limits of 0.1 or 0.01 eV. The 10t option of GENIUS, using ten tons of enriched Germanium, may even probe values down to $2 \cdot 10^{-3}$ eV.

There is also the possibility that heavy left-handed neutrinos (i.e. heavier than about 1 GeV) trigger neutrinoless double beta decay. Then the propagator in Eq. (2.3) simplifies to $m_i/(q^2 - m_i^2) \simeq -1/m_i$ and the inverse half-life can now be written as

$$(T_{1/2}^{0\nu})^{-1} = A' \left| \sum_i U_{ei}^2 \frac{1}{m_i} \right|^2. \quad (2.8)$$

Here A' is different from A in Eq. (2.5) and U_{ei} is now the coupling of the heavy neutrino to the electron. With the same half-life limit a bound can be set on the combination of

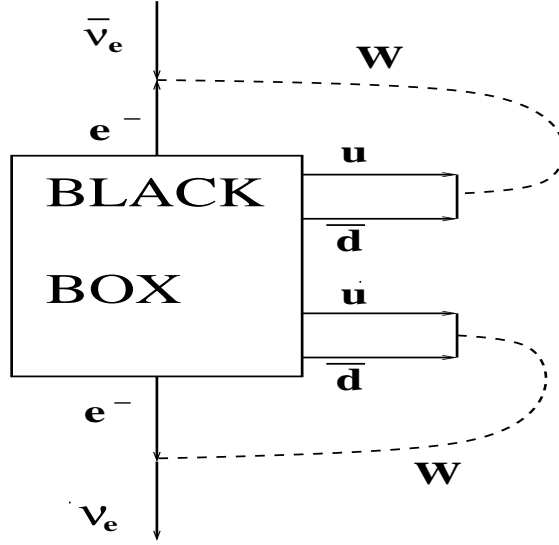


Figure 2.2: Connection between Majorana mass term of ν_e and the existence of $0\nu\beta\beta$.

the coupling U and m_i , the result is [51]

$$\langle \frac{1}{m} \rangle = \sum_i U_{ei}^2 \frac{1}{m_i} < 1.1 \cdot 10^{-8} \text{ GeV}^{-1}. \quad (2.9)$$

Extensive use of these two bounds on $\langle m \rangle$ and $\langle \frac{1}{m} \rangle$ will be made in this and the following chapters.

It is possible that other new physics processes (e.g. supersymmetry or right-handed currents) are responsible for $0\nu\beta\beta$, which can be used to set limits on the particular sector of new physics. We refer to Refs. [57] for a summary of such possibilities. Here we just mention that in gauge theories the detection of $0\nu\beta\beta$ alone is enough to show the existence of a Majorana neutrino mass term for the electron neutrino, as was shown by Schechter and Valle [58]. In Fig. 2.2 the mechanism that governs $0\nu\beta\beta$ is denoted “black box”. It triggers the process $uu \rightarrow dd e^- e^-$. Therefore, crossing permits $0 \rightarrow d\bar{u} d\bar{u} e^- e^-$. By coupling a W to each emitted $d\bar{u}$ and electron, a Majorana mass for the ν_e is produced. A generalization of this argument is presented in Chapter 3. Actually, this loop-induced mass is exceedingly small. Thus, it is clear that any information on $\langle m \rangle$ that can be obtained from oscillation data could help to reveal the true mechanism of $0\nu\beta\beta$.

2.1.1 Calculation of the nuclear matrix elements

In order to obtain a limit on $\langle m \rangle$ from a limit on $T_{1/2}^{0\nu}$, the nuclear matrix elements describing the transition between the two nuclei have to be evaluated. Reviews of this particular area of nuclear physics can be found in [59], here we try to summarize the main points.

In general, the half-life of $0\nu\beta\beta$ mediated by light Majorana neutrinos can be written as

$$(T_{1/2}^{0\nu})^{-1} = G_{0\nu}(E_0, Z) |M_{0\nu}|^2 \langle m \rangle^2, \quad (2.10)$$

where $G_{0\nu}(E_0, Z)$ is a phase space function and $M_{0\nu}$ the nuclear matrix element (NME). The available final state energy is denoted E_0 . The quantity $G_{0\nu}(E_0, Z)$ can be calculated accurately, whereas the NMEs are the source of the mentioned uncertainty of the limit on $\langle m \rangle$. The matrix element is the sum of Fermi and Gamov–Teller operators [60],

$$M_{0\nu} = M_{0\nu}^{GT} - M_{0\nu}^F. \quad (2.11)$$

The two contributions involve spin–spin and isospin–isospin correlations within the nuclei and are hard to calculate. They can be written as

$$\begin{aligned} M_{0\nu}^{GT} &= \sum_{m,n} \langle 0_f^+ \| t_{-m} t_{-n} H(r) \sigma_m \sigma_n \| 0_i^+ \rangle \\ M_{0\nu}^F &= \sum_{m,n} \langle 0_f^+ \| t_{-m} t_{-n} H(r) \| 0_i^+ \rangle \left(\frac{g_V}{g_A} \right)^2, \end{aligned} \quad (2.12)$$

with t_{-} as the isospin ladder operator converting a neutron into a proton, σ the spin operator, $r = |\vec{r}_m - \vec{r}_n|$ and $H(r)$ the neutrino potential, representing the exchange of the neutrino between the two nucleons. The vector and axial–vector weak interaction coupling constants are denoted g_V and g_A , respectively. Transitions to excited states are suppressed. The neutrino potential $H(r)$ stems from integrating the neutrino propagator over a denominator, whose form is given by perturbation theory. It is proportional to $1/r$ for light neutrinos ($m_i \leq 10$ MeV) and has the form of a Yukawa potential for heavy neutrinos. The factors $\langle 0_f^+ \| t_{-m} t_{-n} H(r) \| 0_i^+ \rangle$ and $\langle 0_f^+ \| t_{-m} t_{-n} H(r) \sigma_m \sigma_n \| 0_i^+ \rangle$ have to be computed within a nuclear model for the initial and final wave functions $\|0_i^+\rangle$ and $\|0_f^+\rangle$.

These various models, like Quasiparticle Random Phase Approximation (QPRA), Operator Expansion Method (OEM) or the Shell Model (ShM), result in values of $T_{1/2}^{0\nu}$, which vary within the mentioned factor of up to ten. Table 2.1 shows for three isotopes values of $T_{1/2}^{0\nu} \langle m \rangle^2$, evaluated within several models and variants of the respective models. The calculation from [52] is used to get the limit (2.7) on $\langle m \rangle$. Using all the values from the table results in range of (0.30 . . . 0.98) eV for the upper limit on $\langle m \rangle$.

model	^{76}Ge	^{130}Te	^{136}Xe
ShM [61]	1.67	4.01	—
ShM [62]	17.5	—	12.1
QPRA [63]	2.15	0.52	1.51
QPRA [64]	14	0.66	3.3
QPRA [52]	2.3	0.49	2.2
QPRA [65]	18.4	2.1	2.8
OEM [66]	2.75	0.723	4.29

Table 2.1: Representative values for $T_{1/2}^{0\nu}\langle m \rangle^2$ in 10^{24} y eV^2 for three isotopes, calculated within several nuclear models.

We remark that the respective calculations can have a sizable intrinsic uncertainty due to the unknown particle–particle coupling, whose magnitude can be (within a certain range) inferred from single β decay. In this thesis $\langle m \rangle < 0.35$ eV will be used most of the times. When we consider in the following limits on the neutrino mass, these bounds roughly scale with the $\langle m \rangle$ limit.

2.2 Formalism

2.2.1 General considerations

With the parameterization from Eq. (1.24) the ee element of m reads

$$m_{ee} \equiv \langle m \rangle = c_3^2 \left[c_1^4 m_1^2 + s_1^4 m_2^2 + t_3^4 m_3^2 + 2 \left(m_2 m_3 s_1^2 t_3^2 c_{2(\alpha-\beta)} + c_1^2 m_1 (s_1^2 c_{2\alpha} m_2 + t_3^2 c_{2\beta} m_3) \right) \right]^{1/2}, \quad (2.13)$$

where $t_3 = \tan \theta_3$, $c_{2\alpha} = \cos 2\alpha$ and so on. It is instructive to consider the two-flavor scenario. In this case, using Eq. (1.25), the CP conserving and violating cases read

$$\langle m \rangle = \begin{cases} |m_1 \cos^2 \theta + m_2 e^{2i\phi} \sin^2 \theta| & CP \text{ violation} \\ |m_1 \cos^2 \theta + m_2 \eta_1 \eta_2 \sin^2 \theta| & CP \text{ invariance} \end{cases}. \quad (2.14)$$

Hence, a single CP parity has no physical meaning, only relative values are significant. Note though that the case $\eta_1 \eta_2 = -1$ (opposite parities) and $\phi = \pi/2$ (“maximal” violation) can not be distinguished. This can be also seen from the choice of the mixing matrix $S_{\alpha i}$, which diagonalizes the mass matrix. The case $\eta_1 = -1$ and $S_{e1} = O_{e1}$ is equivalent to $\eta_1 = +1$ and $S_{e1} = e^{-i\pi/2} O_{e1} = -i O_{e1}$. This means that opposite parities with a real mixing matrix are equivalent to equal parities with a complex mixing matrix for a maximal phase. Hence, for “maximal” phases we can not tell from $0\nu\beta\beta$ alone if there is CP violation in the lepton sector and the answer if there is one at all has to come from long-baseline experiments [37]. This is similar to the statement by Pal and Wolfenstein [67] for the decay $\nu_2 \rightarrow \nu_1 \gamma$: for equal (opposite) parities magnetic (electric) dipole radiation occurs. Opposite parities are equivalent to complex mixing matrix elements but do not imply CP violation. This would be suggested only by the presence of both kinds of radiation. For a degenerate scheme with masses discussed in the following sections however, the life time of such a process is about $\tau \gtrsim 10^{48}$ s.

2.2.2 Special cases

2.2.2.1 Single, bi- and trimaximal mixing

Simple forms of $\langle m \rangle$ can be obtained for several special cases. First, one can insert the three special mixing matrices from Section 1.3.2 and finds:

$$\langle m \rangle = \begin{cases} m_1 & \text{single maximal} \\ \frac{1}{2} \sqrt{m_1^2 + m_2^2 + 2 m_1 m_2 c_{2\alpha}} & \text{bimaximal} \\ \frac{1}{3} \sqrt{m_1^2 + m_2^2 + m_3^2 + 2(m_2 m_3 c_{2(\alpha-\beta)} + m_1(m_2 c_{2\alpha} + m_3 c_{2\beta}))} & \text{trimaximal} \end{cases}. \quad (2.15)$$

Note that though for bimaximal mixing only two flavors are present, there is still CP violation induced by the phase α . This fact reflects the Majorana nature of the neutrinos.

The single maximal case is effectively a one flavor problem and thus no CP violating effects are present. The four special CP conserving parity configurations read for bimaximal mixing

$$\langle m \rangle = \frac{1}{2} \begin{cases} (m_2 + m_1) & \text{for } (+ + +) \text{ and } (- - +) \\ (m_2 - m_1) & \text{for } (+ - -) \text{ and } (- + -) \end{cases} \quad (2.16)$$

and for trimaximal

$$\langle m \rangle = \frac{1}{3} \begin{cases} (m_3 + m_2 + m_1) & \text{for } (+ + +) \\ (m_3 + m_2 - m_1) & \text{for } (+ - -) \\ (m_3 - m_2 + m_1) & \text{for } (- + -) \\ (m_3 - m_2 - m_1) & \text{for } (- - +) \end{cases} . \quad (2.17)$$

2.2.2.2 Hierarchical masses

It is often useful to neglect the lightest mass eigenstate m_1 . For $\langle m \rangle$ follows:

$$\langle m \rangle = c_3^2 \sqrt{m_2^2 s_1^4 + m_3^2 t_3^4 + 2 m_2 m_3 c_{2(\alpha-\beta)} s_1^2 t_3^2} . \quad (2.18)$$

Again, we have a two flavor scenario and still CP violation due to the Majorana nature. The three special cases for U yield

$$\langle m \rangle = \begin{cases} 0 & \text{single maximal} \\ \frac{1}{2} m_2 & \text{bimaximal} \\ \frac{1}{3} \sqrt{m_3^2 + m_2^2 + 2 m_2 m_3 c_{2(\alpha-\beta)}} & \text{trimaximal} \end{cases} . \quad (2.19)$$

For bimaximal (single maximal) mixing there is one (no) flavor present, consequently there is no CP violation for these cases. For trimaximal mixing the four special cases read

$$\langle m \rangle = \frac{1}{3} \begin{cases} (m_3 + m_2) & \text{for } (+ + +) \text{ and } (+ - -) \\ (m_3 - m_2) & \text{for } (- + -) \text{ and } (- - +) \end{cases} . \quad (2.20)$$

2.2.2.3 Inverse Hierarchy

If m_3 is the lightest mass eigenstate and in addition $m_1 \simeq m_2 \equiv m_A$ then

$$\langle m \rangle = m_A c_3^2 \sqrt{c_1^4 + s_1^4 + 2 c_1^2 s_1^2 c_{2\alpha}} . \quad (2.21)$$

The three special mixing matrices give

$$\langle m \rangle = m_A \begin{cases} 1 & \text{single maximal} \\ c_\alpha & \text{bimaximal} \\ \frac{2}{3} c_\alpha & \text{trimaximal} \end{cases} . \quad (2.22)$$

Applying the CP conserving cases to bimaximal mixing gives

$$\langle m \rangle = \begin{cases} m_A & \text{for } (+++) \text{ and } (- - +) \\ 0 & \text{for } (+ - -) \text{ and } (- + -) \end{cases} \quad (2.23)$$

and $2/3$ times these value for trimaximal mixing.

2.2.2.4 Degenerate neutrinos

For degenerate masses the mass difference can be neglected with respect to the total mass, i.e. $m_0 \equiv m_1 \simeq m_2 \simeq m_3$. The total mass scale m_0 is bounded by measurements of the tritium spectrum, which limits [33]

$$\sum_i |U_{ei}|^2 m_i^2 = m_0^2 < (2.2 \text{ eV})^2 . \quad (2.24)$$

The effective neutrino mass reads now

$$\langle m \rangle = m_0 c_3^2 \sqrt{c_1^4 + s_1^4 + t_3^4 + 2(s_1^2 t_3^2 c_{2(\alpha-\beta)} + c_1^2 (s_1^2 c_{2\alpha} + t_3^2 c_{2\beta}))} . \quad (2.25)$$

The four CP conserving configurations yield

$$\tilde{m} \equiv \frac{\langle m \rangle}{m_0} = c_3^2 (\eta_1 c_1^2 + \eta_2 s_1^2 + \eta_3 t_3^2) = \begin{cases} 1 & (+++) \\ |1 - 2 c_1^2 c_3^2| & (+ - -) \\ |1 - 2 s_1^2 c_3^2| & (- + -) \\ \cos 2\theta_3 & (- - +) \end{cases} , \quad (2.26)$$

where we defined an ‘‘average mass’’ \tilde{m} which lies in the range from zero to one. Note that for the $(- - +)$ case $\langle m \rangle$ is independent on the solar solution. The three special mixing matrices give

$$\tilde{m} = \begin{cases} 1 & \text{single maximal} \\ c_\alpha & \text{bimaximal} \\ \frac{1}{3} \sqrt{3 + 2(c_{2\alpha} + c_{2\beta} + c_{2(\alpha-\beta)})} & \text{trimaximal} \end{cases} . \quad (2.27)$$

Applying the three special matrices to this gives for bimaximal

$$\tilde{m} = \begin{cases} 1 & \text{for } (+++) \text{ and } (- - +) \\ 0 & \text{for } (+ - -) \text{ and } (- + -) \end{cases} \quad (2.28)$$

and for trimaximal

$$\tilde{m} = \begin{cases} 1 & \text{for } (+++) \\ \frac{1}{3} & \text{for } (+ - -), (- + -) \text{ and } (- - +) \end{cases} . \quad (2.29)$$

2.2.2.5 Vanishing mixing with one state

Global analyses as well as reactor data imply that the mixing of the electron neutrino with the mass state m_3 is very small. Thus, setting in (2.13) $\theta_3 = 0$ yields

$$\langle m \rangle = \sqrt{(m_1 c_1^2 + m_2 s_1^2)^2 - 4 m_1 m_2 c_1^2 s_1^2 s_\alpha^2}. \quad (2.30)$$

Setting then m_1 to zero corresponds to a strong hierarchy as in Section 2.2.2.2 and gives

$$\langle m \rangle = m_2 s_1^2. \quad (2.31)$$

For inverse hierarchy and degeneracy one has $m_1 = m_2 = m$ and therefore

$$\langle m \rangle = m \sqrt{1 - 4s_1^2 c_1^2 s_\alpha^2}. \quad (2.32)$$

For the three special mixing matrices (i.e. $s_1^2 = 0, 1$) and the special values of the mixing matrix one obtains again the formulas (2.15) from (2.30), (2.19,2.20) from (2.31) and (2.21–2.23) as well as (2.27–2.29) from (2.32).

2.2.3 Maximal values for different schemes

As shown in Chapter 1, two main mass schemes exist, the normal and the inverse. Since the lightest mass state is an unknown parameter, its value can be used to further distinguish the schemes. This may be done also by the maximal value that a scheme gives for $\langle m \rangle$. Depending on the magnitude of the smallest mass eigenstate m_1 (m_3), the other two masses are obtained with the two Δm^2 from Eq. (1.50). For the following estimates and the sake of simplicity, $\Delta m_A^2 \gg \Delta m_\odot^2$ is assumed. For LMA and QVO we take $c_1^2 = s_1^2$, for SMA $s_1^2 = 0$.

- **A** Normal scheme

1. Hierarchical scheme

This occurs for $m_1 \ll \sqrt{\Delta m_\odot^2} \lesssim 10^{-3}$ eV. Then $m_3 \simeq \sqrt{\Delta m_A^2} \gg m_2 \simeq \sqrt{\Delta m_\odot^2} \gg m_1 \simeq 0$. The maximal value of $\langle m \rangle$ reads

$$\langle m \rangle \lesssim \begin{cases} s_3^2 \sqrt{\Delta m_A^2} & \text{SMA} \\ s_1^2 \sqrt{\Delta m_\odot^2} + s_3^2 \sqrt{\Delta m_A^2} & \text{LMA, QVO} \end{cases}. \quad (2.33)$$

The LMA solution delivers the highest $\langle m \rangle$ in the hierarchical scheme. This scheme corresponds to the special case in Section 2.2.2.2.

2. Partial hierarchical scheme

This occurs when $m_1 \simeq \sqrt{\Delta m_A^2} \simeq 0.05$ eV. It follows $m_3 \simeq \sqrt{2} \sqrt{\Delta m_A^2} > m_2 \simeq m_1$. The maximal value is therefore independent on the solar solution,

$$\langle m \rangle \lesssim \sqrt{\Delta m_A^2} (1 + \sqrt{2} s_3^2). \quad (2.34)$$

This maximum is higher than the one for the hierarchical scheme.

- **B** Inverse scheme

1. Inverse hierarchical scheme

As in the hierarchical scheme, the smallest mass eigenstate is much lighter than the other two, i.e. $m_3 \ll \sqrt{\Delta m_{\odot}^2} \lesssim 10^{-3}$ eV. Then, $m_1 \simeq m_2 \simeq \sqrt{\Delta m_{\text{A}}^2} \gg m_3 \simeq 0$. For the maximal effective mass holds

$$\langle m \rangle \leq \sqrt{\Delta m_{\text{A}}^2} \quad , \quad (2.35)$$

which is independent on the solar solution and s_3^2 . This scheme corresponds to the one given in Section 2.2.2.3.

2. Partial inverse hierarchical scheme

Apart from having a terrible name, the smallest mass has to be around the atmospheric scale, $m_3 \simeq \sqrt{\Delta m_{\text{A}}^2} \simeq 0.05$ eV. The masses are $m_1 \simeq m_2 \simeq \sqrt{2}\sqrt{\Delta m_{\text{A}}^2} > m_3$. The maximal value of $\langle m \rangle$ is again independent on the solar solution,

$$\langle m \rangle \lesssim \sqrt{\Delta m_{\text{A}}^2} (\sqrt{2} + s_3^2) \quad , \quad (2.36)$$

and is higher than the one for the inverse hierarchical scheme.

- **C** Degenerate scheme

The form of $\langle m \rangle$ in this case has been given in 2.2.2.4. In this case, $m_0^2 \equiv m_1^2 \simeq m_2^2 \simeq m_3^2 \gg \Delta m_{\text{A}}^2$. A common mass higher than 0.3 eV has implications on cosmology and can be probed in next generation direct mass searches [68]. Due to unitarity, $\langle m \rangle \leq m_0$. This means that a measurement of $m_0 > \langle m \rangle$ would mean that $0\nu\beta\beta$ is caused by another mechanism, i.e. not via light left-handed Majorana neutrino exchange. A value of $m_0 > \langle m \rangle$ will prove the existence of cancellations of terms.

Therefore, we can order the schemes with respect to their maximal value for $\langle m \rangle$, it holds

$$\text{degenerate} > \text{partial inverse} > \text{partial} > \text{inverse} > \text{normal} \quad . \quad (2.37)$$

Next, the dependence on the parameters for the three extreme schemes, **A1**, **B1** and **C** will be analyzed, inserting typical numerical values.

To sum up, several simple forms of $\langle m \rangle$ have been obtained, using the two different schemes, the form of the mixing matrix and the value of the smallest mass state. All of these possibilities represent the open problems of neutrino physics as mentioned in the introduction. The given idealizations are a useful compilation of formulas and will be very helpful when we in the next sections analyze $\langle m \rangle$ in different situations and study the resulting consequences.

2.3 Dependence on the parameters

2.3.1 Hierarchical scheme

The form of $\langle m \rangle$ neglecting m_1 but including terms proportional to s_3 reads

$$\langle m \rangle = \sqrt{\Delta m_{\odot}^2 s_1^4 + \Delta m_{\text{A}}^2 s_3^4 + 2 \sqrt{\Delta m_{\odot}^2 \Delta m_{\text{A}}^2} c_{2\phi} s_1^2 s_3^2}, \quad (2.38)$$

where $\phi = \alpha - \beta$. For the SMA solution one has

$$\langle m \rangle \simeq \sqrt{\Delta m_{\text{A}}^2} s_3^2 \lesssim 2 \cdot 10^{-4} \text{ eV}, \quad (2.39)$$

which will not be accessible in currently planned experiments. For LMA and small s_3 the first term in Eq. (2.38) dominates, for larger s_3 the third term can cancel the first two when $\phi = \pi/2$. For QVO the second term dominates in Eq. (2.38) and $\langle m \rangle$ is proportional to s_3^2 . This can be seen in Fig. 2.3, where $\langle m \rangle$ is shown as a function of ϕ , for the LMA and QVO case, different s_3^2 and t_1^2 . It will be very difficult to measure $\langle m \rangle$ in the hierarchical scheme when QVO is the solar solution. In order to give an accessible $\langle m \rangle$, s_3^2 has to be very close to its current limit. For the LMA solution, $\langle m \rangle$ can lie above $2 \cdot 10^{-3}$ eV even for vanishing s_3 . If the two phases conspire to fulfill $\alpha \simeq \pi + \beta$ then cancellation occurs and $\langle m \rangle$ can vanish. This happens also for the $(- - +)$ configuration. For $\langle m \rangle \gtrsim 0.01$ eV the hierarchical scheme with a small Δm_{\odot}^2 as in the plot will be ruled out. With the extreme values of the parameters from Table 1.2 one can obtain $\langle m \rangle$ as high as 0.02 eV.

2.3.2 Inverse hierarchical scheme

Here $\langle m \rangle$ reads (see Eq. (2.21)),

$$\langle m \rangle \simeq \sqrt{\Delta m_{\text{A}}^2} \sqrt{1 - 4 s_1^2 c_1^2 s_{\alpha}^2} = \frac{\sqrt{\Delta m_{\text{A}}^2}}{1 + t_1^2} \sqrt{(1 + t_1^2)^2 - 4 t_1^2 s_{\alpha}^2}. \quad (2.40)$$

Note that it is not a function of Δm_{\odot}^2 . It allows complete cancellation only for $t_1^2 \geq 1$. For SMA it simplifies to

$$\langle m \rangle \simeq \sqrt{\Delta m_{\text{A}}^2} \lesssim 6 \cdot 10^{-3} \text{ eV}, \quad (2.41)$$

which is accessible in the GENIUS 10t experiment. Fig. 2.4 shows $\langle m \rangle$ as a function of α for different t_1^2 . For non-maximal mixing $\langle m \rangle$ can be probed regardless of the phase and complete cancellation is only possible for $t_1^2 = 1$. If $\langle m \rangle \gtrsim 0.1$ eV, the inverse hierarchical scheme will be ruled out. The case $\alpha = \pi/2$ corresponds also to the $(+ - -)$ and the $(- + -)$ configurations. From Eq. (2.40), α can be calculated for a given t_1^2 , Δm_{A}^2 and $\langle m \rangle$:

$$s_{\alpha}^2 \simeq \frac{1}{4 t_1^2} (1 + t_1^2)^2 \left(1 - \frac{\langle m \rangle^2}{\Delta m_{\text{A}}^2} \right) \simeq 1 - \frac{\langle m \rangle^2}{\Delta m_{\text{A}}^2}, \quad (2.42)$$

where the last approximation holds for $t_1^2 \simeq 1$. If e.g. $\langle m \rangle = 0.01$ then $s_{\alpha}^2 \simeq 0.97$ for $\Delta m_{\text{A}}^2 = 3 \cdot 10^{-3} \text{ eV}^2$. If one replaces Δm_{A}^2 with m_0^2 then the last equation holds also for a degenerate scheme with $s_3^2 = 0$, see Section 2.3.3.2.

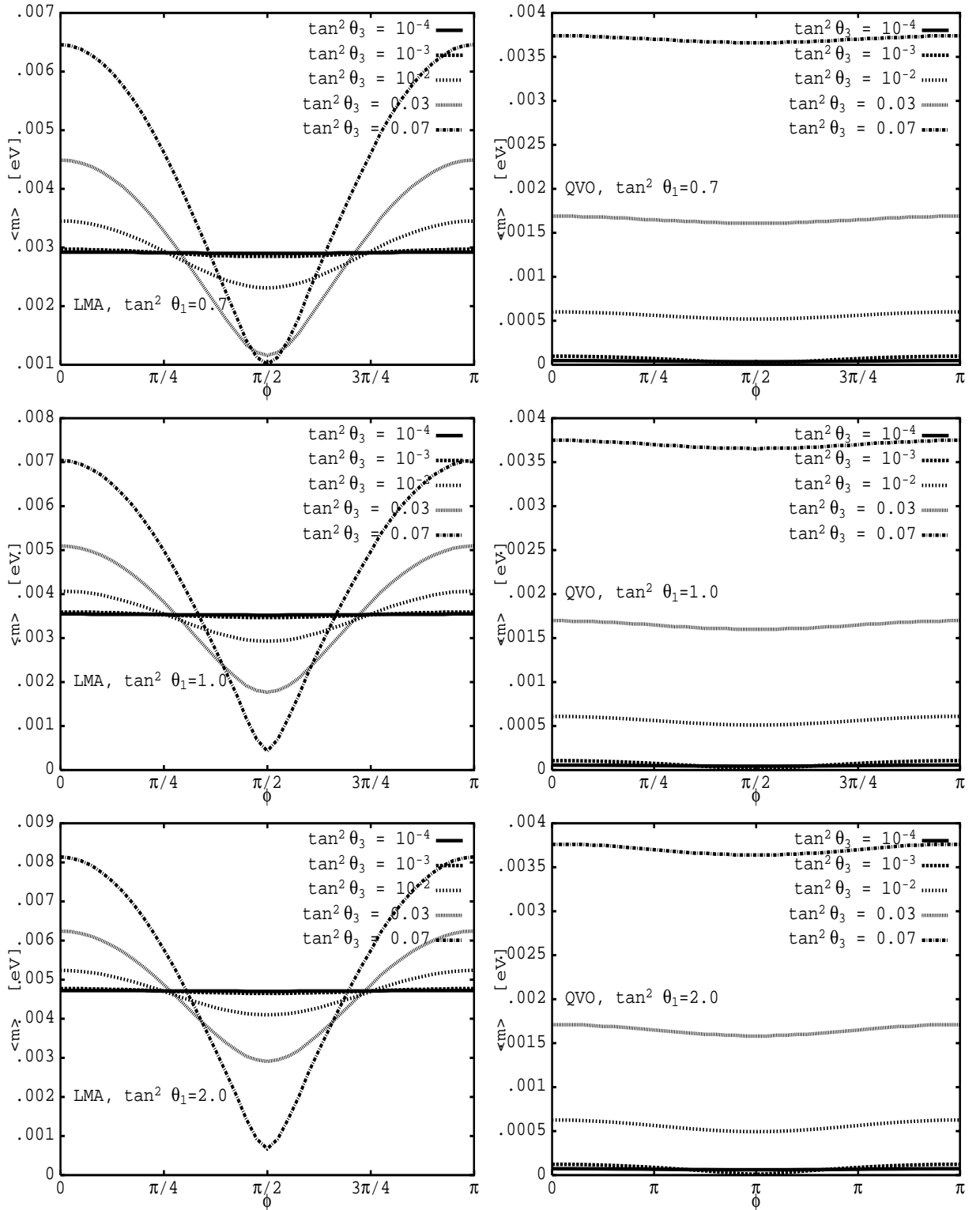


Figure 2.3: $\langle m \rangle$ in the hierarchical scheme as a function of ϕ for different s_3^2 and t_1^2 . The smallest mass is $m_1 = 10^{-6}$ eV, $\Delta m_A^2 = 3.2 \cdot 10^{-3}$ eV². For LMA (QVO) we took $\Delta m_\odot^2 = 5 \cdot 10^{-5}$ (10^{-8}) eV².

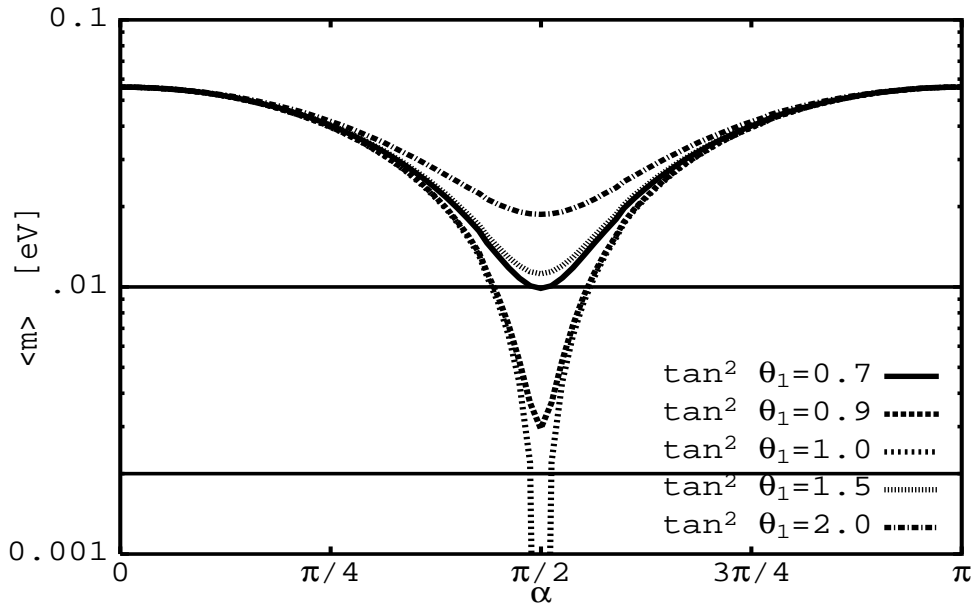


Figure 2.4: $\langle m \rangle$ in the inverse hierarchical scheme as a function of α for different t_1^2 . The smallest mass is $m_3 = 10^{-6}$ eV, $\Delta m_A^2 = 3.2 \cdot 10^{-3}$ eV², $\Delta m_\odot^2 = 5 \cdot 10^{-5}$ eV², $s_3^2 = 0.01$ and $\beta = 0$.

2.3.3 Degenerate scheme

In this section we are interested in bounds on m_0 in a degenerate scheme [1]. The most definite statements can be made with a $\langle m \rangle$ value, which corresponds to a certain scheme. Therefore, with the current limit of 0.35 eV, the degenerate scheme is of interest. If in the following the limit on m_0 approaches 0.1 eV, then the bound applies for the smallest mass in an intermediate mass scheme, i.e. the partial hierarchies. All limits on m_0 are proportional to $\langle m \rangle$ and can thus be easily tuned when new data appears.

2.3.3.1 CP conservation

We shall start with the CP conserving case, $\tilde{m} \equiv \langle m \rangle / m_0$ is given in Eq. (2.26). When the $(+++)$ configuration holds, $\langle m \rangle = m_0$ and the bounds on both quantities are the same. For the $(--+)$ case, \tilde{m} is independent on the solar angle θ_1 . Fig. 2.5 shows the allowed area in the s_3^2 - m_0 space in this situation. Due to the smallness of θ_3 , the value of $\langle m \rangle$ corresponds approximately to the value of m_0 in this scenario. A limit of $\langle m \rangle \lesssim 0.1$ eV would start to jeopardize this scenario.

Figs. 2.6 and 2.7 show for $\langle m \rangle = 0.35$ eV the maximal allowed m_0 as a function of s_3^2 for the $(+--)$ and $(-+-)$ cases, respectively. For the $(+--)$ configuration the

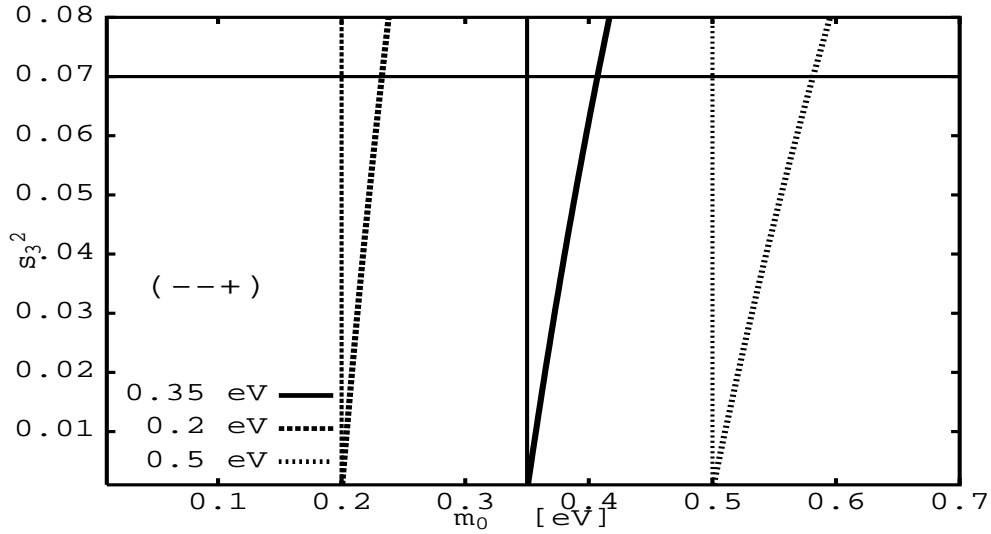


Figure 2.5: s_3^2 - m_0 space for the $(- - +)$ signature of the CP parities for different $\langle m \rangle$. Allowed is the range below the $s_3^2 = 0.07$ line and the two curves belonging to the respective $\langle m \rangle$ value.

bound on m_0 ,

$$m_0 \leq \frac{\langle m \rangle}{1 - 2c_1^2 c_3^2} = \langle m \rangle \frac{1 + t_1^2}{t_1^2 + 2s_3^2 - 1}, \quad (2.43)$$

explodes when the denominator approaches zero. Since $m_0 < 2.2 \text{ eV}$, certain values of s_3 and t_1 can be ruled out when $\langle m \rangle$ is known. From Fig. 2.6 it can be seen that $t_1^2 = 0.9$ and maximal mixing are ruled out for the $(+ - -)$ case. Also, for $s_3^2 \lesssim 0.02$, $t_1^2 = 0.8$ is forbidden. For the SMA solution one arrives again at the $(- - +)$ case.

In the $(- + -)$ scenario the bound on m_0 reads

$$m_0 \leq \frac{\langle m \rangle}{1 - 2s_1^2 c_3^2} = \langle m \rangle \frac{1 + t_1^2}{1 + t_1^2(2s_3^2 - 1)}, \quad (2.44)$$

and explodes for $t_1^2 = (2c_3^2 - 1)^{-1}$, which lies between 1 and 1.16. As can be seen from Fig. 2.7, maximal mixing is ruled out. For $s_3^2 \lesssim 0.04$, $t_1^2 = 0.9$ is forbidden. When the value on $\langle m \rangle$ decreases, these values are allowed. For small t_1^2 , i.e. the SMA solution, one arrives again at the $(+ + +)$ configuration.

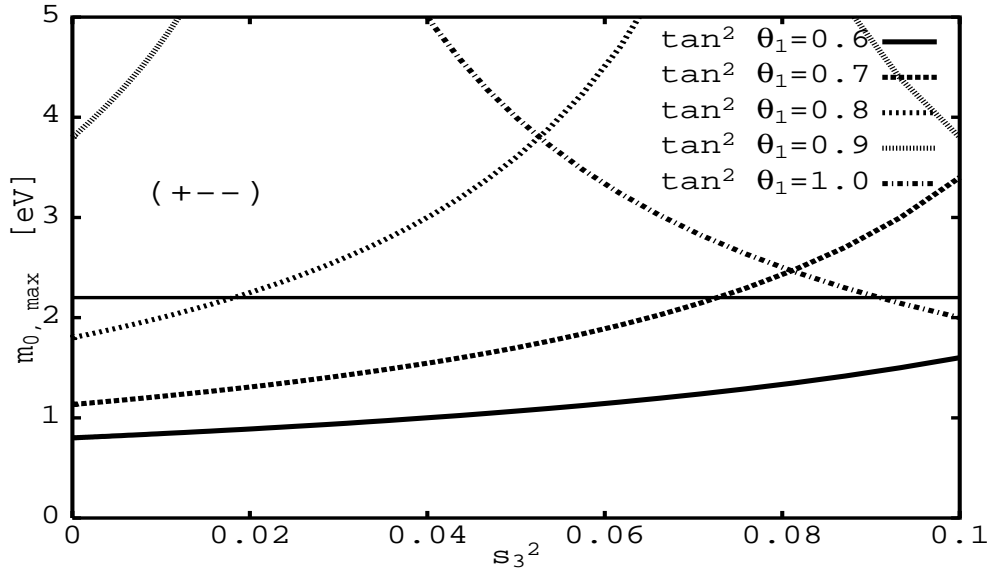


Figure 2.6: s_3^2 - m_0 space for the $(+--)$ signature of the CP parities for $\langle m \rangle = 0.35$ eV. Allowed is the range below the $m_0 = 2.2$ eV line.

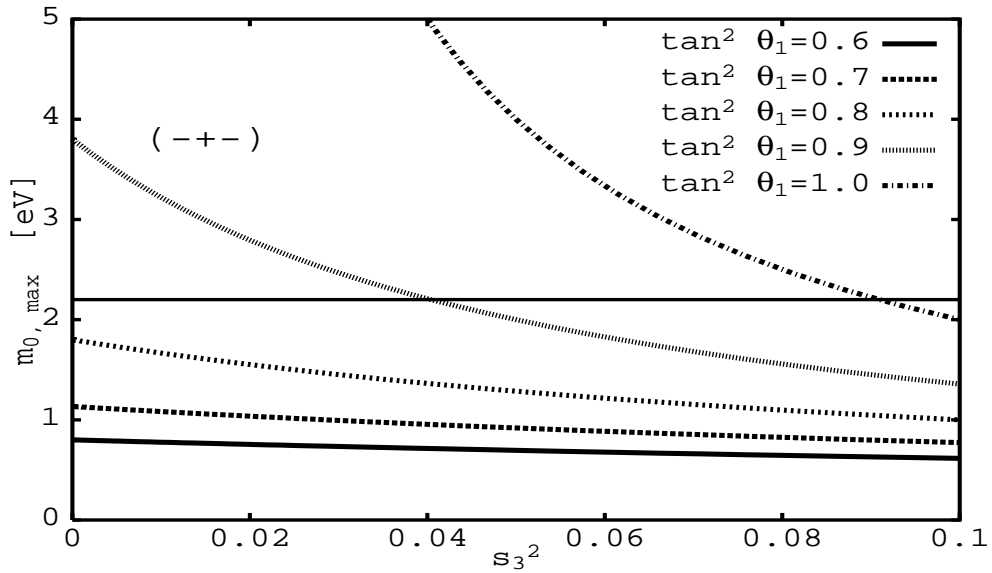


Figure 2.7: s_3^2 - m_0 space for the $(-+-)$ signature of the CP parities for $\langle m \rangle = 0.35$ eV. Allowed is the range below the $m_0 = 2.2$ eV line.

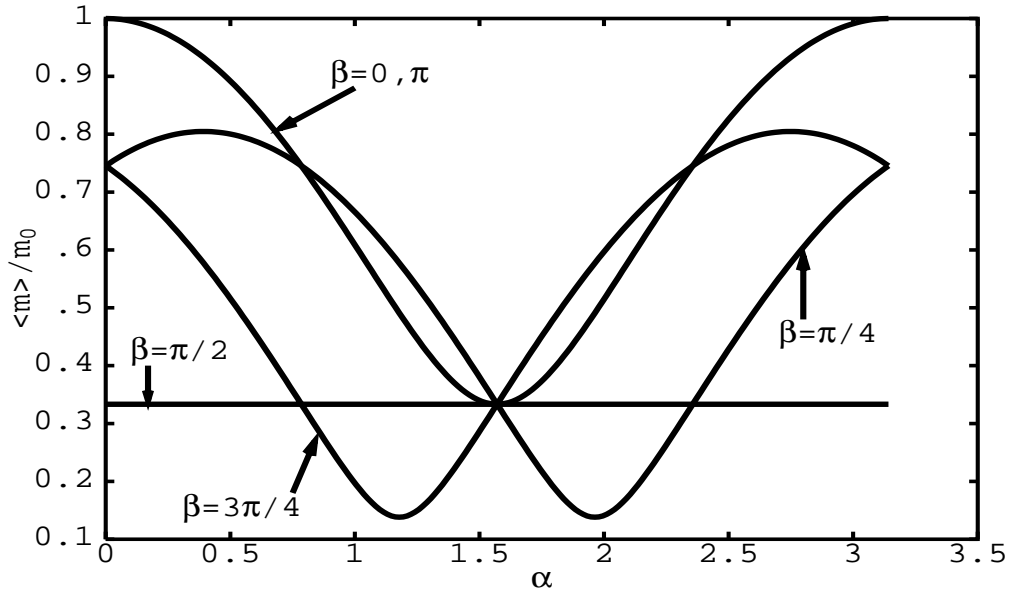


Figure 2.8: \tilde{m} for trimaximal mixing as a function of one CP violating phase for different values of the second phase.

For $s_3^2 = 0$ the $(-+-)$ and $(+--)$ cases give the same result. When a measurement of m_0 has been made, $\langle m \rangle$ can be predicted for a given t_1^2 . For example, when $t_1^2 = 0.8(1, 1.2)$, then $\langle m \rangle$ will be around $0.11(0, 0.09)m_0$. The $(+--)$ and $(-+-)$ cases are connected, because if one replaces $\theta_1 \rightarrow \pi/2 - \theta_1$ then $c_1 \rightarrow s_1$. Therefore, e.g. $t_1^2 = 0.5$ in the $(+--)$ case is identical to the case $t_1^2 = 2.0$ in the $(-+-)$ configuration. For $t_1^2 = 1$ the $(+--)$ and $(-+-)$ cases show no difference since $c_1^2 = s_1^2$.

In Reference [69] plots of the allowed c_1^2 and s_3^2 were given for $m_0 = 1.7$ eV, $\langle m \rangle \lesssim 0.5$ eV and all three nontrivial parity configurations. Their conclusion that small s_3 requires near-maximal (i.e. not the SMA solution) mixing for the $(-+-)$ and $(+--)$ case is consistent with our formalism, since $\langle m \rangle \simeq m_0$ for the SMA case, which contradicts the assumed m_0 value. However, in their approach they consider all $(\pm\pm\pm)$ configurations *and* varied the phases at the same time, which is incorrect. Reference [70] also plots c_1^2 against s_3^2 for different situations resulting in similar conclusions as ours. Our plots are thus different projections of the five-dimensional parameter space giving complementary and additional information. Both mentioned works use cosmological arguments to set m_0 between 1.7 and 4 eV, whereas our approach using \tilde{m} allows to investigate different situations like positive results on $\langle m \rangle$ and/or m_0 .

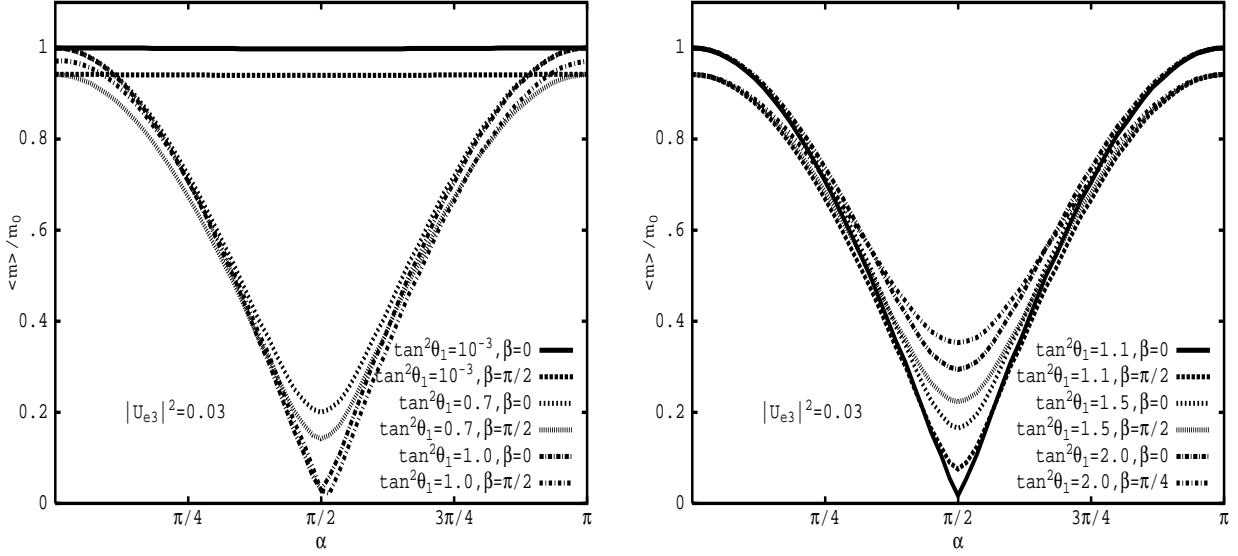


Figure 2.9: \tilde{m} as a function of one phase α for different values of the second phase β and different t_1^2 . Displayed are the ‘‘light side’’ $\tan^2 \theta_1 < 1$ (left) and the ‘‘dark side’’ $\tan^2 \theta_1 > 1$ (right). It is assumed that $|U_{e3}|^2 = 0.03$.

2.3.3.2 CP violation

Looking back at Eq. (2.27) it is seen that for exact single maximal mixing, no CP violation exists. For bimaximal mixing, the phase α is given by

$$c_\alpha = \frac{\langle m \rangle}{m_0}. \quad (2.45)$$

For $m_0 = 2$ (1) eV and the current $\langle m \rangle$ limit it holds $\alpha \lesssim 79.9^0$ (69.5^0). For trimaximal mixing Fig. 2.8 shows the dependence of \tilde{m} on α for different β . Note the constant value for $\beta = \pi/2$.

Returning to the general case, in Fig. 2.9 we plot \tilde{m} as a function of α for different values of $\tan^2 \theta_1$ and β whilst assuming $|U_{e3}|^2 = 0.03$. Maximal mixing allows almost complete cancellation, whereas for other values a non-vanishing minimal \tilde{m} is achieved. If $\langle m \rangle$ is much smaller than m_0 then $\alpha \simeq \pi/2$. For $\langle m \rangle \simeq m_0$ the phase α has to be very small or close to π . The dependence on the second phase is rather small which can be explained by the smallness of $|U_{e3}|$. Note that in the trimaximal case (Fig. 2.8) the dependence on the second phase is rather strong. For smaller values of $|U_{e3}|$ the dependence on β is almost non existing, consequences of this fact will be studied in Chapter 4. As an extreme example we show in Fig. 2.10 the ‘‘iso- \tilde{m} ’’ lines in α - β space for a specific set of parameters. A broad range of values for the two phases, especially for β , is allowed. This is of course explained by the fact that only one observable is used to

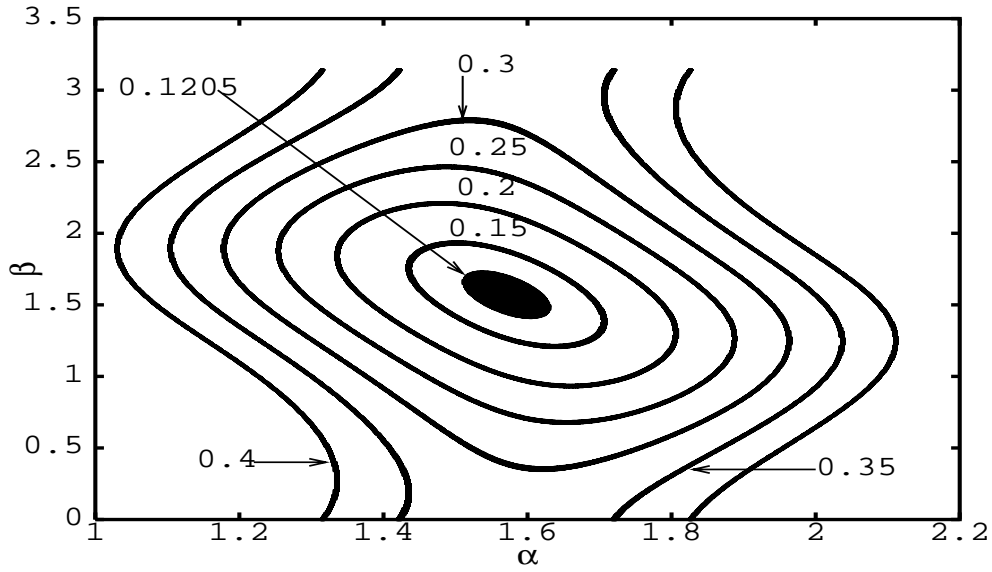


Figure 2.10: "Iso- \tilde{m} " lines in the α - β space for $t_1^2 = 0.6$ and $|U_{e3}|^2 = 0.1$. For $\tilde{m} = 0.1205$ a precision of 5 % is assumed, the other values are for an exact measurement.

constrain two parameters. See [70, 71] for a detailed analysis of the range of the phases in different scenarios.

In Fig. 2.11 we show for $\langle m \rangle = 0.35$ eV, $\beta = \pi/2$ and different $|U_{e3}|^2$ the allowed area in the m_0 - α space for different $\tan^2 \theta_1$. For very small s_3 and large mixing, $\langle m \rangle$, m_0 and α are connected via Eq. (2.42),

$$s_\alpha^2 \simeq \frac{1}{4t_1^2}(1+t_1^2)^2 \left(1 - \frac{\langle m \rangle^2}{m_0^2}\right) \simeq 1 - \frac{\langle m \rangle^2}{m_0^2}, \quad (2.46)$$

where the approximation holds again for $t_1^2 \simeq 1$. If $\langle m \rangle$ is close to m_0 then $\alpha \simeq 0$ or π . Fig. 2.11 shows that large m_0 requires $\alpha \simeq \pi/2$ and t_1^2 close to one. Since the bound on m_0 decreases with $\langle m \rangle$, α has to be the closer to $\pi/2$ the smaller $\langle m \rangle$ is.

When one considers \tilde{m} , the following situations can occur:

- If an upper limit $\langle m \rangle$ and on m_0 exists, nothing specific can be said.
- An upper limit on $\langle m \rangle$ and a value for m_0 results in an upper limit on \tilde{m} .
- An upper limit on m_0 and a value for $\langle m \rangle$ results in a lower limit on \tilde{m} .
- A value for $\langle m \rangle$ and m_0 results in a value for \tilde{m} .

Obviously, the last case would be the most welcome one. As an example, consider the value 0.7 in Fig. 2.9. For large mixing, a value of $\tilde{m} = (\leq, \geq)0.7$ corresponds to

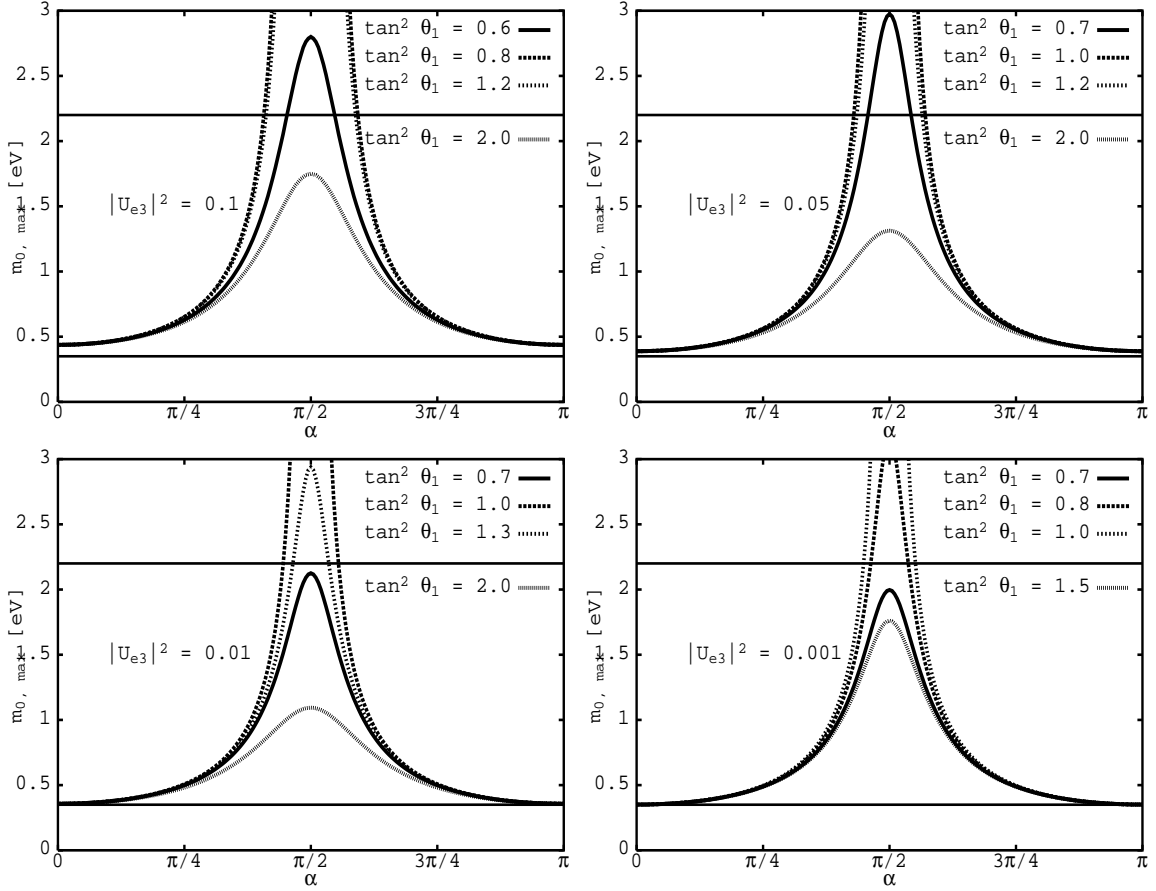


Figure 2.11: α - m_0 space for $\beta = \pi/2$, different $|U_{e3}|^2$ and $\tan^2 \theta_1$. Allowed is the area under the respective curve. We assumed $\langle m \rangle = 0.35$ eV.

$\alpha \simeq (\lesssim, \gtrsim)\pi/4$, largely independent on β and $\tan^2 \theta_1$. Values of \tilde{m} smaller than 0.2 are able to rule out certain solar angles, e.g. $\tilde{m} \leq 0.15$ rules out $\tan^2 \theta_1 \lesssim 0.7$ or $\tan^2 \theta_1 \gtrsim 1.5$, respectively.

It is possible to verify CP violation in the lepton sector through neutrinoless double beta decay. If one calculates for a given t_1^2 the value or range of \tilde{m} , then plots like Fig. 2.12 are produced. From the figures, one can easily analyze some specific configurations: For example, for $\tilde{m} < 0.6$ the $(- - +)$ configuration is ruled out and for $\tilde{m} > 0.6$ the $(+ - -)$ and $(- + -)$ cases, independent on the solar solution and the value of $|U_{e3}|$. In general, the difference between the CP conserving curve and the CP violating area is larger for small s_3^2 . This key value of 0.6 would prove that there is CP violation in the lepton sector. In principle, every value of \tilde{m} between one and $2 \cdot 10^{-3}/2.2 \simeq 9 \cdot 10^{-4}$ is possible, so that this remarkable experimental verification of CP violation is possible. The general case of CP violation in all schemes, i.e. with arbitrary m_1 (m_3), is studied in the next section.

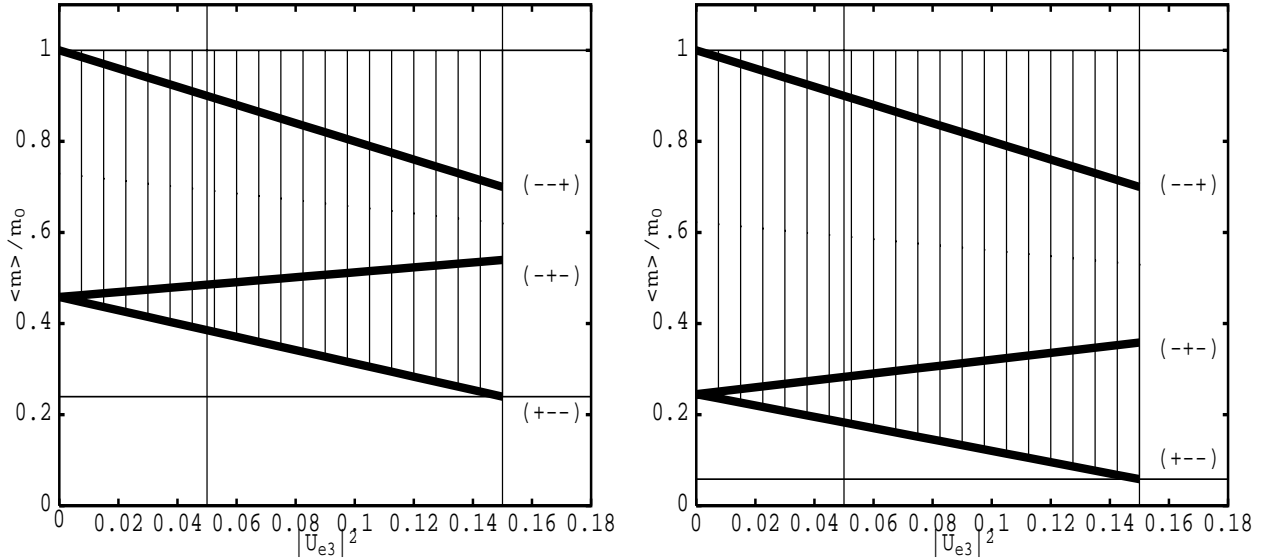


Figure 2.12: \tilde{m} as a function of $|U_{e3}|^2$ for $\tan^2 \theta_1 = 0.4$ (left) and $\tan^2 \theta_1 = 0.6$ (right). Displayed is the range for the CP violating case and all CP conserving parity configurations except the trivial $(+++)$ case.

There is a small possibility to calculate the phase β in the SMA solution. Since $s_1^2 \simeq 0$, the phase α does hardly contribute to $\langle m \rangle$. If in Eq. (2.25) $c_1 \simeq 1$ then one gets $\tilde{m}^2 \simeq 1 + s_3^2 c_{2\beta}$ and thus

$$c_{2\beta} \simeq \frac{1}{2s_3^2}(\tilde{m}^2 - 1). \quad (2.47)$$

If e.g. $\langle m \rangle = 0.35$ eV, $m_0 = 0.37$ eV and $s_3^2 = 0.06$ then $c_{2\beta} \simeq -0.88$. A much larger m_0 is not possible, in the next section it will in fact be shown that for SMA holds $m_0 \leq 0.39$ eV. Therefore, this situation seems unlikely, since all parameters have to be close to their current limit and in addition m_0 must be close to the lowest experimentally accessible value.

2.3.4 Summary

In the normal hierarchy a sizable $\langle m \rangle$ can only be expected for the LMA solution, unless $\phi = \alpha - \beta \simeq \pi/2$. The larger s_3 , the larger is the maximal $\langle m \rangle$ as a function of ϕ . The dependence on ϕ vanishes for small s_3 . For QVO, $\langle m \rangle$ is approximately proportional to s_3^2 and only for values of s_3 close to its current bound a measurable $\langle m \rangle$ can be expected. Not much dependence on the phases exists. In case of the SMA solution, the value of $\langle m \rangle$ is one order of magnitude below the sensitivity of currently planned experiments and insensitive on the phases.

In the inverse hierarchy, $\langle m \rangle$ is basically independent on Δm_{\odot}^2 and measurable even for the SMA solution. For large mixing, $\langle m \rangle$ is larger and the results are depending on the phase α , which can cause cancellation if its value is around $\pi/2$. It can be related to t_1^2 , $\langle m \rangle$ and Δm_{Λ}^2 , thus providing a possibility to measure it.

With the parameters used in this section, $\langle m \rangle \gtrsim 0.01$ eV would rule out the normal hierarchy. If $\langle m \rangle \gtrsim 0.1$ eV would be measured, then also the inverse hierarchy would be ruled out. In the next section the complete allowed data set will be used, which slightly modifies these values.

To sum up our results for the degenerate scheme, for the $(+++)$ configuration holds $\langle m \rangle = m_0$ and a limit on $\langle m \rangle$ smaller than 0.1 eV will jeopardize this scenario. For the $(--+)$ case, which yields results independent on the solar solution, the same holds for very small s_3^2 . For larger s_3^2 only a small parameter space remains. For the $(+-)$ and $(-+-)$ configurations, maximal mixing is ruled out when $\langle m \rangle$ is close to its current limit. Regarding CP violation, large m_0 and small $\langle m \rangle$ requires near-maximal mixing and $\alpha \simeq \pi/2$. Consequently, large m_0 , maximal mixing and $\alpha \simeq \pi/2$ is ruled out when $\langle m \rangle$ is close to its current bound. For the SMA solution it holds $\langle m \rangle \simeq m_0$, unless s_3 is close to its current bound. The phase β can then be calculated via Eq. (2.47). In general, β will not be strongly constrained due to the smallness of s_3 . The “average mass” \tilde{m} is used to study the degenerate scheme and consequences of measurements of $\langle m \rangle$ and /or m_0 are discussed. The presence of CP violation can be shown, especially when s_3^2 is small. For large mixing, the phase α can be obtained from Eq. (2.46).

2.4 An analysis of $\langle m \rangle$ as a function of the smallest mass state

We present in this section an analysis on the allowed values of $\langle m \rangle$ as a function of the smallest mass eigenstate. The used data sets of the oscillation parameters are provided by Carlos Peña–Garay [42]. They include the five oscillation parameters $\tan^2 \theta_1$, $\tan^2 \theta_2$, $\tan^2 \theta_3$, Δm_{\odot}^2 and Δm_{A}^2 . The data was obtained by fitting the parameters to the rates of the Homestake, SAGE, GALLEX and GNO experiments and to 1117 days of SK data including the recoil energy spectrum. For the atmospheric data the analysis uses the contained events and the upward–going ν –induced muon fluxes, including the previous data samples of Frejus, IMB, Nusex, and Kamioka experiments as well as the full 71 kton–yr (1144 days) SK data set, the recent 5.1 kton–yr contained events of Soudan2 and the results on up–going muons from the MACRO detector. The reactor data comes from the CHOOZ experiment, see [42] for details. The size of the files is some ten thousand to some hundred thousand lines.

For the analysis, the smallest mass is varied between 10^{-5} eV and the maximal allowed value. For every mass value the files are read and for every quintet of parameters the phases α and β are varied between zero and π to find the minimum of $\langle m \rangle$. The maximum is the sum of the absolute values of the three terms in $\langle m \rangle$. It is obtained for $\alpha = \beta = \pi$. For the CP conserving parity configurations, α and β are fixed to the values given in Eq. (1.36). Both cases, CP violation and conservation, are analyzed separately.

2.4.1 Best–fit values

For the sake of simplicity we start with the best–fit points of the combined analysis of all data, which are given in Table 2.2. Fig. 2.13 shows for the two hierarchies and the three solar solutions the allowed range of $\langle m \rangle$ as a function of the smallest mass eigenvalue. In this and all following figures we include a $\langle m \rangle$ –limit of 0.2 eV and some limits achievable by several planned or proposed experiments, 0.1 , $3 \cdot 10^{-2}$, $2 \cdot 10^{-2}$ and $2 \cdot 10^{-3}$ eV. For the SMA case the minimum lies at ($s_1^2 \simeq 0$)

$$m_1 \simeq \frac{s_3^2 m_3}{c_1^2} \simeq s_3^2 m_3 \simeq s_3^2 \sqrt{\Delta m_{\text{A}}^2} \simeq 2.7 \cdot 10^{-4} \text{ eV} ,$$

as long as m_1 and m_3 have different signs, i.e. for the $(+ - -)$ and the $(- - +)$ cases. For the inverse hierarchy, one has

$$\langle m \rangle \simeq \sqrt{\Delta m_{\text{A}}^2} \pm m_3 s_3^2 \simeq \sqrt{\Delta m_{\text{A}}^2} ,$$

so that the different parities have not much influence on the minimal or maximal value of $\langle m \rangle$. The different cases are indistinguishable in the logarithmic plot.

solar region	$\tan^2 \theta_3$	$\tan^2 \theta_1$	Δm_{21}^2 [eV ²]	Δm_{32}^2 [eV ²]
LMA	0.005	0.36	$3.3 \cdot 10^{-5}$	$3.1 \cdot 10^{-3}$
QVO	0.005	0.58	$9.6 \cdot 10^{-8}$	$3.1 \cdot 10^{-3}$
SMA	0.005	$6.8 \cdot 10^{-4}$	$5.1 \cdot 10^{-6}$	$3.1 \cdot 10^{-3}$

Table 2.2: Best-fit points for the combined analysis of atmospheric, solar and reactor neutrino data.

For the LMA and QVO solutions in the normal hierarchy the situation is slightly different. Now that the three contributions to $\langle m \rangle$ are comparable, it is possible that phases $\alpha, \beta \neq \pi/2, \pi$ exist, which also result in a vanishing $\langle m \rangle$. This leads to a broader minimum. One notes that for LMA and QVO the CP conserving cases two minima exist, the position of which differs but the gap between them is about the same. These minima occur in the $(+ - -)$ and $(- + -)$ case for LMA (QVO) at

$$m_1 = \tan^2 \theta_1 \sqrt{\Delta m_{\odot}^2} \pm \frac{\sqrt{\Delta m_A^2}}{\cos^2 \theta_1} \tan^2 \theta_3 \simeq \begin{cases} 2.4 \cdot 10^{-3} (6.2 \cdot 10^{-4}) \text{ eV} & \text{for } (+ - -) \\ 1.7 \cdot 10^{-3} (2.6 \cdot 10^{-4}) \text{ eV} & \text{for } (- - +) \end{cases} .$$

The difference is independent on Δm_{\odot}^2 and reads

$$2 \frac{\sqrt{\Delta m_A^2}}{\cos^2 \theta_1} \tan^2 \theta_3 \simeq 8 \cdot 10^{-4} \text{ eV} .$$

As mentioned before, for small m_1 the highest $\langle m \rangle$ is obtained in the LMA solution.

In the inverse hierarchical scheme, one finds from Eq. (2.21) that $\langle m \rangle$ lies between

$$\sqrt{\Delta m_A^2} \cos 2\theta_1 \lesssim \langle m \rangle \lesssim \sqrt{\Delta m_A^2} ,$$

where the upper limit is about 0.06 eV and the lower one 0.026 (0.015) for LMA (QVO). The lower limit occurs when the first and second mass have opposite signs, i.e. in the $(+ - -)$ and $(- + -)$ cases. As discussed in the last section, for small m_3 the maximal value of $\langle m \rangle$ is independent on the solar solution.

2.4.2 Results for the complete data set

We turn now to the general case of allowed values in the five-dimensional parameter space, treating the CP conserving and violating cases separately.

Figs. 2.14 to 2.16 show the range of $\langle m \rangle$ as a function of the smallest mass eigenstate for the three solar solutions and both hierarchies. Due to the smallness of $\tan^2 \theta_1$ there is not much difference with respect to the best-fit plot for the SMA solution (Fig. 2.14). Regarding LMA and QVO, the broad range of oscillation parameters results in a broader

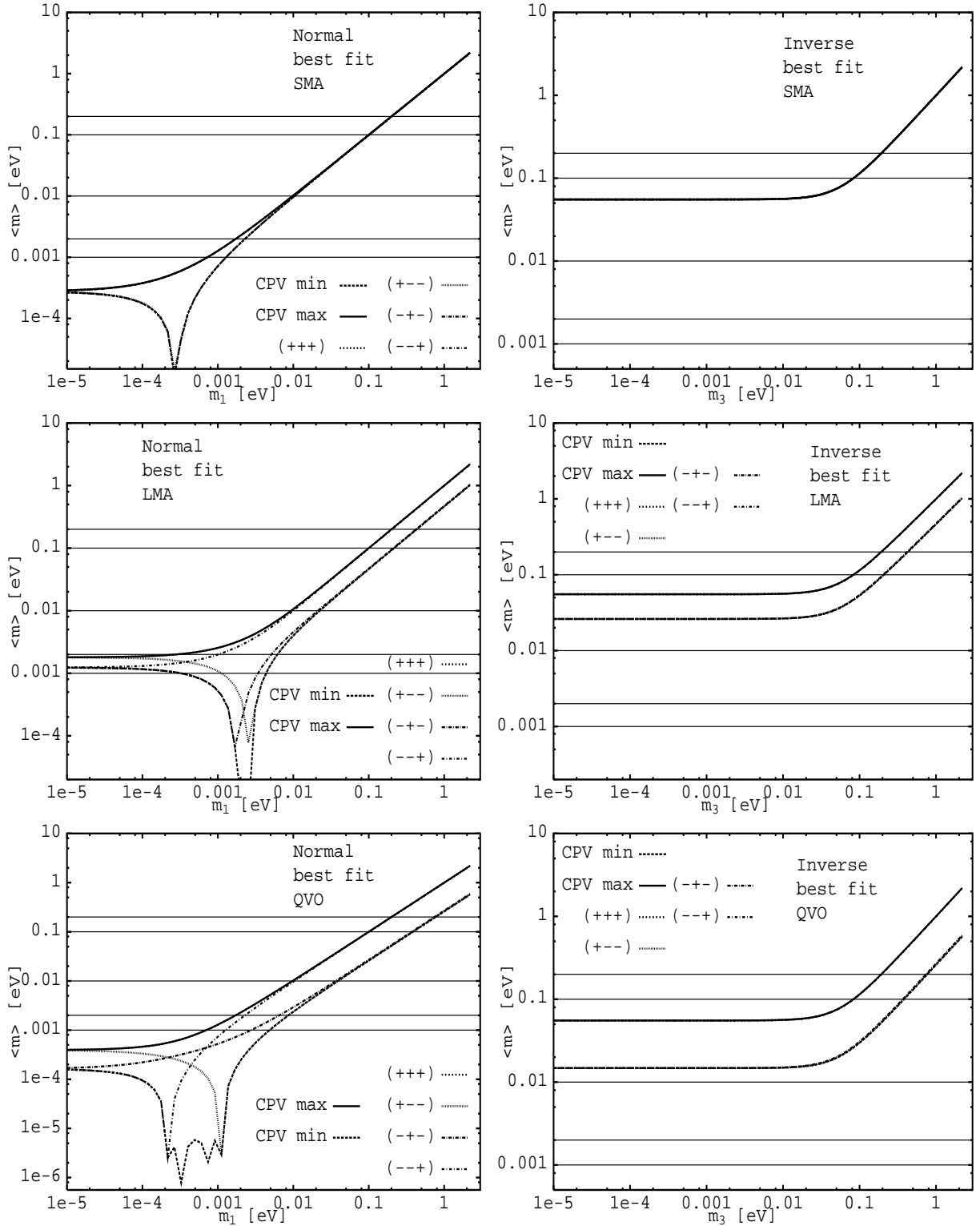


Figure 2.13: $\langle m \rangle$ in both hierarchies as a function of the smallest mass eigenvalue for the best-fit point of the respective solar solution.

	SMA	LMA		QVO	
	light	dark	light	dark	light
$\langle m \rangle^{(1)}$	$(1.9-2.0) \cdot 10^{-3}$	$(2.6-4.9) \cdot 10^{-4}$	$(5.0-8.6) \cdot 10^{-4}$	$(3.8-9.7) \cdot 10^{-4}$	$(1.0-1.7) \cdot 10^{-3}$
$\langle m \rangle^{(2)}$	$(0.5-6.2) \cdot 10^{-6}$	$(0.2-1.8) \cdot 10^{-2}$	$(0.05-1.4) \cdot 10^{-2}$	$(1.0-1.6) \cdot 10^{-3}$	$(0.3-1.0) \cdot 10^{-3}$
$\langle m \rangle^{(3)}$	$(0-2.7) \cdot 10^{-3}$	0	$(0-3.5) \cdot 10^{-3}$	$(0-2.7) \cdot 10^{-3}$	$(0-2.7) \cdot 10^{-3}$

Table 2.3: Ranges of the three contributions to $\langle m \rangle$ in eV using the 99 % C.L. data set of the respective region and assuming normal mass hierarchy. The value for the smallest mass eigenvalue is $2 \cdot 10^{-3}$ (10^{-3}) eV for SMA and QVO (LMA).

	SMA	LMA		QVO	
	light	dark	light	dark	light
$\langle m \rangle^{(1)}$	$(3.6-7.6) \cdot 10^{-2}$	$(1.4-3.4) \cdot 10^{-2}$	$(2.1-6.5) \cdot 10^{-3}$	$(0.9-3.7) \cdot 10^{-2}$	$(1.8-5.6) \cdot 10^{-2}$
$\langle m \rangle^{(2)}$	$(0.07-1.3) \cdot 10^{-4}$	$(1.9-4.4) \cdot 10^{-2}$	$(0.7-3.5) \cdot 10^{-2}$	$(2.0-5.4) \cdot 10^{-2}$	$(0.8-3.8) \cdot 10^{-2}$
$\langle m \rangle^{(3)}$	$(0-1.0) \cdot 10^{-4}$	0	$(0-8.0) \cdot 10^{-5}$	$(0-1.0) \cdot 10^{-4}$	$(0-1.0) \cdot 10^{-4}$

Table 2.4: Ranges of the three contributions to $\langle m \rangle$ in eV using the 99 % C.L. data set of the respective region and assuming inverse mass hierarchy. The value for the smallest mass eigenvalue is $2 \cdot 10^{-3}$ (10^{-3}) eV for SMA and QVO (LMA).

minimum as a function of the smallest mass state. Curves which are far below the ones for the maximal values do not appear in the respective plots. Furthermore, these curves often show a “chaotic” behavior, as can be also seen in the best-fit QVO plot of Fig. 2.13.

Tables 2.3 and 2.4 show for a specific m_1 (m_3) the ranges of the three terms of $\langle m \rangle$, which are denoted

$$\langle m \rangle^{(i)} \equiv |U_{ei}|^2 m_i.$$

The range is given for the hierarchical schemes and the light and dark side of the parameter space. The tables show e.g. that for the SMA case with inverse hierarchy and the $(- - +)$ as well as the $(+ - -)$ case cancellation is possible, because $\langle m \rangle^{(1)}$ and $\langle m \rangle^{(3)}$ can have the same size. For the inverse scheme no cancellation is possible because $\langle m \rangle^{(1)}$ is at least two orders of magnitude higher than $\langle m \rangle^{(2)}$ and $\langle m \rangle^{(3)}$. Regarding LMA, in the normal hierarchical scheme complete cancellation is possible when the first and second $\langle m \rangle^{(i)}$ have opposite sign. For the QVO solution all $\langle m \rangle^{(i)}$ are of comparable size for all m_1 in the normal hierarchical scheme. When $\langle m \rangle^{(1)}$ and $\langle m \rangle^{(2)}$ have the same sign, $\langle m \rangle^{(3)}$ can cancel them *only* for $m_1 \simeq 2 \cdot 10^{-3}$ eV. In the inverse scheme, $\langle m \rangle^{(3)}$ is again very small and $\langle m \rangle$ vanishes if $\langle m \rangle^{(1)}$ and $\langle m \rangle^{(2)}$ have opposite sign.

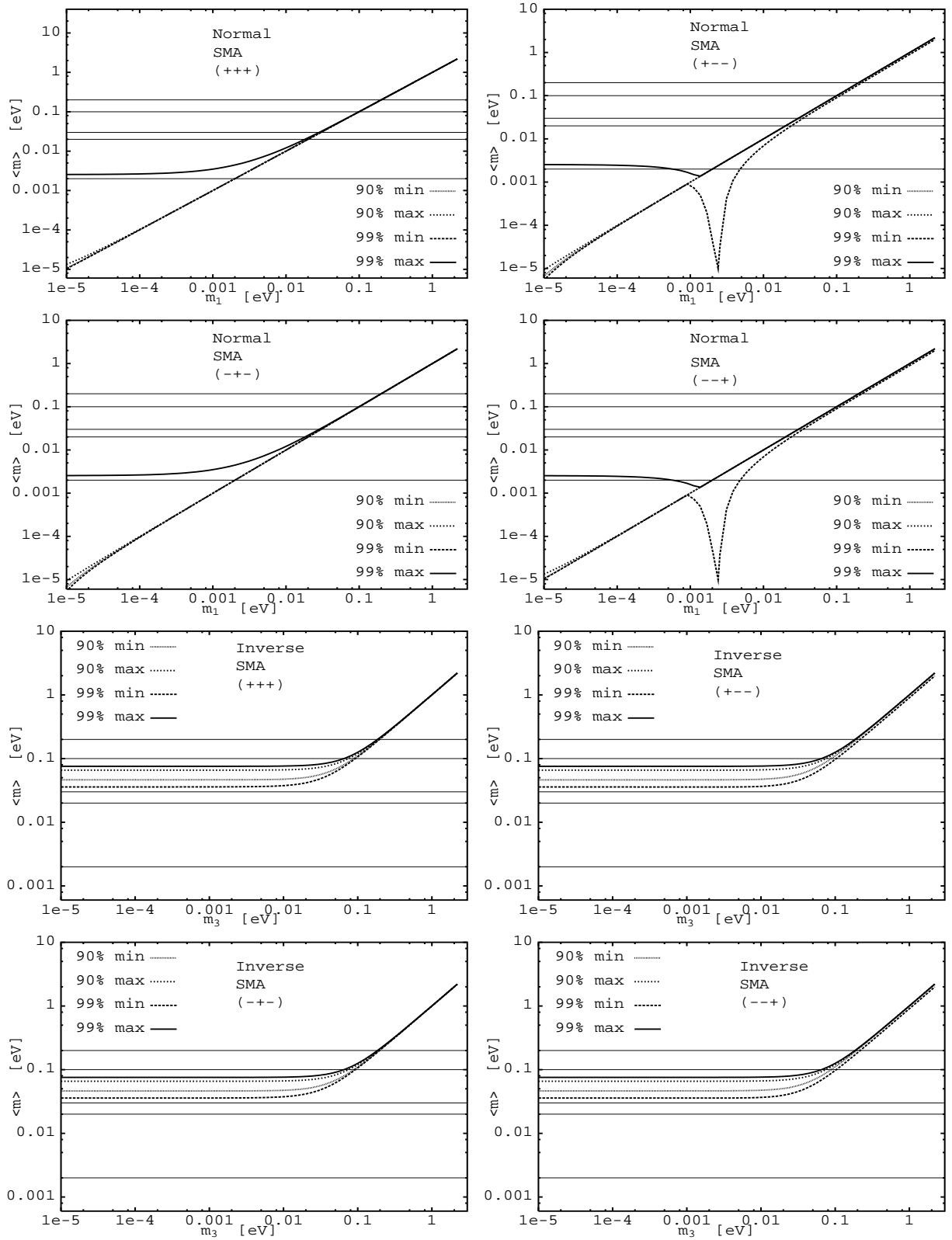


Figure 2.14: $\langle m \rangle$ as a function of the smallest mass eigenvalue for the 90 and 99 % C.L. SMA region and the 4 CP conserving parity configurations.

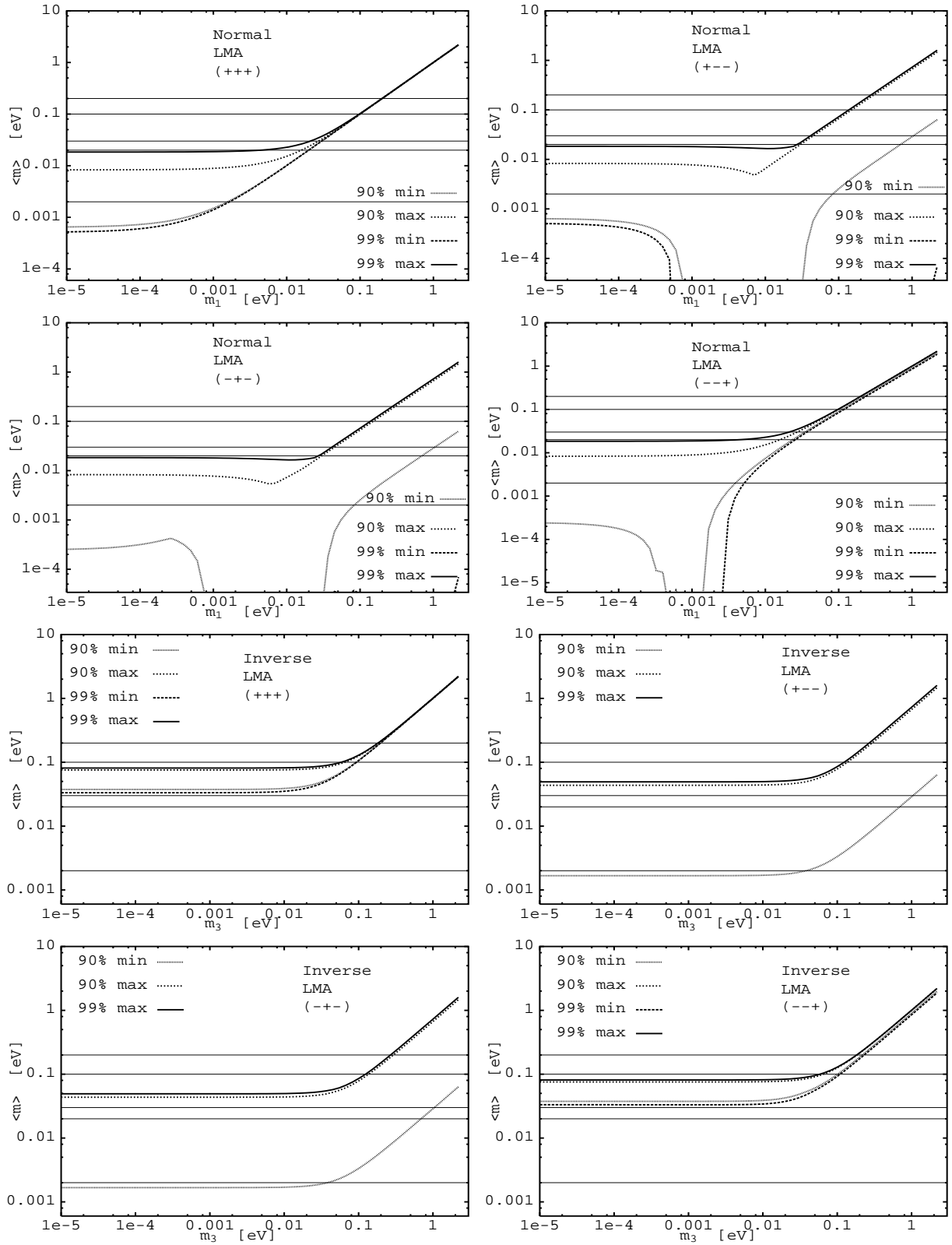


Figure 2.15: $\langle m \rangle$ as a function of the smallest mass eigenvalue for the 90 and 99 % C.L. LMA region and the 4 CP conserving parity configurations.

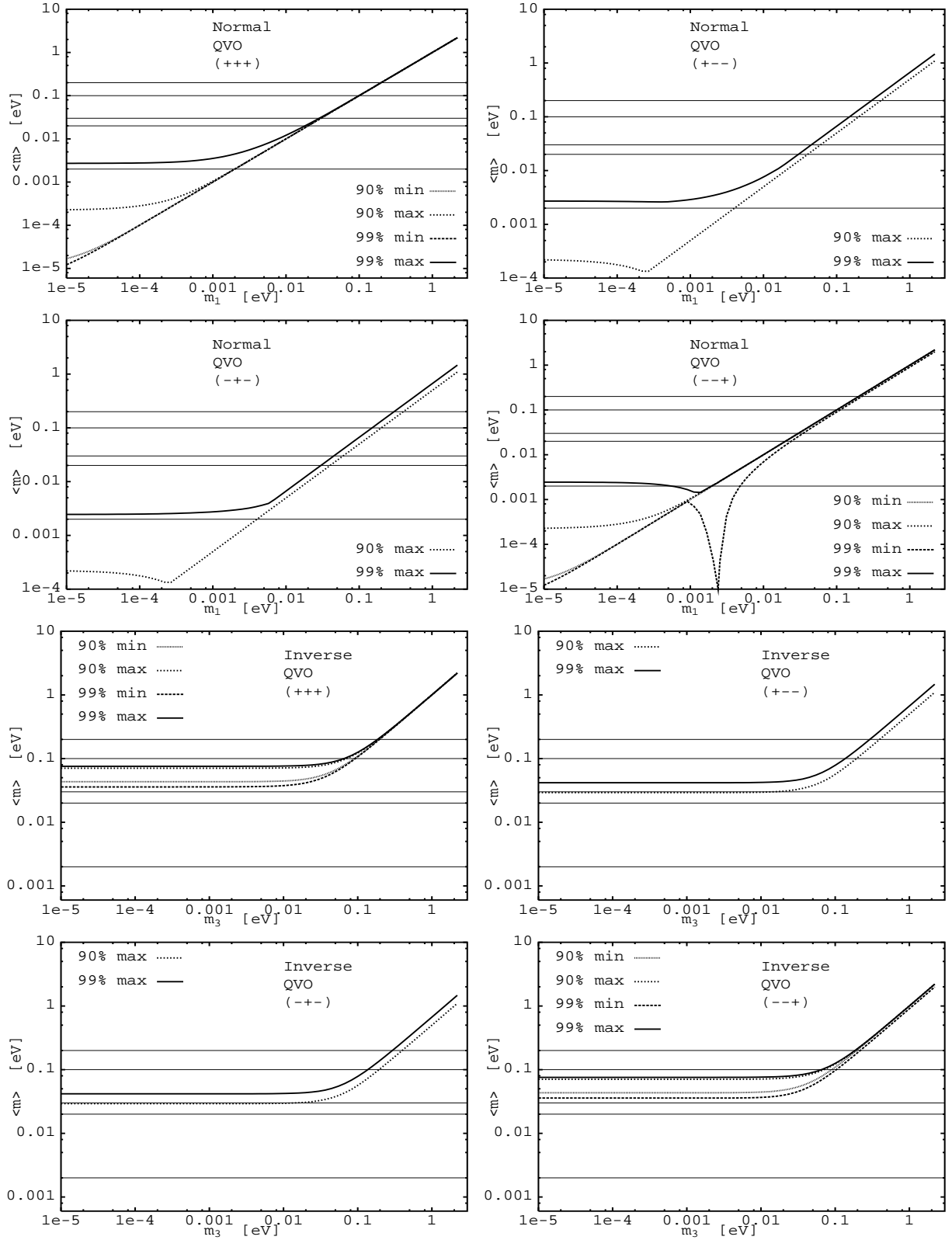


Figure 2.16: $\langle m \rangle$ as a function of the smallest mass eigenvalue for the 90 and 99 % C.L. QVO region and the 4 CP conserving parity configurations.

Fig. 2.17 is the master plot of this chapter. Several key scales of $\langle m \rangle$ and the smallest mass state can be identified and their consequences described. In addition, when one solar solution and/or a hierarchy will be identified, important statements can be made. Some of them have already been made in the examples given above and are now confirmed by the detailed analysis. For instance:

- If $\langle m \rangle \lesssim 0.03$ eV is measured...
...then the inverse scheme with the SMA solution is ruled out. This means that when for these $\langle m \rangle$ values SMA is verified, the mass scheme has to be the normal one. On the other hand, when the inverse scheme is verified, SMA can not be the solar solution. If however SMA *and* the inverse scheme are measured, neutrinos are Dirac particles.
- If $m_0 \gtrsim 0.4$ eV is measured...
...then the SMA is ruled out in both schemes. If SMA is verified then neutrinos are Dirac particles.
- If SMA is ruled out and $\langle m \rangle \leq 0.1$ eV is measured...
...then m_1 (m_3) has to be smaller than 0.09 (0.07) eV for the normal (inverse) scheme. This limit is one order of magnitude better than the ones expected from the next generation ^3H experiments. The scheme is then not degenerate. If a larger mass is measured, neutrinos are Dirac particles.
- If QVO is verified and $\langle m \rangle \leq 0.01$ eV is measured...
...then m_1 has to be smaller than 0.006 eV for the normal scheme. This limit is two order of magnitude better than the ones expected from the next generation ^3H experiments. The scheme is then hierarchical. If a larger mass is measured, neutrinos are Dirac particles.

The maximal value of m_0 for the SMA solution is 0.39 eV (which roughly scales with the limit on $\langle m \rangle$) and 2.2 eV for the LMA and QVO case. Since for SMA $\langle m \rangle \simeq m_0(1+s_3^2e^{2i\beta})$, such a high m_0 requires s_3 close to its current limit and $\beta \simeq \pi/2$, see Eq. (2.47) and the discussion thereafter. Regarding large mixing, it was shown in Section 2.3.3.2 that high m_0 and $\langle m \rangle$ close to its current limit forbids $\alpha \simeq \pi/2$. For $\langle m \rangle > m_0$ unitarity is violated and some “new physics” process causes neutrinoless double beta decay.

Limits depending on the parity configuration can also be derived. Some of them are

- If $\langle m \rangle \lesssim 0.02$ eV is measured...
...then the normal and inverse scheme together with the LMA solution are ruled out when the (+ - -) or (- - +) configurations are realized.
- If $\langle m \rangle \gtrsim 0.1$ eV and $m_0 \gtrsim 0.5$ eV is measured...
...then the case inverse scheme, LMA (QVO), (+ + +) and (+ - -) are ruled out. Also the (+ + +) case for LMA (QVO) and the normal scheme are not possible.

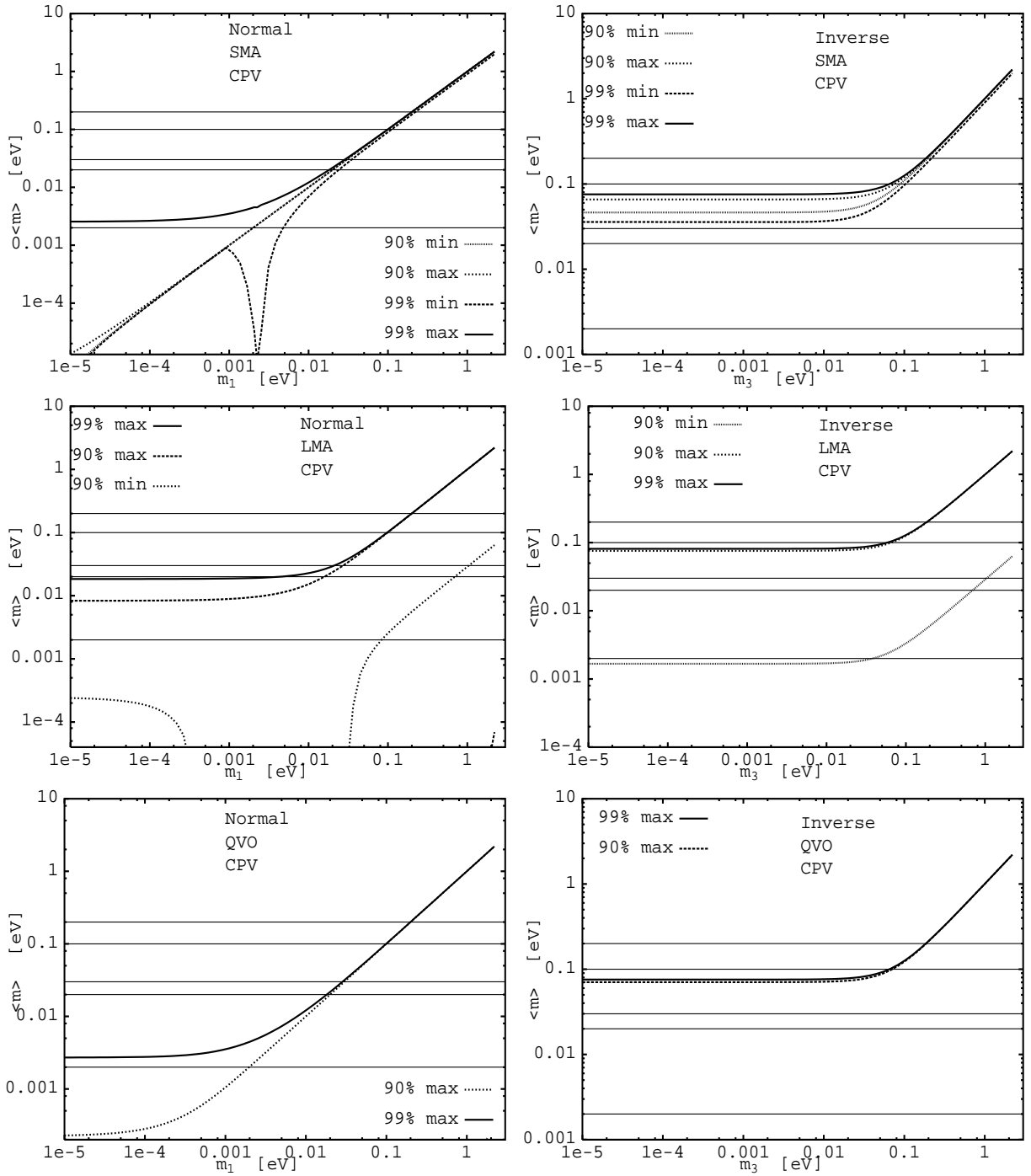


Figure 2.17: $\langle m \rangle$ in both hierarchies as a function of the smallest mass eigenvalue for the 90 and 99 % C.L. data sets of all three regions and the general CP violating case.

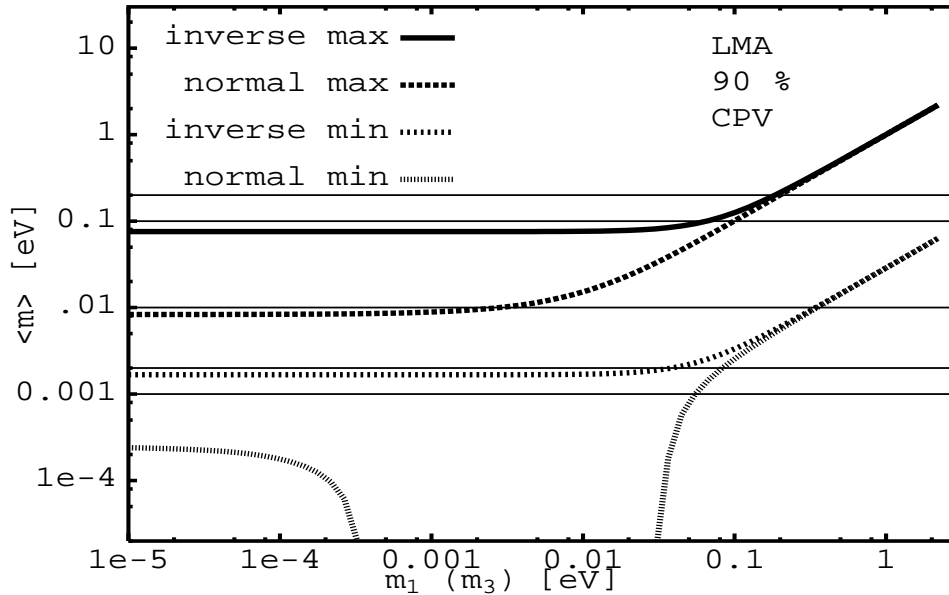


Figure 2.18: $\langle m \rangle$ as a function of the smallest mass eigenvalue in both hierarchies for the 90 % C.L. region of the LMA solution in the general CP violating case.

This means that $0\nu\beta\beta$ can give complementary information about the solar solution and the mass hierarchy, in addition to that given by direct mass searches and oscillation experiments. For certain cases limits on the smallest mass eigenstate better by two orders of magnitude can be set. Some statements, namely the character of the neutrino and the values of the phases or parities, can only be given by $0\nu\beta\beta$. The key scales to make such powerful statements are $\langle m \rangle \simeq 0.1, 0.01, 0.03$ eV and $m_0 \simeq 0.4$ eV. In contrast to recent claims, $\langle m \rangle \lesssim 0.01$ eV does not disfavor the LMA solution in the inverse scheme.

One can use the value $m_1(m_3) \leq 10^{-3}$ eV to define the normal (inverse) hierarchical scheme. Then, Fig. 2.17 shows that a value of $\langle m \rangle \gtrsim 0.004(0.02, 0.004)$ eV rules out the normal hierarchical scheme for the SMA (LMA, QVO) solution. The inverse hierarchical scheme would be ruled out for $\langle m \rangle \gtrsim 0.08$ eV.

In Fig. 2.18 we show $\langle m \rangle$ as a function of the smallest mass eigenstate for both hierarchies. When both schemes give the same value of $\langle m \rangle$, then the scheme is degenerate. This happens for a mass of about 0.2 eV, which is of the order of the current limit on $\langle m \rangle$. Therefore, at present one can not distinguish the normal from the inverse scheme in $0\nu\beta\beta$.

The existence of CP violation might be probed. Taking the 90 % C.L. data set we plot in Fig. 2.19 the maximal values of $\langle m \rangle$ for CP violation and the CP conserving parity configurations. The area below the “CPV” line and the next $(\pm\pm\pm)$ line is only

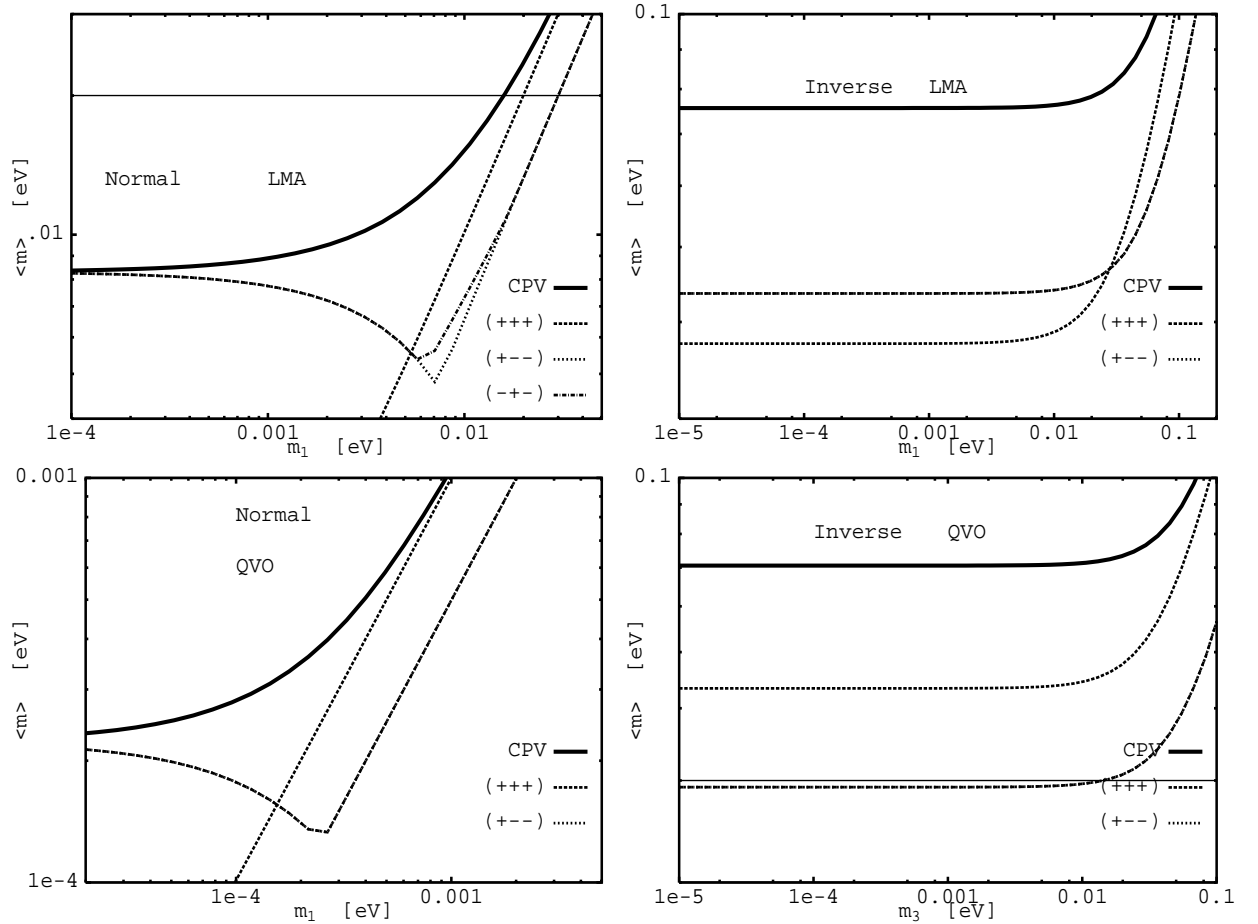


Figure 2.19: Maximal $\langle m \rangle$ in both hierarchies as a function of the smallest mass eigenvalue for the LMA and QVO solution and the 90 % C.L. data set. The area below the ‘‘CPV’’ line and the next $(\pm\pm\pm)$ line is only possible for CP violation.

possible for CP violation. One sees that this will be easiest to verify for the inverse hierarchy. If $\langle m \rangle$ is between 0.07 and 0.04 eV and m_3 is below 0.01 eV, then CP violation takes place. However, these small values of $\langle m \rangle$ and m_0 can not be probed. When the scheme becomes degenerate, the difference between the CP violating and conserving curves becomes very small and the other solar parameters have to be known in good precision, not to mention the uncertainty in the calculation of the nuclear matrix elements has to be fixed. See Fig. 2.9 for the situation in the degenerate scheme. In general, the ‘‘ CP violating’’ area is larger in the inverse scheme than in the normal one.

In general, for the normal scheme the distinction of the two cases takes place at values of $\langle m \rangle$ and m_1 typically one order of magnitude smaller than in the inverse scheme. Also, the CP violating area is larger in the inverse scheme. For SMA the difference is negligible.

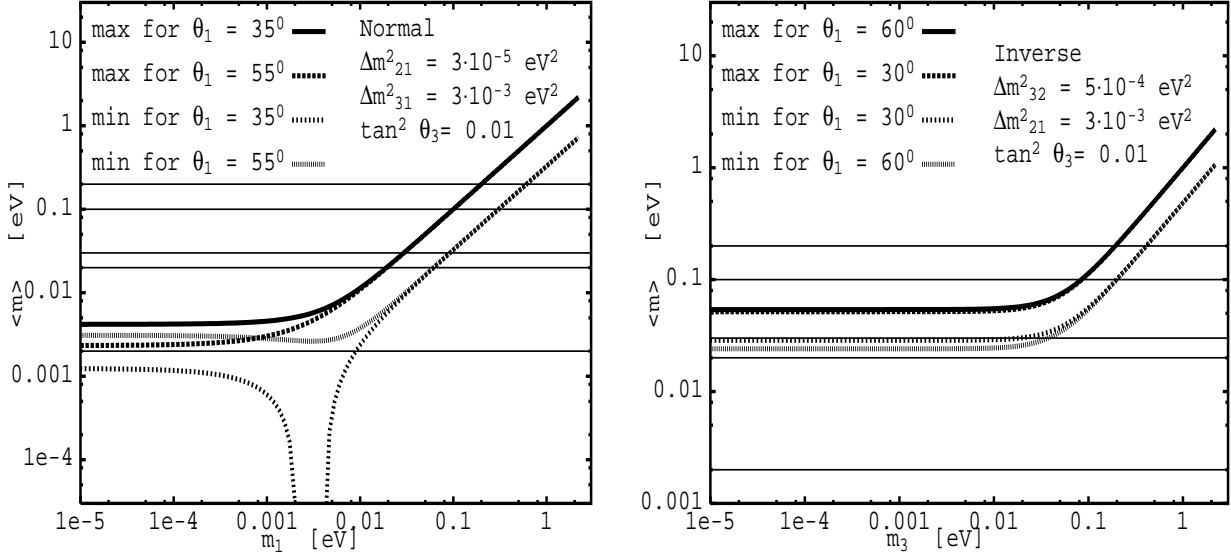


Figure 2.20: $\langle m \rangle$ as a function of the smallest mass eigenvalue in the normal (left) and inverse (right) hierarchy for a special choice of parameters from the LMA region. Shown is the minimal and maximal value for two values of θ_1 .

2.4.3 Implications from the dark side

The importance of taking also the dark side into account is shown in Fig. 2.20, where for a choice of parameters from the LMA region the minimal and maximal values are plotted. The minimum is found only for the angle from the light side. However, this difference shows up only for the normal hierarchy as can be seen in Fig. 2.20, where the difference between the two choices for θ_1 is hard to see. For more typical, lower values of $\tan^2 \theta_3$ and Δm_{\odot}^2 the difference is even harder to see. In Fig. 2.21 the difference between light and dark side is shown for the complete 99 % LMA parameter range and a special phase configuration. If $\langle m \rangle \leq 0.01$ eV would be measured then a limit of $m_1 \leq 1$ eV is obtained using only the dark side whereas $m_1 \leq 2.2$ eV is the bound from the light side. Tables 2.3 and 2.4 give the ranges of the three contributions to $\langle m \rangle$ using the 99 % C.L. data set of the respective region. The nontrivial correlation of the five oscillation parameters has been taken into account to obtain the given values. The fact that only the light side gives cancellation for LMA — for all parity configurations — is confirmed by the numbers. For QVO however, both parts of the parameter space can give $\langle m \rangle^{(i)}$ of similar magnitude and cancellation can occur for both parts of the parameter space.

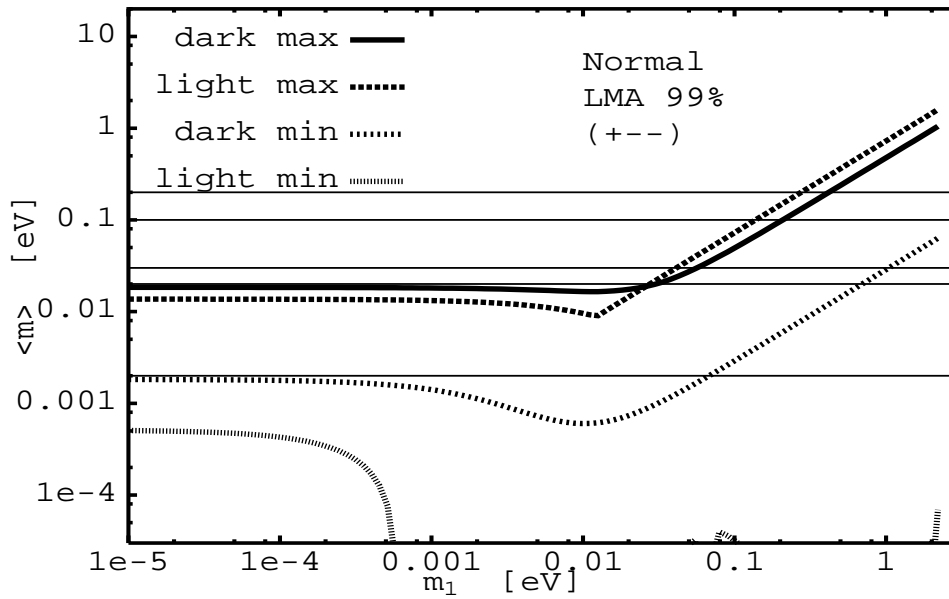


Figure 2.21: $\langle m \rangle$ as a function of the smallest mass eigenvalue m_1 in the normal hierarchy for the LMA solution and the $(+--)$ case. Shown are the minimal and maximal values for the dark and light side of the parameter space.

Another interesting conclusion follows from the fact that for QVO the solar mass scale tends to be lower on the dark side. Therefore in the normal hierarchy, where $\langle m \rangle^{(2)} \propto \sqrt{\Delta m_{\odot}^2}$, it follows that $\langle m \rangle$ is smaller for $\tan^2 \theta_1 > 1$.

2.5 Summary and final remarks

Neutrinoless double beta decay can provide unique information about the character of the neutrino and the value of the CP phases or parities. Complementary statements about the solar solution, mass scheme and the presence of leptonic CP violation can be given. Limits on the mass eigenstates can be obtained, which are up to two orders of magnitude better than from direct searches.

The formalism of the connection of neutrino oscillation and $0\nu\beta\beta$ has been reviewed and many special cases have been given. The dependence of $\langle m \rangle$ on the parameters has been analyzed in specific mass hierarchies. An analysis of $\langle m \rangle$ as a function of the smallest mass eigenstate has been presented, which includes for the first time the correlation of the different angles and Δm^2 . Using this, a limit on m_0 of 0.39 eV for the SMA solution could be given. This would only be possible for $\beta \simeq \pi/2$ and large s_3 . For the other solutions the tritium limit of 2.2 eV applies. However, when the $\langle m \rangle$ limit decreases to, say, 10^{-2} eV, such a high m_0 requires close-to-maximal mixing and $\alpha \simeq \pi/2$. The normal and inverse scheme give the same result for $\langle m \rangle$ when the smallest mass state is about 0.2 eV. Independent on the solar solution, the normal (inverse) hierarchical scheme is ruled out for $\langle m \rangle \gtrsim 0.02$ (0.1) eV. There are CP violating areas in the parameter space, which are in general larger for the inverse scheme than for the normal one. It will however be very difficult to verify CP violation, given that all parameters have to be known to a good precision and that the largest difference between CP conservation and violation occurs for very small neutrino masses. It has been commented on the implications from the dark side of the solar parameter space. It was found that for LMA only the light side can give complete cancellation. The QVO tends to have a lower $\langle m \rangle$ on the dark side and different limits on m_0 are obtained for data from both sides.

The connection of the CP conserving and violating case through the parities of the mass eigenstate has been stressed. Since β is always connected to the small quantity s_3 , a derivation of this phase remains doubtful. In fact, a large range for β will be allowed. However, for degenerate or inverse schemes, which may deliver a sizable $\langle m \rangle$, the phase α might be inferred via Eqs. (2.42) or (2.46), respectively. When s_3 is sizable, $\langle m \rangle$ has some dependence on β . However, then only one observable exists to constrain the two phases. Only for the SMA solution, large s_3 and m_0 larger than the $\langle m \rangle$ limit, $\beta \simeq \pi/2$ could be inferred through Eq. (2.47). In the normal hierarchical scheme the derivation of the phases will be very difficult because $\langle m \rangle$ is very small in this case.

Apart from just being parameters of a theory, the CP violating phases have important consequences in cosmology. The baryon asymmetry of the universe can be created through leptogenesis [72], which denotes the CP and L violating out-of-equilibrium decay of heavy Majorana neutrinos in the early universe. By solving equation (1.16) for M_R and diagonalizing this matrix one knows the right-handed heavy Majorana masses and can calculate the baryon asymmetry, which therefore depends also on the phases in U . A

particularly simple connection is possible in left–right symmetric models, where one can show that for the LMA or QVO solution holds [73]

$$Y_B \cdot 10^{10} \lesssim 4.1 \frac{1}{1 - 2 s_3 c_\delta} \left(\frac{m}{\text{GeV}} \right)^2 \left\{ (s_{2\alpha} + 4 s_3 s_\delta c_{2\alpha}) \frac{m_1}{\sqrt{\Delta m_\odot^2}} + 2(s_{2(\beta+\delta)} - 2 s_3 s_{2\beta+\delta}) \frac{m_1}{\sqrt{\Delta m_A^2}} \right\},$$

where m is the largest entry in m_D . Once the phases are known, a better understanding of leptogenesis will be possible and different models might be distinguished [74]. Moreover, the right–handed neutrinos required for leptogenesis are too heavy to be produced at colliders. Therefore, the verification of leptonic CP violation and the Majorana nature of neutrinos is perhaps the only possibility to validate leptogenesis. Neutrinoless double beta decay might just show both of these properties.

In Chapters 3 and 4 examples on analogue processes are given, which will quantify that $0\nu\beta\beta$ is the only process capable to directly probe $m_{\alpha\beta}$.

Chapter 3

Analogues of $0\nu\beta\beta$ I: Production of heavy Majorana Neutrinos at Colliders

High energy analogues of $0\nu\beta\beta$ can give information on the Majorana sector in a very different mass range. The slope of a typical cross section as a function of the Majorana mass m_i is easily understood from the two extreme limits of (compare with Eq. (2.3))

$$\sigma \propto \frac{m_i^2}{(q^2 - m_i^2)^2} \rightarrow \begin{cases} m_i^2 & \text{for } m_i^2 \ll q^2 \\ \frac{1}{m_i^2} & \text{for } m_i^2 \gg q^2 \end{cases}, \quad (3.1)$$

where q is the momentum of the Majorana neutrino. The highest signal is thus expected for an intermediate mass, the precise value depends on the energy scale of the experiment.

As in $0\nu\beta\beta$, the Majorana nature shows up in final states with two leptons of the same charge, like-sign dileptons (LSD). Since this production in analogy to $0\nu\beta\beta$ has been studied in great detail in the past for hadron-hadron collisions [75–77], we shall focus here on yet unstudied neutrino-nucleon and positron-proton scattering. Due to the higher available energy at colliders, it is now possible that the two LSD have different flavor.

First, in Section 3.1, the simplest example for a collider process involving Majorana neutrinos is discussed. It is the process $e^-e^- \rightarrow W^-W^-$, which has been studied in various ways in recent years [78, 79]. Most properties of analogue $\Delta L = 2$ processes are understood in this simple reaction and can be derived analytically. Several limits on mass and mixing of the neutrinos have to be obeyed, constraining the signal significantly. Especially the limit (2.9) from $0\nu\beta\beta$ on heavy Majorana neutrinos strongly suppresses final states with electrons, as will be illustrated also for the other processes in this chapter.

In Sections 3.2 and 3.3 a similar process for neutrino–nucleon scattering is analyzed. We consider both, past fixed target experiments as well as future high–energy neutrino factories. Section 3.4 sees the discussion of a similar process in the form of positron–proton scattering at HERA. In Section 3.5 an example for a phenomenological effect of heavy Majorana neutrinos is given: a possible explanation of the events with an isolated lepton and large missing transverse momentum found by the H1 collaboration at HERA. Though two like–sign dileptons are produced, the experimental cuts tend to ignore one of them. Therefore one observes only one isolated lepton together with missing transverse momentum. Finally, this chapter is summarized in Section 3.6.

3.1 Calculation of inverse neutrinoless double beta decay

The process $e^-e^- \rightarrow W^-W^-$ allows to study the property of Majorana neutrino production in a simple manner. Since the diagram is in fact the central part of the $0\nu\beta\beta$ diagram, it is of general interest and is known as “inverse neutrinoless double beta decay”. The proposed next generation e^+e^- colliders, such as TESLA [80], may be also run in an e^-e^- mode, which would provide the opportunity to search for this process. There also exist other (mostly new physics) applications, which make the e^-e^- mode an interesting alternative [81]. Among them are production of Z' bosons, dileptons, leptoquarks, doubly charged Higgs bosons, supersymmetric particles and so on. Some of them can provide complementary information to those gathered in the e^+e^- mode, others are solely possible in the e^-e^- mode. Here we shall however focus on the exchange of Majorana neutrinos in the t and u channel, updating the discussion performed in [82].

At the beginning there is the SM Lagrangian for the coupling of a neutrino ν_α with a charged lepton α ,

$$\mathcal{L} = \frac{g}{\sqrt{2}} U_{\alpha i} \bar{\nu}_i \gamma_\mu \gamma_- \alpha W^{\mu-}. \quad (3.2)$$

The notation of the diagram is given in Fig. 3.1, the matrix element reads

$$-i\mathcal{M} \equiv -i(\mathcal{M}_1 + \mathcal{M}_2) = \left(\frac{ig}{\sqrt{2}} \right)^2 U_{ei}^2 [\bar{\nu}_i \gamma_\mu \gamma_- e_1 \bar{\nu}_i \gamma^\nu \gamma_- e_2 \epsilon_1^{\mu*} \epsilon_2^{\nu*} + (\gamma_\mu \leftrightarrow \gamma_\nu)], \quad (3.3)$$

with the obvious notation $e_1 = e(p_1)$ and $\epsilon_1 = \epsilon(k_1)$. Starting with \mathcal{M}_1 one may use the identity¹

$$\bar{\nu}_i \gamma_\mu \gamma_- e_1 = -\bar{e}_1^c \gamma_\mu \gamma_+ \nu_i^c. \quad (3.4)$$

Since $\nu_i = \nu_i^c$ and $\nu_i \bar{\nu}_i = -i(\not{q} - m_i)^{-1}$, where q is the momentum of the neutrino, \mathcal{M}_1 reads

$$-i\mathcal{M}_1 = \frac{ig^2}{2} U_{ei}^2 \frac{1}{t - m_i^2} \bar{e}_1^c \gamma_\mu \gamma_+ (\not{q} + m_i) \gamma_\nu \gamma_- e_2 \epsilon_1^{\mu*} \epsilon_2^{\nu*}. \quad (3.5)$$

Here s , t and u denote the usual Mandelstam variables. It is trivial to show that $\gamma_+(\not{q} + m_i) \gamma_\nu \gamma_- = m_i \gamma_+ \gamma_\nu$. For the expansion in terms of spinors and creation/annihilation operators the following relations are valid [83]:

$$\begin{aligned} \mu &\propto fu + \bar{f}^+ v \\ \bar{\mu}^c &\propto \bar{f}^+ \bar{u} + f\bar{v} \end{aligned} \quad (3.6)$$

¹ $\bar{\nu}_i \gamma_\mu \gamma_- e_1 = (\bar{\nu}_i^c)^c \gamma_\mu \gamma_- (e_1^c)^c = -(\nu_i^c)^T C^{-1} \gamma_\mu \gamma_- C \bar{e}_1^{cT} = (\nu_i^c)^T (\gamma_\mu \gamma_+)^T \bar{e}_1^{cT} = -\bar{e}_1^c \gamma_\mu \gamma_+ \nu_i^c$. The last sign comes from the interchange of two fermion fields. We used the definition of charge conjugation from Eq. (1.6).

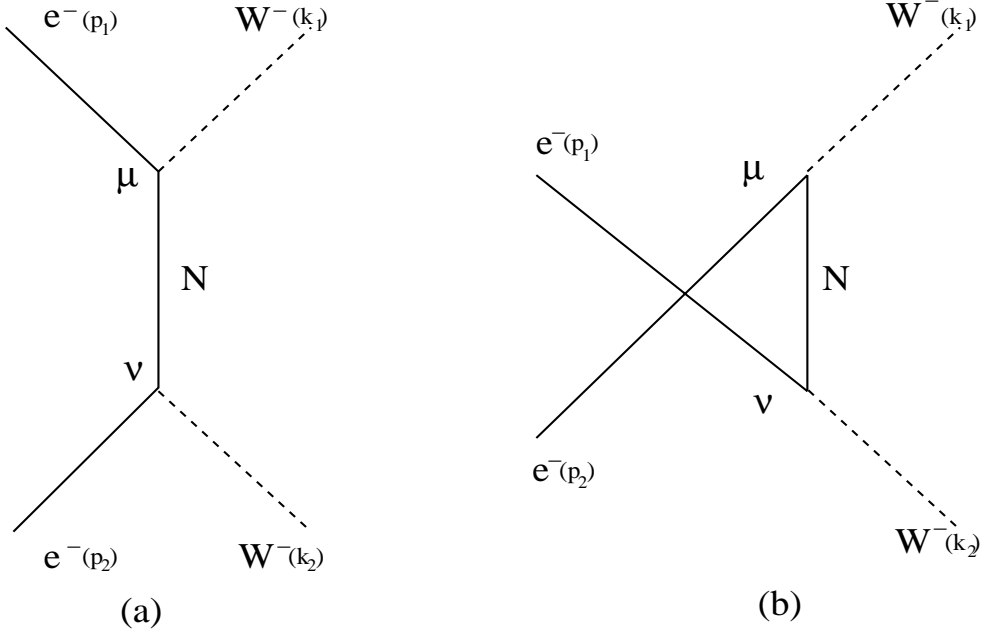


Figure 3.1: Feynman diagram for $e^-e^- \rightarrow W^-W^-$. \mathcal{M}_1 is given in (a) and the crossed diagram is described by (b).

Here f annihilates a particle and \bar{f}^+ creates an antiparticle. Therefore,

$$\mathcal{M}_1 = \frac{-g^2}{2} U_{ei}^2 m_i \frac{1}{t - m_i^2} \bar{v}_1 \gamma_- \gamma_\mu \gamma_\nu u_2 \epsilon_1^{\mu*} \epsilon_2^{\nu*}, \quad (3.7)$$

and the crossed diagram is now obtained by also replacing t with u in addition to $\gamma_\mu \leftrightarrow \gamma_\nu$. Note that — in contrast to the usual Feynman rules — one γ_- is now a γ_+ and \bar{v}_1 instead of u_1 is used for an incoming electron. Averaging over the spin of the two initial electrons, we find

$$\begin{aligned} |\overline{\mathcal{M}}|^2 &= \frac{1}{4} 8 G_F^2 m_i m_j U_{ei}^2 U_{ej}^2 \\ &\left[\frac{1}{(t - m_i^2)(t - m_j^2)} (4 m_W^6 - (t + u)(t^2 + 4 m_W^4) + 2 m_W^2 t(t + 2u)) + (t \leftrightarrow u) \right. \\ &\quad \left. + \frac{2}{(t - m_i^2)(u - m_j^2)} (4 m_W^6 - t u (4 m_W^2 - s)) \right]. \end{aligned} \quad (3.8)$$

The cross section in the center-of-mass system is obtained by

$$\frac{d\sigma}{d\cos\theta} = \frac{1}{2} \frac{1}{32\pi s} \sqrt{1 - \frac{4 m_W^2}{s}} |\overline{\mathcal{M}}|^2. \quad (3.9)$$

The factor 1/2 is due to fact that there are two identical particles in the final state.

It is an excellent approximation to neglect the mass of the W with respect to \sqrt{s} . Then, neglecting all terms proportional to m_W ,

$$\frac{d\sigma}{d\cos\theta} = \frac{G_F^2}{32\pi} \left\{ m_i U_{ei}^2 \left(\frac{t}{t - m_i^2} + \frac{u}{u - m_i^2} \right) \right\}^2. \quad (3.10)$$

Two interesting special cases exist, corresponding to very light (heavy) neutrinos, i.e. $m_i^2 \ll s$ ($m_i^2 \gg s$). Inserting this in the last equation gives

$$\sigma \simeq \begin{cases} \frac{G_F^2}{4\pi} (m_i U_{ei}^2)^2 & = 4.2 \left(\frac{\langle m \rangle}{\text{eV}} \right)^2 \cdot 10^{-18} \text{ fb} & s \gg m_i^2 \\ \frac{G_F^2}{16\pi} s^2 \left(\frac{U_{ei}^2}{m_i} \right)^2 & = 1.1 \left(\frac{\langle \frac{1}{m} \rangle}{10^{-8} \text{ GeV}^{-1}} \right)^2 \left(\frac{s}{\text{TeV}^2} \right)^2 \cdot 10^{-4} \text{ fb} & s \ll m_i^2 \end{cases}. \quad (3.11)$$

For light neutrinos, the proportionality to $\langle m \rangle^2$ is the same as in $0\nu\beta\beta$. In the last chapter, hand-waving arguments for this fact were given, the calculation in this section confirms the result. As a function of the neutrino mass, the extreme limits from Eq. (3.1) are obtained. Clearly, both cases are unobservable when we use the bounds from Eqs. (2.7) and (2.9). The cross sections for light and heavy neutrinos are $5.2 \cdot 10^{-19}$ fb and $1.3 \cdot 10^{-4}$ fb for $\sqrt{s} = 1$ TeV, respectively.

3.1.1 Unitarity

In the limit $s \rightarrow \infty$ the cross section reads

$$\sigma = \frac{G_F^2}{4\pi} \left| \sum U_{ei}^2 m_i \right|^2, \quad (3.12)$$

i.e. it tends towards a constant and, since the matrix element grows with \sqrt{s} , violates unitarity. Two easy ways out of this misery exist, both are related to the mechanism, which provides neutrinos with mass. First, a left-handed Higgs triplet can be introduced, which includes a doubly charged Higgs boson. This participates in the reaction $e^-e^- \rightarrow W^-W^-$ via s channel production and restores unitarity. This was already noted in the first publications devoted to the process [78].

Second, if the left-handed triplet is absent, the usual see-saw mechanism might be active. In the simple two-dimensional scenario of Section 1.2 the sum in Eq. (3.12) is

$$m_\nu \cos\theta + M_R \sin\theta = -\frac{m_D^2}{M_R} \cdot 1 + M_R \frac{m_D^2}{M_R^2} = 0 \quad (3.13)$$

and the problem solves itself. Actually, M_R is a right-handed neutrino whose inclusion may result in a different cross section. However, it turns out to be described by the same cross section and the interference terms between the left- and right-handed contributions cancel. For a proper treatment of $e^-e^- \rightarrow W^-W^-$ in left-right symmetric models, see [84]. We shall return to these unitarity considerations in Section 4.5.2.

3.1.2 Limits on heavy neutrinos and properties of the cross section

As shown, using the bounds on the very light and very heavy neutrinos from $0\nu\beta\beta$ yields unobservable cross sections. However, we may vary the mass of the Majorana and look for observable effects of neutrinos with intermediate mass. The result for the case of one mass m_i and $U_{ei} = 1$ is shown in Fig. 3.2a. As an integrated luminosity for TESLA one usually assumes $\mathcal{L} = 80 \text{ s/TeV}^2 \text{ fb}^{-1}$. Asking for five events, this corresponds to masses between 0.1 and $6.4 \cdot 10^5 \text{ GeV}$ for $\sqrt{s} = 0.5 \text{ TeV}$. For $\sqrt{s} = 2 \text{ TeV}$ masses between 0.03 and $4.3 \cdot 10^7 \text{ GeV}$ can be probed. The values for different center-of-mass energies are given in Table 3.1 in the “no limits” column.

However, the mixing parameter of electrons with heavy neutrinos, U_{ei} , is not a free parameter. Various observables, such as spectra of meson decays, limit $|U_{ei}|$ for various m_i . For a summary of these limits we refer to the Particle Data Group (PDG) [85]. The limit we will use the most applies especially to heavy neutrinos. The three known light neutrinos ν_α are expressed as mixtures of light and heavy particles, this can be written as

$$\nu_\alpha \rightarrow \cos \theta_\alpha \nu_\alpha + \sin \theta_\alpha N_\alpha \quad (3.14)$$

in the (unmixed) Lagrangian for each family. For the sake of simplicity we take $N_\alpha = N$. The Lagrangian now reads:

$$\begin{aligned} -\mathcal{L} = & \frac{g}{\sqrt{2}} W_\mu^- \left\{ \cos \theta_\alpha \bar{\nu}_\alpha \gamma^\mu \gamma_- l_\alpha + \sin \theta_\alpha \bar{N} \gamma^\mu \gamma_- l_\alpha \right\} \\ & + \frac{g}{2 \cos \theta_W} Z_\mu \left\{ \cos^2 \theta_\alpha \bar{\nu}_\alpha \gamma^\mu \gamma_- \nu_\alpha + \sin 2\theta_\alpha \bar{N} \gamma^\mu \gamma_- \nu_\alpha - \frac{1}{2} \sin^2 \theta_\alpha \bar{N} \gamma_\mu \gamma_5 N \right\} + \text{h.c.} \end{aligned} \quad (3.15)$$

Note that there is no vector current between the heavy Majoranas \bar{N} and N due to their Majorana nature². The last equation as a function of $\sin^2 \theta_\alpha$ can now be fitted to weak interaction processes such as muon decay or neutrino nucleon scattering, and a limit on the mixing angle can be set. If ν_α mixes with more than one heavy neutrino, $\sin^2 \theta_\alpha$ has to be replaced with $\sum_i |U_{\alpha i}|^2$. The obtained limits read [86]

$$\begin{aligned} \sum |U_{ei}|^2 & \leq 6.6 \cdot 10^{-3} \\ \sum |U_{\mu i}|^2 & \leq 6.0 \cdot 10^{-3} \quad . \\ \sum |U_{\tau i}|^2 & \leq 1.8 \cdot 10^{-2} \end{aligned} \quad (3.16)$$

These bounds are essentially independent of the $SU(2)_L$ transformation properties of the neutrino with which the ν_α mixes. For later use we remark that they therefore also apply to mixture with heavy right-handed neutrinos. In addition, the limit is quite conservative — it allows for the possibility that the other charged fermions also mix with new charged particles. If one assumes that the only new particles are neutrinos, then the

² $\bar{N} \gamma_\nu N = \bar{N}^c \gamma_\nu N^c = -N^T C^{-1} \gamma_\nu C \bar{N}^T = N^T \gamma_\nu^T \bar{N}^T = -\bar{N} \gamma_\nu N$.

\sqrt{s} [TeV]	no limits	limits	$0\nu\beta\beta$ limits
0.5	$0.1 \dots 6.4 \cdot 10^5$	$70 \dots 3.6 \cdot 10^3$	—
1	$0.05 \dots 5.3 \cdot 10^6$	$70 \dots 3.0 \cdot 10^4$	—
2	$0.03 \dots 4.3 \cdot 10^7$	$70 \dots 2.4 \cdot 10^5$	—
4	$0.01 \dots 3.5 \cdot 10^8$	$70 \dots 2.1 \cdot 10^6$	$1.8 \cdot 10^3 \dots 2.0 \cdot 10^6$
10	$5 \cdot 10^{-3} \dots 5.4 \cdot 10^9$	$70 \dots 3.3 \cdot 10^7$	$9.2 \cdot 10^2 \dots 3.1 \cdot 10^7$

Table 3.1: The Majorana neutrino masses in GeV that can be probed in the reaction $e^-e^- \rightarrow W^-W^-$ at various center-of-mass energies. Five events are required. Shown are the results for applying no limits, the limits on mixing from various experiments and these limits together with the one from $0\nu\beta\beta$.

above limit improves somewhat.

In Fig. 3.2b the result of these limits on the cross section is seen. From $m_i \simeq 70$ GeV on, only the limits from (3.16) exist so that the accessible mass range starts with this value. The mass range that may be probed now is given in the “limits” column of Table 3.1. The upper mass is now reduced by two orders of magnitude.

Now the result from $0\nu\beta\beta$ comes into play. If there is only one heavy mass eigenstate m_i , then Eq. (2.9) sets a strong limit on the mixing, namely

$$|U_{ei}|^2 \leq 1.1 \cdot 10^{-8} \frac{m_i}{\text{GeV}}. \quad (3.17)$$

This limit is stronger than the one from Eq. (3.16) up to masses of $m_i \leq 6 \cdot 10^5$ GeV. In Fig. 3.2c the consequences of imposing this limit on the cross section are seen. From the figure and the “ $0\nu\beta\beta$ limits” column in Table 3.1 one finds that the process renders unobservable at e^-e^- colliders with $\sqrt{s} \leq 2$ TeV. For an energy of 3 TeV, masses between 5 and 750 TeV may be probed.

The situation improves when one considers $\mu^-\mu^- \rightarrow W^-W^-$ or $e^-\mu^- \rightarrow W^-W^-$. For the former case, Fig. 3.2b and the “limits” column of Table 3.1 apply, the latter might allow detection of the process from about 1 TeV on. These utopian possibilities will however not be considered here.

The current limits on Majorana neutrino masses lie below the values that may be probed in inverse neutrinoless double beta decay. Searches for so-called “Heavy Neutral Leptons” have extensively been performed at the LEP collider. The best limits come from the L3 experiment using an integrated luminosity of 506 pb^{-1} and center-of-mass energies from 133 to 208 GeV. Due to different detection techniques and efficiencies the bounds are different for different final states. Assuming no universality of coupling the

limits read [87]

$$\begin{aligned}
 m_i &> 89.5 \text{ GeV} && \text{coupling to } e \\
 m_i &> 90.7 \text{ GeV} && \text{coupling to } \mu \quad . \\
 m_i &> 80.5 \text{ GeV} && \text{coupling to } \tau
 \end{aligned}
 \tag{3.18}$$

These limits together with the bounds on $\sum |U_{\alpha i}|^2$ from Eq. (3.16) will be used in the this and the following Chapter.

3.1.3 Evading the limits

It is possible to evade some of the statements regarding the observability of $e^-e^- \rightarrow W^-W^-$ [82]. These cases do however require construction of contrived models. Assume that there is a neutrino of $m_1 = 2$ TeV with $U_{e1}^2 = 5 \cdot 10^{-3}$. In order to fulfill the constraints in Eqs. (2.9,3.16) another neutrino with e.g. $m_2 = 400$ GeV and $U_{e2}^2 = -1 \cdot 10^{-3}$ has to be introduced. This would at $\sqrt{s} = 2$ TeV result in a cross section of about 31.1 fb and will be observable. However, neutrinos with $m_i < \sqrt{s}$ will be detected directly in the reaction $e^+e^- \rightarrow \nu_e N$ [88]. Then the presence of the heavier one can be inferred from Eq. (2.9). An exclusive discovery may be realized via $m_1 = 2$ TeV with $U_{e1}^2 = 6 \cdot 10^{-4}$ and $m_1 = 10$ TeV with $U_{e2}^2 = -2.9 \cdot 10^{-3}$. The cross section at $\sqrt{s} = 2$ TeV will be 0.16 fb, again observable. Here, the heavier neutrino possesses a larger mixing with the electron, something usually considered as unnatural.

There is also the possibility that the heavy neutrinos are degenerate, i.e. $m_1 = m_2 = M$. Then the mixing is given by $\sum U_{ei}^2 \leq 1.1 \cdot 10^{-8} M/\text{GeV}$. The largest cross section that one can obtain in this scenario is the limit $m_i^2 \gg s$ from Eq. (3.11).

All these examples get the more baroque and unlikely the more additional heavy neutrinos one introduces. Therefore, from here on it will be assumed that there is no fine-tuning in order to evade the $0\nu\beta\beta$ constraint on heavy neutrino mixing. This is identical to the case that the processes under study are governed by only one neutrino.

The limit on heavy neutrinos from $0\nu\beta\beta$ does strictly speaking only hold for left-handed neutrinos. We can however assume that effects of right-handed neutrinos will be of the same order of magnitude. Thus, also the bound Eq. (2.9) applies, at least order-of-magnitude wise. Eq. (3.16) also holds for right-handed neutrinos, and therefore our considerations about the observability of $e^-e^- \rightarrow W^-W^-$ will not change for heavy right-handed neutrinos. In the following we will mostly discuss processes involving left-handed Majorana neutrinos. An explicit example for right-handed neutrinos is given in Section 3.3.

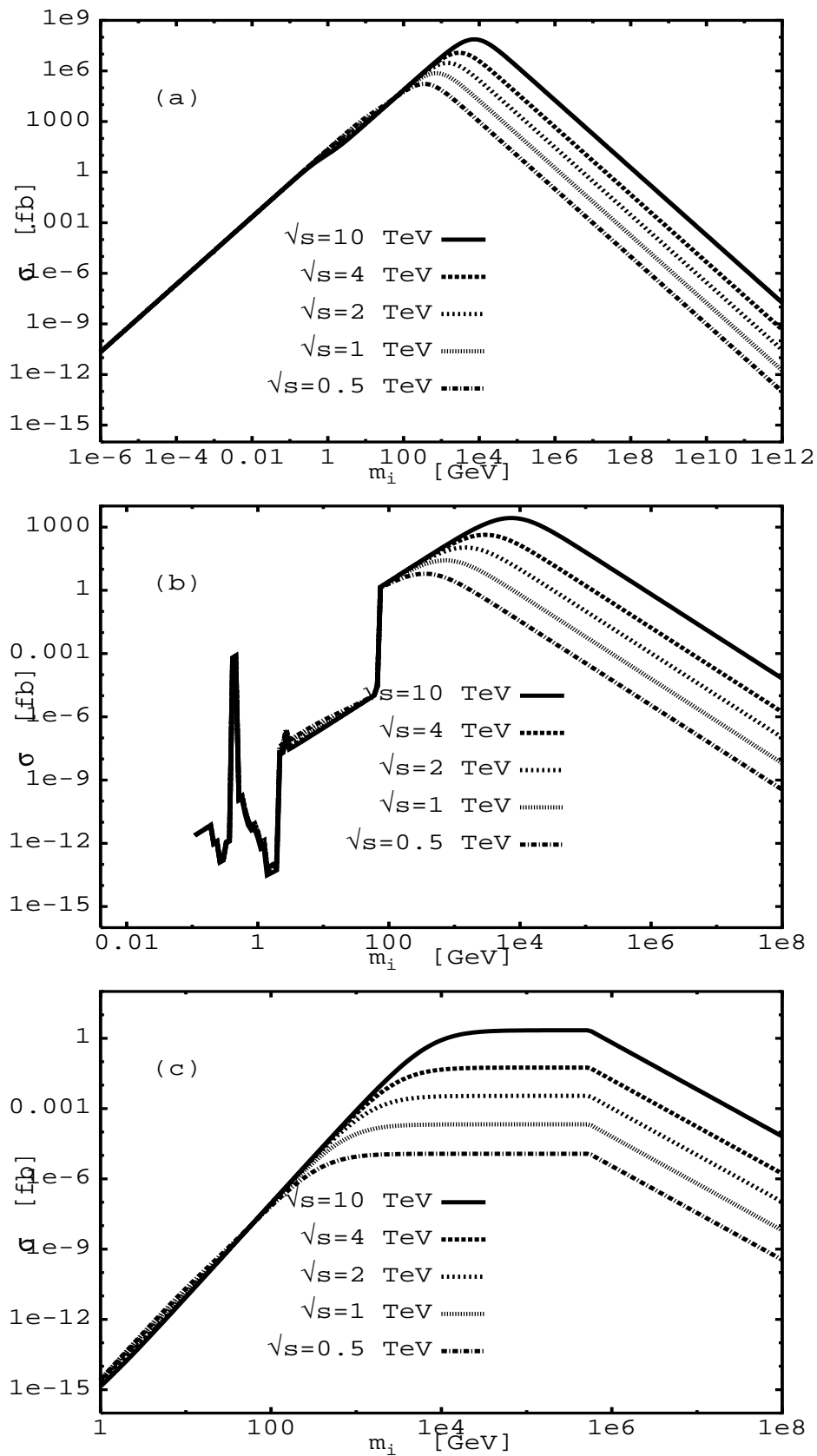


Figure 3.2: Cross section of $e^-e^- \rightarrow W^-W^-$ against mass of the intermediate Majorana neutrino for (a) no limit on the mixing, (b) limits from various experiments and (c) these limits together with the one from neutrinoless double beta decay.

3.2 Neutrino–nucleon scattering

A high–energy analogue of $0\nu\beta\beta$ can be realized e.g. in neutrino–nucleon scatterings such as $\nu_\mu N \rightarrow \mu^- \mu^+ \mu^+ X$ or positron–proton scattering $e^+ p \rightarrow \bar{\nu}_e \mu^+ \mu^+ X$. The core diagram $W^- W^- \rightarrow e^- e^-$ has been calculated in Section 3.1. In order to calculate a process with an intermediate Majorana neutrino, the matrix element has to be changed: If the W couples to a weak interaction vertex, the polarization tensor just has to be replaced with the usual charged current (CC) term.

3.2.1 Calculation

As a first example, we study trimuon production in neutrino–nucleon scattering [2],

$$\nu_\mu N \rightarrow \mu^- \mu^+ \mu^+ X . \quad (3.19)$$

The diagram, which also defines the kinematics, is given in Fig. 3.3. Using the trick from Eq. (3.4) one obtains for the matrix element:

$$\begin{aligned} \mathcal{M}_1 &\propto U_{\mu i}^{*2} \bar{\mu}_2^c \gamma_\rho \gamma_- \nu_i \bar{\nu}_i \gamma_\pi \gamma_+ \mu_3 \\ &= U_{\mu i}^{*2} [\bar{u}(k_2) \gamma_\rho \gamma_- (\not{q}_2 + m_i) \gamma_\pi \gamma_+ v(k_3)] \frac{1}{q_2^2 - m_i^2} \\ &= U_{\mu i}^{*2} m_i [\bar{u}(k_2) \gamma_\rho \gamma_- \gamma_\pi v(k_3)] \frac{1}{q_2^2 - m_i^2} . \end{aligned} \quad (3.20)$$

In the crossed diagram, described by \mathcal{M}_2 , q_2 is replaced by \tilde{q}_2 and k_2 by k_3 . Finally, the interference term is given by

$$-\mathcal{M}_1^* \mathcal{M}_2 \propto \bar{v}(k_3) \gamma_\nu \gamma_+ \gamma_\mu u(k_2) \bar{u}(k_3) \gamma_\alpha \gamma_- \gamma_\beta v(k_2) . \quad (3.21)$$

It has a relative sign with respect to \mathcal{M}_1 due to the interchange of two identical fermion lines. Using the identities $\bar{v} = -u^T C^{-1}$ and $u = C \bar{v}^T$ this can be written in a form suitable for using the completeness relations for the spinors:

$$\begin{aligned} \bar{v}(k_3) \gamma_\nu \gamma_+ \gamma_\mu u(k_2) &= -u^T(k_3) C^{-1} \gamma_\nu \gamma_+ \gamma_\mu C \bar{v}^T(k_2) \\ &= -u^T(k_3) (\gamma_\mu \gamma_+ \gamma_\nu)^T \bar{v}^T(k_2) = \bar{v}(k_2) \gamma_\mu \gamma_+ \gamma_\nu u(k_3) . \end{aligned} \quad (3.22)$$

Putting all the couplings and propagators together, the matrix element for *one* intermediate Majorana and scattering with a quark can be written as (using the Feynman–gauge for the W propagator)

$$\begin{aligned}
|\overline{\mathcal{M}}|^2 &= |\overline{\mathcal{M}}_1|^2 + |\overline{\mathcal{M}}_2|^2 + 2\text{Re} \left(\overline{\mathcal{M}}_1^* \overline{\mathcal{M}}_2 \right) \\
&= \left(U_{\mu i}^{*2} m_i \right)^2 64 G_F^4 M_W^8 \left| \frac{1}{q_1^2 - M_W^2} \frac{1}{q_3^2 - M_W^2} \right|^2 \\
&\text{Tr} \left\{ \gamma_+ \gamma^\mu \not{p}_1 \gamma^\beta (\not{k}_1 + m_\mu) \right\} \text{Tr} \left\{ \gamma^\nu \gamma_- (\not{p}_2 + m_q) \gamma^\alpha \gamma_- (\not{k}_4 + m_{q'}) \right\} \\
&\quad \left[\left| \frac{1}{q_2^2 - m_i^2} \right|^2 \text{Tr} \left\{ \gamma_\mu \gamma_- \gamma_\nu (\not{k}_3 - m_\mu) \gamma_\alpha \gamma_+ \gamma_\beta (\not{k}_2 + m_\mu) \right\} \right. \\
&\quad + \left| \frac{1}{\bar{q}_2^2 - m_i^2} \right|^2 \text{Tr} \left\{ \gamma_\mu \gamma_- \gamma_\nu (\not{k}_2 - m_\mu) \gamma_\alpha \gamma_+ \gamma_\beta (\not{k}_3 + m_\mu) \right\} \\
&\quad \left. - 2 \left| \frac{1}{q_2^2 - m_i^2} \frac{1}{\bar{q}_2^2 - m_i^2} \right| \text{Tr} \left\{ \gamma_\beta \gamma_+ \gamma_\alpha (\not{k}_3 + m_\mu) \gamma_\mu \gamma_- \gamma_\nu (\not{k}_2 - m_\mu) \right\} \right] \\
&= \left(U_{\mu i}^{*2} m_i \right)^2 G_F^4 M_W^8 \left| \frac{1}{q_1^2 - M_W^2} \frac{1}{q_3^2 - M_W^2} \right|^2 2^{12} (p_1 \cdot p_2) \\
&\quad \left[\left| \frac{1}{q_2^2 - m_i^2} \right|^2 (k_1 \cdot k_2)(k_3 \cdot k_4) + \left| \frac{1}{\bar{q}_2^2 - m_i^2} \right|^2 (k_2 \cdot k_4)(k_1 \cdot k_3) \right. \\
&\quad \left. - \left| \frac{1}{q_2^2 - m_i^2} \frac{1}{\bar{q}_2^2 - m_i^2} \right| ((k_2 \cdot k_3)(k_1 \cdot k_4) - (k_2 \cdot k_4)(k_1 \cdot k_3) - (k_1 \cdot k_2)(k_3 \cdot k_4)) \right].
\end{aligned} \tag{3.23}$$

Here are m_q and $m_{q'}$ the masses of the scattered initial and final state partons, respectively. Coupling to an antiquark is identical to replacing k_4 with p_2 . The formulas for anti-neutrino scattering and intermediate right-handed neutrinos are given in Appendix B. The two short traces describe the SM $V - A$ vertices, the ones inside the square brackets the $0\nu\beta\beta$ -like core process. Averaging over the parton spin adds an additional factor $1/2$. The long traces were computed with the MATHEMATICA [89] package TRACER [90].

As can be seen, in the low mass regime the matrix element is proportional to m_{μ}^2 . For heavy neutrinos the dependence goes as $(U_{\mu i}^2/m_i)^2$.

3.2.2 Results of the Monte Carlo

For the evaluation of the total and differential cross sections a Monte Carlo program calling the phase space routine GENBOD [91] was written. The chosen parton distributions are GRV 98 ($\overline{\text{MS}}$) NLO [92] at $Q^2 = s = (p_1 + p_2)^2 = x^2 M_p^2 + 2x M_p E_\nu$. Here M_p denotes the proton mass, E_ν the energy of the incoming neutrino and x the Björken variable. We set $Q^2 = Q_{\text{min}}^2$ whenever Q^2 went under the minimal allowed value of 0.8 GeV^2 . To get the averaged neutrino–nucleon cross section we assumed an isoscalar target and replaced up and down quarks to get the parton distributions for the neutron.

Before presenting the results we estimate the ratio with respect to the total neutrino–nucleon cross section. As mentioned, the typical suppression factor one encounters when dealing with Majorana instead of Dirac neutrinos is m_i/E in the matrix elements with

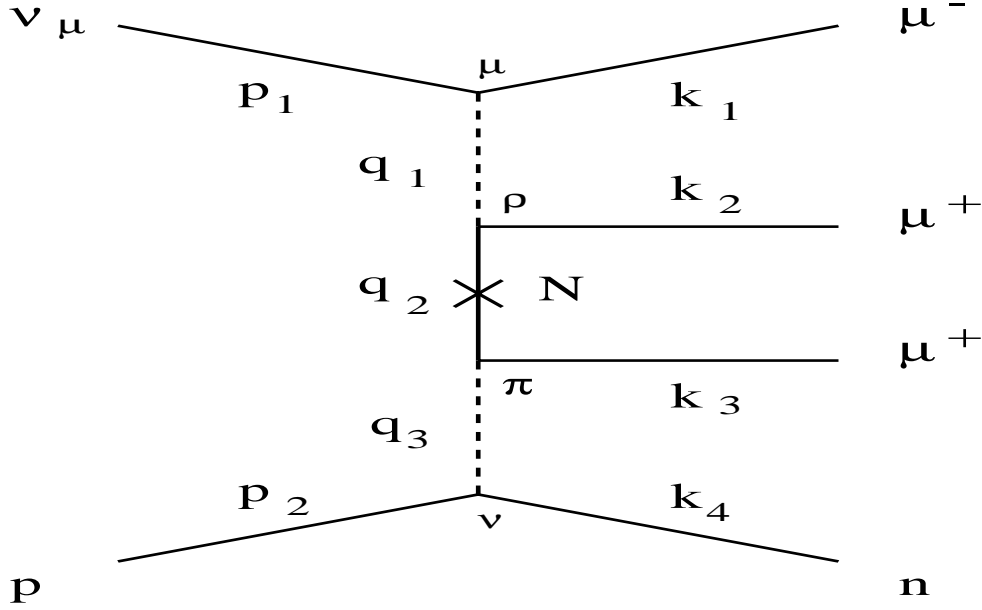


Figure 3.3: Feynman diagram for trimuon production in neutrino-nucleon scattering. It is $q_2 = q_1 - k_2 = p_1 - k_1 - k_2$. For the crossed diagram k_2 and k_3 are exchanged and the corresponding momentum of the Majorana neutrino is denoted with $\tilde{q}_2 = q_1 - k_3 = p_1 - k_1 - k_3$. For the W momenta holds: $q_1 = p_1 - k_1$ and $q_3 = k_4 - p_2$.

m_i being the Majorana mass and E its energy. For the ratio R of the cross sections we have therefore:

$$R = \frac{\sigma(\nu_\mu N \rightarrow \mu^- \mu^+ \mu^+ X)}{\sigma(\nu_\mu N \rightarrow \mu^- X)} \propto \left(\frac{m_i}{E}\right)^2 G_F^2 M_W^4 \sim \begin{cases} 10^{-24} & \text{for } m_i = 0.35 \text{ eV} \\ 10^{-13} & \text{for } m_i = 170 \text{ keV} \\ 10^{-4} & \text{for } m_i = 5 \text{ GeV} \end{cases}, \quad (3.24)$$

where we took as a typical value $E = 30 \text{ GeV}$. For heavy neutrinos the behavior changes significantly: Instead of m_i/E we have now m_i^{-2} and the ratio goes as

$$R \propto \frac{G_F^2 M_W^4 M_p^2}{m_i^2} \sim 10^{-7} \text{ for } m_i = 100 \text{ GeV}. \quad (3.25)$$

These ratios will of course be further suppressed by a very small phase space factor, which rises slightly with energy and turns out to be about 10^{-7} . In addition, small factors arising from bounds on the mixing with heavy neutrinos apply.

As expected, the cross section is tiny: If we use for the mass of the Majorana neutrino the current limit from the direct muon neutrino mass search, $m_i = 170 \text{ keV}$ [34], we find that the cross section for energies in the range (5...500) GeV is of the order

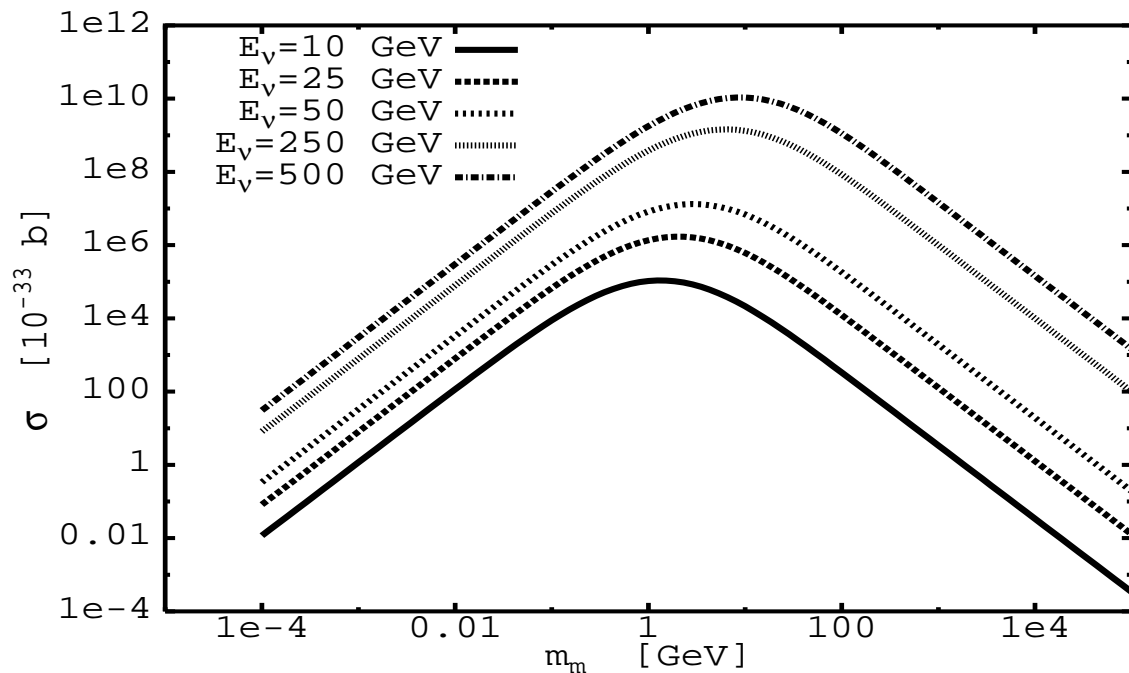


Figure 3.4: Total cross section for a left-handed Majorana neutrino as a function of its mass for different neutrino beam energies.

$\sigma(3\mu) \simeq (1 \dots 10^2) \cdot 10^{-33}$ b, being 20 orders of magnitude lower than the total neutrino nucleon CC cross section of $\sigma_{CC} \simeq (1 \dots 10^2) \cdot 10^{-14}$ b for the same energy range. See Chapter 4 for an interesting way to still do something useful with these small numbers, namely setting (admittedly not very physical) limits on light and heavy neutrinos.

Despite the small values, the ratio of the trimuon process described here is significantly more sensitive on $m_{\mu\mu}$ than previously discussed processes: Abad et al. [93] obtain for the decay $K^+ \rightarrow \pi^- \mu^+ \mu^+$ a branching ratio of $2 \cdot 10^{-22}$ while Missimer et al. [94] estimate the ratio of $(\mu^- \mu^+)$ -conversion via capture in ^{44}Ti with respect to a normal CC reaction to be $4 \cdot 10^{-25}$, both for a few hundred keV Majorana neutrino. Thus the process discussed here is therefore about two orders of magnitude closer to the relevant standard model process than previously discussed Majorana induced muon–number violating processes.

In Fig. 3.4 we show the cross section as a function of m_i for different neutrino energies. The cross section is too small to be observed. Differential cross sections of the momenta of the three muons are presented in Fig. 3.5.

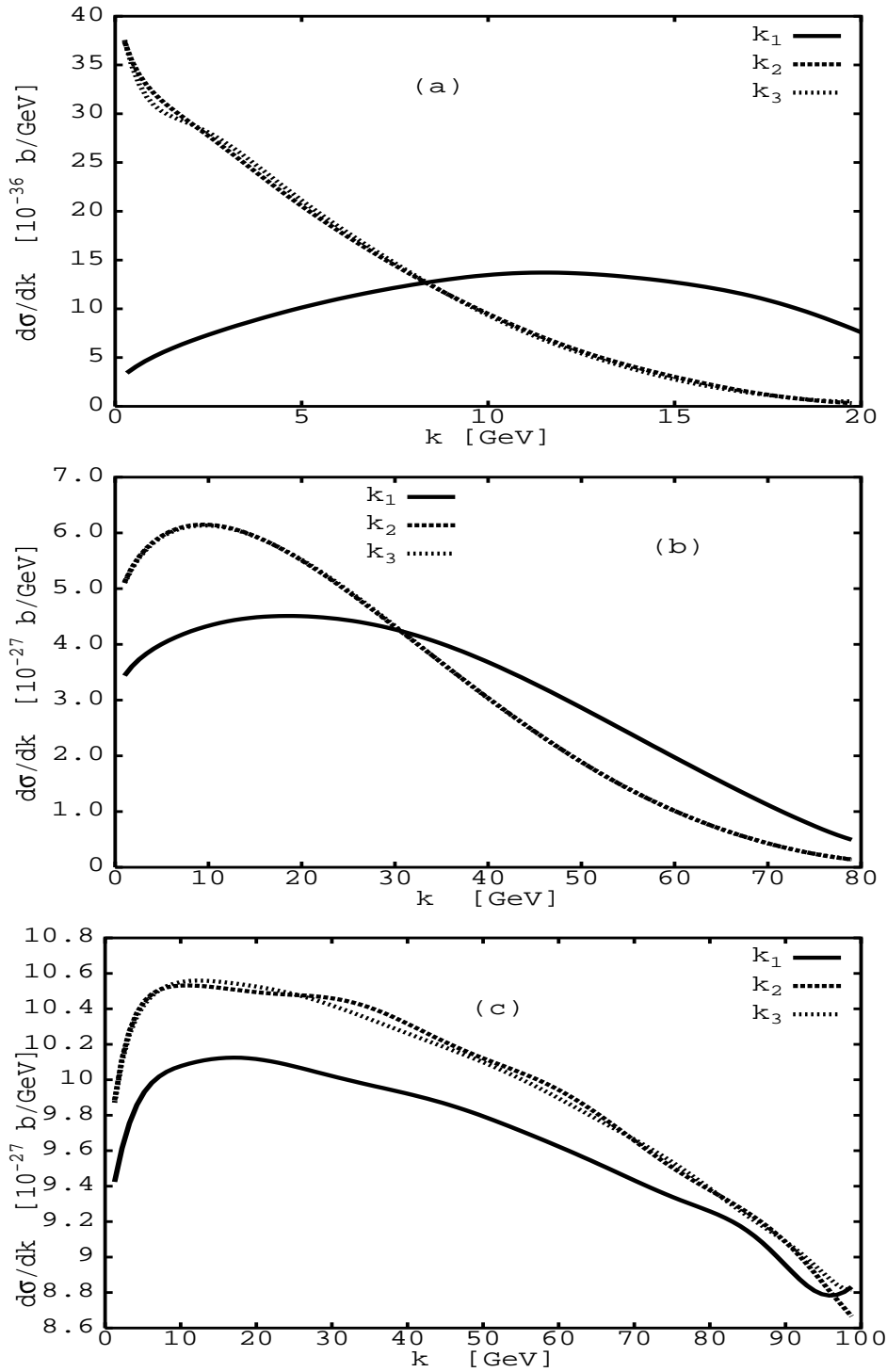


Figure 3.5: Differential cross sections of the muon momenta for different energies and Majorana masses. (a) $m_i = 170$ keV and $E_\nu = 25$ GeV, (b) $m_i = 5$ GeV and $E_\nu = 100$ GeV and (c) $m_i = 80$ GeV and $E_\nu = 500$ GeV. No limit on $U_{\mu i}^2$ was applied.

3.2.3 Experimental considerations

Though one can not expect a signal of trimuon production from processes with a Majorana neutrino in intermediate states, some words from the experimental point of view are appropriate. Several experiments reported the observation of trimuon events [95–97]. The observed ratio of trimuon events (having a lepton number conserving $(- - +)$ signature of the muon charges) with respect to single charged current events is of the order 10^{-5} . First thought to provide evidence for physics beyond the SM, the explanation was soon given in terms of CC reactions with dimuon production via meson decay, radiative processes or direct muon pair production from subsequent hadronic interactions [98–100]. An acceptance cut on muon momenta to be larger than about 5 GeV was applied by all experiments to reduce the background.

To extract a $(- + +)$ signature several background processes occurring in typical wide band neutrino beams have to be considered. Among them, the most severe are lepton pair creation due to antineutrino contaminations of the beam (also having a $(- + +)$ signature) and charm production with an associated pion or kaon decay as well as overlaying events with beam muons. Furthermore, going to high momenta some misidentification in the charge might lead to additional background.

A complete listing of all relevant distributions is not our aim, however, for the sake of completeness, the distributions of the muon momenta, which might be used to identify the process, are given. From Fig. 3.5 it can be seen, that for light m_i the two μ^+ have relatively low energy, while the μ^- from the upper $V - A$ vertex has a broad spectrum with significantly higher energy. This is no longer valid for a heavy Majorana where the difference of the muon momenta is less clear, but is becoming larger with increasing neutrino energy. However, the like-sign muons have typically the same momentum distributions, which is an important experimental signature. It is a general feature that the momentum difference gets bigger when the energy E_ν is significantly higher than the mass of the intermediate Majorana. For mass and energy being equal the distributions are more or less identical.

The developed strategies as described here could be of some use when one searches for similar processes triggered by non SM effects, such as supersymmetry. As will be argued in Section 3.3, one may expect a sizable signal from these sector.

3.3 High energy neutrino factory

The physics potential of a muon storage ring is rich and exciting. Especially the option of using the neutrinos from the μ decay has received large attention [101]. Typically the main focus lies in long baseline oscillation experiments [47] with source–detector distances from 730 up to 10000 km and muon energies of 10 to 50 GeV. This development is driven by the urge to find out about oscillation phenomena in more detail and to gain additional information, be it about CP violation, the mass scheme, the size of $|U_{e3}|$ or the existence of sterile neutrinos.

An additional option is the installation of a detector directly at the storage ring site together with a very large muon energy. This will probably be done in the form of a $\mu^- \mu^+$ collider, whose primary goal will be to do precision Higgs physics. Neutrino interactions of up to 10^{13} /y provide also the possibility of high precision experiments regarding CKM matrix elements, structure functions, electroweak parameters, charm physics or other phenomena, see [102] for some possibilities. As in any other new experiment, new physics may lurk in the results.

The process under study in this section is [5]

$$\bar{\nu}_\delta^{(-)} N \rightarrow \delta^\mp \alpha^\pm \beta^\pm X, \text{ where } \delta = e, \mu \text{ and } \alpha, \beta = e, \mu, \tau. \quad (3.26)$$

In the Monte Carlo program, outlined in the last section, an integration over the neutrino spectrum is included. A simple phase space calculation (see Appendix C) for the $\mu \rightarrow e\nu_e\nu_\mu$ decay gives for the normalized distribution in the lab frame:

$$\begin{aligned} \frac{dN}{dE_\nu}(\nu_\mu) &= \frac{2}{E_\mu^3} E_\nu^2 \left(3 - 2\frac{E_\nu}{E_\mu} \right), \\ \frac{dN}{dE_\nu}(\nu_e) &= \frac{12}{E_\mu^3} E_\nu^2 \left(1 - \frac{E_\nu}{E_\mu} \right). \end{aligned} \quad (3.27)$$

The maximal neutrino energy is E_μ and the mean value is $\langle E_\nu \rangle = 7/10$ ($3/5$) E_μ for ν_μ (ν_e).

For a $\mu^- \mu^+$ -collider or a muon storage ring four different signals are possible, corresponding to incoming $\nu_\mu, \nu_e, \bar{\nu}_\mu$ or $\bar{\nu}_e$. In Fig. 3.6 we plot for all four possibilities the cross section for the production of two muons, including the limits on heavy neutrino mixing as given in Eq. (3.16). The figure shows that the muon neutrino from the μ^- decay gives the highest cross section.

We will also consider now the case when the two leptons from the intermediate “ $WW \rightarrow \alpha\beta$ ” diagram are not of the same flavor. An interesting statistical effect occurs when one considers the relative difference between, say, the $\mu\mu$ and the μe final state (mass effects play no role for e and μ): first, there is no phase space factor $\frac{1}{2}$ for the latter case, since two different particles are now in the final state. Then, there is the possibility

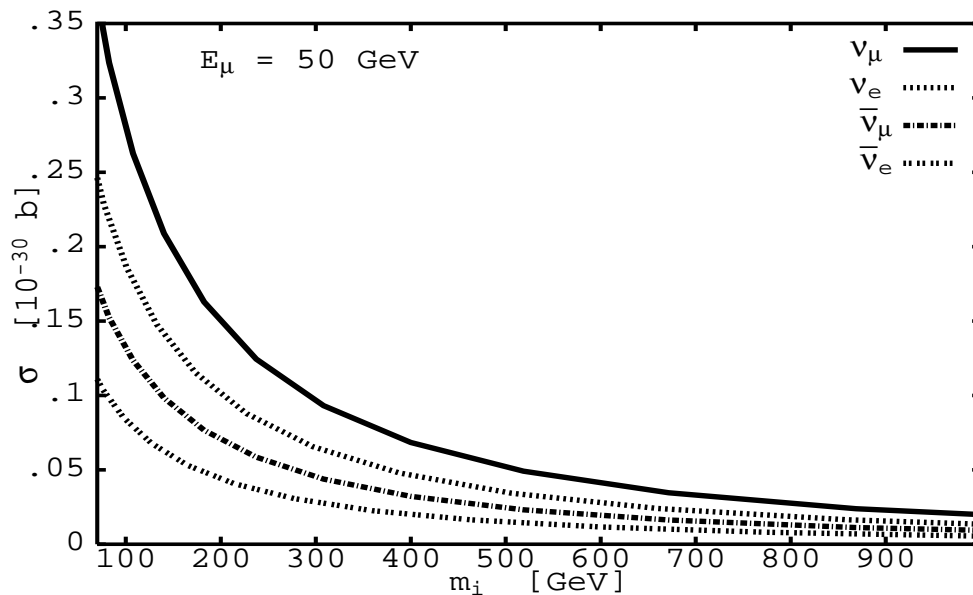


Figure 3.6: Total cross section for $\nu_l N \rightarrow l\mu\mu X$ for ν_μ , ν_e , $\bar{\nu}_\mu$ and $\bar{\nu}_e$ as a function of the Majorana mass for a μ energy of 50 GeV. The limits on $U_{\mu i}$ are applied.

that an electron is produced at the (“upper”) $\nu l W$ vertex or at the (“lower”) $qq'W$ vertex. Both diagrams are topologically distinct and thus have to be treated separately. This means, four diagrams lead to the μe final state, whereas only two lead to the $\mu\mu$ final state. We see that there is a relative factor 4 between the two cases. Note though that now the interference terms are *added* to the two squared amplitudes since there is no relative sign between the two diagrams. This reduces the relative factor to about 3. However, effects of kinematical cuts and the limits of Eq. (3.16) wash out this phenomenon.

In Fig. 3.8 the total cross section for the reaction $\nu_\mu N \rightarrow \mu^- \alpha^+ \beta^+ X$ with the $\mu\mu$, $\mu\tau$ and $\tau\tau$ final states for three different muon energies is shown. For the statistical arguments to be valid, the mass of the final state leptons has to be negligible. This is the case for muon energies higher than about 3 TeV: the $\mu\tau$ final state is the leading signal for $E_\mu = 4$ TeV.

Finally, we give in Fig. 3.9 the cross section for $\nu_\mu N \rightarrow \mu^- \mu^+ \mu^+ X$ with two possible other realizations, namely via an intermediate right-handed Majorana neutrino and via right-handed interactions with a W_R -mass of 720 GeV, the current lower bound [103]. See Appendix B for the relevant formulas. It can be seen that a left-handed heavy neutrino gives the highest contribution. As argued before, effects of left- and right-handed neutrinos are of similar magnitude. Of course it is possible that all these realizations contribute and thus interfere.

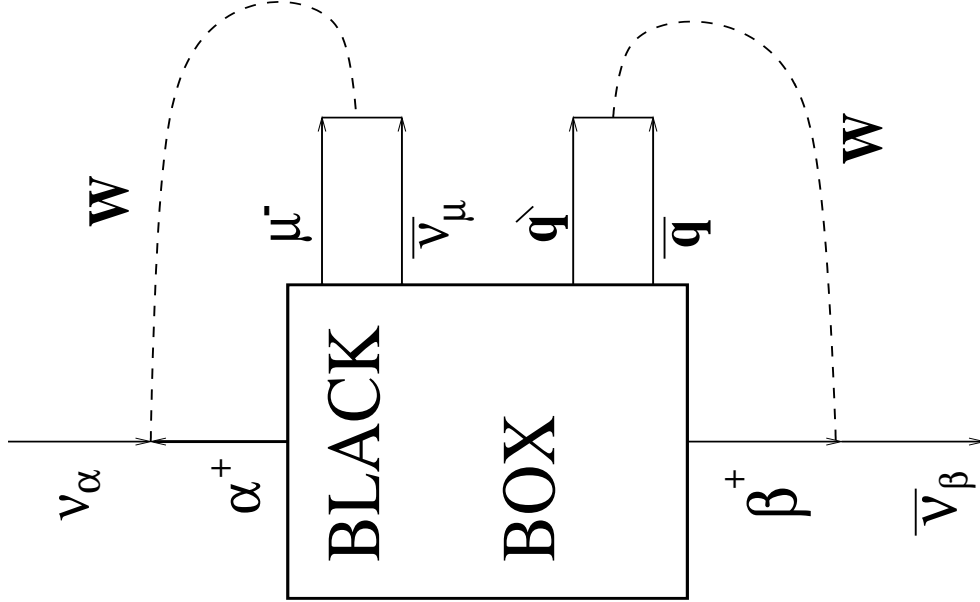


Figure 3.7: Connection between Majorana mass term of ν_α and ν_β and the existence of process $\nu_\mu N \rightarrow \mu^- \alpha^+ \beta^+ X$.

We checked the dependence of the results on oscillation parameters by integrating over simple two-flavor formulas. Even for $E_\mu = 50$ GeV, a detector–source distance of 1 km and LSND–like values of Δm^2 ($\simeq 0.1$ eV²) and $\sin^2 2\theta$ ($\simeq 10^{-3}$) the relative suppression of the signal was not more than $\mathcal{O}(10^{-6})$. Inserting typical parameters of atmospheric or solar experiments has an even smaller effect.

The question arises if one can conclude that a Majorana mass term is present if a process like Eq. (3.26) is measured. Here, a simple generalization of the Schechter and Valle [58] arguments from Section 2.1 for $0\nu\beta\beta$ applies. Assuming we found convincing evidence for $\nu_\mu q \rightarrow \mu^- \alpha^+ \beta^+ q'$, then crossing permits the process $0 \rightarrow \bar{\nu}_\mu \mu^- \alpha^+ \beta^+ q' \bar{q}$, realized by the “black box” in Fig. 3.7. Any reasonable gauge theory will have W ’s couple to quarks and leptons, so that a Majorana mass term for ν_α and ν_β is produced by coupling one W to the $\alpha^+ \nu_\mu \mu^-$ and one W to the $\beta^+ q' \bar{q}$ vertex. Since we do not know which two quarks participate and which neutrino couples to the quark this theorem is a straightforward generalization of the Schechter and Valle argument.

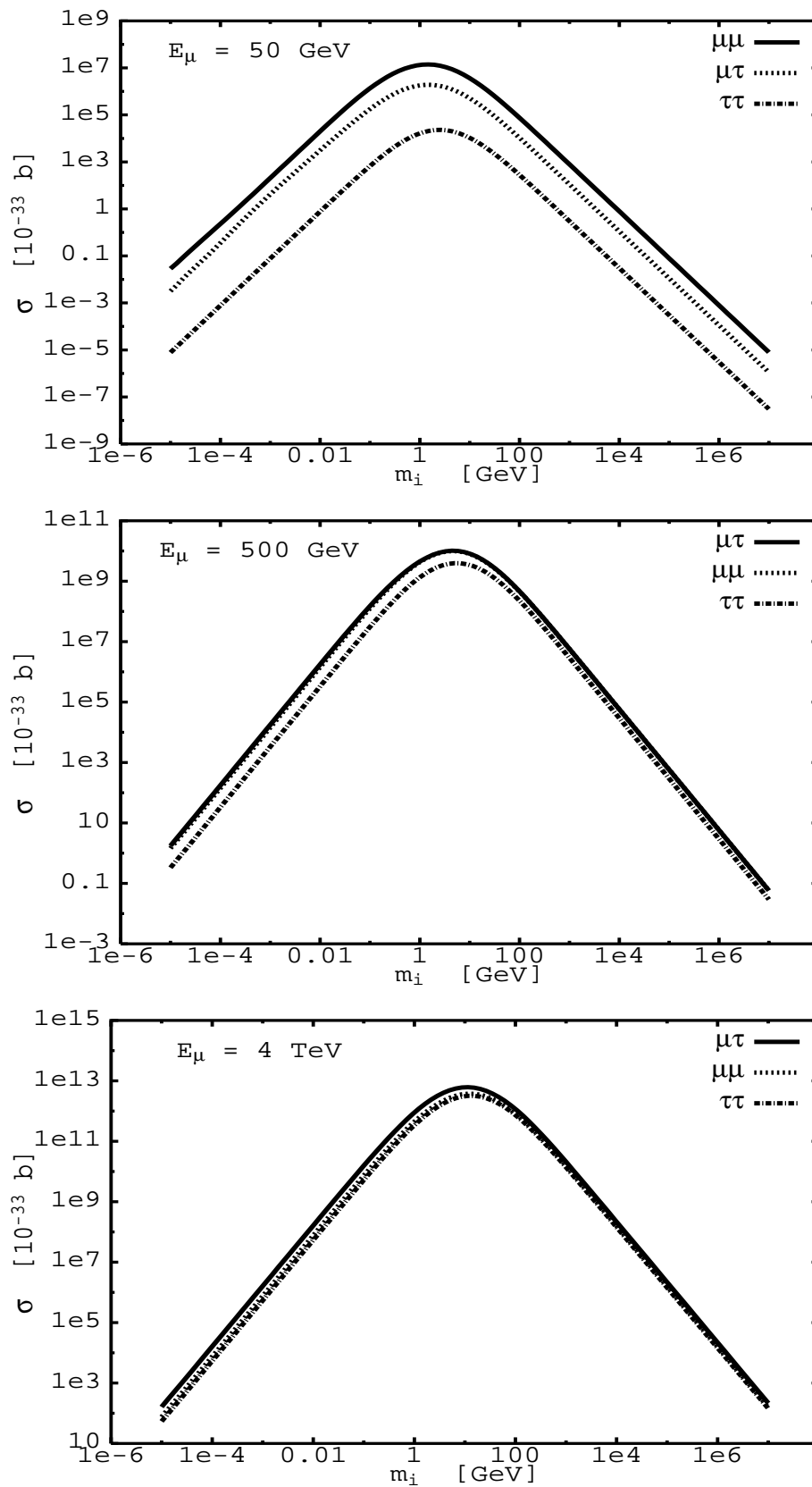


Figure 3.8: Total cross section for the reaction $\nu_\mu N \rightarrow \mu^- \alpha^+ \beta^+ X$ with the $\mu\mu$, $\mu\tau$ and $\tau\tau$ final states for three different muon energies. No limit on $U_{\mu i}$ was applied.

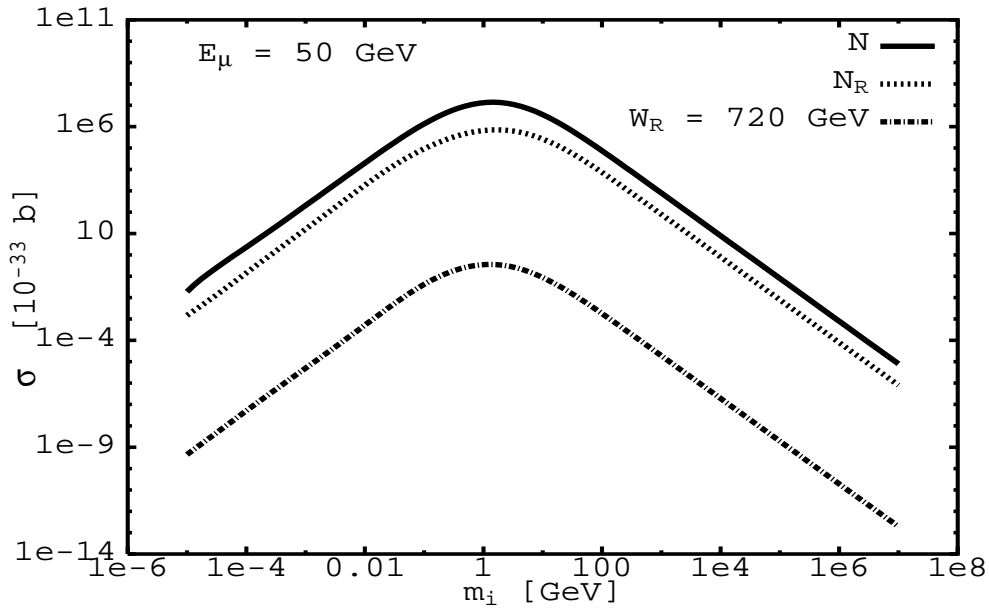


Figure 3.9: Total cross section for $\nu_\mu N \rightarrow \mu^- \mu^+ \mu^+ X$ as a function of the Majorana mass for a μ^- energy of 50 GeV and different possible realizations of the process. N is a left-handed, N_R a right-handed Majorana and W_R denotes the process with a right-handed W boson and a left-handed Majorana. No limits on $U_{\mu i}$ are applied.

3.3.1 Properties of neutrino factories

Several proposals for a muon storage ring have been discussed, the number of expected neutrino interactions differs. The formula used for the luminosity in units of $\text{cm}^{-2} \text{s}^{-1}$ is [104]

$$\mathcal{L}' = N_A f N_\mu l, \quad (3.28)$$

where N_A is the Avogadro number, N_μ the number of muons injected in the ring per second, f the fraction of the collider ring occupied by the production straight section and l the mass depth of the target in g cm^{-2} . Typical numbers are $f = 0.02$, $l = 1000 \text{ g cm}^{-2}$ and $N_\mu = (10^{12} \dots 10^{14}) \text{ s}^{-1}$. Let us be optimistic and assume $N_\mu = 10^{14} \text{ s}^{-1}$ with a “year” of 10^7 s running time. With this parameter set one gets $\mathcal{L} = 10^{46} \text{ cm}^{-2}$ integrated luminosity. The neutrinos from the μ -decay will all end inside the detector since their opening angle is just $\theta \simeq 1/\gamma_\mu = m_\mu/E_\mu$. Typical distances between detector and muon ring are 10^2 to 10^3 m , discussed energies go up to 10^6 GeV . A complete scope of all possible options is not our aim. If definite plans for experiments and machines are made, our results can easily be rescaled with the help of relation (3.28).

3.3.2 Experimental considerations

Because of the smallness of the cross section of the process discussed here, one might ask if SM processes exist, which fake the signal. A discussion of this kind has already been done for trimuon production in conventional $\nu_\mu N$ scattering in Section 3.2.3.

The “normal” trimuon production in $\nu_\mu N$ scattering has a $(-++)$ signature. Due to the principle creation of conventional neutrino beams by using pion- and kaon-decays, there is always a “ $\bar{\nu}_\mu$ -pollution” in the beam which can give a $(-++)$ signal through muon pair production, be it radiatively or in the hadronic final state via e.g. vector meson production. These effects exist on the level of maximally 10^{-5} of the total observed charged current events. Kinematical cuts to suppress this background, e.g. using the invariant mass or angular isolation have been developed. For previous experiments however, it was found that for trimuon production via Majorana neutrinos the signal-to-background ratio is far too small.

Nevertheless, for a muon storage ring we know exactly what neutrino flavor is in the initial state and thus in the case of μ^- -decay there is no SM process to give a $(-++)$ event. The only exception is $\nu_\mu N \rightarrow \mu^- e^+ \mu^+ X$ which might be faked by a $\bar{\nu}_e$ CC event with $\mu^+ \mu^-$ production in the jet or via bremsstrahlung. However, as shown, final states with electrons cannot be expected due to the severe limits from $0\nu\beta\beta$. Because of the $\nu_\mu \bar{\nu}_e$ or $\bar{\nu}_\mu \nu_e$ structure of the beam, ratios between observed types of events (coming from each neutrino species) could be used to establish a signal. Also polarization of the muon beam could be useful because it allows to change the neutrino spectra and therefore the event ratios in a predictable way. Possible channels involving τ leptons in the final state might be investigated by topological and kinematical methods as used by CHORUS and NOMAD.

Up to now we ignored in this section effects of neutrino oscillations. An incoming $\bar{\nu}_e$ could oscillate into a $\bar{\nu}_\mu$ and create via the aforementioned processes a $(-++)$ signal. The relevant oscillation parameters are now given by atmospheric ($\Delta m^2 \simeq 10^{-3} \text{ eV}^2$) and CHOOZ ($\sin^2 2\theta \lesssim 0.2$) data. Integrating the CC cross section of the $\bar{\nu}_e$ over a two-flavor formula and taking also into account the trimuon suppression factor 10^{-5} , yields numbers smaller than the ratio of process (3.26) with the (CC + NC) cross section by at least two orders of magnitude, even for a $L = 1 \text{ km}$ and $E_\mu = 50 \text{ GeV}$ option of the experiment.

For the other final states there is no SM background: Typical events with additional leptons are production of gauge bosons, which however are always accompanied with neutrinos or extra jets and thus in principle distinguishable.

E_μ	$\frac{\sigma_{\mu\mu}}{\sigma_{CC+NC}}$	$\frac{\sigma_{\mu\tau}}{\sigma_{CC+NC}}$	$\frac{\sigma_{\tau\tau}}{\sigma_{CC+NC}}$	N^{CC+NC}
50	$1 \cdot 10^{-20}$	$7 \cdot 10^{-21}$	$7 \cdot 10^{-22}$	$4 \cdot 10^9$
100	$1 \cdot 10^{-19}$	$1 \cdot 10^{-19}$	$7 \cdot 10^{-20}$	$8 \cdot 10^9$
200	$7 \cdot 10^{-19}$	$2 \cdot 10^{-18}$	$2 \cdot 10^{-18}$	$2 \cdot 10^{10}$
300	$3 \cdot 10^{-18}$	$7 \cdot 10^{-18}$	$1 \cdot 10^{-17}$	$2 \cdot 10^{10}$
400	$7 \cdot 10^{-18}$	$2 \cdot 10^{-17}$	$4 \cdot 10^{-17}$	$4 \cdot 10^{10}$
500	$1 \cdot 10^{-17}$	$4 \cdot 10^{-17}$	$7 \cdot 10^{-17}$	$4 \cdot 10^{10}$
10^3	$7 \cdot 10^{-17}$	$4 \cdot 10^{-16}$	$7 \cdot 10^{-16}$	$8 \cdot 10^{10}$
$2 \cdot 10^3$	$7 \cdot 10^{-16}$	$3 \cdot 10^{-15}$	$7 \cdot 10^{-15}$	$1 \cdot 10^{11}$
$4 \cdot 10^3$	$5 \cdot 10^{-15}$	$2 \cdot 10^{-14}$	$5 \cdot 10^{-14}$	$2 \cdot 10^{11}$
10^4	$4 \cdot 10^{-14}$	$2 \cdot 10^{-13}$	$5 \cdot 10^{-13}$	$5 \cdot 10^{11}$
10^5	$2 \cdot 10^{-12}$	$1 \cdot 10^{-11}$	$2 \cdot 10^{-11}$	$3 \cdot 10^{12}$
10^6	$4 \cdot 10^{-11}$	$8 \cdot 10^{-10}$	$4 \cdot 10^{-10}$	$8 \cdot 10^{12}$

Table 3.2: Maximal ratio of $\nu_\mu N \rightarrow \mu^- \alpha^+ \beta^+ X$ and sum of CC and NC for ν_μ for different final states and muon energies in GeV. Indirect bounds on mixing matrix elements are applied. The last column displays the expected number of (CC + NC) events from ν_μ with the parameter set given in Section 3.3.1.

3.3.3 Is it observable?

Unfortunately, the bounds on neutrinos and their mixing severely restrict the prospects of detecting a signal from $B - L$ violating mass terms at the discussed experiments. For example, let us consider a 4 TeV muon source and the $\mu\mu$ channel. The maximum cross section is achieved for a mass eigenstate of about 10 GeV, $\sigma_{\mu\mu}(m_i \simeq 10 \text{ GeV}) \simeq 10^{-20}$ b. A few years of running with an integrated luminosity of $\mathcal{L} \simeq 10^{46}$ cm⁻² per year could establish an observation. However, for the minimal allowed mass of 90.7 GeV, the cross section reduces to $\sigma_{\mu\mu}(m_i = 90.7 \text{ GeV}) \simeq 1.7 \cdot 10^{-21}$ b, which is then further suppressed by the $U_{\mu i}$ limit to $6.3 \cdot 10^{-26}$ b.

Roughly the same numbers hold for the ee channel, and for the $e\mu$ channel about three times this number. However, for these channels the value from Eq. (2.9) comes into play: Assuming one mass eigenstate of 89.5 GeV one gets $U_{ei}^2 < 9.9 \cdot 10^{-7}$, resulting in $\sigma_{ee}(m_i = 89.5 \text{ GeV}) \simeq 10^{-33}$ b. The cross section stays constant till $m_i = 6 \cdot 10^5$ GeV and scales with m_i^{-2} for larger masses. For the $e\mu$ and $e\tau$ channel the cross sections are $\sigma_{e\mu} \simeq 2 \cdot 10^{-31}$ b/ m_i [GeV] and $\sigma_{e\tau} \simeq 8 \cdot 10^{-31}$ b/ m_i [GeV], respectively. Again it was shown that electron final states of processes like (3.26) provide no real chance for observation.

Now we investigate possible event numbers: to be independent on the concrete values of the experimental parameters we calculate the ratio of our process with the

usual charged and neutral current (NC) cross sections. The well known formulas for deep inelastic neutrino–nucleon scattering (see, e.g. [105]) are integrated over the energy spectrum (3.27) with the GRV 92 and 98 [92,106] parton distributions including c and b quark contributions. The maximal value of the Majorana neutrino process is obtained with the minimal allowed value of m_i from Eq. (3.18) and the maximal value of $|U_{\alpha i}|^2$ from Eq. (3.16). With this we give the maximal ratio, shown in Table 3.2. We considered only the muonic and tauonic final states and took for the $\mu\tau$ channel the value $m_i = 90.7$ GeV. The last column gives the number of ν_μ (CC + NC) events with the parameter set given after Eq. (3.28). Only the highest discussed energies, more than $E_\mu = 10^4$ TeV, provide a chance for observation. However, the realization of this kind of machine remains doubtful, but might be realized in a form of a new high–energy physics laboratory [107]. In addition, the masses that may be probed (maximally a few 100 GeV) lie below the ones that are accessible in linear colliders, i.e. there will be information on this mass range before such a high–energy muon storage ring is build.

Though the numbers are no reason to be overoptimistic, the same final state we discussed might have contributions from other channels as the ones plotted in Fig. 3.9. For $0\nu\beta\beta$ many limits on beyond–SM parameters were derived, see [57] for a review. A simple estimation shows the power of such a neutrino factory: For a 4 TeV energy and a 100 keV neutrino, the cross section is about 10^{-29} b. Other contributions might not need a helicity flip and are thus larger by roughly a factor of $(E/m_i)^2 \simeq 10^{13}$, where E is the energy of the Majorana neutrino. With the mentioned 10^{39} cm $^{-2}$ s $^{-1}$ luminosity we would have 10^6 events per year, a “new–physics factory”. The process considered here is then a relevant background signal.

3.4 Positron–proton scattering at HERA

The HERA collider can produce intermediate Majorana neutrinos via the reaction [3]

$$e^+p \rightarrow \bar{\nu}_e \alpha^+ \beta^+ X, \text{ with } (\alpha, \beta) = (e, \tau), (\mu, \tau), (\mu, \mu) \text{ and } (\tau, \tau), \quad (3.29)$$

where the electron and proton energies are $E_e = 27.5$ GeV and $E_p = 820$ GeV, respectively. We demand the taus to decay into muons to take advantage of the like–sign lepton signature, which is more unique for muons than electrons. It is evident that such a process has a spectacular signature with large missing transverse momentum (\cancel{p}_T) and two like–sign leptons, isolated from the hadronic remnants.

Direct production of heavy Majoranas N at HERA has been studied before [108] with the process $e^-p \rightarrow XN \rightarrow XW^\pm\alpha^\mp \rightarrow X\nu\beta'^\pm\alpha^\mp$ resulting in two leptons with opposite charge. A discovery limit of about 160 GeV was derived, as long as the Majorana decays into e^+W^- , giving an isolated lepton with different charge than the incoming one. One might argue that this direct Majorana production is more likely to occur since the cross section is larger³. However, due to its unique signature we believe that the process under study deserves some attention. In addition, the limit (2.9) from $0\nu\beta\beta$ has not been applied to the analysis in [108] and a general analysis of all channels ($N \rightarrow \nu Z$, $N \rightarrow \mu W$, ...) remains still to be done. It might be interesting to compare the results of such an analysis with ours in the future.

Until that is done, we also think that process (3.29) is worth considering, inasmuch as we have no restriction to the flavor of the final state lepton and because of its unique signature. The connection of the observation of the signal under study with a Majorana mass term is depicted in Fig. 3.10.

3.4.1 Analysis and results

One should pay more attention to the experimental reality, therefore we include some cuts on the observables, namely $|\eta_{l,X}| \leq 2.0$ and $|\cancel{p}_T| \geq 10$ GeV. Here $|\cancel{p}_T| = \sum \sqrt{(\sum p_x^\nu)^2 + (\sum p_y^\nu)^2}$ is the total missing transverse momentum, with the sum going over all neutrinos, i.e. one neutrino for the $(\mu\mu)$, three for the $(e\tau)$ and $(\mu\tau)$ and five for the $(\tau\tau)$ case. The pseudorapidity of the charged lepton l and the hadronic final state X is $\eta_{l,X} = -\ln \tan(\theta_{l,X}/2)$, where $\theta_{l,X}$ is the polar angle in a system where the z -axis is parallel to the proton direction. In addition, we want the charged leptons to be isolated from the hadrons and demand $\Delta R = \sqrt{(\phi_l - \phi_X)^2 + (\eta_l - \eta_X)^2} > 0.5$ with ϕ being the azimuthal angle.

³Only one coupling U_{ei} is needed in the matrix element.

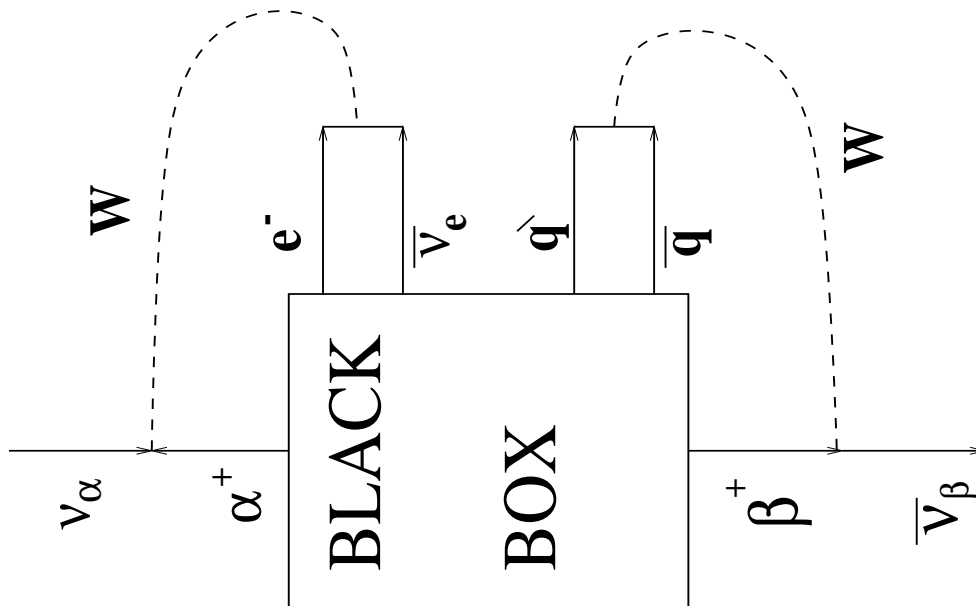


Figure 3.10: Connection between Majorana mass term of ν_α and ν_β and the existence of process $e^+p \rightarrow \bar{\nu}_e \alpha^+ \beta^+ X$.

In Fig. 3.11 the total cross section as a function of *one* mass eigenvalue is shown for all combinations of final state charged leptons, without applying the above mentioned $U_{\alpha i}$ limits. The condition that the tau decays into a muon is included. The masses of the final state leptons have almost no effect (less than 5 %), so that the only numerical difference comes from the branching ratios, the $U_{\alpha i}$ limits from Eq. (3.16) and the above mentioned statistical factor for the $(e\tau)$ and $(\mu\tau)$ cases.

These limits combined with the tau branching ratio ($\text{BR}(\tau \rightarrow \mu\nu_\mu\nu_\tau) = 0.1732$ [85]) lead to a maximal cross section of about 10^{-23} b in the $(\mu\mu)$ case for a neutrino mass of 80 GeV. It is about 12 orders of magnitude smaller than the SM charged current e^+p cross section of $\sigma_{\text{CC}}(e^+p, Q^2 > 200 \text{ GeV}^2) \simeq 30$ pb [109] (it was checked that the Q^2 condition is not significantly violated for the applied cuts). Nevertheless the above cross section is some orders of magnitude closer to the relevant SM CC process than most other exotic Majorana neutrino induced $\Delta L = 2$ processes such as $K^+ \rightarrow \pi^- \mu^+ \mu^+$ [93, 110] or $\mu^- \mu^+$ -conversion via muon-capture in ^{44}Ti [94]. These have ratios with respect to the relevant SM CC process of at most 10^{-20} . According to Section 3.2, for trimuon production $\nu_\mu N \rightarrow \mu^- \mu^+ \mu^+ X$ a ratio of 10^{-17} for a 500 GeV neutrino beam was achieved, so the process described here results in an improvement of another five orders of magnitude. The other cases, like $(\tau\tau)$, have ratios with respect to the SM CC process maximally one order of magnitude smaller than the $(\mu\mu)$ case.

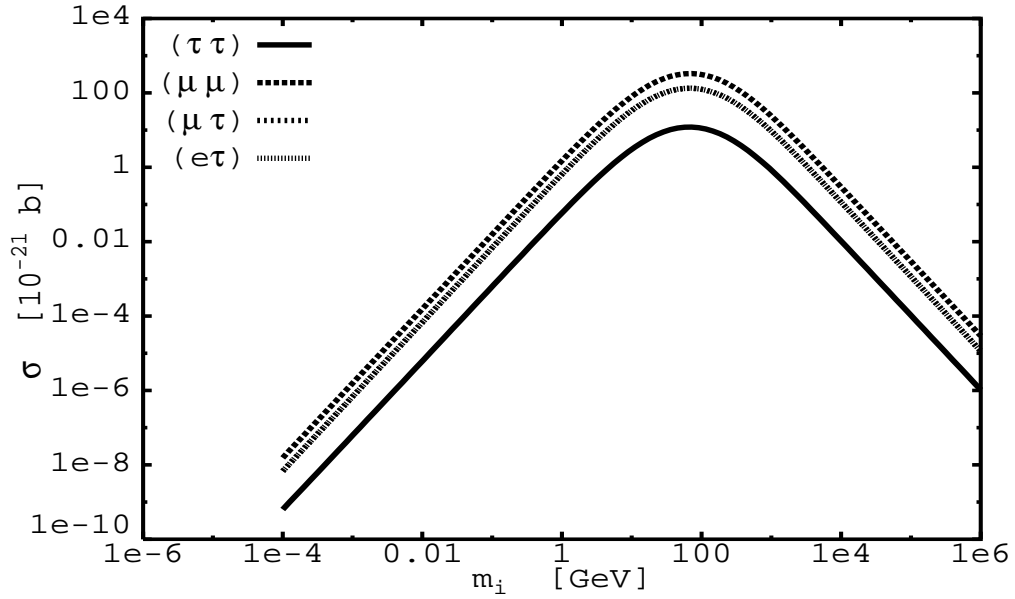


Figure 3.11: Total cross section for $e^+p \rightarrow \bar{\nu}_e \alpha^+ \beta^+ X$ as a function of *one* eigenvalue m_i . No limits on $U_{\alpha i}$ are applied, the branching ratio for taus into muons is included. The $(e\tau)$ and $(\mu\tau)$ cases are indistinguishable in this plot.

As an example for differential cross sections we plot in Fig. 3.12 for $m_i = 80$ GeV the distribution of the missing transverse momentum for the $(\mu\mu)$, $(\mu\tau)$ and $(\tau\tau)$ case. The limits on $|U_{\alpha i}|^2$ from Eq. (3.16) are applied. Note that all these cases have two like-sign muons in the final state. The mean values are $\langle p_T \rangle \simeq 28.3, 37.0$ and 37.3 GeV, respectively. The shape is different for each case, despite the similar mean value of missing transverse momentum. To distinguish, say, $(\mu\tau)$ from $(\tau\tau)$ events, one should consider other distributions, e.g. the invariant mass of the two muons, $m(2\mu)$, as displayed in Fig. 3.13. Whether a muon comes directly from the Majorana vertex or from the tau-decay decreases its energy and momentum fraction of the total available energy and alters also its invariant mass. Here the mean values are $\langle m(2\mu) \rangle \simeq 66.8, 28.1$ and 16.1 GeV, for $(\mu\mu)$, $(\mu\tau)$ and $(\tau\tau)$, respectively. Unfortunately, this procedure requires high statistics. On an event-by-event analysis detailed kinematic reconstruction as well as angular distributions might be more useful, see the next section.

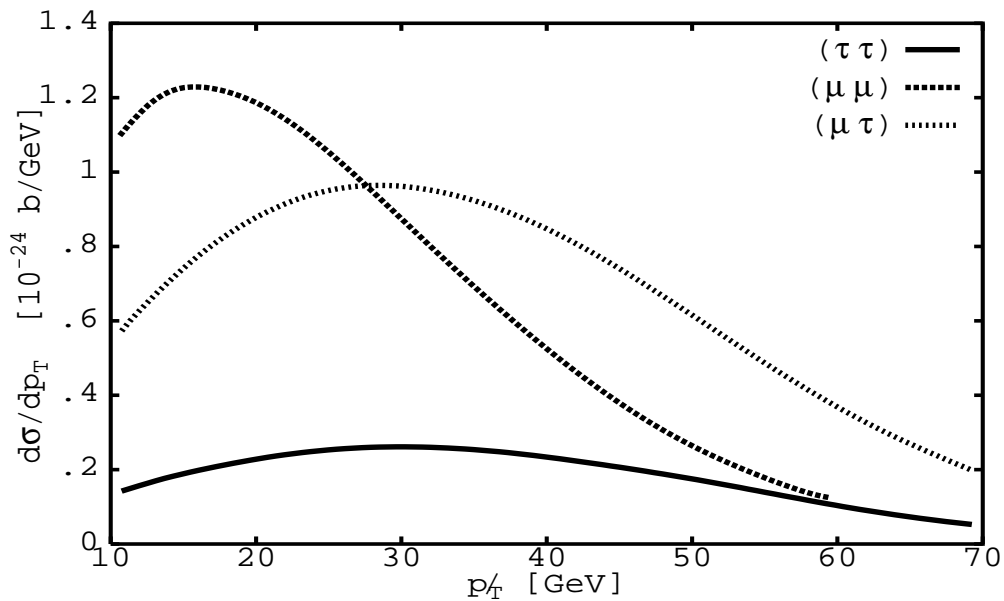


Figure 3.12: Distribution of the total missing transverse momentum p_T for the $(\mu\tau)$, $(\mu\mu)$ and $(\tau\tau)$ case in the reaction $e^+p \rightarrow \bar{\nu}_e \alpha^+ \beta^+ X$ for $m_i = 80$ GeV. The tau branching ratio is not included, the limits on $|U_{\alpha i}|$ are applied.

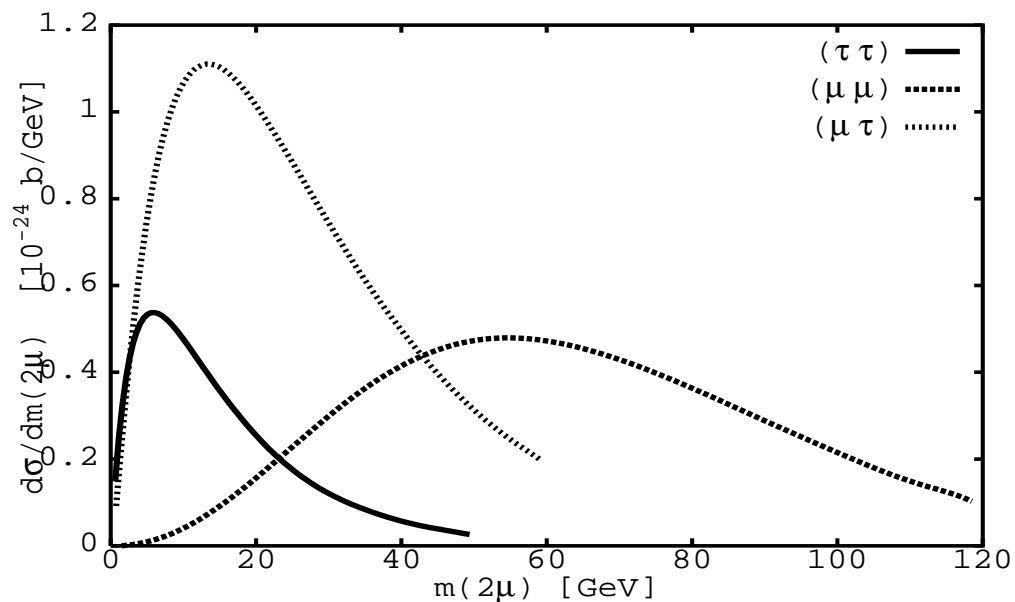


Figure 3.13: Invariant mass distribution for the two like-sign muons given for the same parameters as in the previous figure.

3.4.2 Experimental considerations

Because of its lepton number violating character the discussed process should be background free from SM processes. On the other hand, misidentification of the muon charge might create some like-sign dimuon events. The charge of the LSD corresponds to the one of the incoming lepton. Processes producing opposite sign muon pairs are pair production of heavy quarks, photon-photon interactions, Z -boson production, Drell-Yan pairs from resolved photon-proton interactions, pion punchthrough associated with a single muon event and beam related background.

However, the identification of two like-sign, isolated muons with large p_T in addition to a large missing transverse momentum should indeed be an outstanding signature. At present, no such signal has been observed yet. The observation of such a signature would imply a Majorana mass term, as shown in Fig. 3.10. For the $(e\tau)$ channel, which has a like-sign $e\mu$ signature, single W production [111] is a severe background. However, channels with electrons in the final state will not be observable anyway. Because of this we shall assume zero background. In case of observation a detailed analysis has to be done anyway in order to rule out any of the Standard Model processes as the ones described above. In the next section such an analysis will be performed for a different final state, using realistic cuts and observables.

3.5 HERA's isolated leptons and heavy Majorana neutrinos

One of the anomalies in current high-energy data is the existence of high p_T isolated leptons together with large missing transverse momentum (\cancel{p}_T) at HERA. Since the first event [112] was discovered by H1, five more were found [113] and at least three of them can probably not be explained by W production or other SM processes. To be precise, these five events (found by using 36.5 pb^{-1} integrated luminosity) are now accompanied by four more. However, regarding these four new events, only a conference report is available [114], without many details, so that only the first four will be used in the following analysis. In contrast to H1, ZEUS sees no excess in these events [115], however, at the present statistical level, there is no contradiction [116].

In the last section the process

$$e^+p \rightarrow \bar{\nu}_e \alpha^+ \beta^+ X \text{ with } \alpha, \beta = e, \mu, \tau \quad (3.30)$$

was examined and possible signals of this LSD and high \cancel{p}_T final state were discussed. However, it turns out that when the kinematical cuts used in H1's search for isolated leptons are applied to our process (3.30), they tend to ignore one of the two leptons [4]. Especially the requirement of $p_T > 10 \text{ GeV}$ is often too much for both charged leptons to fulfill. The LSD signal of Eq. (3.30) is thus reduced to *one* isolated lepton with high \cancel{p}_T .

This possibility can be checked by looking for an additional isolated low p_T and/or high pseudorapidity lepton. In addition, it is possible that a produced τ decays hadronically, resulting also in single lepton final states. More than one isolated jet would be a signal for this kind of event. Since process (3.30) gives LSD with the same sign as the incoming lepton we concentrate on H1's positive charged muon events, since there are no positron events found. This fact might be explained if one incorporates also the limit Eq. (2.9) on mixing of heavy neutrinos, as derived from $0\nu\beta\beta$. With this constraint the expected e signal is smaller than the μ signal.

A few words on finite width effects: Eq. (3.15) can be applied to calculate the width of the Majorana, which is dominated by the two-body decays $N \rightarrow W\alpha$ and $N \rightarrow Z\nu_\alpha$, one finds

$$\begin{aligned} \Gamma(N) = \sum_{\alpha} \frac{G_F \sin^2 \theta_{\alpha}}{8\pi\sqrt{2}M_N^3} \left\{ \left[(M_N^4 - M_W^4) + M_W^2(M_N^2 - M_W^2) \right] (M_N^2 - M_W^2) \right. \\ \left. + \cos^2 \theta_{\alpha} \left[(M_N^4 - M_Z^4) + M_Z^2(M_N^2 - M_Z^2) \right] (M_N^2 - M_Z^2) \right\}, \end{aligned} \quad (3.31)$$

where $\sin^2 \theta_{\alpha} = \sum |U_{\alpha i}|^2$. Finite (W and N) width effects were included in the program and found to be negligible.

The statistical peculiarity mentioned in Section 3.3 is refined when different tau decays are considered. For example, consider the $\tau\tau$ case and let the taus decay into different particles (e.g. $e\nu\nu$ and $\mu\nu\nu$). There is no way to tell into what the “upper” or “lower” tau decays, so one has to include both cases. This means that alone from the $\tau\tau$ state, four diagrams contribute the μe signal. The cross section from this case has to be added to the “pure” μe final state, the $e\tau$ case when the tau decays into μ and so on.

In contrast to the signal in neutrinoless double beta decay experiments (two electrons with constant sum in energy) the identification of this process will be very difficult and deciding which $\alpha\beta$ final state was originally produced remains a hard task. In addition, the number of expected events turns out to be far less than one. Nevertheless, the analysis represents a nice explanation of a yet not understood anomaly and is worthwhile considering.

3.5.1 Two become one

The same cuts as H1 in their search for isolated leptons were applied:

- Imbalance in transverse momentum $\not{p}_T \geq 25$ GeV
- Transverse momentum of lepton $p_T \geq 10$ GeV
- Pseudorapidity of lepton $|\eta| \leq 2.436$
- Distance between charged lepton and closest jet in η - ϕ space, $\Delta R \geq 1.5$ where ϕ is the azimuthal angle⁴
- Angle of the hadronic jet(s) $4^\circ \leq \theta^X \leq 178^\circ$

This has to be compared with the cuts in Section 3.4, $\not{p}_T \geq 10$ GeV, $|\eta| \leq 2.0$ for all measured particles and $\Delta R \geq 0.5$ between the charged leptons and the hadronic remnants. It turns out that both sets of cuts deliver cross sections in the same ballpark.

There are now two possibilities for the original LSD signal to appear as one single lepton:

1. One lepton can have high pseudorapidity and/or low p_T . This lepton then also contributes to the missing transverse momentum.
2. If one tau is produced it might decay hadronically, adding one neutrino to the imbalance in p_T and also additional hadronic jets.

⁴Actually H1’s value is 1.0 or 0.5, depending on the way they define jets for their respective analysis. We use a general value of 1.5 to account for hadronization effects.

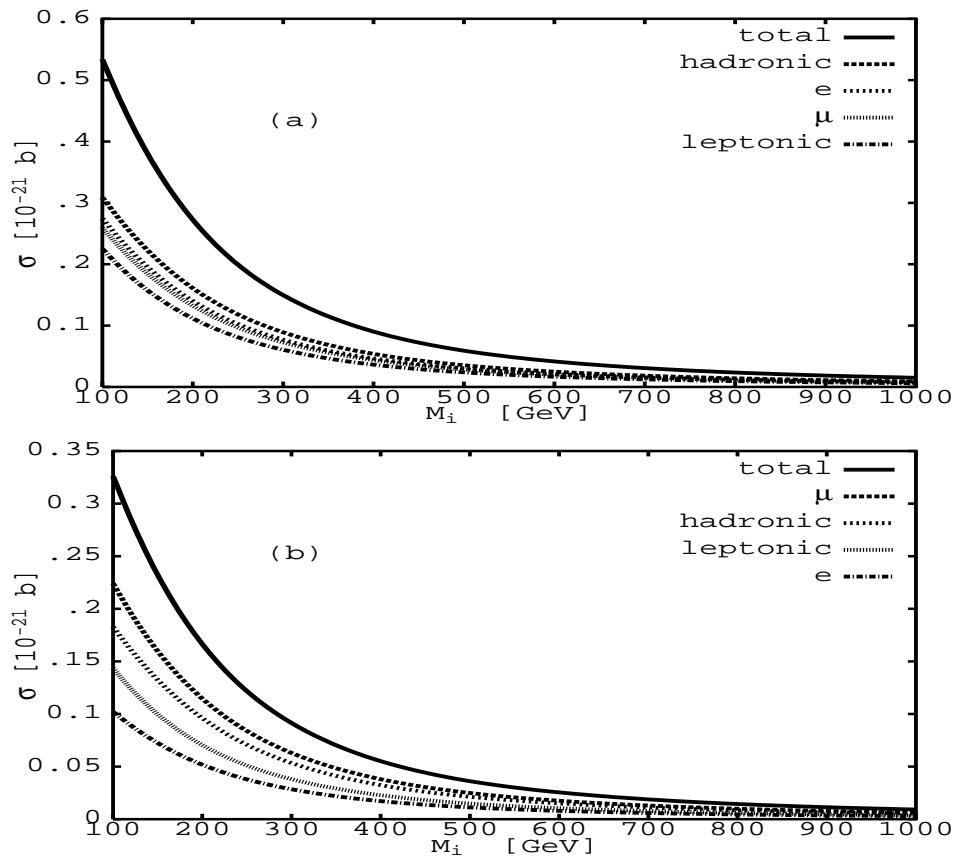


Figure 3.14: Cross section of the expected isolated lepton signal from all possible final states as a function of the Majorana mass m_i . Part (a) shows the composition before, part (b) after applying the limit from $0\nu\beta\beta$ on heavy neutrinos.

A detailed analysis of the LSD signal might be done if one finds such events.

Collecting all possibilities for the $\alpha\beta$ final states and the τ decays results in Fig. 3.14a. We denote with “hadronic” the signal coming from final states which also have additional hadronic activity from a τ decay. Signals are “leptonic” when they stem from events in which two final state leptons are produced from which one escapes the identification criteria. Those include therefore most channels, namely all of them except the ones with hadronic tau decay. One can see that muon events have a smaller cross section than the e signal, coming from the fact that their mixing with the heavy neutrino has the biggest constraint. Mass effects play no significant role.

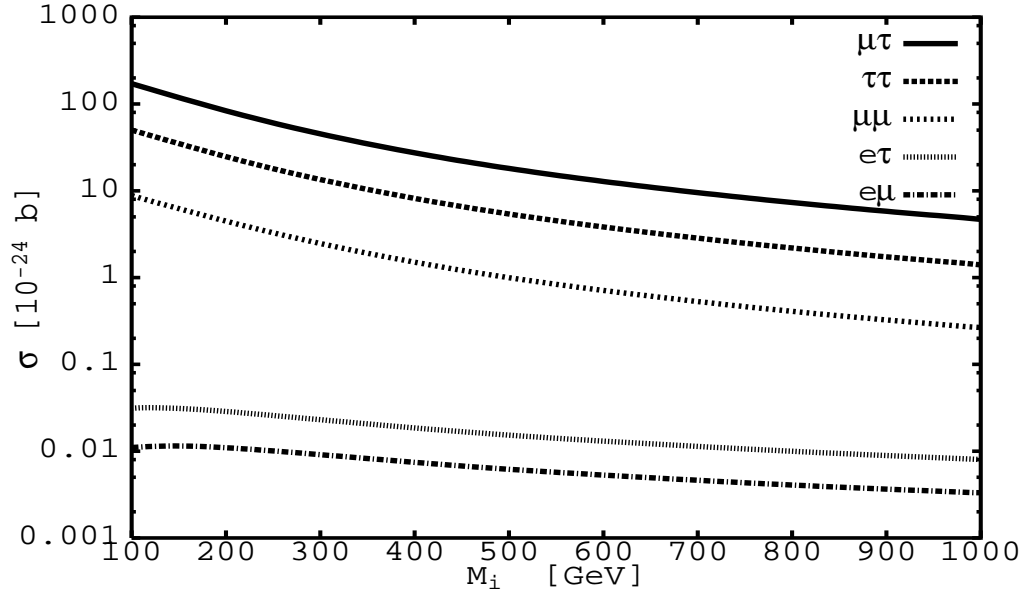


Figure 3.15: Contribution of the different final states to the cross section of the muon signal as a function of the Majorana mass m_i .

If the H1 anomaly is indeed explained by heavy Majorana neutrinos, one might ask why only muon events are detected. A possible reason for that might lie in the fact that the constraint from $0\nu\beta\beta$ on mixing with a heavy Majorana neutrino which reads⁵

$$U_{ei}^2 \leq 5 \cdot 10^{-8} \frac{m_i}{\text{GeV}}. \quad (3.32)$$

Incorporating this in Fig. 3.14a gives Fig. 3.14b. Now the electron signal is far below the muon signal. In Fig. 3.15 we plot how the cross section for the production of a μ is composed. The biggest contribution comes from the $\mu\tau$ channel, which has its reason in the mentioned factor $\simeq 3$ relative to the $\alpha\alpha$ channels and the high hadronic tau branching ratio, $\text{BR}(\tau \rightarrow \nu_\tau \text{ hadrons}) \simeq \frac{2}{3}$. An additional reason why the $\tau\alpha$ channels deliver a large contribution is that when the tau decays it distributes its momentum to three particles, i.e. the p_T is in general lower and it can therefore escape the $p_T \geq 10$ GeV cut more easily and thus has a higher cross section. Admittedly, the process gives only a tiny signal: Multiplying the cross section with the 36.5 pb^{-1} luminosity H1 analyzed, gives $10^{-8} \dots 10^{-9}$.

One sees that many LSD signals produce the same single lepton signature. In the next section possibilities to distinguish different original final states from the measured ones are discussed.

⁵The analysis done in [4] and repeated here was performed with this weaker limit for $\langle \frac{1}{m} \rangle$. This however only strengthens our conclusions.

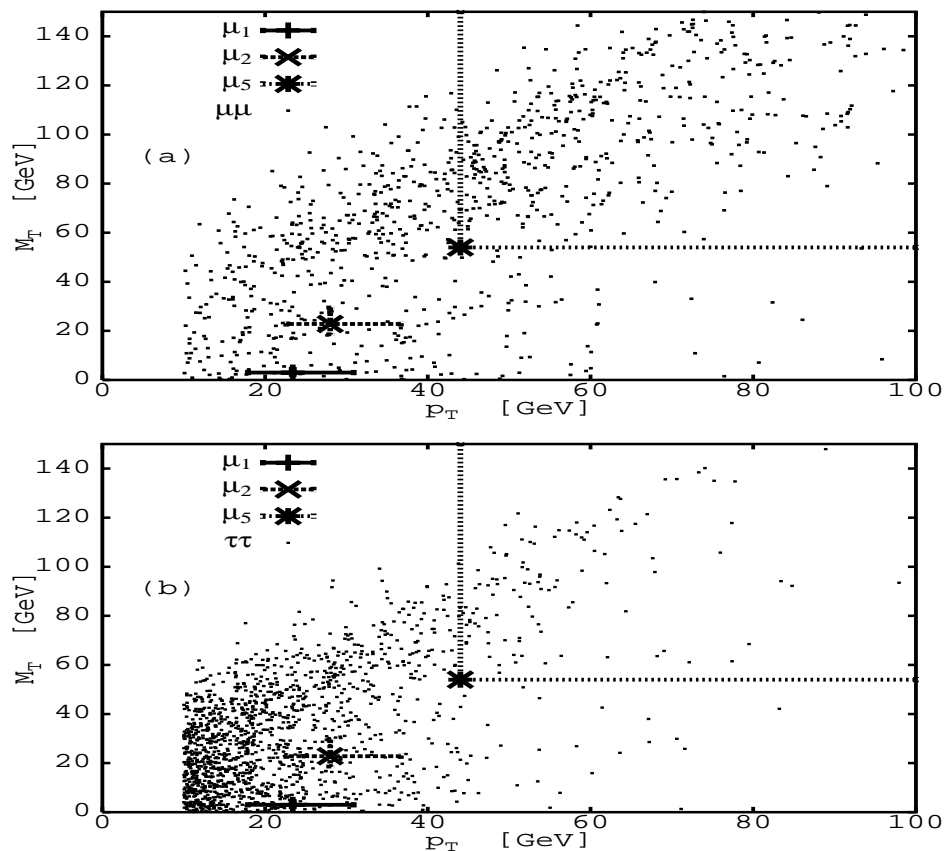


Figure 3.16: Scatter plot of p_T of the measured lepton against M_T for the channels $e^+p \rightarrow \bar{\nu}_e \mu^+ \mu^+ X$ (a) and $e^+p \rightarrow \bar{\nu}_e \tau^+ \tau^+ X$ (b) with one tau decaying hadronically.

3.5.2 Signals and observables

Some kinematic quantities of H1's positive muon events are given in Table 3.3. In the H1 analysis [113] using $36.5 \pm 1.1 \text{ pb}^{-1}$ luminosity at $E_p = 820 \text{ GeV}$ and $E_e = 27.5 \text{ GeV}$, 6 events were found ($0 e^+$, $1 e^-$, $2 \mu^+$, $2 \mu^-$ and 1μ of undetermined charge), where about 2 e and 1 μ are expected from SM processes. From those, the most important ones are W production, NC events (for e^+ events) and photon-photon interactions (μ^\pm). We also include the event with undetermined charge. The e^- and one μ^- events (the latter also includes a e^+) are very likely to stem from W production [112].

In the following we will plot all distributions for $m_i = 200 \text{ GeV}$ since the qualitative conclusions we draw remain valid for all masses considered. In the analysis it turned out that — with the kinematics from Table 3.3 — scatter plots of p_T , \hat{p}_T and the transverse

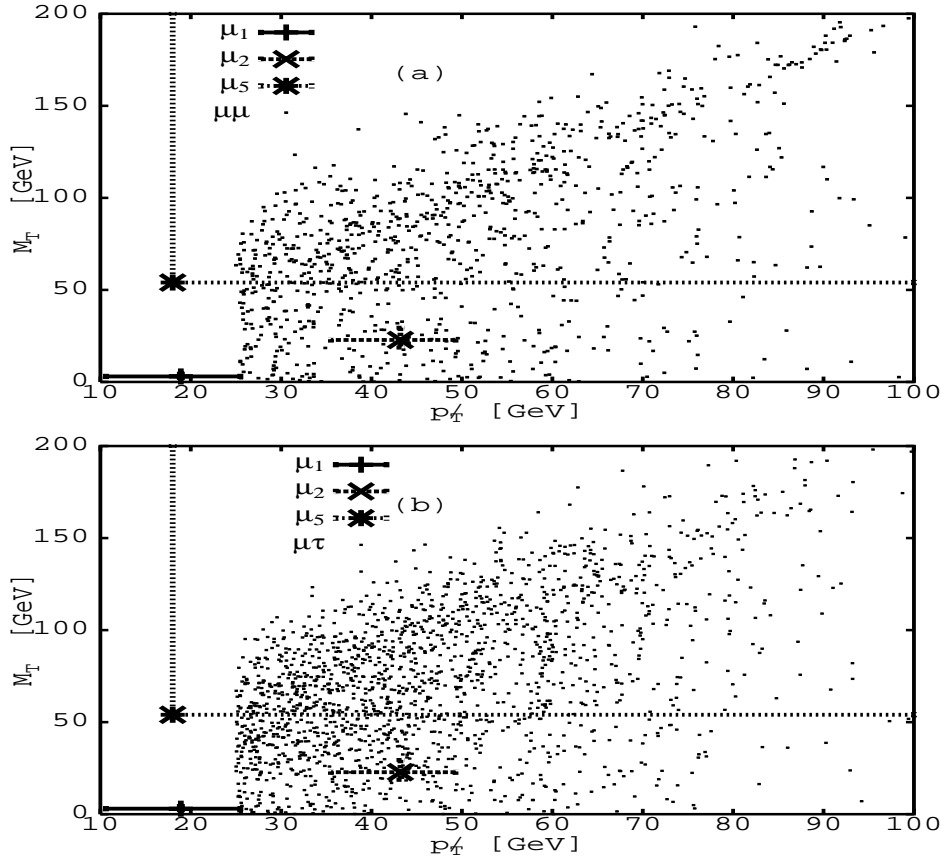


Figure 3.17: Scatter plot of p_T^{miss} against M_T for the channels $e^+p \rightarrow \bar{\nu}_e \mu^+ \mu^+ X$ (a) and $e^+p \rightarrow \bar{\nu}_e \mu^+ \tau^+ X$ (b) with the tau decaying hadronically.

mass $M_T = \sqrt{(p_T^{\text{miss}} + p_T)^2 - (\vec{p}_T^{\text{miss}} + \vec{p}_T)^2}$ are most useful. We stress again that for different final states the composition of the missing transverse momentum can be made of two (for $\mu\mu$ or ee final states) to six (1 lepton and five neutrinos, $\tau\tau$ channel with two leptonic decays) particles, thus changing the area in which events populate, say, the M_T - p_T space.

The transverse momentum is also very sensitive to the original final state since τ decays share the initial momentum to three particles, thereby reducing the average p_T . This is displayed in Fig. 3.16 for the $(\mu\mu)$ and $(\tau\tau, \text{one hadronic decay})$ case. If both taus decay leptonically the distribution looks similar to the one in Fig. 3.16a. Obviously, the $\tau\tau$ case has in general low p_T and M_T , whereas the $\mu\mu$ case displays an uniform distribution with a slight band in the center region indicated.

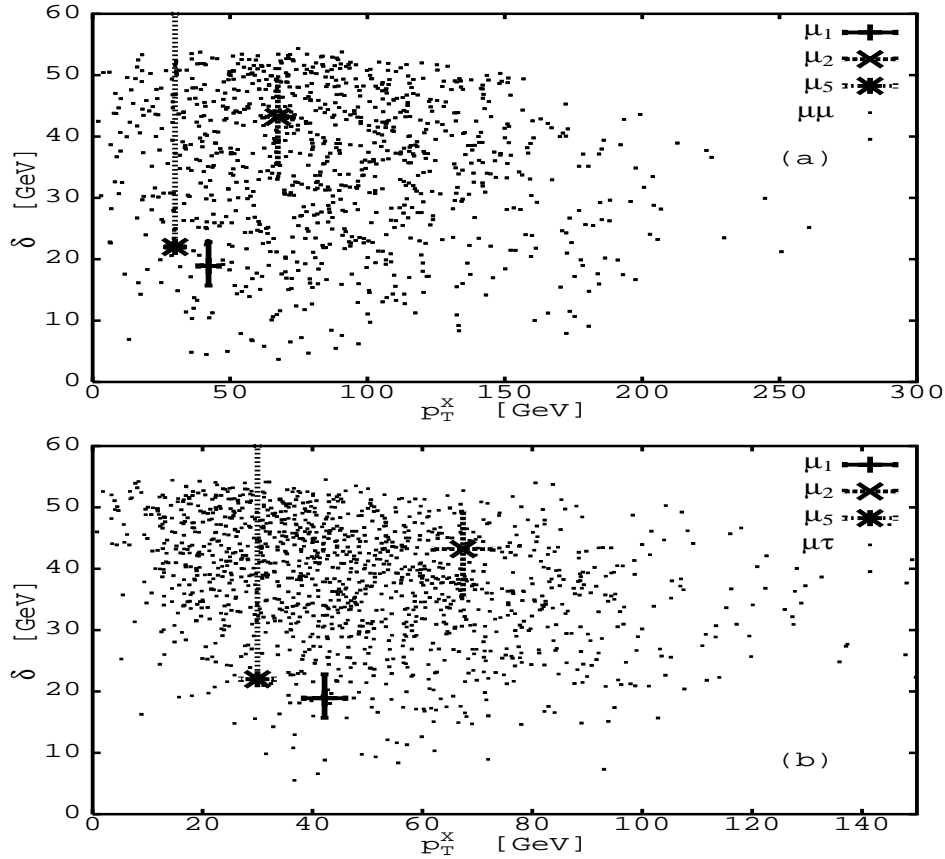


Figure 3.18: Scatter plot of p_T^X against δ for the channels $e^+p \rightarrow \bar{\nu}_e \mu^+ \mu^+ X$ (a) and $e^+p \rightarrow \bar{\nu}_e \mu^+ \tau^+ X$ (b) with the tau decaying hadronically. Note that the p_T^X range is half as wide in part (b).

Turning now to \hat{p}_T we see in Fig. 3.17 for the $(\mu\mu)$ and $(\mu\tau, \text{hadronic decay})$ case that the situation is not as clear in the “mixed” channels, i.e. channels with two different final state charged leptons. Though the population in $\hat{p}_T - M_T$ space is different (lower values in the latter case), the difference is not as obvious as for the $(\mu\mu)/(\tau\tau)$ case. In all figures event μ_1 seems to be disfavored due to its low M_T , however, no definite statement can be made.

Now we consider the quantities connected with the hadronic remnants. We found that the muon signal is composed of roughly 1/3 purely leptonic final states and 2/3 events with additional jets. An interesting quantity is $\delta = \sum E_i(1 - \cos \theta_i)$, where the sum goes over all measured final state particles. In Fig. 3.18 one sees that the presence of three jets keeps δ in more or less the same area whereas the transverse momentum of the hadronic system p_T^X is shifted towards lower values. Also in these plots μ_1 lies in a less crowded area.

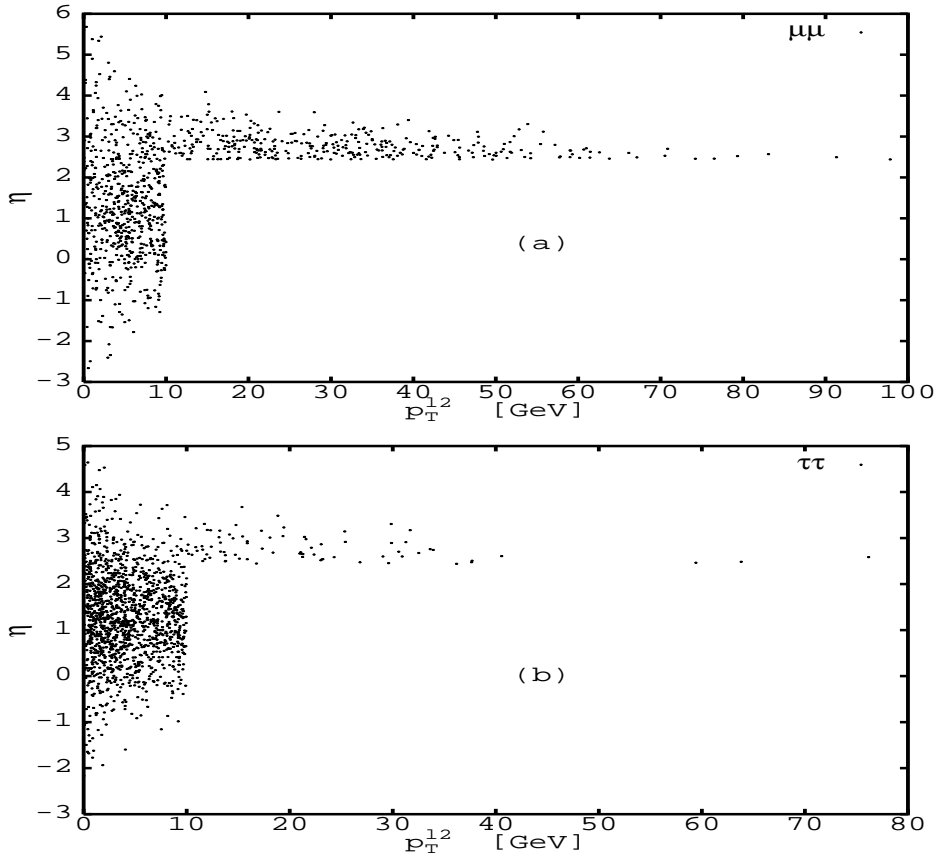


Figure 3.19: Scatter plot of p_T of the escaping charged lepton against its pseudorapidity for the channels $e^+p \rightarrow \bar{\nu}_e \mu^+ \mu^+ X$ (a) and $e^+p \rightarrow \bar{\nu}_e \tau^+ \tau^+ X$ (b) with the tau decaying hadronically. The sharp edge is due to the applied cuts.

What are now the signals of the escaping charged lepton (if there is one)? In Fig. 3.19 we plot the pseudorapidity η of the undetected lepton against its transverse momentum. Again, the $\mu\mu$ and the $\tau\tau$ case can be distinguished since the latter has lower p_T . The τ boosts its decay products more or less in its forward direction so that η does not alter much. Therefore, one would expect rather a low p_T than a high η lepton. The problem one might encounter is that the escaping lepton is hiding in the hadronic jet. Demanding a distance of $\Delta R \geq 1.5$ reduces the cross section by 10 to 15 % but does not change the distributions in Fig. 3.19.

	μ_1	μ_2	μ_5
p_T^l	$23.4^{+7.5}_{-5.5}$	$28.0^{+8.7}_{-5.4}$	> 44
\hat{p}_T	$18.9^{+6.6}_{-8.3}$	$43.2^{+6.1}_{-7.7}$	> 18
M_T	$3.0^{+1.5}_{-0.9}$	$22.8^{+6.7}_{-4.2}$	> 54
δ	$18.9^{+3.9}_{-3.2}$	$17.1^{+2.5}_{-1.7}$	> 22
p_T^X	42.2 ± 3.8	67.4 ± 5.4	30.0 ± 3.0

Table 3.3: Kinematical quantities of H1's candidates for positively charged muon events. Note that the charge for μ_5 is undetermined. All values in GeV, taken from [113]. The limits for μ_5 correspond to 95 % C.L.

We mimicked the hadronic τ decay via two quark jets and ignored effects of modes like $\tau \rightarrow \pi's \nu_\tau$. Thus, due to the boost of the τ , two of the three jets of events with a hadronically decaying tau will be very close together. Fig. 3.20 displays the normalized distribution of the distance in η - ϕ space. We denote with R_i this distance ordered with ascending value. One distance is centered significantly below one, therefore probably two jets instead of three will be measured. However, the τ identification is hard to do and Fig. 3.20 serves only as an indication of how things might work. Information on the jet multiplicity is not given in Ref. [113], though μ_1 and μ_5 seem to have additional separated tracks in their event displays as can be seen in Fig. 2 of Ref. [113].

To sum up, if there is a LSD signal, one lepton can escape the identification criteria by either having low transverse momentum and/or high pseudorapidity or (if it is a τ) via hadronic decay. All of H1's positive muon events lie in the regions typically populated by the "double beta" process, though μ_1 is always in a less crowded area. Due to its high errors μ_5 is mostly in the favored region (but for the same reason always in the region populated by SM processes [113]). Therefore, if the explanation in this section is correct, event μ_2 seems to be the candidate. Since only one hadronic event is observed in μ_2 [113], some leptonic channel is perhaps the source of event μ_2 . From these leptonic channels, the $(\mu\tau)$ and $(\tau\tau)$ channel have the highest cross sections, producing, as Fig. 3.19 indicates, a low p_T lepton, whose pseudorapidity should not be higher than three.

To confirm our hypothesis, direct production of heavy Majorana neutrinos will be the only possibility since cross sections or branching ratios of other $0\nu\beta\beta$ -like processes are probably too small to be detected, see Chapter 4.

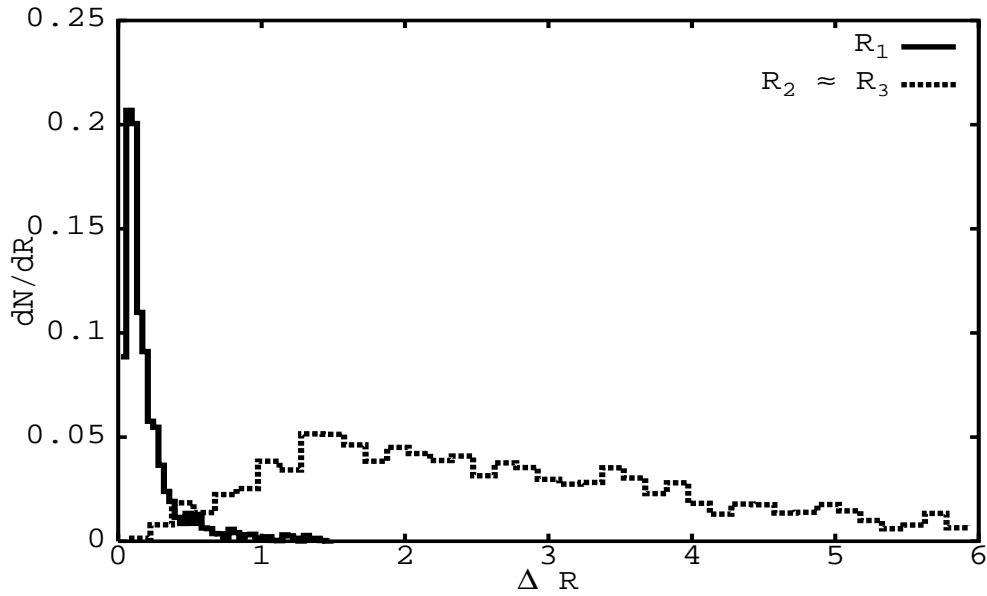


Figure 3.20: Distance of the three jets in η - ϕ space with R_i ordered with ascending value for the process $e^+p \rightarrow \bar{\nu}_e \tau^+ \tau^+ X$ with one τ decaying hadronically.

Other proposed explanations [112] for the events were flavor changing neutral currents interactions (topologically identical to leptoquark production) or high p_T jets from which one fakes a muon signal. Production of supersymmetric particles was suggested in [117] to explain the results. A definite answer regarding all detector/identification issues can only be given by the collaboration itself. From the “new physics” side we believe that — given the overwhelming results on oscillation — massive neutrinos provide one of the most natural possibilities, despite the expected smallness of the signal.

3.6 Summary and final remarks

The production of heavy Majorana neutrinos can be realized in processes analogue to $0\nu\beta\beta$. An extensive study for the Large Hadron Collider (LHC) was recently performed [76], resulting in a discovery limit for the mass of about 250 GeV. Here, as an example for the procedure and calculation of these processes, inverse neutrinoless double beta decay ($e^-e^- \rightarrow W^-W^-$) was studied and the results from [82] rederived. The process renders unobservable for center-of-mass energies below 2 TeV. It was shown for this and the other processes that final states containing electrons are strongly suppressed with respect to the other ones, once one incorporates the bound for heavy neutrinos from $0\nu\beta\beta$.

Two novel analogues of $0\nu\beta\beta$ were presented, neutrino–nucleon scattering [2, 5] and positron–proton scattering at HERA [2, 4]. If compared to previously discussed processes, the obtained cross sections have ratios to the relevant SM processes better by at least two orders of magnitude. Nevertheless, the maximal cross sections are far below experimental access, except for extremely high energies at a neutrino factory. The neutrino masses that may be probed there, will however be investigated experimentally before the construction of such a neutrino factory.

A new phenomenological aspect of positron–proton scattering was discussed, namely the explanation of H1’s events which contain one isolated lepton and large missing transverse momentum. One of the LSD from the $0\nu\beta\beta$ –like process tends to escape the detection criteria and thus produces the observed signature. No positron events were observed, which is explained by the $0\nu\beta\beta$ limit on heavy neutrino mixing. In spite of predicting a tiny event number, the kinematics of the muon events μ_2 and μ_5 seem to be consistent with the proposed explanation, whereas event μ_1 seems to be disfavored. Our proposed signal consists mostly of original ($\mu\tau$) and ($\tau\tau$) states. A low p_T lepton may thus validate our hypothesis.

We end this chapter with remarks on the production of Majorana neutrinos in different reactions. Regarding the next linear collider, the pair production $e^+e^- \rightarrow NN$ produces very few event numbers [118]. Recently it was shown in [119] that for $\sqrt{s} \gtrsim 500$ GeV the “indirect” process $e^+e^- \rightarrow \nu e^\pm W^\mp$ might probe Majorana masses up to the center of mass energy. The same holds for the $e\mu$ option of future colliders via $e^\pm\mu^\mp \rightarrow \nu l^\pm W^\mp$ [120] where also Majorana neutrino pair production will be observable [121]. Processes such as $e^-\gamma \rightarrow \nu_e\alpha^- \beta^+ W^+$ [82] with $\alpha, \beta = \mu, \tau$ or $e^-e^- \rightarrow \mu^-\mu^-$ [122] might also evade the $0\nu\beta\beta$ constraint but require center-of-mass energies in the same region as the ones discussed here. Though these high-energy processes do not suffer from the uncertainty due the calculation of nuclear matrix elements, the signal is in general very small and limited to a small mass range.

Chapter 4

Analogues of $0\nu\beta\beta$ II: Effects of $m_{\alpha\beta}$ and $\frac{1}{m_{\alpha\beta}}$

In the present Chapter the ranges of the remaining five elements of $m_{\alpha\beta}$ are considered. First, in Section 4.1, we estimate the range of the mixing matrix U from fits of atmospheric, solar and reactor data. In Section 4.2 we then study the range of the complete mass matrix $m_{\alpha\beta}$. We apply in Section 4.3 the highest allowed values of $m_{\alpha\beta}$ to some processes, which depend on elements of $m_{\alpha\beta}$ just as $0\nu\beta\beta$ depends on $\langle m \rangle$. Branching ratios or cross sections for these processes are predicted. The fact that only $0\nu\beta\beta$ supplies information and/or restrictions for the two Majorana phases results in an uncertainty for the other elements of $m_{\alpha\beta}$ of one order of magnitude.

We define *direct* limits, which are obtained just by using experimental information of a given process and *indirect* limits, which are obtained through oscillation data. A novel collider ansatz for direct limits on the tau sector of $m_{\alpha\beta}$ is presented, which is at present the only way to get information about these elements. The difference of direct and indirect limits is quantified and discussed.

Then, in Section 4.4 an analogue of $m_{\alpha\beta}$ for heavy Majorana neutrinos, $\frac{1}{m_{\alpha\beta}}$, is introduced and direct and indirect limits on it are defined and compared. Its form is given by the fact that processes with heavy Majorana neutrinos have a different behavior as a function of the mass, as was shown before. Processes depending on elements of $\frac{1}{m_{\alpha\beta}}$ are found and the expected cross sections or branching ratios are estimated. As for $m_{\alpha\beta}$, no effects of $\frac{1}{m_{\alpha\beta}}$ (except for $\langle \frac{1}{m} \rangle$, of course) can be expected.

Finally, in Section 4.4.4 we discuss direct limits to be obtained in the future. Some model dependent and unitarity limits on heavy Majorana neutrinos are discussed in Section 4.5. As always, the chapter is summarized and adorned with some final remarks in Section 4.6.

4.1 The entries of the mixing matrix

As can be seen from Eq. (1.24), the phases α and β do not influence the absolute values of the entries of U . The only phase governing the magnitude is therefore δ so that we consider both cases, $\delta = 0$ and $\delta \neq 0$.

As mentioned already, the fitted data on the mixing angles and the mass squared stems purely from oscillation and are thus independent on the value of the lowest mass eigenvalue, which is bounded to be smaller than 2.2 eV. The additional information one has to include is the limit from $0\nu\beta\beta$, which further restricts the angles. For masses bigger than 0.35 eV all mixing angles are not allowed, thus the magnitude of $U_{\alpha i}$ is a function of the lowest mass eigenvalue. To be consistent, we have to treat each of the four CP conserving signatures when we consider CP conservation. However, no big difference is found, with the exception that the $(+++)$ and the $(-- +)$ cases are not allowed for high masses, see Chapter 2. The other two signatures give similar values for U .

We use again the data from a pre-SNO analysis and read the 99 % C.L. range of the solar and atmospheric parameters from plots displayed in [42] and given in Tables 1.1 and 1.2. A random scan over the allowed ranges of the angles, the mass squared differences and δ is performed, including α and β to obtain $\langle m \rangle$ whenever necessary, i.e. when the smallest mass eigenstate is larger than 0.35 eV. The inclusion of the SNO data is not expected to change our general conclusions. We give the numerical values with three decimals in order to show more clearly the difference of the various cases under consideration.

4.1.1 CP violating case, $\delta \neq 0$

The following ranges of the mixing matrix elements are found for $m_1 = 10^{-5}$ eV, i.e. when no constraint from $0\nu\beta\beta$ is included:

$$|U| \simeq \left\{ \begin{array}{l} \left(\begin{array}{ccc} 0.969 \dots 1.000 & 0.014 \dots 0.055 & 0 \dots 0.245 \\ 0.007 \dots 0.226 & 0.492 \dots 0.848 & 0.529 \dots 0.866 \\ 0.004 \dots 0.211 & 0.528 \dots 0.870 & 0.485 \dots 0.845 \end{array} \right) \text{ SMA} \\ \left(\begin{array}{ccc} 0.495 \dots 0.954 & 0.299 \dots 0.866 & 0 \dots 0.265 \\ 0.016 \dots 0.765 & 0.146 \dots 0.823 & 0.529 \dots 0.866 \\ 0.057 \dots 0.783 & 0.169 \dots 0.843 & 0.482 \dots 0.845 \end{array} \right) \text{ LMA} \\ \left(\begin{array}{ccc} 0.400 \dots 0.953 & 0.297 \dots 0.912 & 0 \dots 0.224 \\ 0.016 \dots 0.800 & 0.049 \dots 0.821 & 0.529 \dots 0.866 \\ 0.063 \dots 0.830 & 0.093 \dots 0.846 & 0.487 \dots 0.845 \end{array} \right) \text{ QVO} \end{array} \right. \quad (4.1)$$

Note that the departure from exactly maximal mixing for $U_{\mu 3}$ and $U_{\tau 3}$ can be more than 40 %. The reason is that c_2 can be as low as 0.5 for the allowed $t_2^2 = 3$. For sizable s_3 , which itself causes corrections of order 10 %, this value is even further reduced. For SMA the values that should be zero if single maximal mixing was true can in fact be very small, of order 0.01. However, since $|U_{e3}|$ can be as large as 0.25, the maximal values of these entries can be quite sizable.

Now we take the highest possible mass eigenvalue, which is 0.39 eV for the SMA solution and 2.2 eV for the other two. The ranges are

$$|U| \simeq \left\{ \begin{array}{l} \left(\begin{array}{ccc} 0.9691 \dots 0.9693 & 0.022 \dots 0.027 & 0.245 \\ 0.129 \dots 0.226 & 0.495 \dots 0.794 & 0.594 \dots 0.840 \\ 0.099 \dots 0.210 & 0.608 \dots 0.869 & 0.485 \dots 0.767 \end{array} \right) \text{ SMA} \\ \left(\begin{array}{ccc} 0.634 \dots 0.761 & 0.617 \dots 0.761 & 0 \dots 0.200 \\ 0.188 \dots 0.690 & 0.238 \dots 0.681 & 0.529 \dots 0.866 \\ 0.268 \dots 0.698 & 0.298 \dots 0.723 & 0.493 \dots 0.845 \end{array} \right) \text{ LMA} \\ \left(\begin{array}{ccc} 0.609 \dots 0.761 & 0.611 \dots 0.761 & 0 \dots 0.224 \\ 0.189 \dots 0.710 & 0.180 \dots 0.704 & 0.530 \dots 0.866 \\ 0.261 \dots 0.733 & 0.231 \dots 0.727 & 0.487 \dots 0.845 \end{array} \right) \text{ QVO} \end{array} \right. \quad (4.2)$$

The first thing one notices is that for SMA only $s_3^2 = 0.06$ is allowed. Due to this fact, the ranges of the other entries are significantly reduced with respect to the case of $m_1 = 10^{-5}$ eV, up to 25 %. The reason for the high s_3 is that for $\langle m \rangle \simeq m_0(1 + s_3^2 e^{2i\beta}) \leq 0.35$ eV the second term has to compensate the first term. Also for the other solar solutions the ranges are smaller, however the difference is not as severe as for the SMA case. The normal and inverse scheme have not to be treated separately, since for smallest mass larger than 0.35 eV the scheme is degenerate.

It is also instructive to calculate the rephasing invariant Jarlskog invariant J_{CP} [123], which reads

$$J_{CP} = \frac{1}{8} \sin 2\theta_1 \sin 2\theta_2 \sin 2\theta_3 \cos \theta_3 \sin \delta \quad (4.3)$$

in the parametrisation (1.24). For SMA the maximal value is 0.0046 for $m_1 = 10^{-5}$ eV and lies between 0.0022 and 0.0033 for $m_1 = 0.39$ eV. For the LMA solution, $J_{CP} \lesssim 0.058$ (0.047) for $m_1 = 10^{-5}$ (2.2) eV. In case of the QVO solution no dependence on the scheme is found, $J_{CP} \lesssim 0.053$ for all m_1 . Such large values of J_{CP} may be probed in neutrino factory experiments, provided the solar solution is LMA and Δm_{\odot}^2 is not too low. We note that our values for U display a broader range than the ones in [124]. The reason is that we use the 99 % C.L. values of the fit from [42]. Because of this, our maximal value

of J_{CP} exceeds the one from [124] by 50 %. The dependence of U and J_{CP} on m_1 has to our best knowledge not been stressed before.

4.1.2 CP conserving case, $\delta = 0$

For $m_1 = 10^{-5}$ eV the range is

$$U \simeq \left\{ \begin{array}{l} \left(\begin{array}{ccc} 0.969 \dots 1.000 & 0.014 \dots 0.055 & 0 \dots 0.245 \\ -0.226 \dots -0.007 & 0.491 \dots 0.845 & 0.529 \dots 0.866 \\ -0.180 \dots -0.047 & -0.870 \dots -0.534 & 0.485 \dots 0.845 \end{array} \right) \text{ SMA} \\ \left(\begin{array}{ccc} 0.495 \dots 0.954 & 0.299 \dots 0.866 & 0 \dots 0.265 \\ -0.769 \dots -0.152 & 0.144 \dots 0.804 & 0.529 \dots 0.866 \\ 0.050 \dots 0.750 & -0.846 \dots -0.268 & 0.482 \dots 0.845 \end{array} \right) \text{ LMA} \\ \left(\begin{array}{ccc} 0.400 \dots 0.953 & 0.297 \dots 0.913 & 0 \dots 0.224 \\ -0.802 \dots -0.152 & 0.046 \dots 0.801 & 0.529 \dots 0.866 \\ 0.044 \dots 0.790 & -0.851 \dots -0.219 & 0.487 \dots 0.845 \end{array} \right) \text{ QVO} \end{array} \right. \quad (4.4)$$

For SMA, three entries are smaller than zero and two entries for the other solutions. The absolute values are similar to the ones for $\delta \neq 0$.

For the highest allowed m_1 and $\alpha = \beta = \pi/2$ the entries read:

$$U \simeq \left\{ \begin{array}{l} \left(\begin{array}{ccc} 0.9691 \dots 0.9693 & 0.022 \dots 0.027 & 0.245 \\ -0.226 \dots -0.168 & 0.494 \dots 0.787 & 0.594 \dots 0.840 \\ -0.180 \dots -0.098 & -0.869 \dots -0.618 & 0.485 \dots 0.767 \end{array} \right) \text{ SMA} \\ \left(\begin{array}{ccc} 0.648 \dots 0.761 & 0.617 \dots 0.761 & 0 \dots 0.200 \\ -0.686 \dots -0.325 & 0.236 \dots 0.642 & 0.529 \dots 0.866 \\ 0.238 \dots 0.659 & -0.736 \dots -0.348 & 0.490 \dots 0.845 \end{array} \right) \text{ LMA} \\ \left(\begin{array}{ccc} 0.648 \dots 0.761 & 0.607 \dots 0.761 & 0 \dots 0.224 \\ -0.695 \dots -0.324 & 0.189 \dots 0.641 & 0.529 \dots 0.866 \\ 0.220 \dots 0.659 & -0.746 \dots -0.347 & 0.487 \dots 0.845 \end{array} \right) \text{ QVO} \end{array} \right. \quad (4.5)$$

Comparing this equation with the previous three shows that the ranges are the more restricted the more constraints are active. The smallest range appears for this last case, when CP is conserved and the limit for $\langle m \rangle$ has to be respected due to a high m_1 .

The idealized case of single maximal mixing is not possible for sizable m_1 since U_{e3} has to be sizable too in this case. For the same reason, $U_{\mu 1}$ and $U_{\tau 1}$ can be very low for the case $\delta \neq 0$ and hierarchical scheme, whereas they are at least of the order 0.1 for large m_1 . U_{e2} is always of the order 10^{-2} . Exact bimaximal mixing is possible for all m_1 . The values of U are closer to the exact bimaximal mixing case when more constraints are applied.

4.2 The other entries of the mass matrix

It is interesting to compare the behavior of $\langle m \rangle$ with the one of the other five independent entries in $m_{\alpha\beta}$. The formulas of these parameters can be found in Appendix A. Since, as we will see, the hopes to measure these quantities are rather low, it is not necessary to analyze them in such details as $\langle m \rangle$ has been. Therefore we do not include all $(\pm \pm \pm)$ signatures of the mass states and also do not use the full correlated data set from [42]. It takes far less time to do a random scan of the allowed parameters, similar to the one performed for U in the last section. For later use we denote the limits obtained in this section *indirect limits*.

In addition to that analysis, both mass hierarchies have now to be considered. In the program, m_1 (m_3) and s_3^2 are run. The remaining seven parameters (2 masses, 2 angles and 3 phases) are generated within their allowed range by a random number generator. We take 10^5 parameter sets for each mass m_1 (m_3) and s_3 and calculate the minimal and maximal value for each of the five $m_{\alpha\beta}$. As a constraint we demand that $\langle m \rangle$ is not larger than 0.35 eV. The result can be seen for some cases in Fig. 4.1. All properties of the remaining entries of $m_{\alpha\beta}$ can be seen in these examples.

4.2.1 Properties of the plots

The extreme cases of the plots in Fig. 4.1 can be easily explained. For example, for large m_1 (m_3) a sharp decrease of the minimal $m_{\alpha\beta}$ is observed, regardless of the solar solution. It occurs when the smallest mass is greater than 0.35 eV, i.e. in the degenerate scheme.

First, consider the SMA case and $m_{e\mu}$ as an example. In order to have a m_0 heavier than 0.35 eV, large s_3^2 and a tuned β is required. This restricts the values for the other $m_{\alpha\beta}$ significantly: it can be seen from Eq. (1.24) that for $\tan^2 \theta_1 \simeq 0$, $c_3 \simeq 1$ and the degenerate scheme

$$m_{e\mu} \simeq m_0 s_3 \sqrt{2} s_\beta . \quad (4.6)$$

With the same simplifications we get for $\langle m \rangle$ from Eq. (2.47)

$$\langle m \rangle \simeq m_0 \sqrt{1 + 2 s_3^2 c_{2\beta}} . \quad (4.7)$$

For $m_0 = 0.37$ eV, nonzero s_3^2 is required to obtain $\langle m \rangle \leq 0.35$ eV. In fact, only the maximal $s_3^2 = 0.06$ is allowed. With this value one finds that the phase β is restricted to $c_{2\beta} \lesssim -0.88$. Thus, s_β is close to one and therefore $m_{e\mu} \simeq 0.1$ eV, as confirmed by Fig. 4.1a.

Similar considerations can be done for the maximal mixing case. For $m_{e\tau}$ and exactly bimaximal mixing one finds

$$m_{e\tau} \simeq \frac{m_0}{\sqrt{2}} s_\alpha . \quad (4.8)$$

However, for the same mixing matrix we find from Eq. (2.28) that $\langle m \rangle = m_0 c_\alpha$. If we take $m_0 = 1$ eV then it follows $c_\alpha \leq 0.35$ which translates into 0.66 eV $\lesssim m_{e\tau} \lesssim 0.71$ eV, as confirmed by Fig. 4.1b.

If we consider now $m_{\mu\mu}$ and the SMA case in the extreme hierarchical case $m_1 = 0$ then

$$m_{\mu\mu} \simeq \frac{1}{2} \sqrt{\Delta m_A^2 + 2 \sqrt{\Delta m_A^2 \Delta m_\odot^2} c_\phi} \quad (4.9)$$

with $\phi = 2(\alpha - \beta - \delta)$. Inserting the maximal and minimal values of the mass scales for $s_3^2 = 0$ from Tables 1.1 and 1.2 gives values between 0.01 and 0.04 eV, as confirmed in Fig. 4.1c. Calculating the same element for the bimaximal case yields

$$m_{\mu\mu} \simeq \frac{1}{2} \sqrt{\Delta m_A^2 + \sqrt{\Delta m_A^2 \Delta m_\odot^2} c_\phi} \quad (4.10)$$

which is about $\frac{1}{2} \sqrt{\Delta m_A^2}$ for low Δm_\odot^2 and can vanish for the case of more sizable Δm_\odot^2 as for the LMA case. In Fig. 4.1d it is seen that the element can indeed become very small for this solution. For the QVO solution, a lower limit of about 0.01 eV is found.

Going now to the inverse hierarchy, it is of course noticed that the considerations for m_1 (m_3) larger than 0.35 eV apply for this scheme as well. For the SMA solution $m_{\mu\tau}$ is estimated to be

$$m_{\mu\tau} \simeq \frac{\sqrt{\Delta m_A^2}}{2} \sqrt{1 - 2 s_3^2 c_{2(\alpha-\delta)}} \quad (4.11)$$

which lies between 0.01 and 0.04 eV. This is again confirmed by Fig. 4.1e. For exact bimaximal mixing one finds

$$m_{\tau\tau} \simeq \frac{\sqrt{\Delta m_A^2}}{2\sqrt{2}} \sqrt{1 + c_{2\alpha}} \quad (4.12)$$

which is smaller than 0.04 eV and allows for complete cancellation, as can be seen in Fig. 4.1f. Similar to $\langle m \rangle$, the maximal values for the inverse hierarchical scheme are not depending on the solar solution.

The constraint that $\langle m \rangle$ should be smaller than 0.35 eV has consequences on the range of the other elements. In Fig. 4.2 the difference of $m_{\mu\mu}$ is shown for the LMA case in the normal hierarchy. Constraining $\langle m \rangle$ decreases the maximal value and increases the minimal value. The difference can be up to 20 %.

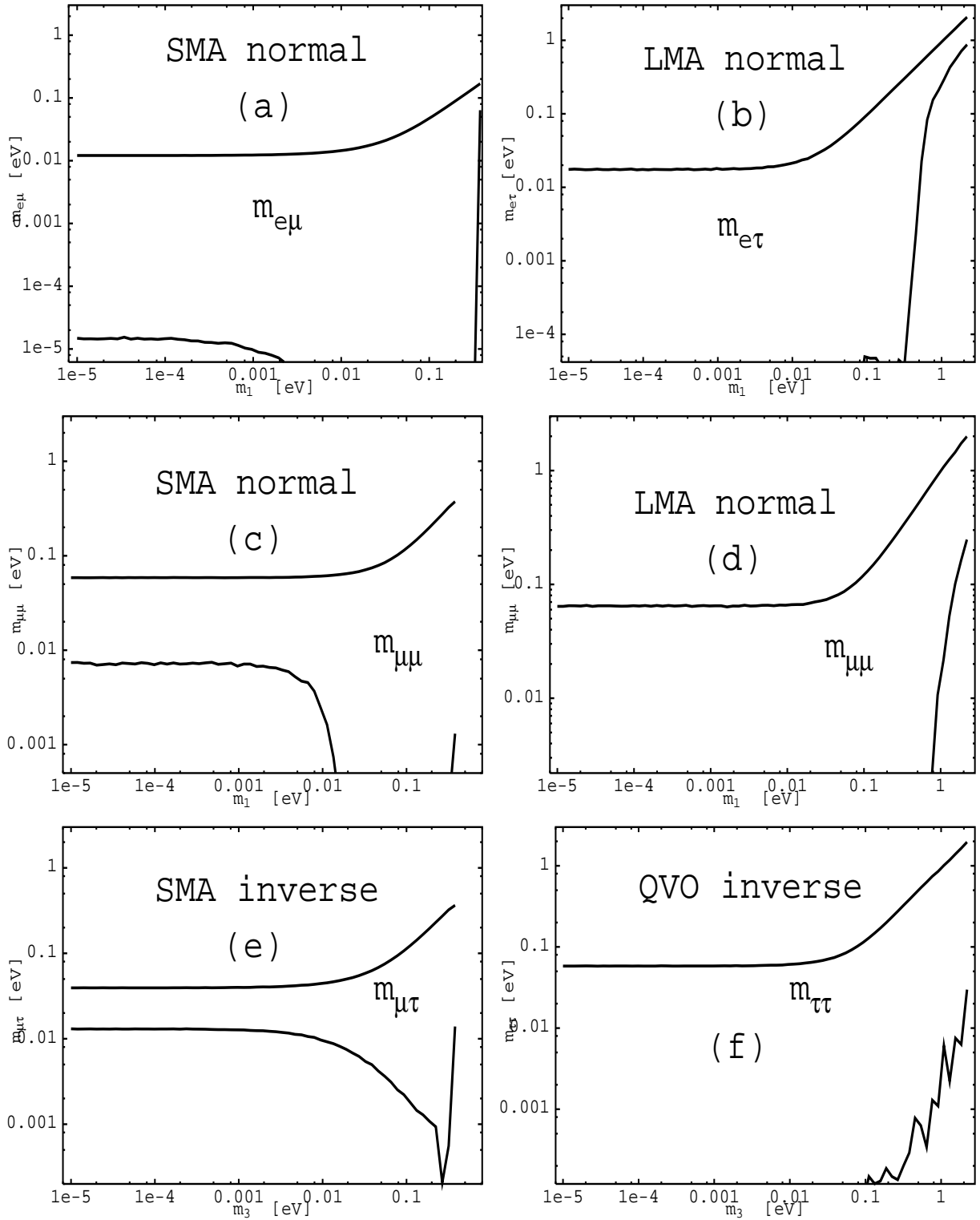


Figure 4.1: Allowed range of some elements of $m_{\alpha\beta}$ for different solar solutions and both hierarchies.

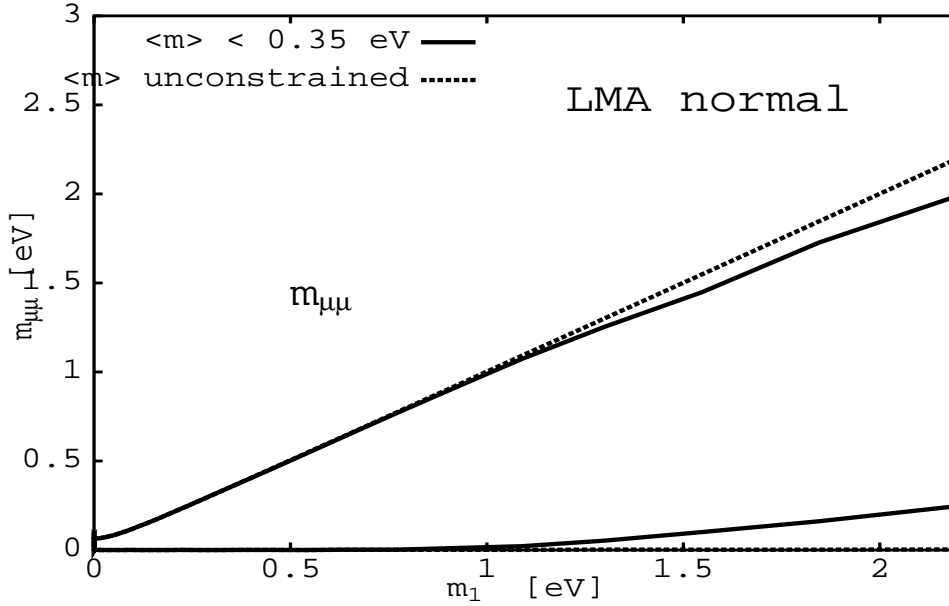


Figure 4.2: $m_{\mu\mu}$ as a function of the smallest mass eigenvalue m_1 in the normal hierarchy for the LMA case. Shown are the minimal and maximal ranges for scanning the allowed parameters demanding the $\langle m \rangle$ to be within its experimental value and without constraining it.

4.2.2 Summary of the allowed range of $m_{\alpha\beta}$

We summarize the derived indirect limits. For the hierarchical scheme we find in the normal hierarchy (setting values smaller than 10^{-4} eV to zero and taking $m_1 = 10^{-5}$ eV)

$$m_{\alpha\beta} \simeq \left\{ \begin{array}{l} \left(\begin{array}{ccc} 0 \dots 2.6 \cdot 10^{-3} & 0 \dots 1.2 \cdot 10^{-2} & 0 \dots 1.1 \cdot 10^{-2} \\ & 7.4 \cdot 10^{-3} \dots 5.9 \cdot 10^{-2} & 1.2 \cdot 10^{-2} \dots 4.1 \cdot 10^{-2} \\ & & 5.5 \cdot 10^{-3} \dots 5.6 \cdot 10^{-2} \end{array} \right) \text{eV} \quad \text{SMA} \\ \left(\begin{array}{ccc} 0 \dots 1.8 \cdot 10^{-2} & 1.6 \cdot 10^{-5} \dots 1.8 \cdot 10^{-2} & 0 \dots 1.8 \cdot 10^{-2} \\ & 1.1 \cdot 10^{-3} \dots 6.4 \cdot 10^{-2} & 8.4 \cdot 10^{-3} \dots 5.0 \cdot 10^{-2} \\ & & 0 \dots 6.1 \cdot 10^{-2} \end{array} \right) \text{eV} \quad \text{LMA} \\ \left(\begin{array}{ccc} 0 \dots 2.7 \cdot 10^{-3} & 0 \dots 1.2 \cdot 10^{-2} & 0 \dots 1.1 \cdot 10^{-2} \\ & 9.0 \cdot 10^{-3} \dots 5.8 \cdot 10^{-2} & 1.3 \cdot 10^{-2} \dots 3.9 \cdot 10^{-2} \\ & & 7.5 \cdot 10^{-3} \dots 5.5 \cdot 10^{-2} \end{array} \right) \text{eV} \quad \text{QVO} \end{array} \right. \quad (4.13)$$

For the inverse scheme we find

$$m_{\alpha\beta} \simeq \left\{ \begin{array}{l} \left(\begin{array}{ccc} 3.6 \cdot 10^{-2} \dots 7.6 \cdot 10^{-2} & 0 \dots 1.4 \cdot 10^{-2} & 0 \dots 1.3 \cdot 10^{-2} \\ & 6.5 \cdot 10^{-3} \dots 5.6 \cdot 10^{-2} & 1.3 \cdot 10^{-2} \dots 3.9 \cdot 10^{-2} \\ & & 8.7 \cdot 10^{-3} \dots 5.8 \cdot 10^{-2} \end{array} \right) \text{eV} & \text{SMA} \\ \\ \left(\begin{array}{ccc} 0 \dots 8.1 \cdot 10^{-2} & 0 \dots 6.3 \cdot 10^{-2} & 0 \dots 6.6 \cdot 10^{-2} \\ & 0 \dots 5.4 \cdot 10^{-2} & 0 \dots 3.9 \cdot 10^{-2} \\ & & 0 \dots 5.8 \cdot 10^{-2} \end{array} \right) \text{eV} & \text{LMA} \\ \\ \left(\begin{array}{ccc} 0 \dots 7.6 \cdot 10^{-2} & 0 \dots 6.4 \cdot 10^{-2} & 0 \dots 6.6 \cdot 10^{-2} \\ & 0 \dots 5.5 \cdot 10^{-2} & 0 \dots 3.9 \cdot 10^{-2} \\ & & 0 \dots 5.8 \cdot 10^{-2} \end{array} \right) \text{eV} & \text{QVO} \end{array} \right. \quad (4.14)$$

For degenerate schemes the ranges are

$$m_{\alpha\beta} \simeq \left\{ \begin{array}{l} \left(\begin{array}{ccc} 0.31 \dots 0.35 & 6.4 \cdot 10^{-2} \dots 0.17 & 4.7 \cdot 10^{-2} \dots 0.16 \\ & 1.3 \cdot 10^{-3} \dots 0.39 & 7.4 \cdot 10^{-3} \dots 0.38 \\ & & 7.7 \cdot 10^{-4} \dots 0.39 \end{array} \right) \text{eV} & \text{SMA} \\ \\ \left(\begin{array}{ccc} 0 \dots 0.35 & 0.69 \dots 2.00 & 0.87 \dots 2.06 \\ & 0.25 \dots 1.99 & 0.61 \dots 1.27 \\ & & 0.08 \dots 1.86 \end{array} \right) \text{eV} & \text{LMA} \\ \\ \left(\begin{array}{ccc} 1.7 \cdot 10^{-4} \dots 0.35 & 0.56 \dots 2.04 & 0.78 \dots 2.11 \\ & 0.17 \dots 2.08 & 0.47 \dots 1.27 \\ & & 0.03 \dots 1.96 \end{array} \right) \text{eV} & \text{QVO} \end{array} \right. \quad (4.15)$$

4.3 Direct and indirect limits on and from $m_{\alpha\beta}$

4.3.1 Analogues of neutrinoless double beta decay

The dependence of neutrinoless double beta decay on $\langle m \rangle$ has been studied extensively in Chapter 2. However, there are other processes, which depend on the other elements of $m_{\alpha\beta}$ just as $0\nu\beta\beta$ depends on $\langle m \rangle$.

One of the first analogues of neutrinoless double beta decay studied was the decay $K^+ \rightarrow \pi^- \mu^+ \mu^+$, sometimes denoted “neutrinoless double muon decay”. In Fig. 4.3 we show the Feynman diagram for the process. Lately, two groups recalculated the branching ratio as a function of the intermediate Majorana mass [125,126]. Some consequences of a new experimental limit [127] were studied in [128,129]. Reference [125] focused on an enhancement effect: When the Majorana mass is of the order of the kaon mass, its propagator displays a resonance. Applying the usual replacement $m_i \rightarrow m_i - \frac{i}{2}\Gamma_i$ where Γ_i is the decay width of the Majorana with mass m_i , allowed to set stringent limits on the mixing parameter $U_{\mu i}$ in the mass region between 245 and 389 MeV.

In [126] only the extreme cases of very light and very massive neutrinos were studied, but many other channels of B^+ and K^+ decays were discussed, including all possible lepton pairs in the final state. Another process under study was (μ^-, e^+) conversion. A recent calculation for the case of light neutrinos for the process $^{48}\text{Ti}(\mu^-, e^+)^{48}\text{Ca}$ was performed in [130]. A rough estimate of (μ^-, μ^+) conversion on ^{44}Ti was made in [94].

Assuming now that the branching ratio is proportional to $m_{\alpha\beta}^2$ one can use the experimental limit on the branching ratio to obtain a limit on $m_{\alpha\beta}$. The bound derived by this approach is denoted *direct limit*, which has to be compared with the *indirect limits* as obtained from oscillation data. A drawback of these considerations is the fact that no experimental limit on the τ sector of $m_{\alpha\beta}$ can be calculated due to the lack of experimental limits on processes like $B^+ \rightarrow \pi^- \tau^+ \tau^+$. Here, the “collider approach” introduced in [2] and generalized in [3] is of help. Especially the process

$$e^+ p \rightarrow \bar{\nu}_e \alpha^+ \beta^+ X$$

at HERA allowed to set for the first time limits on these quantities. The highest cross section and some phenomenological aspects were studied in Chapter 3.

In Table 4.1 we show the results of this program. Some remarks are required. Two processes for each element of $m_{\alpha\beta}$ are given. The column “experiment” gives the experimental information on this process, which is the half life $T_{1/2}^{0\nu}$ for $0\nu\beta\beta$ (using the calculation of [52]) and the BR for the K and B decays. For the conversion $^{48}\text{Ti}(\mu^-, e^+)^{48}\text{Ca}$ the ratio R with respect to muon capture $^{48}\text{Ti}(\mu^-, \nu_\mu)^{48}\text{Sc}$ is given. For the scattering processes at HERA the integrated luminosity, collected in searches for isolated leptons (cf. with Section 3.5) is used, where no LSD event was found. The BR

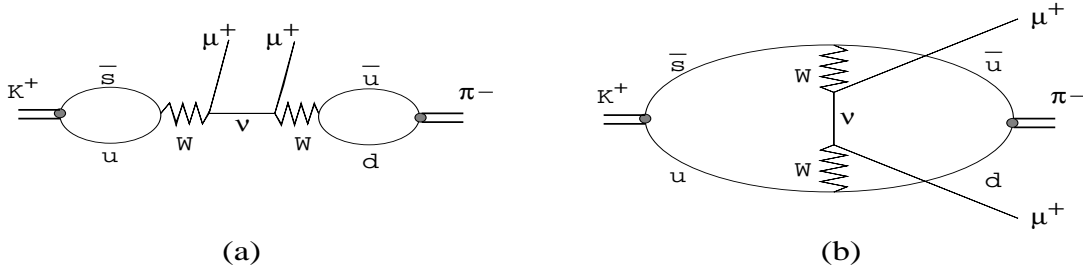


Figure 4.3: The Feynman diagram for $K^+ \rightarrow \pi^- \mu^+ \mu^+$. The tree diagram (a) dominates over the loop diagram (b). Taken from [125].

of the produced taus into muons is included in the limit, because the dimuon channel is expected to be much more free from background than the dielectron channels [2, 3].

Two numbers for $K^+ \rightarrow \pi^- \mu^+ \mu^+$ are available, stemming from two calculations [125] and [126], which agree within a factor of two. We take the number from the calculation of [126] to be consistent with the other elements. In addition, since the resulting BRs are way beyond experimental access, a precise treatment is not that necessary. Furthermore, for the B decays a range within a factor of six is given in [126], without specifying why this comes about. The highest value is taken. Due to the smallness of the resulting BRs, the uncertainty of the hadronic matrix elements can be safely neglected.

B decays may yield similar limits on $m_{\alpha\tau}$ as the ones from the HERA processes if BRs of order 10^{-10} are available. Currently, the BR for $B^+ \rightarrow \pi^- e^+ e^+$ is 3.9×10^{-3} [85]. Using this value as an example leads to limits in the order of 10^4 TeV, much worse than the one stemming from HERA data. Using the BR of 9.1×10^{-3} for $B^+ \rightarrow \pi^- \mu^+ \mu^+$ [85] leads again to limits of the same order. For identical experimental limits on the BRs, limits on $m_{\alpha\beta}$ are more stringent when taken from K decays than from B decays.

As one sees, there is a spread of fourteen orders of magnitude from the ee to the $\tau\tau$ element. The kaon decay gives the second best limit, namely about 89 GeV on $m_{e\mu}$. Comparing the collider limit with the kaon decay limit shows that both bounds are comparable for $m_{\mu\mu}$. As already mentioned, the tau sector is currently only accessible through the HERA data.

Of course, the limits are unphysical. Since we assumed the neutrinos to be light, we can assume $U_{\alpha i} = \mathcal{O}(1)$ and thus apply the limit on $m_{\alpha\beta}$ directly on the plots of the cross section against m_i . For the decay of a K^+ a Majorana neutrino of almost 90 GeV is certainly not a “light” neutrino. For these masses, the BR is proportional to m_i^{-2} and

element	process	experiment	direct limit [TeV]
$\langle m \rangle$	$0\nu\beta\beta$	$T_{1/2}^{0\nu} > 1.9 \cdot 10^{25}$ y	$0.35 \cdot 10^{-12}$
	$K^+ \rightarrow \pi^- e^+ e^+$	BR $< 6.4 \cdot 10^{-10}$	0.11
$m_{e\mu}$	$^{48}\text{Ti}(\mu^-, e^+)^{48}\text{Ca}$	R $< 4.3 \cdot 10^{-12}$	2.9
	$K^+ \rightarrow \pi^- e^+ \mu^+$	BR $< 5.0 \cdot 10^{-10}$	0.09
$m_{e\tau}$	$B^+ \rightarrow \pi^- e^+ \tau^+$	—	—
	$e^+ p \rightarrow \bar{\nu}_e e^+ \tau^+ X$	$\mathcal{L} = 82 \text{ pb}^{-1}$	3.0
$m_{\mu\mu}$	$K^+ \rightarrow \pi^- \mu^+ \mu^+$	BR $< 3.0 \cdot 10^{-9}$	0.46
	$e^+ p \rightarrow \bar{\nu}_e \mu^+ \mu^+ X$	$\mathcal{L} = 82 \text{ pb}^{-1}$	0.85
$m_{\mu\tau}$	$B^+ \rightarrow \pi^- \mu^+ \tau^+$	—	—
	$e^+ p \rightarrow \bar{\nu}_e \mu^+ \tau^+ X$	$\mathcal{L} = 82 \text{ pb}^{-1}$	3.1
$m_{\tau\tau}$	$B^+ \rightarrow \pi^- \tau^+ \tau^+$	—	—
	$e^+ p \rightarrow \bar{\nu}_e \tau^+ \tau^+ X$	$\mathcal{L} = 82 \text{ pb}^{-1}$	14.6

Table 4.1: Element of the Majorana mass matrix $m_{\alpha\beta}$, two processes which are sensitive on the respective element, the experimental information on the process and the direct limit obtained from it.

not to m_i^2 as assumed to get the limit. In order to get a limit of order MeV on $m_{\mu\mu}$ one would need a limit on the BR of 10^{-20} , a limit comparable to the one from $0\nu\beta\beta$ on $\langle m \rangle$ requires even 10^{-32} , certainly a sophisticated if not impossible task.

4.3.2 Limits on lepton number violating processes from indirect limits on $m_{\alpha\beta}$

Now we estimate the BRs and ratios on lepton number and flavor violating processes when the indirect limits from Section 4.2 are inserted. Some previous work on this topic can be found in [6], here the analysis is more detailed.

As we have seen, the bounds are a function of the smallest mass eigenstate, the scheme and the solar solution. The results are given in Tables 4.2 to 4.6. The column “max [eV]” shows the maximal value of $m_{\alpha\beta}$ for the given solar solution and scheme, “ratio (max)” displays the BR, ratio or half-life of the process when this maximal value of $m_{\alpha\beta}$ is inserted. In “indirect/direct” the quotient of the indirect limit with the direct limit from Table 4.1 is given. As in Table 4.1, two processes per element of $m_{\alpha\beta}$ are presented, taken from the same references. For the HERA scattering, R denotes the ratio of the cross section with the usual CC cross section of $\sigma(e^+ p \rightarrow \bar{\nu}_e X, Q^2 \geq 200 \text{ GeV}^2) \simeq 30.3 \text{ pb}$ [109]. Table 4.2 gives the values for the SMA solution in the normal hierarchy for $m_1 = 10^{-5} \text{ eV}$. The maximal values of $m_{\alpha\beta}$ for the inverse scheme are similar.

Table 4.3 shows the values for the LMA solution, which has very similar values as the

element	max [eV]	process	ratio (max)	indirect/direct
$\langle m \rangle$	$2.6 \cdot 10^{-3}$	$0\nu\beta\beta$ $K^+ \rightarrow \pi^- e^+ e^+$	$T_{1/2}^{0\nu} = 3.5 \cdot 10^{29}$ y BR = $3.3 \cdot 10^{-37}$	$7.3 \cdot 10^{-3}$ $2.3 \cdot 10^{-14}$
$m_{e\mu}$	$1.2 \cdot 10^{-2}$	$^{48}\text{Ti}(\mu^-, e^+)^{48}\text{Ca}$ $K^+ \rightarrow \pi^- e^+ \mu^+$	R = $7.3 \cdot 10^{-41}$ BR = $8.9 \cdot 10^{-36}$	$4.1 \cdot 10^{-15}$ $1.3 \cdot 10^{-13}$
$m_{e\tau}$	$1.1 \cdot 10^{-2}$	$B^+ \rightarrow \pi^- e^+ \tau^+$ $e^+ p \rightarrow \bar{\nu}_e e^+ \tau^+ X$	BR = $2.9 \cdot 10^{-39}$ R = $5.4 \cdot 10^{-33}$	— $3.6 \cdot 10^{-15}$
$m_{\mu\mu}$	$5.9 \cdot 10^{-2}$	$K^+ \rightarrow \pi^- \mu^+ \mu^+$ $e^+ p \rightarrow \bar{\nu}_e \mu^+ \mu^+ X$	BR = $1.3 \cdot 10^{-34}$ R = $2.0 \cdot 10^{-30}$	$2.1 \cdot 10^{-13}$ $7.0 \cdot 10^{-14}$
$m_{\mu\tau}$	$4.0 \cdot 10^{-2}$	$B^+ \rightarrow \pi^- \mu^+ \tau^+$ $e^+ p \rightarrow \bar{\nu}_e \mu^+ \tau^+ X$	BR = $3.8 \cdot 10^{-38}$ R = $6.7 \cdot 10^{-32}$	— $1.3 \cdot 10^{-14}$
$m_{\tau\tau}$	$5.6 \cdot 10^{-2}$	$B^+ \rightarrow \pi^- \tau^+ \tau^+$ $e^+ p \rightarrow \bar{\nu}_e \tau^+ \tau^+ X$	BR = $3.0 \cdot 10^{-39}$ R = $5.9 \cdot 10^{-33}$	— $3.8 \cdot 10^{-15}$

Table 4.2: Maximal indirect limit of $m_{\alpha\beta}$ for the SMA solution in the normal hierarchy for $m_1 = 10^{-5}$ eV.

QVO case. Table 4.4 gives the numbers for the inverse hierarchy and the QVO solution, for $m_3 = 10^{-5}$ eV. These values are similar to the ones obtained for the LMA inverse case. Finally, Tables 4.5 and 4.6 give the numbers for the highest allowed mass of the lightest eigenstate, for the LMA (the same as for the QVO case) and the SMA case, respectively.

The square of the value in the “indirect/direct” column is the factor, which an experimental limit on a BR or ratio would have to be improved in order to be comparable to the indirect limits on $m_{\alpha\beta}$. Ignoring $0\nu\beta\beta$ for the moment (it has extensively been discussed before), this number is between 10^{24} and 10^{29} for hierarchical schemes and between 10^{23} and 10^{27} for degenerate schemes. The same statement is that the indirect limits are more stringent than the direct ones by 12 to 14 (hierarchical scheme) or 12 to 13 (degenerate) orders of magnitude.

The element $m_{e\mu}$ is “closest” to experiment, typically two orders of magnitude better than the $\tau\tau$ element, which is always the most poorly known one. The reason is the low limit on the BR for $K^+ \rightarrow \pi^- \mu^+ e^+$ and the tiny cross section for $e^+ p \rightarrow \bar{\nu}_e \tau^+ \tau^+ X$.

Tables similar to the ones given here have also been presented in [126], using however inconsistent values for the elements of $m_{\alpha\beta}$. In that reference a limit on $\langle m \rangle$ of 0.35 eV was assumed together with a bound of about 3 eV on the total mass from the tritium spectrum. With these values they use a limit of 9 eV on the other five $m_{\alpha\beta}$, which is obviously not possible if one believes in unitarity. The same mistake has been made in [125].

element	max [eV]	process	ratio (max)	indirect/direct
$\langle m \rangle$	$1.8 \cdot 10^{-2}$	$0\nu\beta\beta$ $K^+ \rightarrow \pi^- e^+ e^+$	$T_{1/2}^{0\nu} = 7.1 \cdot 10^{27}$ y BR = $2.0 \cdot 10^{-35}$	$5.2 \cdot 10^{-2}$ $1.8 \cdot 10^{-13}$
$m_{e\mu}$	$1.8 \cdot 10^{-2}$	$^{48}\text{Ti}(\mu^-, e^+)^{48}\text{Ca}$ $K^+ \rightarrow \pi^- e^+ \mu^+$	R = $1.7 \cdot 10^{-40}$ BR = $2.0 \cdot 10^{-35}$	$6.2 \cdot 10^{-15}$ $2.0 \cdot 10^{-13}$
$m_{e\tau}$	$1.8 \cdot 10^{-2}$	$B^+ \rightarrow \pi^- e^+ \tau^+$ $e^+ p \rightarrow \bar{\nu}_e e^+ \tau^+ X$	BR = $7.8 \cdot 10^{-39}$ R = $1.4 \cdot 10^{-32}$	— $6.0 \cdot 10^{-15}$
$m_{\mu\mu}$	$6.4 \cdot 10^{-2}$	$K^+ \rightarrow \pi^- \mu^+ \mu^+$ $e^+ p \rightarrow \bar{\nu}_e \mu^+ \mu^+ X$	BR = $1.5 \cdot 10^{-34}$ R = $2.3 \cdot 10^{-30}$	$2.2 \cdot 10^{-13}$ $7.6 \cdot 10^{-14}$
$m_{\mu\tau}$	$5.0 \cdot 10^{-2}$	$B^+ \rightarrow \pi^- \mu^+ \tau^+$ $e^+ p \rightarrow \bar{\nu}_e \mu^+ \tau^+ X$	BR = $6.0 \cdot 10^{-38}$ R = $1.0 \cdot 10^{-31}$	— $1.6 \cdot 10^{-14}$
$m_{\tau\tau}$	$6.1 \cdot 10^{-2}$	$B^+ \rightarrow \pi^- \tau^+ \tau^+$ $e^+ p \rightarrow \bar{\nu}_e \tau^+ \tau^+ X$	BR = $3.6 \cdot 10^{-39}$ R = $7.0 \cdot 10^{-33}$	— $4.2 \cdot 10^{-15}$

Table 4.3: Same as previous table for the LMA solution.

element	max [eV]	process	ratio (max)	indirect/direct
$\langle m \rangle$	$7.6 \cdot 10^{-2}$	$0\nu\beta\beta$ $K^+ \rightarrow \pi^- e^+ e^+$	$T_{1/2}^{0\nu} = 4.0 \cdot 10^{26}$ y BR = $2.9 \cdot 10^{-34}$	0.22 $6.8 \cdot 10^{-13}$
$m_{e\mu}$	$6.4 \cdot 10^{-2}$	$^{48}\text{Ti}(\mu^-, e^+)^{48}\text{Ca}$ $K^+ \rightarrow \pi^- e^+ \mu^+$	R = $2.1 \cdot 10^{-39}$ BR = $2.5 \cdot 10^{-34}$	$2.2 \cdot 10^{-14}$ $7.1 \cdot 10^{-13}$
$m_{e\tau}$	$6.6 \cdot 10^{-2}$	$B^+ \rightarrow \pi^- e^+ \tau^+$ $e^+ p \rightarrow \bar{\nu}_e e^+ \tau^+ X$	BR = $1.0 \cdot 10^{-37}$ R = $1.9 \cdot 10^{-31}$	— $2.2 \cdot 10^{-14}$
$m_{\mu\mu}$	$5.5 \cdot 10^{-2}$	$K^+ \rightarrow \pi^- \mu^+ \mu^+$ $e^+ p \rightarrow \bar{\nu}_e \mu^+ \mu^+ X$	BR = $1.1 \cdot 10^{-34}$ R = $1.7 \cdot 10^{-30}$	$1.9 \cdot 10^{-13}$ $1.8 \cdot 10^{-14}$
$m_{\mu\tau}$	$3.9 \cdot 10^{-2}$	$B^+ \rightarrow \pi^- \mu^+ \tau^+$ $e^+ p \rightarrow \bar{\nu}_e \mu^+ \tau^+ X$	BR = $3.7 \cdot 10^{-38}$ R = $6.3 \cdot 10^{-32}$	— $1.3 \cdot 10^{-14}$
$m_{\tau\tau}$	$5.8 \cdot 10^{-2}$	$B^+ \rightarrow \pi^- \tau^+ \tau^+$ $e^+ p \rightarrow \bar{\nu}_e \tau^+ \tau^+ X$	BR = $3.2 \cdot 10^{-39}$ R = $6.4 \cdot 10^{-33}$	— $4.0 \cdot 10^{-15}$

Table 4.4: Same as previous table for the inverse hierarchy with $m_3 = 10^{-5}$ eV and the QVO solution.

element	max [eV]	process	ratio (max)	indirect/direct
$\langle m \rangle$	0.35	$0\nu\beta\beta$ $K^+ \rightarrow \pi^- e^+ e^+$	$T_{1/2}^{0\nu} = 1.9 \cdot 10^{25} \text{ y}$ BR = $6.2 \cdot 10^{-33}$	1 $3.1 \cdot 10^{-12}$
$m_{e\mu}$	2.00	$^{48}\text{Ti}(\mu^-, e^+)^{48}\text{Ca}$ $K^+ \rightarrow \pi^- e^+ \mu^+$	R = $2.0 \cdot 10^{-36}$ BR = $2.5 \cdot 10^{-31}$	$6.9 \cdot 10^{-13}$ $2.2 \cdot 10^{-11}$
$m_{e\tau}$	2.06	$B^+ \rightarrow \pi^- e^+ \tau^+$ $e^+ p \rightarrow \bar{\nu}_e e^+ \tau^+ X$	BR = $1.0 \cdot 10^{-34}$ R = $1.9 \cdot 10^{-28}$	— $6.8 \cdot 10^{-13}$
$m_{\mu\mu}$	2.00	$K^+ \rightarrow \pi^- \mu^+ \mu^+$ $e^+ p \rightarrow \bar{\nu}_e \mu^+ \mu^+ X$	BR = $1.5 \cdot 10^{-31}$ R = $2.2 \cdot 10^{-27}$	$7.0 \cdot 10^{-13}$ $2.4 \cdot 10^{-12}$
$m_{\mu\tau}$	1.27	$B^+ \rightarrow \pi^- \mu^+ \tau^+$ $e^+ p \rightarrow \bar{\nu}_e \mu^+ \tau^+ X$	BR = $3.9 \cdot 10^{-35}$ R = $6.7 \cdot 10^{-29}$	— $4.1 \cdot 10^{-13}$
$m_{\tau\tau}$	1.86	$B^+ \rightarrow \pi^- \tau^+ \tau^+$ $e^+ p \rightarrow \bar{\nu}_e \tau^+ \tau^+ X$	BR = $3.3 \cdot 10^{-36}$ R = $6.6 \cdot 10^{-30}$	— $1.3 \cdot 10^{-13}$

Table 4.5: Same as previous Table for the LMA solution and $m_0 = 2.2 \text{ eV}$.

element	max [eV]	process	ratio (max)	indirect/direct
$\langle m \rangle$	0.35	$0\nu\beta\beta$ $K^+ \rightarrow \pi^- e^+ e^+$	$T_{1/2}^{0\nu} = 1.9 \cdot 10^{25} \text{ y}$ BR = $6.2 \cdot 10^{-33}$	1 $3.1 \cdot 10^{-12}$
$m_{e\mu}$	0.17	$^{48}\text{Ti}(\mu^-, e^+)^{48}\text{Ca}$ $K^+ \rightarrow \pi^- e^+ \mu^+$	R = $1.5 \cdot 10^{-38}$ BR = $1.8 \cdot 10^{-33}$	$5.9 \cdot 10^{-14}$ $1.9 \cdot 10^{-12}$
$m_{e\tau}$	0.15	$B^+ \rightarrow \pi^- e^+ \tau^+$ $e^+ p \rightarrow \bar{\nu}_e e^+ \tau^+ X$	BR = $5.4 \cdot 10^{-38}$ R = $1.0 \cdot 10^{-30}$	— $5.0 \cdot 10^{-14}$
$m_{\mu\mu}$	0.37	$K^+ \rightarrow \pi^- \mu^+ \mu^+$ $e^+ p \rightarrow \bar{\nu}_e \mu^+ \mu^+ X$	BR = $5.1 \cdot 10^{-33}$ R = $7.7 \cdot 10^{-29}$	$1.3 \cdot 10^{-12}$ $4.4 \cdot 10^{-13}$
$m_{\mu\tau}$	0.37	$B^+ \rightarrow \pi^- \mu^+ \tau^+$ $e^+ p \rightarrow \bar{\nu}_e \mu^+ \tau^+ X$	BR = $3.3 \cdot 10^{-36}$ R = $5.7 \cdot 10^{-30}$	— $1.2 \cdot 10^{-13}$
$m_{\tau\tau}$	0.38	$B^+ \rightarrow \pi^- \tau^+ \tau^+$ $e^+ p \rightarrow \bar{\nu}_e \tau^+ \tau^+ X$	BR = $1.4 \cdot 10^{-37}$ R = $2.7 \cdot 10^{-31}$	— $2.6 \cdot 10^{-14}$

Table 4.6: Same as previous figure for the SMA solution and $m_0 = 0.39 \text{ eV}$.

Finally we note that decays like $\mu \rightarrow e\gamma$ are also sensitive on neutrino masses. However, the branching ratio is depending on the quantity [15]

$$\overline{m_{e\mu}^2} \equiv \sum U_{\mu i}^* U_{ei} m_i^2$$

and reads

$$\text{BR}(\mu \rightarrow e\gamma) \simeq \frac{3\alpha}{32\pi M_W^4} \overline{m_{e\mu}^2} \simeq 5 \cdot 10^{-48} \left(\frac{\overline{m_{e\mu}^2}}{\text{eV}^2} \right)^2.$$

This is much smaller than the processes considered here, since $\overline{m_{e\mu}^2}$ is maximally of the order of Δm_A^2 . In fact, for bimaximal mixing it holds

$$\overline{m_{e\mu}^2} = -\overline{m_{e\tau}^2} \simeq \Delta m_{21}^2 \frac{1}{2\sqrt{2}} \quad \text{and} \quad \overline{m_{\mu\tau}^2} \simeq \frac{1}{4}(\Delta m_{31}^2 + \Delta m_{32}^2)$$

and for $c_1 \simeq 1$:

$$\overline{m_{e\mu}^2} = \overline{m_{e\tau}^2} \simeq \Delta m_{31}^2 \frac{s_3}{\sqrt{2}} e^{i\delta} \quad \text{and} \quad \overline{m_{\mu\tau}^2} \simeq \frac{1}{2} \Delta m_{32}^2$$

Inserting the experimental limit of $\text{BR}(\mu \rightarrow e\gamma) \leq 1.2 \cdot 10^{-10}$ [131] yields $\sqrt{\overline{m_{e\mu}^2}} \lesssim 1$ GeV being more than 12 orders of magnitude higher than the value from oscillation.

However, the process is obviously also possible for the case of Dirac neutrinos, since only lepton flavor and not lepton number is violated. Also the fact that $\overline{m_{\alpha\beta}^2}$ depends only on δ and the Δm^2 shows that Dirac neutrinos are sufficient to trigger these decays. Similar arguments hold for decays like $\mu \rightarrow 3e$.

To sum up this section, direct limits on $m_{\alpha\beta}$ are physically not meaningful and except for $0\nu\beta\beta$ no observable effect of $m_{\alpha\beta}$ can be expected. However, the situation for lepton flavor violating modes like $\mu \rightarrow e\gamma$ is even worse. The fact that only $0\nu\beta\beta$ provides knowledge about the Majorana mass matrix is somewhat not surprising because using some 10 kg of ^{76}Ge for a $0\nu\beta\beta$ experiment correspond to about 10^{26} atoms. It is not possible to generate the same number of kaons or CC interactions.

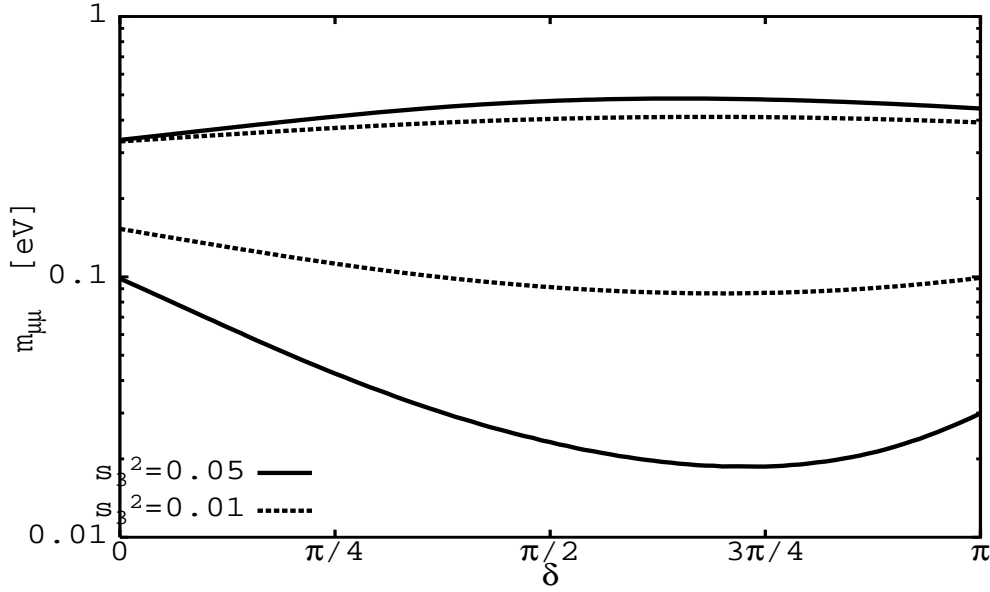


Figure 4.4: $m_{\mu\mu}$ as a function of the CKM phase δ for two different values of s_3^2 . The other parameters are $t_1^2 = t_2^2 = 0.7$, $\Delta m_A^2 = 3 \cdot 10^{-3} \text{ eV}^2$, $\Delta m_\odot^2 = 5 \cdot 10^{-5} \text{ eV}^2$, $m_1 = 0.6 \text{ eV}$ and $\langle m \rangle = 0.2 \text{ eV}$.

4.3.3 More on the influence of $\langle m \rangle$ on $m_{\alpha\beta}$

As shown, no observable effect of an element of $m_{\alpha\beta}$ other than $\langle m \rangle$ can be expected. Therefore, information about the phases α and β can only come from $0\nu\beta\beta$. In Section 2.3.3.2 it was shown that even if all masses and mixing angles are exactly known, a large range in (α, β) -space can give the same $\langle m \rangle$. Especially the phase β , which in our parametrisation is always connected with the small quantity s_3 , may be known to a bad precision. For the SMA solution the situation will be even worse because then α will be also connected with a small quantity, s_1 .

However, in $m_{\mu\mu}$ the dependence on β goes with $|U_{\mu 3}|^2 = s_2^2 c_3^2 \simeq 1/2$ and this fact will result in a large uncertainty. This is quantified in Fig. 4.4, where for two parameter sets the range of $m_{\mu\mu}$ is given as a function of the third phase δ . For large s_3^2 the allowed range can be up to a factor 25. This is however a rather extreme value, normally the relative difference does not exceed a factor of order one. Nevertheless, this factor is of the same order of magnitude as the one stemming from the uncertainty in the calculation of the nuclear matrix elements.

4.4 Effective heavy Majorana masses: $\frac{1}{m_{\alpha\beta}}$

We study now the experimental information on “the inverse effective Majorana neutrino mass”, defined as

$$\begin{aligned} \frac{1}{m_{\alpha\beta}} &= |(U \text{diag}(\frac{1}{m_1}, \frac{1}{m_2}, \frac{1}{m_3}, \dots) U^T)_{\alpha\beta}| \\ &= \left| \sum \frac{1}{m_i} U_{\alpha i} U_{\beta i} \right| \leq \sum \frac{1}{m_i} |U_{\alpha i} U_{\beta i}| \text{ with } \alpha, \beta = e, \mu, \tau. \end{aligned} \quad (4.16)$$

The sum over i is not the same as in $m_{\alpha\beta}$: For $m_{\alpha\beta}$ it goes over all “light” mass eigenstates and in $\frac{1}{m_{\alpha\beta}}$ over all “heavy” states. The attribute “light” or “heavy” depends on the energy scale of the process one considers to obtain information about the respective element. For example, a heavy neutrino is heavier than 1 GeV for $0\nu\beta\beta$ and heavier than 100 GeV for collider processes. Note that we indicated that the sum goes up to a number greater than three. It is however also possible that only one additional very heavy neutrino exists. Apart from theoretical prejudices, a priori we do not know how many there are.

The form of the matrix (4.16) might seem somewhat artificial; its form comes from the fact that — as we have seen — heavy Majorana neutrinos force cross sections or branching ratios (typically processes analogous to $0\nu\beta\beta$) to have mass⁻² dependence, see Eq. (3.1).

4.4.1 Direct limits on $\frac{1}{m_{\alpha\beta}}$

Reference [126] has given also the BRs of K and B decays for heavy Majorana neutrinos. We can use their numbers to set *direct* limits on the elements of $\frac{1}{m_{\alpha\beta}}$, along the same lines as in the previous section for $m_{\alpha\beta}$. For the tau sector we apply again the collider approach from [3], including the BR of taus into muons. The result is shown in Table 4.7.

Here there is a spread of “only” eight orders of magnitude, six orders of magnitude less then for $m_{\alpha\beta}$. The reason for this is that the high-energy processes at HERA are better suited for effects of very massive particles. This can be seen also when one compares the limit on $\frac{1}{m_{\mu\mu}}$ from HERA data and the kaon BR. The high-energy value is three orders of magnitude better and therefore the BR would have to be improved by a factor of 10^6 to get a comparable limit. The same holds for BRs of the rare B decays, which must be of the order of 10^{-15} in order to compete with the HERA limits. The limit on $m_{\mu\mu}$ from kaon decay and the collider process is of similar magnitude.

Again, the limits on $\frac{1}{m_{\alpha\beta}}$ except for $\langle \frac{1}{m} \rangle$ are unphysical, i.e. for $\frac{1}{m_{\alpha\beta}}$ of order 1 GeV^{-1}

element	process	experiment	direct limit [GeV ⁻¹]
$\langle \frac{1}{m} \rangle$	$0\nu\beta\beta$ $K^+ \rightarrow \pi^- e^+ e^+$	$T_{1/2}^{0\nu} > 1.9 \cdot 10^{25}$ y BR $< 6.4 \cdot 10^{-10}$	$1.1 \cdot 10^{-8}$ 852.8
$\frac{1}{m_{e\mu}}$	$K^+ \rightarrow \pi^- e^+ \mu^+$ $e^+ p \rightarrow \bar{\nu}_e e^+ \mu^+ X$	BR $< 5.0 \cdot 10^{-10}$ $\mathcal{L} = 82$ pb ⁻¹	762.5 0.73
$\frac{1}{m_{e\tau}}$	$B^+ \rightarrow \pi^- e^+ \tau^+$ $e^+ p \rightarrow \bar{\nu}_e e^+ \tau^+ X$	— $\mathcal{L} = 82$ pb ⁻¹	— 1.3
$\frac{1}{m_{\mu\mu}}$	$K^+ \rightarrow \pi^- \mu^+ \mu^+$ $e^+ p \rightarrow \bar{\nu}_e \mu^+ \mu^+ X$	BR $< 3.0 \cdot 10^{-9}$ $\mathcal{L} = 82$ pb ⁻¹	$3.5 \cdot 10^3$ 0.98
$\frac{1}{m_{\mu\tau}}$	$B^+ \rightarrow \pi^- \mu^+ \tau^+$ $e^+ p \rightarrow \bar{\nu}_e \mu^+ \tau^+ X$	— $\mathcal{L} = 82$ pb ⁻¹	— 1.3
$\frac{1}{m_{\tau\tau}}$	$B^+ \rightarrow \pi^- \tau^+ \tau^+$ $e^+ p \rightarrow \bar{\nu}_e \tau^+ \tau^+ X$	— $\mathcal{L} = 82$ pb ⁻¹	— 5.7

Table 4.7: Element of the Majorana mass matrix $\frac{1}{m_{\alpha\beta}}$, two processes, which are sensitive on the respective element, the experimental information on the process and the direct limit obtained from it.

the neutrino is light, not heavy. The same holds for $\frac{1}{m_{\mu\mu}} \simeq 10^3$ GeV⁻¹, which corresponds to a MeV neutrino, whose mass is “light” in a collider process.

4.4.2 Indirect limits on $\frac{1}{m_{\alpha\beta}}$

We recall the limits on heavy neutrinos, assuming no universality of coupling they read

$$\begin{aligned}
\sum |U_{ei}|^2 &< 6.6 \cdot 10^{-3}, \quad m_i > 89.5 \text{ GeV}, \\
\sum |U_{\mu i}|^2 &< 6.0 \cdot 10^{-3}, \quad m_i > 90.7 \text{ GeV}, \\
\sum |U_{\tau i}|^2 &< 1.8 \cdot 10^{-2}, \quad m_i > 80.5 \text{ GeV}.
\end{aligned} \tag{4.17}$$

With these numbers the maximal values of $\frac{1}{m_{\alpha\beta}}$ can be calculated, again assuming that there are no baroque models,

$$\frac{1}{m_{\alpha\beta}} \lesssim \begin{pmatrix} 7.4 \cdot 10^{-5} & 6.9 \cdot 10^{-5} & 1.2 \cdot 10^{-4} \\ & 6.6 \cdot 10^{-5} & 1.1 \cdot 10^{-4} \\ & & 2.2 \cdot 10^{-4} \end{pmatrix} \text{GeV}^{-1}. \tag{4.18}$$

Here we used the heavier limit on m_i for the mixed terms, i.e. 90.7 GeV for $\frac{1}{m_{e\mu}}$.

If one assumes universality, a common bound of 90.7 GeV on all m_i applies. However, the limits do not change, except for $\langle \frac{1}{m} \rangle$ and $\frac{1}{m_{\tau\tau}}$, which are now $7.3 \cdot 10^{-5}$ and $2.0 \cdot 10^{-4}$

element	max [GeV ⁻¹]	process	ratio (max)	indirect/direct
$\langle \frac{1}{m} \rangle$	$1.1 \cdot 10^{-8}$	$0\nu\beta\beta$ $K^+ \rightarrow \pi^- e^+ e^+$	$T_{1/2}^{0\nu} = 1.9 \cdot 10^{25}$ y BR = $1.1 \cdot 10^{-33}$	1 $1.3 \cdot 10^{-11}$
$\frac{1}{m_{e\mu}}$	$8.5 \cdot 10^{-7}$	$K^+ \rightarrow \pi^- e^+ \mu^+$ $e^+ p \rightarrow \bar{\nu}_e e^+ \mu^+ X$	BR = $6.2 \cdot 10^{-28}$ R = $5.5 \cdot 10^{-16}$	$1.1 \cdot 10^{-9}$ $1.2 \cdot 10^{-6}$
$\frac{1}{m_{e\tau}}$	$1.5 \cdot 10^{-6}$	$B^+ \rightarrow \pi^- e^+ \tau^+$ $e^+ p \rightarrow \bar{\nu}_e e^+ \tau^+ X$	BR = $1.4 \cdot 10^{-27}$ R = $5.6 \cdot 10^{-16}$	— $1.2 \cdot 10^{-6}$
$\frac{1}{m_{\mu\mu}}$	$6.6 \cdot 10^{-5}$	$K^+ \rightarrow \pi^- \mu^+ \mu^+$ $e^+ p \rightarrow \bar{\nu}_e \mu^+ \mu^+ X$	BR = $1.4 \cdot 10^{-24}$ R = $1.8 \cdot 10^{-12}$	$2.1 \cdot 10^{-8}$ $6.8 \cdot 10^{-5}$
$\frac{1}{m_{\mu\tau}}$	$1.1 \cdot 10^{-4}$	$B^+ \rightarrow \pi^- \mu^+ \tau^+$ $e^+ p \rightarrow \bar{\nu}_e \mu^+ \tau^+ X$	BR = $7.5 \cdot 10^{-24}$ R = $3.0 \cdot 10^{-12}$	— $8.7 \cdot 10^{-5}$
$\frac{1}{m_{\tau\tau}}$	$2.0 \cdot 10^{-4}$	$B^+ \rightarrow \pi^- \tau^+ \tau^+$ $e^+ p \rightarrow \bar{\nu}_e \tau^+ \tau^+ X$	BR = $4.8 \cdot 10^{-23}$ R = $5.0 \cdot 10^{-13}$	— $3.5 \cdot 10^{-5}$

Table 4.8: Element of the Majorana mass matrix $\frac{1}{m_{\alpha\beta}}$, maximal indirect limit on it, two processes, which are sensitive on the respective element and the quotient of this indirect limit with the direct limit from Table 4.7.

GeV⁻¹, respectively.

If we include the limit from neutrinoless double beta decay the values of U_{ei} are significantly constrained. One finds

$$\frac{1}{m_{\alpha\beta}} \lesssim \begin{pmatrix} 1.1 \cdot 10^{-8} & 8.5 \cdot 10^{-7} & 1.5 \cdot 10^{-6} \\ & 6.6 \cdot 10^{-5} & 1.1 \cdot 10^{-4} \\ & & 2.2 \cdot 10^{-4} \end{pmatrix} \text{GeV}^{-1}. \quad (4.19)$$

Two orders of magnitude are gained for the electron sector of the matrix. Assuming now again universality we find

$$\frac{1}{m_{\alpha\beta}} \lesssim \begin{pmatrix} 1.1 \cdot 10^{-8} & 8.5 \cdot 10^{-7} & 1.5 \cdot 10^{-6} \\ & 6.6 \cdot 10^{-5} & 1.1 \cdot 10^{-4} \\ & & 2.0 \cdot 10^{-4} \end{pmatrix} \text{GeV}^{-1}. \quad (4.20)$$

These are the values used in the following. They are denoted *indirect limits*. We remark that in [126] a lower limit on heavy neutrinos of 84.1 GeV was used and $\frac{1}{m_{\alpha\beta}} < (84.1 \text{ GeV})^{-1}$ for all elements except $\langle \frac{1}{m} \rangle$ was taken. This is a too high value since the mixing with these neutrinos has to be included.

4.4.3 Limits on lepton number violating processes from indirect limits of $\frac{1}{m_{\alpha\beta}}$

We can use the indirect limits on $\frac{1}{m_{\alpha\beta}}$, as displayed in Eq. (4.20), to predict the BRs and ratios of lepton number and flavor violating processes. The result is seen in Table 4.8. Comparing the “indirect/direct” column with its analogues for $m_{\alpha\beta}$ shows that for heavy neutrinos the situation is much better than for light ones. The reason lies in the already mentioned fact that high-energy processes are much better suited for effects of heavy particles. Furthermore, the bounds on heavy neutrinos are not comparable to the ones for light neutrinos. For them, much information from oscillation, neutrinoless double beta decay and the tritium spectrum exists.

To sum up this section, direct limits on elements of $\frac{1}{m_{\alpha\beta}}$ other than $\langle\frac{1}{m}\rangle$ are physically not meaningful. Indirect limits can not produce observable effects. The situation is however much better than for effects of light neutrinos.

4.4.4 An example for future limits: high energy Neutrino factory

In this subsection the achievable limits on $m_{\alpha\beta}$ and $\frac{1}{m_{\alpha\beta}}$ are given, when one considers the process

$$\nu_{\delta}^{(-)} N \rightarrow \delta^{\mp} \alpha^{\pm} \beta^{\pm} X, \text{ where } \delta = e, \mu \text{ and } \alpha, \beta = e, \mu, \tau \quad (4.21)$$

at a neutrino factory [5]. For the luminosity we use the same parameters as in Section 3.3. As has been shown there, the cross section is highest when the incoming neutrino is a ν_{μ} . Table 4.9 shows what *direct* limits could be achieved for luminosity per year given by the parameter set after Eq. (3.28) in Section 3.3.1. The improvement would be tremendous.

Since the direct limits are proportional to the inverse of the square root of the integrated luminosity, we expect for a given \sqrt{s} a limit better by a factor of

$$\sqrt{\frac{\mathcal{L}^{\nu \text{ factory}}}{\mathcal{L}^{\text{HERA}}}} = \sqrt{\frac{10^{46} \text{ cm}^2}{82 \text{ pb}^{-1}}} \simeq 10^4. \quad (4.22)$$

In fact, HERA’s center-of-mass energy corresponds to $E_{\mu} \simeq 10^4$ GeV and for this energy the limit on $m_{\mu\mu}$ is 0.3 GeV. This value is — as expected from Eq. (4.22) — four orders of magnitude better than the one from HERA, which is about 800 GeV. The same holds for the limits on $\frac{1}{m_{\alpha\beta}}$.

Even for $E_{\mu} = 20$ GeV the direct limit on $m_{\mu\tau}$ is comparable to the one from kaon decay. Comparing the limits on $m_{\alpha\beta}$ for $E_{\mu} = 50$ GeV with the plot of the cross section

E_μ	$m_{\mu\mu}$	$m_{\mu\tau}$	$m_{\tau\tau}$	$\frac{1}{m_{\mu\mu}}$	$\frac{1}{m_{\mu\tau}}$	$\frac{1}{m_{\tau\tau}}$
20	86.7	$1.4 \cdot 10^3$	$1.9 \cdot 10^7$	54.7	$7.0 \cdot 10^3$	—
50	38.3	$7.8 \cdot 10^2$	$3.1 \cdot 10^4$	9.3	32.6	$6.4 \cdot 10^2$
100	19.9	$2.5 \cdot 10^2$	$3.4 \cdot 10^3$	2.5	55.5	$3.5 \cdot 10^2$
200	10.3	91.1	$7.2 \cdot 10^2$	0.6	11.0	46.7
300	7.0	52.8	$3.5 \cdot 10^2$	0.3	4.5	16.9
400	5.3	37.2	$2.2 \cdot 10^2$	0.2	2.4	8.6
500	4.3	28.5	$1.6 \cdot 10^2$	0.1	1.5	5.2
10^3	2.2	12.7	60.6	$2.9 \cdot 10^{-2}$	0.4	1.2
$2 \cdot 10^3$	1.1	6.0	26.2	$7.9 \cdot 10^{-3}$	$9.5 \cdot 10^{-2}$	0.3
$4 \cdot 10^3$	0.6	3.0	12.2	$2.2 \cdot 10^{-3}$	$2.5 \cdot 10^{-2}$	$7.4 \cdot 10^{-2}$
10^4	0.3	1.2	4.8	$4.6 \cdot 10^{-4}$	$4.6 \cdot 10^{-3}$	$1.4 \cdot 10^{-2}$
10^5	$9.6 \cdot 10^{-3}$	0.1	0.4	$1.6 \cdot 10^{-5}$	$1.1 \cdot 10^{-4}$	$3.6 \cdot 10^{-4}$
10^6	$3.2 \cdot 10^{-4}$	$1.3 \cdot 10^{-3}$	$9.9 \cdot 10^{-4}$	$7.9 \cdot 10^{-7}$	$4.3 \cdot 10^{-6}$	$2.0 \cdot 10^{-5}$

Table 4.9: Obtainable direct limits for $m_{\alpha\beta}$ and $\frac{1}{m_{\alpha\beta}}$ (in GeV and GeV^{-1}) for different muon energies in GeV. It holds $\langle m \rangle \simeq m_{\mu\mu} \simeq 1/3 m_{e\mu}$ and $\frac{1}{m_{ee}} \simeq \frac{1}{m_{\mu\mu}} \simeq 1/3 \frac{1}{m_{e\mu}}$. For the luminosity the parameter set given in Section 3.3.1 is used. The branching ratio of $\tau \rightarrow \mu$ has been applied. For $\frac{1}{m_{\tau\tau}}$ and $E_\mu = 20$ GeV the program could not handle the small numbers.

in Fig. 3.8 one sees that the limit is however unphysical, since the cross section is proportional to m_i^{-2} for these masses. At HERA however, such masses would be “light” ones, as can be seen in Fig. 3.11. Physically meaningful limits can be achieved for muon energies higher than 500 GeV: Looking at Fig. 3.8 one sees that for the limit on $m_{\mu\mu}$ of 4 GeV the cross section is still rising with m_i^2 .

Going now to heavy Majoranas, the situation turns out to be different. The HERA limit on $\frac{1}{m_{\mu\mu}}$ of 1 GeV^{-1} is obtained for a muon energy of 200 GeV, showing again that for effects of heavy particles high center-of-mass energies are required. However, even the limit for $E_\mu = 20$ GeV is already better than the one from kaon decay. For $E_\mu = 500$ GeV the limit on $\frac{1}{m_{\mu\mu}}$ reads 0.1 GeV^{-1} , which together with $|U_{\mu i}|^2 \leq 6 \cdot 10^{-3}$ corresponds to $m_i \geq 0.06 \text{ GeV}$, certainly not a heavy neutrino. Only from energies higher than 10 TeV one finds m_i corresponding to heavy neutrinos. However, all of them are lower than the limit from the L3 experiment, 90.7 GeV. Regarding the μ and τ sector of $\frac{1}{m_{\alpha\beta}}$, it is seen that for extreme high muon energies (10^5 GeV and higher) the direct limits are better than the indirect ones.

Some words on future limits for Majorana neutrinos. Production of Majorana neu-

trinos is also possible for hadron–hadron colliders, such as LHC [75, 76]. Regarding the direct limits on $m_{\alpha\beta}$ and $\frac{1}{m_{\alpha\beta}}$ it was found that the cross section for $pp \rightarrow 2 \text{ jets } \alpha^\pm \alpha^\pm$ is about 10^{-29} (10^{-20}) pb for Majorana masses of 1 eV (10^9 GeV) [132]. Assuming 100 fb^{-1} luminosity per year results in limits of 1 TeV (10^{-2} GeV^{-1}) for $m_{\alpha\alpha}$ and $\frac{1}{m_{\alpha\alpha}}$, respectively. These are again unphysical values, since 1 TeV is clearly not a light neutrino and $\frac{1}{m_{\alpha\alpha}} \simeq 10^{-2} \text{ GeV}^{-1}$ corresponds to $m_i \simeq 1 \text{ GeV}$, which is not a heavy neutrino. Similar arguments hold for production at the TeVatron.

Lately it was argued [76] that Majorana masses up to about 250 GeV may be probed by the LHC machine. These values will improve the indirect bounds on $\frac{1}{m_{\alpha\beta}}$. In addition, linear colliders will probe Majorana neutrinos of maximally \sqrt{s} [88], i.e. in the foreseeable future at most 1 TeV. The indirect bounds on $\frac{1}{m_{\alpha\beta}}$ will therefore not be improved by more than one or two orders of magnitude. Regarding future limits, we note that it has been shown [2] that the direct bounds from HERA can not be expected to be improved by more than one order of magnitude. The direct limits on $\langle m \rangle$ and $\langle \frac{1}{m} \rangle$ can be improved by the GENIUS experiment by two orders of magnitude.

4.5 Model dependent considerations for heavy neutrinos

The bounds discussed so far are all for left-handed Majorana neutrinos but were largely model independent. Now we discuss some more model dependent cases, concentrating on see-saw inspired heavy Majorana neutrinos.

4.5.1 Right-handed Majorana neutrinos and see-saw models

As we have seen in Chapter 3, the cross sections for left- and right-handed Majorana neutrinos are comparable and therefore the limits on the right-handed $\frac{1}{m_{\alpha\beta}}$ can be assumed to be comparable.

According to the PDG, the limit on a right-handed neutrino is [85]

$$M_R \geq 1.2 \frac{G_F}{G_R}, \quad (4.23)$$

where G_F is the usual Fermi constant and G_R its analogue for the right-handed sector. Assuming that the coupling constant of the left- and right-handed sectors are identical, G_F/G_R is equal to $(M_{W_R}/M_W)^2$ where M_{W_R} is the right-handed W boson. Using the lower bound of 720 GeV on its mass [103], we find that $M_R \gtrsim 96$ GeV. This is interestingly of the same order of magnitude as the bound on left-handed Majorana neutrinos from the LEP experiments. Recall that the limits on the mixing U_{ei} with heavy neutrinos also apply to right-handed ones. Thus our derived indirect limits on $\frac{1}{m_{\alpha\beta}}$ also apply to right-handed neutrinos.

In the most simple see-saw models one expects $U_{\alpha i} \sim m_D/M_R$ and $M_R \sim m_D^2/m_\nu$ which, for $m_D \sim$ GeV and $m_\nu \sim$ meV results in $\frac{1}{m_{\alpha\beta}} \sim 10^{-36}$ GeV $^{-1}$. Then the BR for $K^+ \rightarrow \pi^- \mu^+ \mu^+$ will be about 10^{-52} .

Less severe reduction is expected from the following argument: the see-saw model predicts in general (see Section 1.2)

$$U_{ei}^2 M_{Ri} = m_L - \langle m \rangle, \quad (4.24)$$

where m_L is the Majorana mass from the left-handed Higgs triplet and M_{Ri} the masses of the right-handed neutrinos. If the left-handed triplet is absent one finds for one neutrino M_R

$$U_{ei}^2 M_R = -\langle m \rangle \Rightarrow \frac{|U_{ei}^2|}{M_R} = \frac{\langle m \rangle}{M_R^2} \lesssim 3.8 \cdot 10^{-14} \text{ GeV}^{-1}, \quad (4.25)$$

which is five orders of magnitude more stringent than the $\langle \frac{1}{m} \rangle$ limit from $0\nu\beta\beta$. In natural left-right symmetric models (see e.g. [73]) one expects m_L to be of the order

of $m_{\alpha\beta}$ so that the same holds true for the case of non-vanishing m_L . In these models, M_R of order 10^{10} GeV or more is expected so that again $\langle \frac{1}{m} \rangle$ will be very small, much smaller than our indirect limits.

One can avoid the extreme heaviness of the neutrinos. A simple example has been presented in [133]: if the neutrino mass matrix is given by

$$m = \begin{pmatrix} m_L & m_D \\ m_D & M_R \end{pmatrix} \quad (4.26)$$

and $m_L M_R = m_D^2$ accidentally or due to some symmetry, one finds the exact result

$$\begin{aligned} m_1 &= 0 \\ m_2 &= m_L + M_R \\ \tan \theta &= \sqrt{\frac{m_L}{M_R}} \end{aligned} \quad (4.27)$$

The symmetry can be broken¹ and give a non-vanishing neutrino mass m_1 . Unlike the usual see-saw models, the mixing angle is not a function of the ratio m_1/m_2 and can be large. Experimentally, $\sin^2 \theta \leq 6.6 \cdot 10^{-3}$, which corresponds to

$$150 m_L \lesssim M_R. \quad (4.28)$$

With this constraint, it is possible to evade the very small U_{ei} and the large M_R predicted by the usual see-saw model and get values of $\frac{1}{m_{\alpha\beta}}$ as low as our indirect limits.

4.5.2 Unitarity revisited

Unitarity allows to set an *upper* limit on the mass scale of the new physics responsible for neutrino mass [134]. As shown in Section 3.1, for light neutrinos and $\sqrt{s} \gg m_i$ the high energy limit of the cross section for $e^-e^- \rightarrow W^-W^-$ is

$$\sigma = \frac{G_F^2}{4\pi} \langle m \rangle^2. \quad (4.29)$$

As already mentioned there, this violates unitarity since the amplitude grows with \sqrt{s} .

The following argument is analogue to the one which shows that Fermi theory breaks down at about 300 GeV energy. The inelastic cross section can be bounded if one uses partial wave expansion and the optical theorem:

$$\sigma_{\text{in}} \leq \frac{1}{4} \frac{4\pi}{2s} \sum_l (2l+1)(1-\eta_l^2), \quad (4.30)$$

¹In fact, when $m_L M_R = m_D^2(1+\epsilon)$ then one finds for $\epsilon \ll 1$ that $m_1 \simeq \epsilon m_L M_R / (m_L + M_R) \simeq \epsilon m_L / M_R$, $m_2 \simeq m_L + M_R$ and $\tan \theta \simeq \sqrt{m_L / M_R}$.

where l is the angular momentum and η_l is the inelasticity parameter, which is smaller than one. The factors $1/4$ and $1/2$ are due to spin averaging and two identical particles in the final state, respectively. The value of \sqrt{s} that corresponds to this limit of σ_{in} can be identified with $\Lambda_{\text{Majorana}}$, the scale of new physics. For $l = 0$ one finds

$$\Lambda_{\text{Majorana}} \leq \frac{\sqrt{2}\pi}{G_F} \frac{1}{\langle m \rangle} \simeq 3.8 \cdot 10^{14} \left(\frac{\text{eV}}{\langle m \rangle} \right) \text{ GeV}. \quad (4.31)$$

We can identify this scale with $U_{ei}^2 M_i$, where M_i is a heavy neutrino. Therefore,

$$\langle \frac{1}{m} \rangle \leq \frac{3.8 \cdot 10^{14}}{M_i^2} \left(\frac{\text{eV}}{\langle m \rangle} \right) \text{ GeV}^{-1}. \quad (4.32)$$

With $M_i \gtrsim 100$ GeV one obtains the lower bound on the BR of $K \rightarrow \pi^- e^+ e^+$ of about 10^{-45} (10^{-42} , 10^{-40}) for $\langle m \rangle = 0.01$ (0.35, 2.2) eV. Similar arguments hold of course for the other entries of $m_{\alpha\beta}$. If we identify $\Lambda_{\text{Majorana}}$ with $\langle \frac{1}{m} \rangle^{-1}$ then the lower bound on the BR of $K \rightarrow \pi^- e^+ e^+$ increases 4 orders of magnitude.

4.6 Summary and final remarks

The allowed ranges of the elements of the MNS matrix U are derived. It is found that — if one incorporates the bound on $\langle m \rangle$ — this range is a function of the smallest mass eigenstate, though it does not influence the oscillations. This effect is quantified for the first time. The cases of CP violation and conservation are considered and their differences are discussed.

Regarding the range of $m_{\alpha\beta}$, some analytical examples are given, which explain the properties of the allowed values found in a numerical analysis. Branching ratios, cross sections and similar observables depending on elements of $m_{\alpha\beta}$ are estimated. Because of their smallness, no measurable effect of an element of $m_{\alpha\beta}$ can be expected. Therefore only $\langle m \rangle$ can give information about $m_{\alpha\beta}$. Even worse, provided one knows all neutrino parameters except the three phases *exactly*, the other elements of $m_{\alpha\beta}$ still have an uncertainty within one order of magnitude. This is an uncertainty in addition to the one from the calculation of the nuclear matrix elements for $0\nu\beta\beta$.

Direct and indirect limits on $m_{\alpha\beta}$ and $\frac{1}{m_{\alpha\beta}}$ are defined and estimated. For the τ sector a collider approach is introduced, which gives currently the only limits on these entries. It is found that indirect limits on $m_{\alpha\beta}$ are more stringent by up to 14 orders of magnitude. Setting direct limits on the elements — other than $\langle m \rangle$ and $\langle \frac{1}{m} \rangle$ — makes no sense: no physically meaningful values can be obtained. Expecting signals from light neutrinos participating in oscillation experiments makes also no sense: the ratios with the relevant SM processes are extremely tiny, at most 10^{-23} .

The current information on heavy neutrinos can be used to set indirect limits on $\frac{1}{m_{\alpha\beta}}$. For low energy processes such as meson decays, the ratios are again tiny, for high energy analogues they can be up to 10^{-12} , which is however still not accessible in experiments. There is not much information on heavy Majorana neutrinos so that the difference of direct and indirect limits is less severe, in fact six orders of magnitude less than for light neutrinos. The direct limits on $\frac{1}{m_{\alpha\beta}}$ from the collider approach are better than the ones from BRs because high-energy processes are better suited for effects of heavy particles.

Model dependent bounds can be derived for heavy right-handed neutrinos, which are expected to produce very similar BRs as heavy left-handed ones. For simple see-saw models the resulting limits are tens of orders of magnitude more stringent than the indirect ones. Unitarity gives an *upper* bound on the heavy Majorana neutrinos, which is inverse proportional to $\langle m \rangle$, thus connecting the light and heavy sector in a model independent way.

A simple model is presented, which can produce mixing parameters and masses close to their current experimental limits. However, as shown in this Chapter, even when one

inserts the current bounds for Majorana neutrinos and their mixing, $m_{\alpha\beta}$ or $\frac{1}{m_{\alpha\beta}}$ do not produce sizable effects outside $0\nu\beta\beta$. Therefore, if (typically LSD) signals of the processes considered here are found, it will mean that other “new physics” is responsible.

Chapter 5

Summary

It was the main goal of this thesis to look for observable effects of Majorana neutrinos. The implied lepton number violation is the key signature of their Majorana character and some consequences in low- and high-energy processes have been studied. In any gauge theory, the observation of processes considered in this thesis implies a Majorana mass term, regardless of the mechanism causing it. This loop-induced mass will however be exceedingly small and therefore any information on $m_{\alpha\beta}$ or $\frac{1}{m_{\alpha\beta}}$ from oscillation or high-energy data can help to reveal the true mechanism of lepton number violation.

In Chapter 2 the connection of neutrinoless double beta decay and neutrino oscillation was studied. The form of $\langle m \rangle$ in all relevant schemes was given and the dependence on the oscillation parameters presented. In a degenerate scheme several limits on the common mass scale were given, where both the CP conserving and violating cases were analyzed. For large mixing in the inverse (Eq. (2.42)) and degenerate (Eq. (2.45)) scheme it may be possible to infer the value of the phase α , whereas the second phase β will be hard to measure since s_3 is small. In a special situation for the SMA solution however (Eq. (2.47)), β may be accessible.

For the first time a correlated data set was used and an analysis of the range of $\langle m \rangle$ as a function of the smallest mass state was presented. For the SMA solution, a limit on 0.39 eV for the smallest neutrino mass was obtained, which is possible for s_3 close to its upper bound and the phase β to be around $\pi/2$. For the other solar solutions, the tritium limit of 2.2 eV applies, which however requires the phase α to be the closer to $\pi/2$ the smaller the $\langle m \rangle$ limit is. Independent on the solar solution, the normal (inverse) hierarchical scheme is ruled out for $\langle m \rangle \gtrsim 0.02$ (0.1) eV. When the value of the smallest mass state is approximately 0.2 eV, the normal and inverse scheme merge into each other.

It was distinguished between CP conservation and violation and the area in which the distinction between this two cases is possible was identified. This area is in general larger for the inverse scheme. In addition, the difference occurs at larger values of

$\langle m \rangle$ and the neutrino mass for the inverse scheme. It was emphasized that in certain situations $0\nu\beta\beta$ can provide complementary information about the solar solution and the mass scheme. Moreover, limits on the smallest mass eigenstate better by two orders of magnitude than from direct searches are possible. For the first time, aspects of the “dark side” of the parameter space were discussed, which showed the different consequences of both sectors for $\langle m \rangle$.

In Chapter 3 the production of heavy Majorana neutrinos in different reactions was studied, focusing on diagrams analogous to $0\nu\beta\beta$. First, inverse neutrinoless double beta decay ($e^-e^- \rightarrow W^-W^-$) was analyzed, where all relevant properties of the reaction are easily derived and the existing limits on mass and mixing show their effect most clearly. The process renders unobservable for center-of-mass energies below 2 TeV.

Then, for the first time, the $0\nu\beta\beta$ diagram was applied to neutrino–nucleon scattering (conventional experiments and future neutrino factories) and electron–proton scattering. The general case with two like–sign dileptons of arbitrary flavor in the final state was considered, applying realistic experimental cuts and including τ leptons with their decay.

Though the expected signal is very small, a possible explanation of an anomaly in the H1 experiment was discussed. In this experiment, several events containing one isolated lepton and missing transverse momentum were found. The original like–sign dilepton signal of the process analogous to $0\nu\beta\beta$ has the property that one of the leptons can escape the experimental cuts and thus is observed as only one isolated lepton. In all of the processes under study it has been shown that final states with electrons are strongly suppressed due to the limit (2.9) on heavy neutrino mixing from $0\nu\beta\beta$.

Finally, in Chapter 4 we analyzed the complete range of the Majorana mass matrix $m_{\alpha\beta}$. After estimating the range of the MNS matrix, showing that it is a function of the smallest mass state, the range of $m_{\alpha\beta}$ was given for all hierarchies and solar solutions (“indirect limits”). Then, for the first time, “direct limits” on all elements of $m_{\alpha\beta}$ were obtained, using existing limits on BRs and similar ratios of lepton number and flavor violating processes. These are depending on elements of $m_{\alpha\beta}$ just as $0\nu\beta\beta$ depends on $\langle m \rangle$. For the τ sector of $m_{\alpha\beta}$ a collider approach was proposed, which gives better limits on the respective elements, unless the BR limit on e.g. $B^+ \rightarrow \pi^- \tau^+ \tau^+$ is lower than 10^{-10} . The obtained limits on $m_{\alpha\beta}$ are unphysical, which means that their values correspond to heavy, not light neutrinos. However they were quantified for the first time. The values of $m_{\alpha\beta}$ obtained from the oscillation data are used to predict the rates for lepton number and flavor violating processes. These indirect limits are (with the notable exception of $0\nu\beta\beta$) up to 14 orders of magnitude more stringent than the direct ones.

A similar analysis was also performed for effects of heavy Majorana neutrinos. A matrix analogous to $m_{\alpha\beta}$ was defined, which has a form suitable to take into account the mass⁻² dependence of processes involving heavy particles. The limits are again

unphysical, which means that their values correspond to light, not heavy neutrinos. The situation is better than for light neutrinos, where the direct and indirect limits differ by “only” eight orders of magnitude. This happens because the information about oscillations and light neutrino masses is not comparable to the one about heavy neutrinos. It was found that for heavy Majorana neutrinos the collider approach gives better limits than BRs because high-energy processes are better suited for effects of heavy particles.

Another novel aspect presented in this thesis was the influence of a measurement of $\langle m \rangle$ on the magnitude of the other elements of $m_{\alpha\beta}$. Since only one observable is used, which depends on two phases (from which one is connected to the small quantity s_3), a large area in α - β space is allowed. This results for the other elements of $m_{\alpha\beta}$ in an uncertainty of the same order as the one stemming from the calculation of nuclear matrix elements for the limit on $\langle m \rangle$.

To conclude, the detection of lepton number violation induced by Majorana neutrinos and the derivation of the light and heavy mass matrices is a big challenge. Probably only neutrinoless double beta decay will be capable of providing information on this sector of particle physics. Effects of analogues of $0\nu\beta\beta$ for light and heavy neutrinos are extremely small relative to the relevant processes of the Standard Model. Production at colliders does not involve the uncertainty due to the calculation of nuclear matrix elements in $0\nu\beta\beta$, but predicts extremely small cross sections or is limited to a small mass range. However, a measurement of $0\nu\beta\beta$ can give additional and unique information on a variety of neutrino parameters and deserves future attention.

Appendix A

Mass matrix elements

We give now — in our paramterisation (1.24) the form of all entries of $m_{\alpha\beta}$ as needed for the estimates in Chapter 4. The by far most important element $\langle m \rangle$ is depending on two phases, the other five elements depend on all three phases.

$$\langle m \rangle^2 = c_3^4 \left(c_1^4 m_1^2 + s_1^4 m_2^2 + t_3^4 m_3^2 + 2(m_2 m_3 s_1^2 t_3^2 c_{2(\alpha-\beta)} + c_1^2 m_1 (s_1^2 c_{2\alpha} m_2 + t_3^2 c_{2\beta} m_3)) \right) \quad (\text{A.1})$$

$$m_{e\mu}^2 = c_3^2 \left(((m_1 - m_2 c_{2\alpha}) c_1 c_2 s_1 + m_1 c_\delta c_1^2 s_2 s_3 + (- (m_3 c_{2\beta+\delta}) + m_2 c_{2\alpha+\delta} s_1^2) s_2 s_3)^2 + (m_2 c_1 c_2 s_{2\alpha} s_1 - m_1 c_1^2 s_\delta s_2 s_3 + (m_3 s_{2\beta+\delta} - m_2 s_{2\alpha+\delta} s_1^2) s_2 s_3)^2 \right) \quad (\text{A.2})$$

$$m_{e\tau}^2 = c_3^2 \left(-((m_1 - m_2 c_{2\alpha}) c_1 s_1 s_2) + m_1 c_\delta c_1^2 c_2 s_3 + c_2 (- (m_3 c_{2\beta+\delta}) + m_2 c_{2\alpha+\delta} s_1^2) s_3 \right)^2 + (m_2 c_1 s_{2\alpha} s_1 s_2 + m_1 c_1^2 c_2 s_\delta s_3 + c_2 (- (m_3 s_{2\beta+\delta}) + m_2 s_{2\alpha+\delta} s_1^2) s_3)^2 \quad (\text{A.3})$$

$$m_{\mu\mu}^2 = \left(c_1 (m_1 s_\delta - m_2 s_{2\alpha+\delta}) s_1 2s_2 c_2 s_3 + s_2^2 (m_3 c_3^2 s_{2(\beta+\delta)} + m_2 s_{2(\alpha+\delta)} s_1^2 s_3^2) + c_1^2 (m_2 c_2^2 s_{2\alpha} + m_1 s_{2\delta} s_2^2 s_3^2) \right)^2 + \left(m_3 c_{2(\beta+\delta)} c_3^2 s_2^2 + 2m_2 s_{2\alpha} s_\delta s_1 s_2 s_3 (c_1 c_2 - c_\delta s_1 s_2 s_3) + m_1 \left(- (c_1^2 s_\delta^2 s_2^2 s_3^2) + (c_2 s_1 + c_\delta c_1 s_2 s_3)^2 \right) + m_2 c_{2\alpha} \left(- (s_\delta^2 s_1^2 s_2^2 s_3^2) + (c_1 c_2 - c_\delta s_1 s_2 s_3)^2 \right) \right)^2 \quad (\text{A.4})$$

$$\begin{aligned}
m_{\mu\tau}^2 = & \left(- (m_2 c_{2\alpha} c_1^2 c_2 s_2) + m_3 c_{2(\beta+\delta)} c_2 c_3^2 s_2 - m_1 c_2 s_1^2 s_2 + m_1 c_\delta c_1 c_2^2 s_1 s_3 - \right. \\
& m_2 c_{2\alpha+\delta} c_1 c_2^2 s_1 s_3 - m_1 c_\delta c_1 s_1 s_2^2 s_3 + m_2 c_{2\alpha+\delta} \\
& \left. c_1 s_1 s_2^2 s_3 + m_1 c_{2\delta} c_1^2 c_2 s_2 s_3^2 + m_2 c_{2(\alpha+\delta)} c_2 s_1^2 s_2 s_3^2 \right)^2 + \\
& (c_1 (c_2^2 - s_2^2) (m_1 s_\delta - m_2 s_{2\alpha+\delta}) , s_1 s_3 + c_1^2 c_2 s_2 (- (m_2 s_{2\alpha}) + m_1 s_{2\delta} s_3^2) + \\
& \left. c_2 s_2 (m_3 c_3^2 s_{2(\beta+\delta)} + m_2 s_{2(\alpha+\delta)} s_1^2 s_3^2) \right)^2
\end{aligned} \tag{A.5}$$

$$\begin{aligned}
m_{\tau\tau}^2 = & \left(m_3 c_{2(\beta+\delta)} c_2^2 c_3^2 - 2 m_2 c_2 s_{2\alpha} s_\delta s_1 s_3 (c_1 s_2 + c_\delta c_2 s_1 s_3) + \right. \\
& m_1 \left(- (c_1^2 c_2^2 s_\delta^2 s_3^2) + (s_1 s_2 - c_\delta c_1 c_2 s_3)^2 \right) + m_2 c_{2\alpha} \left(- (c_2^2 s_\delta^2 s_1^2 s_3^2) + \right. \\
& \left. (c_1 s_2 + c_\delta c_2 s_1 s_3)^2 \right) \left. \right)^2 + \left(m_3 c_2^2 c_3^2 s_{2(\beta+\delta)} + 2 m_1 c_1 c_2 s_\delta s_3 (- (s_1 s_2) \right. \\
& \left. + c_\delta c_1 c_2 s_3) + 2 m_2 c_{2\alpha} c_2 s_\delta s_1 s_3 (c_1 s_2 + c_\delta c_2 s_1 s_3) + \right. \\
& \left. m_2 s_{2\alpha} \left(- (c_2^2 s_\delta^2 s_1^2 s_3^2) + (c_1 s_2 + c_\delta c_2 s_1 s_3)^2 \right) \right)^2
\end{aligned} \tag{A.6}$$

Appendix B

The matrix element

B.1 Left-handed Majorana neutrino

The calculation for the process $\nu_\mu q \rightarrow \mu^- \mu^+ \mu^+ q'$ has been outlined in Chapter 3. To analyze the $0\nu\beta\beta$ diagram at various other collider and accelerator types and for right-handed neutrinos and/or interactions, the derivation has to be modified. This can be done via the exchange of $\gamma_- \leftrightarrow \gamma_+$ before the computation of the traces. In the following, we skip the prefactor

$$\left(U_{\mu i}^2 m_i\right)^2 G_F^4 M_W^8 2^{12} \left(\frac{1}{q_1^2 - M_W^2} \frac{1}{q_1^2 - M_W^2}\right)^2$$

and start with the basic diagram

$$|\mathcal{M}|^2(\nu_\mu q \rightarrow \mu^- \mu^+ \mu^+ q') \equiv |\mathcal{M}^{\nu_{--}}|^2 =$$

$$(p_1 \cdot p_2) \left[\frac{1}{(q^2 - m_i^2)^2} (k_1 \cdot k_2)(k_3 \cdot k_4) + \frac{1}{(\tilde{q}^2 - m_i^2)^2} (k_1 \cdot k_3)(k_2 \cdot k_4) - \right. \quad (\text{B.1})$$

$$\left. \frac{1}{(q^2 - m_i^2)(\tilde{q}^2 - m_i^2)} \{ (k_2 \cdot k_3)(k_1 \cdot k_4) - (k_1 \cdot k_3)(k_2 \cdot k_4) + (k_1 \cdot k_2)(k_3 \cdot k_4) \} \right].$$

The upper index denotes the incoming particle and the two lower ones correspond to γ_\pm at the respective vertex. Scattering with an antiquark yields

$$|\mathcal{M}|^2(\nu_\mu \bar{q} \rightarrow \mu^- \mu^+ \mu^+ \bar{q}') \equiv |\mathcal{M}^{\nu_{-+}}|^2 = |\mathcal{M}^{\nu_{--}}|^2(p_2 \leftrightarrow k_4) \quad (\text{B.2})$$

and the respective processes with an antineutrino read

$$|\mathcal{M}|^2(\bar{\nu}_\mu q \rightarrow \mu^+ \mu^- \mu^- q') \equiv |\mathcal{M}^{\nu_{++}}|^2 = |\mathcal{M}^{\nu_{-+}}|^2 \quad (\text{B.3})$$

and

$$|\mathcal{M}|^2(\bar{\nu}_\mu \bar{q} \rightarrow \mu^+ \mu^- \mu^- \bar{q}') \equiv |\mathcal{M}^{\nu_{++}}|^2 = |\mathcal{M}^{\nu_{--}}|^2, \quad (\text{B.4})$$

respectively. Applying the procedure to HERA results in

$$\begin{aligned}
|\mathcal{M}|^2(e^+ q \rightarrow \bar{\nu}_e \mu^+ \mu^+ q') &\equiv |\mathcal{M}_{+-}^e|^2 = |\mathcal{M}_{--}^\nu|^2(p_1 \leftrightarrow k_1) \\
|\mathcal{M}|^2(e^+ \bar{q} \rightarrow \bar{\nu}_e \mu^+ \mu^+ \bar{q}') &\equiv |\mathcal{M}_{++}^e|^2 = |\mathcal{M}_{--}^\nu|^2(p_1 \leftrightarrow k_1, p_2 \leftrightarrow k_4) \\
|\mathcal{M}|^2(e^- q \rightarrow \nu_e \mu^- \mu^- q') &\equiv |\mathcal{M}_{--}^e|^2 = |\mathcal{M}_{++}^e|^2 \\
|\mathcal{M}|^2(e^- \bar{q} \rightarrow \nu_e \mu^- \mu^- \bar{q}') &\equiv |\mathcal{M}_{-+}^e|^2 = |\mathcal{M}_{+-}^e|^2.
\end{aligned} \tag{B.5}$$

B.2 Right-handed Majorana neutrino

Also for a right-handed Majorana neutrino simple exchanges of γ_+ with γ_- have to be performed. One finds

$$\begin{aligned}
|\mathcal{M}|_R^2(\nu_\mu q \rightarrow \mu^- \mu^+ \mu^+ q') &\equiv |\mathcal{M}_{--}^\nu|_R^2 = |\mathcal{M}_{--}^\nu|^2(k_1 \leftrightarrow p_1, p_2 \leftrightarrow k_4) \\
|\mathcal{M}|_R^2(\nu_\mu \bar{q} \rightarrow \mu^- \mu^+ \mu^+ \bar{q}') &\equiv |\mathcal{M}_{-+}^\nu|_R^2 = |\mathcal{M}_{--}^\nu|^2(p_1 \leftrightarrow k_1) \\
|\mathcal{M}|_R^2(\bar{\nu}_\mu q \rightarrow \mu^+ \mu^- \mu^- q') &\equiv |\mathcal{M}_{+-}^\nu|_R^2 = |\mathcal{M}_{-+}^\nu|_R^2 \\
|\mathcal{M}|_R^2(\bar{\nu}_\mu \bar{q} \rightarrow \mu^+ \mu^- \mu^- \bar{q}') &\equiv |\mathcal{M}_{++}^\nu|_R^2 = |\mathcal{M}_{--}^\nu|_R^2
\end{aligned} \tag{B.6}$$

For HERA:

$$\begin{aligned}
|\mathcal{M}|_R^2(e^+ q \rightarrow \bar{\nu}_e \mu^+ \mu^+ q') &\equiv |\mathcal{M}_{+-}^e|_R^2 = |\mathcal{M}_{--}^\nu|^2(p_2 \leftrightarrow k_4) \\
|\mathcal{M}|_R^2(e^+ \bar{q} \rightarrow \bar{\nu}_e \mu^+ \mu^+ \bar{q}') &\equiv |\mathcal{M}_{++}^e|_R^2 = |\mathcal{M}_{--}^\nu|^2 \\
|\mathcal{M}|_R^2(e^- q \rightarrow \nu_e \mu^- \mu^- q') &\equiv |\mathcal{M}_{--}^e|_R^2 = |\mathcal{M}_{--}^\nu|^2 \\
|\mathcal{M}|_R^2(e^- \bar{q} \rightarrow \nu_e \mu^- \mu^- \bar{q}') &\equiv |\mathcal{M}_{-+}^e|_R^2 = |\mathcal{M}_{+-}^e|_R^2.
\end{aligned} \tag{B.7}$$

For purely right-handed currents, one replaces $\gamma_- \leftrightarrow \gamma_+$ everywhere and the results stays the same.

Appendix C

Derivation of the neutrino spectrum from muon decay

In order to calculate the event numbers for a given process at a neutrino factory, it is necessary to integrate over the energy spectrum of the incoming neutrinos. One starts from the matrix element for the process $\mu(p) \rightarrow \nu_\mu(k_1) e(k_2) \nu_e(k_3)$ multiplied with the phase space,

$$dN \propto |\mathcal{M}|^2 d\Phi(p; k_1, k_2, k_3) \propto (p \cdot k_3)(k_1 \cdot k_2) \frac{d^3 k_1}{2E_1} \frac{d^3 k_2}{2E_2} \frac{d^3 k_3}{2E_3} \delta((p - k_1 - k_2)^2). \quad (\text{C.1})$$

In the rest system of the muon with mass m it holds

$$(p \cdot k_3)(k_1 \cdot k_2) = \frac{1}{2} m^2 E_3 (m - 2 E_3), \quad (\text{C.2})$$

so that after integrating out k_2 one gets:

$$dN \propto E_3^2 (m - 2 E_3) E_1 \delta(m^2 - 2 m(E_1 + E_3) + 2 E_1 E_3 (1 - \cos \theta)) dE_1 dE_3 d \cos \theta, \quad (\text{C.3})$$

where θ is the polar angle between the electron neutrino and the muon neutrino, which is introduced via

$$\frac{d^3 k_1}{2 E_1} \frac{d^3 k_3}{2 E_3} = 2 \pi^2 E_1 E_3 dE_1 dE_3 d \cos \theta. \quad (\text{C.4})$$

One integrates now over $\cos \theta$. Due to

$$\int_a^b dx \delta(x - c) = \theta(b - c) \theta(c - a) \quad (\text{C.5})$$

one has two conditions, coming from the two Heavyside functions:

$$\frac{m}{2} - E_1 < E_3 \text{ and } E_3 < \frac{m}{2}. \quad (\text{C.6})$$

Therefore,

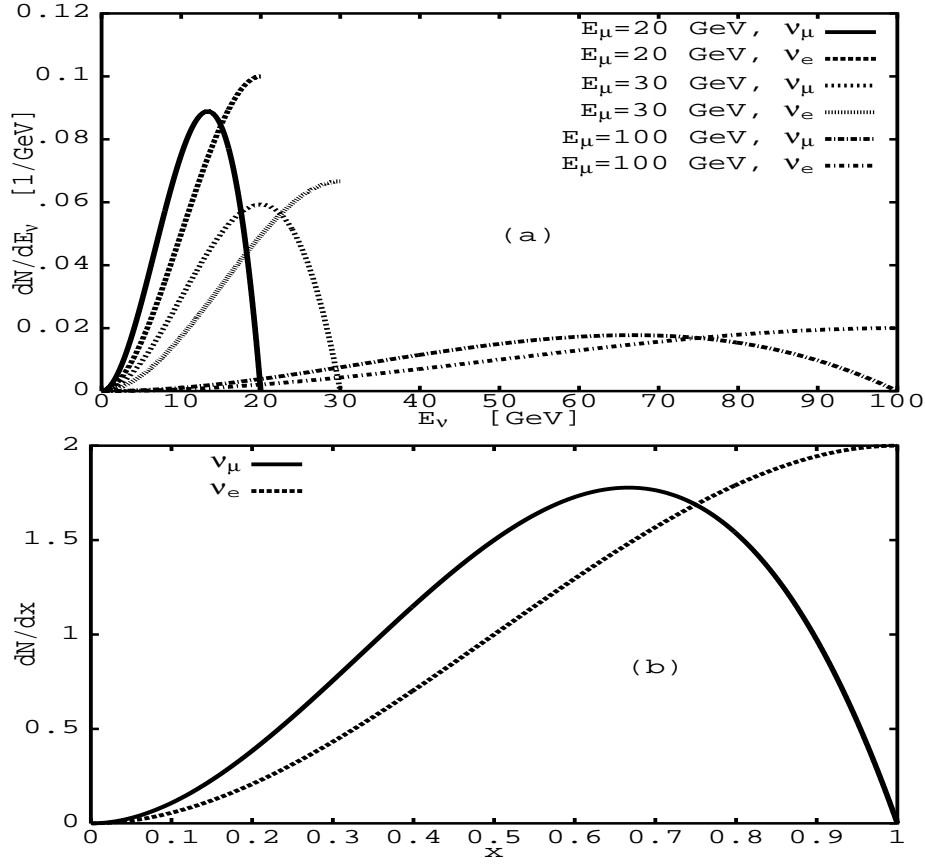


Figure C.1: Energy spectrum of neutrinos from muon decay. In (a) the spectrum for different muon energies is shown and in (b) the normalized spectrum with $x = 2E_\nu/m$.

$$dN \propto \int_0^{m/2} dE_1 \int_{m/2-E_1}^{m/2} dE_3 E_3 (m - 2E_3) \quad (\text{C.7})$$

and from this

$$\frac{dN}{dE_1} \propto E_1^2 (m - \frac{4}{3}E_1). \quad (\text{C.8})$$

Introducing the dimensionless variable $x_1 = 2E_1/m$ which lies between zero and one, and normalizing of the spectrum gives finally

$$\frac{dN}{dx_1} = 2x_1^2 (3 - 2x_1). \quad (\text{C.9})$$

Using $m/2 - E_3 < E_1$ instead of the condition in Eq. (C.6) gives

$$dN \propto \int_0^{m/2} dE_3 \int_{m/2-E_3}^{m/2} dE_1 E_3 (m - 2E_3) \quad (\text{C.10})$$

and in similar manner as before

$$\frac{dN}{dx_3} = 12 x_3^2 (1 - x_3), \quad (\text{C.11})$$

where $x_3 = 2 E_3/m$. Rewriting the two spectra (C.9,C.11) in terms of E_1 and E_3 , respectively, gives the formulas in Eq. (3.27) as written in Section 3.3. Their functional form is displayed in Fig. C.1.

Bibliography

- [1] W. Rodejohann, Nucl. Phys. **B 597**, 110 (2001).
- [2] M. Flanz, W. Rodejohann and K. Zuber, Eur. Phys. J. **C 16**, 453 (2000).
- [3] M. Flanz, W. Rodejohann and K. Zuber, Phys. Lett. **B 473**, 324 (2000), Phys. Lett. **B 480**, 418 (2000) (E).
- [4] W. Rodejohann and K. Zuber, Phys. Rev. **D 62**, 094017 (2000).
- [5] W. Rodejohann and K. Zuber, Phys. Rev. **D 63**, 054031 (2001).
- [6] W. Rodejohann, Phys. Rev. **D 62**, 013011 (2000).
- [7] W. Pauli, letter reprinted in Wolfgang Pauli, Collected Scientific Papers, ed. R. Kronig and V. Weisskopf, Vol. 2, p. 1313 (Interscience, New York) (1964).
- [8] C. L. Cowan, F. Reines *et al.*, *Nature* **178**, 446 (1956).
- [9] B. Pontecorvo, *JETP* **33**, 549 (1957).
- [10] M. Goldhaber, L. Grodzins, and A. W. Sunyar, Phys. Rev. **109**, 1015 (1958).
- [11] G. Danby *et al.*, Phys. Rev. Lett. **9**, 36 (1962).
- [12] Z. Maki, M. Nakagawa, and S. Sakata, Prog. Theo. Phys. **28**, 870 (1962).
- [13] V. Gribov, B. Pontecorvo, Phys. Lett. **B 28**, 493 (1969).
- [14] L. Wolfenstein, Phys. Rev. **D 17**, 2369 (1978); S. P. Mikheyev, A. Yu. Smirnov, *Yad. Fiz.* **42**, 1441 (1985).
- [15] R. N. Mohapatra and P. B. Pal, *Massive neutrinos in physics and astrophysics*, Singapore, Singapore: World Scientific (1991) 318 p. (World Scientific lecture notes in physics, 41); R. N. Mohapatra, *Unification and Supersymmetry*, 2nd edition, Springer Verlag, 1992.

- [16] M. Gell–Mann, P. Ramond and R. Slansky in *Supergravity*, p. 315, edited by F. Nieuwehuizen and D. Friedman, North Holland, Amsterdam, 1979; T. Yanagida, Proc. of the *Workshop on Unified Theories and the Baryon Number of the Universe*, edited by O. Sawada and A. Sugamoto, KEK, Japan 1979; R. N. Mohapatra, G. Senjanovic, Phys. Rev. Lett. **44**, 912 (1980).
- [17] E. Majorana, *Nuovo Cimento* **14**, 171 (1937).
- [18] D. Abbaneo *et al.*, LEP Collaborations, LEP Electroweak Working Group, and SLD Heavy Flavor Group, CERN-EP-2000-016.
- [19] K. Kodama *et al.* (DONUT Collaboration), Phys. Lett. **B 504**, 218 (2001).
- [20] B. T. Cleveland *et al.*, ApJ **496**, 505 (1998).
- [21] K. S. Hirata *et al.*, (Kamiokande Collaboration), Phys. Rev. Lett. **77**, 1683 (1996).
- [22] W. Hampel *et al.*, (GALLEX Collaboration), Phys. Lett. **B 447**, 127 (1999).
- [23] D. N. Abdurashitv *et al.*, (SAGE Collaboration), Phys. Rev. **C 60**, 055801 (1999).
- [24] M. Altmann, *et al.*, (GNO Collaboration), Phys. Lett. **B 490**, 16 (2000).
- [25] S. Fukuda *et al.*, (SuperKamiokande Collaboration), Phys. Rev. Lett. **86**, 5656 (2001).
- [26] Q. R. Ahmad *et al.*, (SNO Collaboration), Phys. Rev. Lett. **87**, 071301 (2001).
- [27] R. Becker–Szendy *et al.*, (IMB Collaboration), Nucl. Phys. (Proc. Suppl.) **38**, 331 (1995).
- [28] W. W. M. Allison *et al.*, (Soudan Collaboration), Nucl. Phys. (Proc. Suppl.) **91**, 134 (2000).
- [29] M. Ambrosio *et al.*, (MACRO Collaboration), Phys. Lett. **B 434**, 1998 (451).
- [30] Y. Fukuda *et al.*, (Kamiokande Collaboration), Phys. Lett. **B 335**, 237 (1994).
- [31] Y. Fukuda *et al.*, (SuperKamiokande Collaboration), Phys. Rev. Lett. **82**, 2644 (1999).
- [32] A. Aguilar *et al.*, (LSND Collaboration), hep-ex/0104049.
- [33] C. Weinheimer *et al.*, (Mainz Collaboration), Nucl. Phys. (Proc. Suppl.) **91**, 273 (2001).
- [34] K. Assamagan *et al.*, Phys. Rev. **D 53**, 6065 (1996).
- [35] R. Barate *et al.* (ALEPH Collaboration), Eur. Phys. J. **C 2**, 395 (1998).

- [36] See e.g. K. Zuber, Phys. Rep. **305**, 295 (1998); S. M. Bilenky, C. Giunti, and W. Grimus, Prog. Part. Nucl. Phys. **43**, 1 (1999).
- [37] M. Koike, J. Sato, Phys. Rev. **D 61**, 073012 (2000); V. Barger *et al.*, Phys. Rev. **D 62**, 073002 (2000). M. Freund, P. Huber, and M. Lindner, Nucl. Phys. **B 615**, 331 (2001).
- [38] M. Apollonio *et al.*, (CHOOZ Collaboration), Phys. Lett. **B 466**, 415 (1999).
- [39] S. P. Rosen, W. Kwong, hep-ph/9501351.
- [40] F. Vissani, hep-ph/9708483.
- [41] P. F. Harrison and W. G. Scott, Phys. Lett. **B 333**, 471 (1994);
- [42] M. C. Gonzalez–Garcia *et al.*, Phys. Rev. **D 63**, 033005 (2001).
- [43] A. de Gouvea, A. Friedland, and H. Murayama, Phys. Lett. **B 490**, 125 (2000); M. C. Gonzalez–Garcia, C. Pena–Garay, Phys. Rev. **D 62**, 031301 (2001).
- [44] A. Piepke *et al.*, (KAMLAND Collaboration), Nucl. Phys. (Proc. Suppl.) **91**, 99 (2001).
- [45] G. Ranucci *et al.*, (BOREXINO Collaboration), Nucl. Phys. (Proc. Suppl.) **91**, 58 (2001).
- [46] G. L. Fogli, E. Lisi, D. Montanino, Phys. Lett. **B 434**, 333 (1998); J. N. Bahcall, M. C. Gonzalez–Garcia, and C. Peña–Garay, J. High Energy Phys. **0108**, 014 (2001).
- [47] V. Barger *et al.*, Phys. Lett. **B 485**, 379 (2000).
- [48] S. M. Bilenky *et al.*, Phys. Rev. **D 54**, 1881 (1996), Phys. Rev. **D 54**, 4432 (1996), Phys. Lett. **B 465**, 193 (1999); V. Barger, K. Whisnant, Phys. Lett. **B 456**, 194 (1999); F. Vissani, J. High Energy Phys. **06**, 022 (1999); M. Czakon, J. Gluza, and M. Zralek, Phys. Lett. **B 465**, 211 (1999); H. V. Klapdor–Kleingrothaus, H. Päs, and A. Yu. Smirnov, Phys. Rev. **D 63**, 073005 (2001); D. Falcone, F. Tramontano, Phys. Rev. **D 64**, 077302 (2001); S. M. Bilenky, S. Pascoli, and S. T. Petcov, Phys. Rev. **D 64**, 053010 (2001); P. Osland, G. Vigdel, Phys. Lett. **B 520**, 143 (2001); M. Czakon *et al.*, hep-ph/0110166; S. Pascoli, S. T. Petcov, and L. Wolfenstein, hep-ph/0110287.
- [49] W. H. Furry, Phys. Rev. **56**, 1184 (1939).
- [50] M. Doi, T. Kotani and E. Takasugi, Prog. Theo. Phys. Suppl. **83**, 1 (1985).
- [51] H. V. Klapdor–Kleingrothaus, H. Päs, Talk presented at COSMO 99: 3rd International Conference on Particle Physics and the Early Universe, Trieste, Italy, 27 Sep - 3 Oct 1999, hep-ph/0002109.

- [52] A. Staudt, K. Muto, and H. V. Klapdor–Kleingrothaus, *Europhys. Lett.* **13**, 31 (1990).
- [53] E. Fiorini *et al.*, (CUORE Collaboration), *Phys. Rep.* **307**, 309 (1998).
- [54] H. Ejiri *et al.*, (MOON Collaboration), *Phys. Rev. Lett.* **85**, 2917 (2000).
- [55] X. Sarazin *et al.*, (NEMO Collaboration), Contributed to 19th International Conference on Neutrino Physics and Astrophysics - Neutrino 2000, Sudbury, Ontario, Canada, 16-21 Jun 2000 and at 30th International Conference on High–Energy Physics (ICHEP 2000), Osaka, Japan, 27 Jul - 2 Aug 2000, hep-ex/0006031.
- [56] H. V. Klapdor–Kleingrothaus *et al.*, (GENIUS Collaboration), Talk given at 2nd International Conference Physics Beyond the Standard Model: Beyond the Desert 99: Accelerator, Nonaccelerator and Space Approaches, Ringberg Castle, Tegernsee, Germany, 6-12 Jun 1999, hep-ph/9910205.
- [57] R. N. Mohapatra, *Nucl. Phys. (Proc. Suppl.)* **77**, 376 (1999). H. V. Klapdor–Kleingrothaus, H. Päs, and U. Sarkar, Talk given at 2nd International Conference Physics Beyond the Standard Model: Beyond the Desert 99: Accelerator, Nonaccelerator and Space Approaches, Ringberg Castle, Tegernsee, Germany, 6-12 Jun 1999, hep-ph/0002118;
- [58] J. Schechter, J. W. F. Valle, *Phys. Rev.* **D 25**, 2951 (1982).
- [59] A. Morales, *Nucl. Phys. (Proc. Suppl.)* **77**, 335 (1999); W. C. Haxton, G. J. Stephenson, *Prog. Part. Nucl. Phys.* **12**, 409 (1984).
- [60] K. Muto, H. V. Klapdor–Kleingrothaus in *Neutrinos*, ed. H. V. Klapdor–Kleingrothaus, Springer 1988.
- [61] W. C. Haxton, G. J. Stephenson Jr., D. Strottman, *Phys. Rev. Lett.* **47**, 153 (1981).
- [62] E. Caurier *et al.*, nucl-th/9601017.
- [63] O. Civitarese, A. Faessler, and T. Tomoda, *Phys. Lett.* **B 194**, 11 (1987).
- [64] J. Engel, P. Vogel, M. R. Zirnbauer, *Phys. Rev.* **C 37**, 731 (1988).
- [65] G. Pantis *et al.*, *Phys. Rev.* **C 53**, 695 (1996).
- [66] X. R. Wu *et al.*, *Phys. Lett.* **B 272**, 169 (1991).
- [67] P. B. Pal and L. Wolfenstein, *Phys. Rev.* **D 25**, 766 (1982).
- [68] A. Osipowicz *et al.*, (KATRIN Collaboration), hep-ex/0109033.
- [69] R. Adhikari, G. Rajasekaran, *Phys. Rev.* **D 61**, 031301 (2000).

- [70] H. Minakata, O. Yasuda, Phys. Rev. **D 56**, 1692 (1997).
- [71] T. Fukuyama *et al.*, Phys. Rev. **D 64**, 013001 (2001).
- [72] For reviews see e.g. A. Pilaftsis, Int. Journal of Modern Physics **14**, 1811 (1999); W. Buchmüller, M. Plümacher, hep-ph/0007176.
- [73] A. S. Joshipura, E. A. Paschos, and W. Rodejohann, Nucl. Phys. **B 611**, 227 (2001); J. High Energy Phys. **0108**, 029 (2001).
- [74] W. Rodejohann, Talk presented at XXV International School of Theoretical Physics, “Particle Physics and Astrophysics — Standard Models and beyond”, Ustroń, Poland, September 10-16, 2001, hep-ph/0110258, to appear in *Acta Phys. Pol. B*.
- [75] D. A. Dicus, D. D. Karatas, and P. Roy, Phys. Rev. **D 44**, 2033 (1991); A. Datta, M. Guchait, and A. Pilaftsis Phys. Rev. **D 50**, 3195 (1994); F. M. L. Almeida, Jr *et al.*, Phys. Rev. **D 62**, 075004 (2000).
- [76] O. Panella, *et al.*, hep-ph/0107308.
- [77] S. T. Petcov, Phys. Lett. **B 139**, 421 (1984);
- [78] T. G. Rizzo, Phys. Lett. **B 116**, 23 (1982).
- [79] C. A. Heusch and P. Minkowski, hep-ph/9611353.
- [80] J. A. Aguilar-Saavedra *et al.*, hep-ph/0106315.
- [81] F. Cuypers, Talk given at 3rd Workshop on Physics and Experiments with e+ e- Linear Colliders (LCWS95), Iwate, Japan, 8-12 Sep 1995, hep-ph/9512201.
- [82] G. Belanger *et al.*, Phys. Rev. **D 53**, 6292 (1996).
- [83] B. Kayser, F. Gibrat-Debu, F. Perrier, *The Physics of Massive Neutrinos*, World Scientific, 1989.
- [84] P. Duka, J. Gluza, and M. Zralek, Phys. Rev. **D 58**, 053009 (1998); J. Maalampi, N. Romanenko, Phys. Rev. **D 60**, 05502 (1999).
- [85] Review of Particle Properties, C. Caso *et al.*, *Eur. Phys. J. C* **3**, 1 (1998).
- [86] E. Nardi, E. Roulet, D. Tommasini, Phys. Lett. **B 344**, 225 (1995).
- [87] P. Achard *et al.*, Phys. Lett. **B 517**, 75 (2001).
- [88] J. Gluza *et al.*, Phys. Lett. **B 407**, 45 (1997).
- [89] S. Wolfram, *Mathematica*, Addison-Wesley, 1991.
- [90] M. Jamin, M. E. Lautenbacher, *Comp. Phys. Comm.* **74**, 265 (1993).

- [91] F. James, CERN 68-15 (1968).
- [92] M. Glück, E. Reya, A. Vogt, *Eur. Phys. J. C* **5**, 461 (1998).
- [93] J. Abad, J. G. Esteve, A. F. Pachero, *Phys. Rev. D* **30**, 1488 (1984).
- [94] J. H. Missimer, R. N. Mohapatra, N. C. Mukhopadhyay, *Phys. Rev. D* **50**, 2067 (1994).
- [95] B. C. Barish *et al.*, *Phys. Rev. Lett.* **38**, 577 (1977).
- [96] A. Benvenuti *et al.*, *Phys. Rev. Lett.* **38**, 1110 (1977), *Phys. Rev. Lett.* **38**, 1183 (1977), *Phys. Rev. Lett.* **42**, 1024 (1979).
- [97] M. Holder *et al.*, *Phys. Lett. B* **70**, 393 (1977); T. Hansl *et al.*, *Nucl. Phys. B* **142**, 381 (1978).
- [98] V. Barger, T. Gottschalk, R. J. N. Phillips, *Phys. Rev. D* **17**, 2284 (1978), *Phys. Rev. D* **18**, 2308 (1978).
- [99] J. Smith, J. A. M. Vermaseren, *Phys. Rev. D* **17**, 2288 (1978).
- [100] R. M. Barnett, L. N. Chang, N. Weiss, *Phys. Rev. D* **17**, 2266 (1978).
- [101] S. Geer, *Phys. Rev. D* **57**, 6989 (1998); D. Ayres *et al.*, physics/9911009; B. Autin, A. Blondel, and J. Ellis (eds.), CERN-99-02; A. Bueno, M. Campanelli and A. Rubbia, *Nucl. Phys. B* **589**, 577 (2000).
- [102] B. J. King, Proc. Workshop on Physics at the First Muon Collider and a the Front End of a Muon Collider, Fermilab, Illinois, 6-9 November, 1997, hep-ex/9907033; E. A. Paschos, DO-TH 98/01, Talk given at Physics at the First Muon Collider and at the Front End of the Muon Collider, Batavia, IL, 6-9 Nov 1997, in "Batavia 1997, Physics at the first muon collider" 370-375; R. D. Ball, D. A. Harris, and K. S. McFarland, hep-ph/0009223.
- [103] DØ Collaboration, S. Abachi *et al.*, *Phys. Rev. Lett.* **76**, 3271 (1996).
- [104] B. J. King, to be published in the proceedings of Workshop on Studies on Colliders and Collider Physics at the Highest Energies: Muon Colliders at 10-TeV to 100-TeV (HEMC 99), Montauk, New York, 27 Sep - 1 Oct 1999, hep-ex/0005007.
- [105] N. Schmitz, *Neutrino Physik*, Teubner Studienbücher, 1997.
- [106] M. Glück, E. Reya and A. Vogt, *Z. Phys. C* **53**, 127 (1992).
- [107] B. J. King, to be published in the proceedings of Workshop on Studies on Colliders and Collider Physics at the Highest Energies: Muon Colliders at 10-TeV to 100-TeV (HEMC 99), Montauk, New York, 27 Sep - 1 Oct 1999, hep-ex/0005008.

- [108] W. Buchmüller, C. Greub, Nucl. Phys. **B 363**, 345 (1988); W. Buchmüller *et al.* in *Physics at HERA*, Proceedings of the workshop, p. 1003, edited by W. Buchmüller and G. Ingelman.
- [109] M. Derrick *et al.*, (H1 Collaboration), Z. Phys. **C 72**, 47 (1996).
- [110] A. Halprin *et al.*, Phys. Rev. **D 13**, 2567 (1976); J. N. Ng, A. N. Kamal, Phys. Rev. **D 18**, 3412 (1978); L. Littenberg, R. E. Shrock, Phys. Rev. Lett. **68**, 443 (1992).
- [111] U. Baur, D. Zeppenfeld, Nucl. Phys. **B 325**, 253 (1989).
- [112] T. Ahmed *et al.*, (H1 Collaboration), DESY 94-248.
- [113] C. Adloff *et al.*, (H1 Collaboration), Eur. Phys. J. **C 5**, 575 (1998).
- [114] M. Kuze, presented at 15th Les Rencontres de Physique de la Vallée d'Aoste: Results and Perspective in Particle Physics, La Thuile, Valle d'Aosta, Italy, 4-10 Mar 2001, hep-ex/0106030
- [115] J. Breitweg *et al.* (ZEUS Collaboration), Phys. Lett. **B 471**, 411 (2000).
- [116] G. Cozzika, Talk given at 13th Topical Conference on Hadron Collider Physics, Mumbai, India, 14-20 Jan 1999, DAPNIA-SPP-99-10.
- [117] T. Kon, T. Kobayashi, S. Kitamura, Phys. Lett. **B 376**, 227 (1996).
- [118] G. Cvetic, C. S. Kim, C. W. Kim, Phys. Rev. Lett. **82**, 4761 (1999).
- [119] F. M. L. Almeida Jr. *et al.*, Phys. Rev. **D 63**, 075005 (2001).
- [120] F. M. L. Almeida Jr. *et al.*, Phys. Lett. **B 494**, 273 (2000).
- [121] G. Cvetic, C. S. Kim, Phys. Lett. **B 461**, 248 (1999), erratum *ibid.* **471**, 471 (2000).
- [122] X. Y. Pham, Phys. Lett. **B 495**, 131 (2000).
- [123] C. Jarlskog, Phys. Rev. Lett. **55**, 1039 (1985).
- [124] M. Fukugita, M. Tanimoto, Phys. Lett. **B 515**, 30 (2001).
- [125] C. Dib *et al.*, Phys. Lett. **B 493**, 82 (2000).
- [126] A. Ali, A. V. Borisov, and N. B. Zamorin, Eur. Phys. J. **C 21**, 123 (2001).
- [127] R. Appel *et al.*, Phys. Rev. Lett. **85**, 2877 (2000).
- [128] K. Zuber, Phys. Lett. **B 479**, 33 (2000).
- [129] L. Littenberg, R. E. Shrock, Phys. Lett. **B 491**, 285 (2000).

- [130] P. Domin, *et al.*, Part. Nucl. Lett. **104**, 40 (2001).
- [131] M. L. Brooks *et al.* (MEGA Collaboration), Phys. Rev. Lett. **83**, 1521 (1999).
- [132] M. Cannoni, private communication.
- [133] J. Gluza, M. Zralek, Phys. Rev. **D 55**, 7030 (1997).
- [134] F. Maltoni, J. M. Niczyporuk, and S. Willenbrock, Phys. Rev. Lett. **86**, 212 (2001).

Acknowledgments

It is a pleasure to thank Prof. E. A. Paschos for scientific guidance, sharing with me his expertise and leaving me the freedom to follow my path. I also thank Prof. W. Grimus for agreeing to act as my co-adviser. This thesis would not have been possible without benefitting from the talents of my co-authors Marion Flanz and Kai Zuber, whose idea ignited all my works. I also thank Marion for being such a nice office-mate for all of the almost five years we spent together. I am also grateful to my colleagues from T III and IV for all the inspiring discussions about (not only) physics.